



FAKULTÄT FÜR VERFAHRENS-
UND SYSTEMTECHNIK

“Analysis and design of center-cut separations using 8-zone simulated moving bed chromatography”

Der Fakultät für Verfahrens- und Systemtechnik
der Otto-Von-Guericke-Universität Magdeburg
Dissertation zur Erlangung des akademischen Grades

**Doktoringenieur
(Dr.-Ing.)**

von Dipl.-Ing. **Francisco Vitor Santos da Silva**
geb. am 7. November 1990 in Curitiba, Brasilien

genehmigt durch die Fakultät für Verfahrens- und Systemtechnik
der Otto-von-Guericke-Universität Magdeburg

Promotionskommission:

Prof. Dr. rer. nat. habil. Dieter Schinzer	(Vorsitz)
Prof. Dr. Diana Cristina Silva de Azevedo	(Gutachter)
Prof. Dr.-Ing. habil. Achim Kienle	(Gutachter)
Prof. Dr.-Ing. habil. Andreas Seidel-Morgenstern	(Gutachter)

eingereicht am:

31. Mai 2017

Promotionskolloquium am:

29. September 2017

Zusammenfassung

Seit ihrer Erfindung als Analysetechnik vor über einem Jahrhundert ist die Chromatographie zu einer der vielseitigsten Technologien geworden, um gelöste Komponenten zu trennen. Da es sich immer noch um einen kostenintensiven Prozess handelt, wurden viele verschiedene kontinuierlich arbeitende Modi vorgeschlagen. Eine der erfolgreichsten Varianten ist der *Simulated-Moving-Bed* (SMB)-Prozess, welcher von D. Broughton et al. 1961 patentiert wurde [1]. Die klassische SMB-Konfiguration kann dabei Gemische nur in zwei Fraktionen trennen, welches den Anwendungsbereich limitiert. Um diesen Nachteil auszugleichen, wurden leistungsstärkere SMB-Variationen, wie z.B. die 8-Zonen-SMB, entwickelt.

Der Gegenstand dieser Dissertation ist es, Möglichkeiten und Limitierungen der 8-Zonen-SMB für die Isolierung von Komponenten mit mittlerer Adsorptionsstärke zu untersuchen. Zunächst wurde für die Prozessanalyse von der Äquivalenz zwischen SMB und dem *True-Moving-Bed* (TMB)-Prozess ausgegangen und darauf aufbauend eine Methode zur Vorhersage der Trennleistung entwickelt. Anschließend wurden ökonomische Parameter zur Analyse hinzugefügt, um die Wirtschaftlichkeit zu maximieren. Überdies wurde ein Entscheidungsbaum für die Wahl zwischen Extrakt- oder Raffinat-Recycling-Konfiguration entwickelt.

Aufgrund bestehender Indikationen, dass die Trennleistung des 8-Zonen-SMB-Verfahrens durch den periodischen Prozessablauf mit Rückführungen nicht immer durch seine geometrische Äquivalenz zum TMB-Prozess beschrieben werden kann. Wurde eine genauere Implementierung des Gleichgewichtsmodells für die Vorhersage des Trennbetriebsbereichs vorgeschlagen und genutzt, um den Trennprozess mit einer Kaskade aus zwei klassischen SMB-Anlagen zu vergleichen.

Abschließend wurden die Betriebsbedingungen, die mit der neu entwickelten Auslegungsmethode identifiziert wurden, mithilfe eines zu trennenden Modellstoffgemisches aus mehreren Lebensmittelfarbstoffen experimentell validiert. Ungeachtet der experimentellen Herausforderungen konnte demonstriert werden, dass das ausgewählte Farbstoffgemisch für die Bewertung verschiedener Flüssigchromatographie-Konfigurationen geeignet ist. Weiterhin gelang es, die mathematischen Relationen, die für das Abschätzen des Betriebsbereiches der 8-Zonen-SMB entwickelt wurden, auch für die Analyse anderer SMB-Konfigurationen mit internem Rückfluss anzuwenden. Auch andere Gleichgewichts-Trennstufenprozesse sollten von den methodischen Ergebnissen, die in dieser Dissertation beschrieben wurden, profitieren können.

Abstract

Since its conception as a laboratory technique over a century ago, chromatography has become one of the most versatile technologies for separating compounds in solution. However, since it is, still, regarded as a cost intensive process, different continuous operating modes have been suggested, of which, the most successful one has been the Simulated Moving Bed (SMB) process, patented by D. Broughton et al. in 1961 [1]. The classical SMB configuration can, however, only separate mixtures in two fractions, narrowing the scope of its potential applications, which led to the development of novel SMB variants to overcome this limitation, such as the 8-zone SMB.

The purpose of this dissertation is to explore the possibilities and limitations of 8-zone SMB for purifying intermediary eluting solutes. Initially assuming equivalence between SMB and the True Moving Bed (TMB) process, an approach for predicting the separation performance was developed. Subsequently, in order to maximize the profitability, economic information was added to the analysis, which led to a strategy for selecting the best operating conditions. Moreover, a decision tree for the choice between extract and raffinate recycle configurations was established.

There have been, however, indications that, due its cyclic nature, the performance of an 8-zone SMB is not always well replicated by an equivalent hypothetical TMB process. Therefore, a more accurate implementation of the equilibrium model for the estimation of the 8-zone SMB operating space was suggested and used for comparing its performance to that of two connected independently operated 4-zone SMB units. Finally, a solution of food dyes was chosen as a model mixture to experimentally validate a separation using the operating conditions identified with help of the developed methodology.

Despite of experimental challenges encountered during the experimental investigations, the potential of studying different continuous liquid chromatographic configurations using dye mixtures could be demonstrated. Furthermore, the mathematical framework created for estimating the operating ranges of 8-zone SMB can be applied for the analysis of other SMB configurations with internal recycle. Different equilibrium staged separation processes, other than chromatography, may also profit from the research described in this dissertation.

Acknowledgments

The work reported in this dissertation was performed in and with financial support from the Max Planck Institute for dynamics of complex and technical systems (Magdeburg, Germany) with some of the funding provided by the branch of the Brazilian Ministry of Education responsible for postgraduate education, CAPES (Coordenação de Aperfeiçoamento de Pessoal de Nível Superior). This work would not have been possible without the tireless commitment and insightful contributions of the main advisor, Professor Dr.-Ing. habil. Andreas Seidel-Morgenstern (Otto-von-Guericke Universität Magdeburg), and without the help of Professor Diana de Azevedo (Universidade Federal do Ceará) with the redaction of the grant proposal.

The research described in this dissertation was greatly supported by the collaboration and fruitful discussions with M.Sc. Bettina Kattein, M.Sc. Rita Ribeiro and M.Sc. Rojari Piskari, who kindly dedicated much of their time to this endeavor. Moreover, necessary acknowledgement is owed to Luise Blach, Jacqueline Kaufmann and Stefanie Leuchtenberg, whose experience and knowledge allowed undertaking the experiments described here. Additionally, the invaluable remarks of Dr. Héctor O. Rubiera Landa, Professor Arvind Rajendran, Professor Tuomo Sainio and Professor Dr.-Ing. habil. Malte Kasperareit to the theoretical framework developed in this work are immensely appreciated. Furthermore, gratitude should be here expressed for the help and technical support of Jan Protzmann and the always-available assistance of the mechanical and electrical workshops at the Max Planck Institute Magdeburg, which made the experimental 8-zone Simulated Moving Bed separation possible.

I am very thankful for the friendship and support of Bettina Kattein, Ivana Mutavdzin, and many others who, over the years, made life in Magdeburg more than an enterprise, a pleasure. I am especially grateful to Marta Brocka for bringing joy and balance to my life. Last but not least, the most important acknowledgement must be granted to my parents, Elaine Maria Santos Silva and Maurício Pereira da Silva, who not only shaped me into the person I am but also and always without hesitation believed in me, even when I did not.

TABLE OF CONTENTS

TABLE OF CONTENTS	5
LIST OF ABBREVIATIONS AND SYMBOLS	8
1. MOTIVATION AND OUTLINE	1
2. PREPARATIVE CHROMATOGRAPHY: STATE OF THE ART	3
2.1. CHROMATOGRAPHIC SEPARATION	3
2.2. ADSORPTION PROCESS	4
2.3. SIMULATED MOVING BED TECHNOLOGY	7
2.4. CENTER-CUT SEPARATIONS	10
2.5. INTEGRATED 8-ZONE SIMULATED MOVING BED	12
2.6. SUMMARY	15
3. MATHEMATICAL MODELING OF CHROMATOGRAPHY	16
3.1. SOLUTE MASS BALANCE IN A CHROMATOGRAPHIC COLUMN	16
3.2. “TRIANGLE THEORY” BASED ON THE TMB ANALOGY	20
3.3. MIXING CELL MODEL OF 8-ZONE SIMULATED MOVING BED	23
3.4. MIXING CELL MODEL OF 8-ZONE TRUE MOVING BED	26
3.5. PERFORMANCE EVALUATION OF CONTINUOUS CHROMATOGRAPHY	30
3.6. SUMMARY	32
4. THEORETICAL BACKGROUND OF THE EXPERIMENTAL METHODS USED	34
4.1. EXPERIMENTAL ESTIMATION OF ADSORPTION ISOTHERMS	34
4.2. MEASUREMENT OF SOLUTE CONCENTRATIONS USING HPLC	37
4.3. MEASUREMENT OF ABSORBANCE SPECTRA	41
4.4. SUMMARY	43
5. OPERATING REGIONS AND ANALYSIS OF 8-ZONE TMB	45
5.1. OPERATING REGIONS OF 8-ZONE TMB WITH EXTRACT RECYCLE	45
5.2. OPERATING REGIONS OF 8-ZONE TMB WITH RAFFINATE RECYCLE	51
5.3. ESTIMATION OF 8-ZONE TMB OUTLET CONCENTRATIONS	54
5.4. ECONOMIC PERFORMANCE OF 8-ZONE TMB	57
5.4.1. <i>Economic analysis</i>	57
5.4.2. <i>Evaluation of extract recycle 8-zone TMB</i>	59
5.4.3. <i>Evaluation of raffinate recycle 8-zone TMB</i>	60
5.4.4. <i>Highest productivity point</i>	61
5.5. OPERATING GUIDELINES FOR 8-ZONE TMB	65

5.6.	DISCUSSION AND OUTLOOK	68
5.7.	CONCLUSIONS.....	70
6.	OPERATING REGIONS OF 8-ZONE SMB	71
6.1.	OPERATING REGIONS OF 8-ZONE SMB WITH 8 COLUMNS.....	71
6.1.1.	<i>Extract recycle 8-zone SMB with 8 columns</i>	<i>72</i>
6.1.2.	<i>Raffinate recycle 8-zone SMB with 8 columns</i>	<i>81</i>
6.2.	8-ZONE SMB VS. TWO INDEPENDENT 4-ZONE SMB UNITS.....	87
6.2.1.	<i>Extract recycle</i>	<i>87</i>
6.2.2.	<i>Raffinate recycle.....</i>	<i>89</i>
6.3.	OPERATING REGIONS OF 8-ZONE SMB WITH 16 COLUMNS.....	92
6.3.1.	<i>Extract recycle 8-zone SMB with 16 columns</i>	<i>92</i>
6.3.2.	<i>Raffinate recycle 8-zone SMB with 16 columns</i>	<i>94</i>
6.4.	LIMITATIONS OF 8-ZONE SMB	96
6.5.	DISCUSSION AND OUTLOOK	97
6.6.	CONCLUSIONS.....	98
7.	EXPERIMENTAL VALIDATION.....	100
7.1.	CHROMATOGRAPHIC SEPARATION OF FOOD DYES.....	100
7.1.1.	<i>Adsorption mechanism of food dyes onto C18 silica.....</i>	<i>103</i>
7.2.	EXPERIMENTAL PROTOCOLS	106
7.2.1.	<i>High performance liquid chromatography.....</i>	<i>107</i>
7.2.2.	<i>Characterization of the 8-zone SMB columns</i>	<i>108</i>
7.2.3.	<i>Adsorption isotherm estimation using frontal analysis</i>	<i>111</i>
7.2.4.	<i>Measurement of absorbance spectra.....</i>	<i>113</i>
7.2.5.	<i>Simulated moving bed chromatography with 8 zones</i>	<i>113</i>
7.2.6.	<i>Estimation of the Prochrom® ICLC-16-10 dead volumes</i>	<i>116</i>
7.3.	EXPERIMENTAL RESULTS AND ANALYSIS THEREOF.....	116
7.3.1.	<i>Measurement of the absorbance spectra.....</i>	<i>116</i>
7.3.2.	<i>Deconvolution of absorbance spectra</i>	<i>118</i>
7.3.3.	<i>Estimation of the adsorption isotherms.....</i>	<i>120</i>
7.4.	SIMULATION OF 8-ZONE SMB SEPARATION OF FOOD DYES.....	123
7.4.1.	<i>Parametric study: 8-zone SMB with extract recycle</i>	<i>124</i>
7.4.2.	<i>Parametric study: 8-zone SMB with raffinate recycle.....</i>	<i>127</i>
7.5.	FOOD DYE SEPARATION USING RAFFINATE RECYCLE 8-ZONE SMB.....	130
7.6.	REPETITION OF THE FOOD DYE SEPARATION USING 8-ZONE SMB	133
7.7.	DISCUSSION AND OUTLOOK	135
7.8.	CONCLUSIONS.....	140
8.	SUMMARY AND GENERAL CONCLUSIONS.....	141
9.	REFERENCES	142

APPENDIX A – 8-ZONE SMB OUTLET CONCENTRATIONS.....	154
APPENDIX B – LIST OF CHEMICALS, EQUIPMENT AND SUPPLIERS.....	160
CURRICULUM VITAE.....	161

List of abbreviations and symbols

Latin characters

$a_{i,\lambda}$	Absorbance of the solute i at wavelength λ [AU] (equation 4-10)
a_i	Detector response to the solute I [arbitrary unit]
$a_{\lambda,Total}$	Absorbance of a mixture at wavelength λ [AU] (equation 4-11)
A	Absorbance spectra of a mixture [AU]
AU	Light Absorbance Units
b_i	Coefficient between detector signal and concentration [$\text{mg}^{-1} \cdot \text{l}$]
$b_{i,\lambda}$	Absorbance coefficient of solute i at wavelength λ [$\text{AU} \cdot \text{mg}^{-1} \cdot \text{l}$]
B	matrix of absorbance coefficients [$\text{AU} \cdot \text{mg}^{-1}$]
c	Concentration of the solute [$\text{mg} \cdot \text{l}^{-1}$]
C	Concentration vector of a mixture [$\text{mg} \cdot \text{l}^{-1}$]
$c_{in,i}(t)$	Concentration profile of the solute i at column inlet [$\text{mg} \cdot \text{l}^{-1}$]
$c_{i,sample}$	Concentration of the solute i in a HPLC sample [$\text{mg} \cdot \text{l}^{-1}$]
CST	Continuously stirred tank
D_{ax}	Diffusion coefficient [$\text{cm} \cdot \text{min}^{-1}$]
$DFFR$	Dimensionless feed flow rate = $FFR \backslash \dot{V}_S$
$DOFR$	Dimensionless outlet flow rate = $OFR \backslash \dot{V}_S$
DP	Dimensionless profit function (defined in equation 5-22)
DSC	Dimensionless solvent consumption = $SC \backslash \dot{V}_S$
F	Phase ration ($(I - \epsilon)/\epsilon$) [dimensionless]
FFR	Feed flow rate [$\text{l} \cdot \text{min}^{-1}$]
FCo	Crude feed costs [$\text{\$} \cdot \text{g}^{-1}$] (defined in Table 5-2)
FCR	Crude feed costs ratio (defined in equation 5-25)
H	Henry adsorption coefficient = $q \backslash c$ [dimensionless]
HPLC	High-performance liquid chromatography
i.d.	Inner diameter [cm]
k_i	Parameter in the Langmuir adsorption isotherm [$\text{mg}^{-1} \cdot \text{l}$]
L	Column length [dm]
M_i	Total mass of a solute i [ng]
m_k	Dimensionless flow rate in zone k
$m_{II(2),min}$	Minimal dimensionless flow rate defined in equation 6-9
$m_{II(1),min}$	Minimal dimensionless flow rate defined in equation 6-10
$m_{III(2),max}$	Maximal dimensionless flow rate defined in equation 6-18
$m_{III(1),max}$	Maximal dimensionless flow rate defined in equation 6-19
n	Number of cells per zone [dimensionless]
NTP	Number of theoretical plates [dimensionless]
OFR	Outlet flow rate [$\text{l} \cdot \text{min}^{-1}$]
P	Profit function [$\text{\$} \cdot \text{min}^{-1}$] (defined in equation 5-21)
Pr	Dimensionless productivity (defined in equation 5-5)
PSP	Product selling price [$\text{\$} \cdot \text{mg}^{-1}$] (defined in Table 5-2)
Pur	Purity ($\frac{c_{Product}}{\sum_{i=1}^n c(i)_{Outlet}}$)
$q_i(c_i)$	Concentration of solute adsorbed i [$\text{mg} \cdot \text{l}^{-1}$]
Rec	Recovery yield (TMB: $\frac{\dot{V}_{Outlet} c_{Product}}{\dot{V}_{Feed} c_{Feed}}$, SMB: $\frac{\dot{V}_{Product} c_{Product}}{\sum \dot{V}_{Outlet} c_{Product}}$)

SC	Solvent consumption [$\text{l}\cdot\text{min}^{-1}$]
SCo	Solvent costs [$\$ \cdot \text{l}^{-1}$] (defined in Table 5-2)
SCR	Solvent costs ratio (defined in equation 5-23)
SMB	Simulated Moving Bed
$SRCo$	Solvent removal costs [$\$ \cdot \text{l}^{-1}$] (defined in Table 5-2)
$SRCR$	Solvent removal costs ratio (defined in equation 5-24)
t^*	Switching interval [min]
t_b	Breakthrough time of the concentration shock front [min]
t_c	Time interval defined in [min]
t_R	Retention time of a single pulse injection [min]
TMB	True Moving Bed
$TSSC$	Total specific solvent consumption [dimensionless]
v	Velocity of a non-adsorbing solvent [$\text{dm}\cdot\text{min}^{-1}$]
V	Band volume [ml]
V_{ads}	Volume of adsorbent inside the column [l]
V_c	Volume of the column [l]
V_{fl}	Volume of solvent inside the column [l]
V_{inj}	Volume of the HPLC sample [ml]
\dot{V}_k	Solvent flow rate in zone k [$\text{l}\cdot\text{min}^{-1}$]
\dot{V}_{out}	Solvent flow rate leaving or entering the system [$\text{l}\cdot\text{min}^{-1}$]
\dot{V}_s	Adsorbent flow rate [$\text{l}\cdot\text{min}^{-1}$]
$w_{1/2}$	Peak width mid-height [min]
z	Longitudinal coordinate axis of the column
Indices	
i	Solute (from 1 to m)
j	Cell (from 1 to n)
k	SMB or TMB zone (from $I(1)$ to $IV(2)$)
x	SMB or TMB subunit ((1) or (2))
Greek characters	
$\alpha_{A,B}$	Selectivity factor = H_B/H_A (dimensionless)
$\alpha_{B,C}$	Selectivity factor = H_C/H_B (dimensionless)
γ	Factor defined in equations 3-31 and 3-33
Δc	Solute concentration increase inside the column [$\text{mg}\cdot\text{l}^{-1}$]
Δc_{in}	Solute concentration increase in the inlet of the column [$\text{mg}\cdot\text{l}^{-1}$]
Δc_{out}	Solute increase at the column outlet [$\text{mg}\cdot\text{l}^{-1}$]
$\Delta q(c)$	Loading increase inside the column [$\text{mg}\cdot\text{l}^{-1}$]
Δz	Width of a cross-section of the column [cm]
Δz_1	Distance shown in Figure 6-2 and in Figure 6-5
Δz_2	Distance shown in Figure 6-2 and in Figure 6-5
ε_{Total}	Total porosity (dimensionless)
η	Factor defined in equations 3-32 and 3-34
λ	Light wavelength [nm]
χ	Flow rate ratio defined in the equation 3-30

1. Motivation and outline

Following the development, in the last decades, of highly specialized and efficient adsorbents, chromatography is now one of the most universal techniques for separating solutes in homogeneous solution. Its production scale application is, however, often regarded as prohibitively expensive, due to the high costs associated with packing material and solvents [2]. Consequently, in order to improve on process economic performance, different counter-current operation modes have been suggested, of which, the most successful one has been the Simulated Moving Bed (SMB) technology. Nonetheless, SMB, as originally conceived, can only split mixtures into two fractions [3] and, thus, different variations have been suggested to allow center-cut separations, such as the 8-zone SMB [4].

The research described in this dissertation is part of a long-lasting effort dedicated to the development of technologies for separating mixtures into three fractions using 8-zone SMB [3-6]. As briefly reviewed in chapter 2, it is the continuation of the research initiated by L. C. Kessler and A. Seidel-Morgenstern [7] and further developed by J. Nowak [8, 9] and D. Kiwala [10] using a Modified Prochrom® ICLC-16-10 unit at the Max Planck Institute in Magdeburg for the purification of intermediary eluting solutes [11]. In the present work, the purpose was the study of the potentials and limitations of 8-zone SMB for separating solutes with linear adsorption isotherms. In chapters 3 and 4, the necessary concepts will be introduced and the main scientific contributions will be reported in the following three parts:

1. Evaluation of the 8-zone SMB separation performance based on the TMB analogy

In chapter 5, the 8-zone True Moving Bed (TMB) will be used as a model for the 8-zone SMB process. The operating parameter space is initially predicted with help of the equilibrium model and the internal concentration profiles are estimated using a mixing cell model. Subsequently, new analytical expressions for the ideal 8-zone TMB outlet concentrations are developed and used in combination with economic information to maximize the process profitability. Finally, explicit criteria are derived and used to create a decision tree for the selection of the system configuration. The results described in this part of the thesis were peer-reviewed and published in the *Journal of Chromatography A* in 2016 [12].

2. Adjustment of the triangle theory to the 8-zone Simulated Moving Bed process

Predictions based on the TMB analogy have not always been accurate. In the analysis presented in chapter 6, the equilibrium model of chromatography will be used to adjust the well established triangle theory [13] to the integrated 8-zone SMB, which allows a more accurate process description and comparison to a cascade of two independently operated 4-zone SMB units as well as the determination of its operating limits.

3. Experimental validation

The impact of theoretical results is increased with an experimental demonstration. Thus, in chapter 7, a model mixture composed of food dyes, will be characterized in terms of its absorbance spectra and adsorption isotherms onto C18 silica. Subsequently, using the tools developed in chapter 6, the operating parameter space will be predicted and adequate operating conditions will be chosen and applied to an 8-zone SMB experimental separation.

2. Preparative chromatography: State of the art

In the first chapter of this dissertation, the foundations and recent developments of the adsorption-based separation technologies pertinent to this work are briefly reviewed. The first section is dedicated to an overview of preparative chromatography, followed by the basic mathematical description of adsorption isotherm models. Next, the reader is invited for a discussion on the applications and limitations of modern continuous chromatography, where particular emphasis is given to center-cut separations – the main focus of the present work – at which point, the concept of 8-zone Simulated Moving Bed (8-zone SMB) is first introduced.

2.1. Chromatographic separation

Preparative chromatography has become an important industrial separation technology over the last century, as highly efficient columns and sophisticated detection systems have become technically feasible. Its begging, however, traces all the way back to the pioneering works of Tswett, in the 1900s, and its first large scale implementation for the separation of rare earth elements as part of the Manhattan Project [2] in the 1940s. As time went by, progressive improvement of the adsorbents, detectors, and pumping systems helped to popularize chromatography as an industrial separation workhorse. Nowadays, examples of its application can be found in the most diverse fields, ranging from the separation of enantiomers [14-46], sugars [47-53], petroleum derivatives [54-61] and proteins [62-68] to viral particles [69, 70] and even isotopes [71-75]. The separation mechanisms involved in the separation of these solutes are just as diverse, including adsorption, ion exchange, size exclusion, immuno-affinity, and many others [76]. Therefore, it can be stated, without exaggeration, that chromatography, and all of its variants, is one of the most universal separation technique in existence.

Despite of the variety of mechanisms, the constituent parts of a chromatographic separation can be broken down in three elements:

1. Solute – These are the chemical entities being separated from each other in the process. They range widely in function and size from single atoms (as for example in the case of the enrichment of noble gases by pressure swing chromatography [77]) to large polymers

and nanoparticles (as in case of the separation of viruses from cell debris by size-exclusion chromatography (SEC) [69, 70]).

2. Solvent – This is the mobile phase, its function is to provide the convective flow of the solutes, that is, ultimately, the driving-force for their separation. It can be found in different states (liquid, gas, or even as a supercritical fluid [20, 78, 79]) as long as it is able to flow through a packed bed. Its composition need not be constant during the separation process either, as in the case of gradient and displacement chromatography.

3. Adsorbent – In this work, it stands for the stationary phase, however the separation principle need not necessarily be adsorption. As a matter of fact, many different separation principles are used for chromatographic separations; ion exchange, size-exclusion and immuno-affinity, being just a few examples. Its purpose is to provide the selective affinity for the different solutes that allows their separation. Therefore, it needs to at least fulfill two requirements: First, it needs to be stationary, at least during the relevant process timeframe. Second, it needs to provide different affinities for the solutes being separated. Often, the adsorbent is in a solid state, however, liquid adsorbents are also possible as long as they are mechanically bound to a support material that prevents them from bleeding out of the chromatographic system during the separation process.

The solutes, the solvent and the adsorbent represent the core of the chromatographic separation. They are, however, not the complete experimental setup. Much more could still be said about the valves, detectors, pumping and control systems that make modern chromatography possible, but these will be left out for now.

2.2. Adsorption process

One of the most important mechanisms for generating the differential retention of solutes, which ultimately allows them to be separated using chromatography, is adsorption. Consequently, a mathematical description of the thermodynamic equilibrium between the solvent and the adsorbent is fundamental for modeling chromatographic separations. For adsorption processes occurring at constant temperature, these correlations are described by so-called *adsorption isotherms*.

In the simplest case (usually, at low concentrations), the loading of a given solute i in the adsorbent $q_i(c_i)$, can be described as a linear function of its concentration in the solvent c_i , according to the adsorption Henry coefficient (H_i):

$$q_i(c_i) = H_i c_i$$

The adsorption isotherms are influenced by many factors, such as temperature, solution ionic strength, the presence of chaotropic agents, interaction with other solutes, pressure, pH, among many others [80].

Broadly speaking, adsorption isotherm models can be categorized into porous and lumped [81]. In the first case, three (or potentially more) phases are considered, the solvent, the solid phase, and an intragranular stagnant fluid phase, which can be further subdivided into different levels, depending on the pore size distribution of the adsorbent particles. Adsorption isotherm models of the second category simplify the mathematical description of the adsorbent to a homogeneous phase.

The decision about the number of layers of complexity necessary to explain practical observations without incurring into data overfitting is one of the major challenges to scientists and engineers trying to model chromatography (or anything else, for that matter). This does not mean, though, that more complex adsorption isotherm models are not relevant (and sometimes vital) to interpret experimental data. However, there is, unfortunately, no ultimate rule for the proper degree of complexity that should ideally be applied for any given problem, much still being left to the researchers' discretion [81].

The work described in this dissertation only considers lumped adsorption isotherms, owing to the fact that detailed information about the environment inside the adsorbent particles is hard to obtain, and, often, can only be, at best, indirectly inferred. Furthermore, considering extra phases in the chromatographic system adds extra degrees of freedom to the interpretation of experimental data, which may confound experimental errors and actual physical phenomena occurring in the system.

Adsorption isotherms can also be classified as either favorable or unfavorable. When adsorption isotherms are favorable, i.e. their curve has a convex shape, the derivative of the adsorption isotherm function over increasing concentrations decreases, typically due to overloading of the adsorbent surface. Conversely, when adsorption isotherms are unfavorable, the derivative of the adsorption isotherm function over increasing concentrations increases, and the resulting adsorption isotherm curve is concave, which is often caused by a synergistic interaction between the adsorbed solutes. Furthermore, the course of adsorption isotherms might have inflexion points, which cause them to have both convex and concave regions. Depending on the mechanisms involved in the process, a series of multilayer adsorption steps might define the resulting curve [81].

The archetypical favorable adsorption model is the Langmuir isotherm (equation 2-2), which is based on a homogeneous surface saturation model. Since this model is thermodynamically consistent and approaches a straight line at low concentrations (a characteristic often experimentally observed in many adsorption systems) the Langmuir model has been very successful for describing experimental data.

$$q_i(c_i) = \frac{H_i c_i}{1 + k_i c_i} \quad 2-2$$

In order to extend the Langmuir approach to adsorbents with energetically heterogeneous adsorbents a second term can be added to generate the bi-Langmuir model [76]:

$$q_i(c_i) = \frac{H_{1,i} c_i}{1 + k_{1,i} c_i} + \frac{H_{2,i} c_i}{1 + k_{2,i} c_i} \quad 2-3$$

Other variations of the Langmuir isotherm, such as the Toth and the Hill isotherm models have been proposed to provide a better fit to experimental data [76]. These models add extra terms to the original function, which allows deviations from ideality to be better accounted for.

Different retention mechanisms, such as ion exchange, on the other hand, can be better described by considering its underlying retention mechanism in the adsorption model. Therefore, steric mass action models have been suggested as a way of incorporating the stoichiometric displacement of ions, which is caused by the adsorption of multivalent solutes, in the mass balance of the columns.

Further extending on the Langmuirian concept, the multicomponent Langmuir isotherm was suggested in order to model the competitive adsorption behavior often observed when different adsorbing solutes are simultaneously present in solution. While not thermodynamically consistent, this model has several free parameters, which result in good experimental data fitting and, thus, normally yields reliable results [76].

A different approach for modeling the adsorption behavior of multicomponent mixtures was suggested by Myers and Prausnitz. The ideal adsorbed solution (IAS) theory, as it came to be known, is based on the Gibbs' adsorption isotherm and provides better extrapolation predictions than most multicomponent isotherms. Its application, however, is often computationally intensive, typically requiring numerical integration steps.

2.3. Simulated Moving Bed technology

Single-column, liquid chromatography is the simplest implementation of the chromatographic principle of separation. It normally consists of an adsorbent bed packed inside a column, a pumping unit and detectors. The solutes are first introduced into the column as a mixture, which is followed by the pumping of solute-free solvent. The solutes are then collected sequentially in the column outlet, ideally, well separated from each other. After re-equilibration of the column with solute-free solvent, the complete procedure can be repeated.

Batch chromatography, as it is commonly referred to, does not make use of any the potential gains associated with continuous operation and complex process layout. Scale-up is, instead, usually achieved using larger columns and/or parallel processing units. It is, however, the method of choice for the separation of many commercially relevant products, such as insulin, paclitaxel, peptides, proteins, polyunsaturated fatty acid ethyl esters and steroids, to name just a few, as high profit margins reduce the potential relative gains from process layout optimization. Instead, much research effort has been directed at improving the adsorbent and solvent composition, mostly aiming at increased purity and easiness of implementation (two aspects highly valued in the fast changing and competitive pharmaceutical industry). Furthermore, significant improvements in batch chromatographic separation have been achieved through better hydraulic systems (pumps, valves and detectors, for example), new solvents and by reducing the adsorbent particle sizes [2].

Despite of its potentially universal applicability, chromatography is still often avoided as a preparative process in the chemical industry. With the exception of a few niche cases (for example, in the separation of the xylenes, C4 isomers and some monosaccharaides), concurring technologies, such as crystallization and distillation, are usually preferred for the separation of solutes. Depending on the case, there might be technical reasons why this is so, however, the main obstacle is often cost effectiveness. Successful chromatographic separations normally rely on high quality specialized adsorbents and large quantities of solvents, which can dramatically increase the overall cost of the production processes.

In order to reduce the consumption of both solvent and adsorbent, several continuous and countercurrent variants of the classical batch chromatographic process have been proposed [2, 11, 76, 81, 82]. By far, the most successful implementation thereof is, still, the Simulated Moving Bed (SMB, Figure 2-2 b)), first patented by D. Broughton et al. in 1961

for the separation of p-xylene from o-xylene, m-xylene and ethylbenzene in the Parex® process [1]. It is based on the principle of the true moving bed (TMB, Figure 2-2 a)), which is itself based on the concept of a continuous countercurrent extractor. The idea behind this process was to maximize the separation driving force by moving the adsorbent and the solvent in opposite directions. In practice, however, moving the adsorbent is not a trivial task, since it is usually composed of small particles and pumping it would cause back-mixing of the solvent, which would reduce resolution power. The solution found for this limitation was to divide the adsorbent bed into sections and instead of moving it in a continuous way, to move the column sections upstream in discrete intervals (or by periodically switching the valve connections downstream, effectively changing the relative positions of the adsorbent sections in the system) [83]. This conversion, however, resulted in the presence of transfer lines between the adsorbent sections, which added dead volumes to the system. Depending on the layout of the SMB unit, these dead volumes can significantly decrease the quality of the separation [84, 85].

The rotary valve patented by patented by D. Broughton [1] for the Sorbex® process family, for example, is not responsible for a significant portion of the system dead volumes (only about 3%). This valve, nevertheless, is optimized for a specific column configuration and, therefore, completely lacks flexibility. Most pilot and laboratory scale SMB units, on the other hand, use distributed valve systems that allow different zone and column configurations to be tested. These systems, however, introduce significant dead volumes to the transfer lines between the columns (around 10% of the total system dead volume, on average). Furthermore, the quality of pilot scale SMB separations can be even more adversely affected by solvent back-mixing if the transfer lines between the columns include check valves and pumps or have an asymmetric distribution [84, 85].

Due to the layout of the classical 4-zone SMB configuration, a single target solute can only be purified from a complex mixture, as the one depicted in Figure 2-1, if it is either the first (Figure 2-1 a)) or the last one (Figure 2-1 b)) to elute. This can be achieved by feeding it into an SMB system as the one shown in the Figure 2-2 b), between zones II and III. As long as the switching intervals and the solvent flow rates are set properly, the net flow of the strongest adsorbing solutes is in the direction of the adsorbent flow and the net flow of the weakest adsorbing solutes is in the direction of the solvent flow. The solvent flow rate in zone I must be set high enough that all strongly adsorbing solutes are eluted from the adsorbent and recovered in the extract port between zones I and II. The solvent flow in zone

IV must be set low enough that the weakly adsorbing solutes are completely removed from the solvent and recovered in the raffinate port between zones III and IV [13, 86].

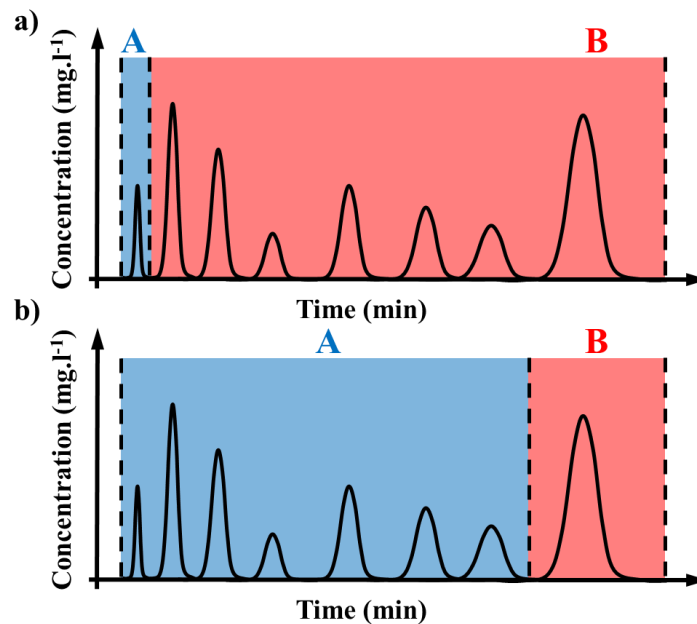


Figure 2-1 - Chromatogram describing a hypothetical mixture composed of 2 fractions. The fraction A has the highest affinity for the adsorbent and the fraction B is the one with the lowest affinity. A target single solute can only be purified using the classical 4-zone SMB configuration if it is either the first (a)) or the last one (b)) to elute.

In recent years, the application of the SMB concept has been mostly studied and applied for the separation of oil derivatives [54, 56, 61, 87-91], sugars [47, 48, 51, 92-102], biotechnological products [28, 63, 65, 66, 70, 79, 103-120], plant extracts [121-128] and chiral molecules [17, 31, 32, 34, 36-38, 129-131]. These separations are typically done using chromatography due to the need to separate solutes with very similar physicochemical properties. Furthermore they are also characterized by small differences in retention coefficients and/or large scale productions and/or expensive solvents, which are all best dealt with using SMB in comparison to batch chromatography.

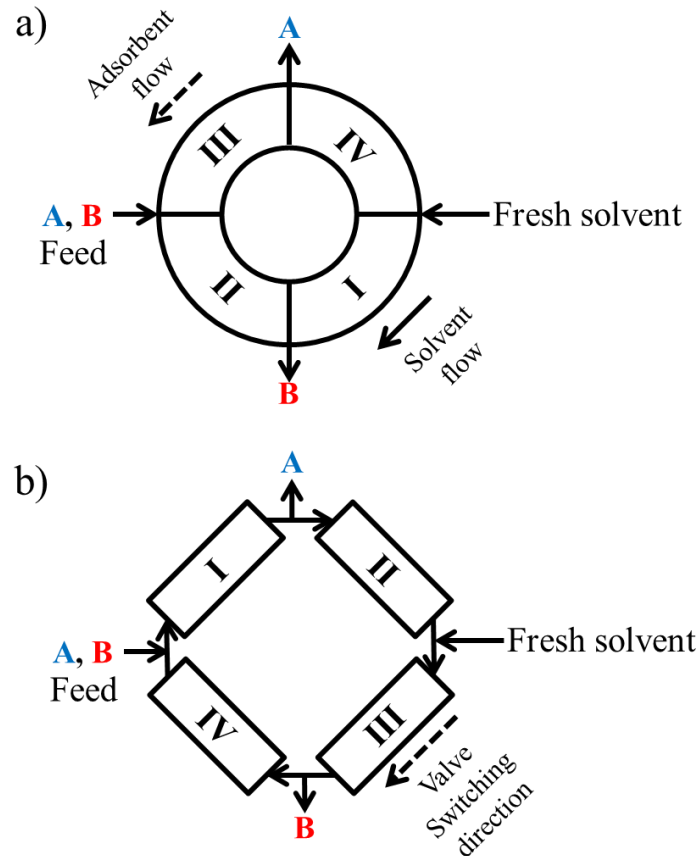


Figure 2-2 – a) True Moving Bed (TMB). The solid line indicates the direction of the solvent flow and the dashed line indicates the direction of the adsorbent flow. b) Simulated Moving Bed (SMB). The adsorbent flow is replaced by a stepwise switching of the inlet and outlet valves in the direction of the solvent flow. A mixture composed of the fractions A and B (as, for example, the mixture depicted in the chromatogram shown in Figure 2-1) is fed into the system between the zones II and III. As the most retained solute(s) (fraction B) move from the feed port in the direction of the adsorbent flow – counterclockwise – and the least retained solute(s) (fraction A) move in the direction of the solvent flow – clockwise – they can be continuously separated from each other and collected in the systems outlet ports as indicated.

2.4. Center-cut separations

A major shortcoming of the classical SMB is that the target solute being isolated must either be the one with the highest or the one with the lowest affinity for the adsorbent [5, 6, 132] (as exemplified in Figure 2-1). This restricts its use to more specific applications, usually simpler mixtures. In the most general case, however, the target solute is part of an intermediary eluting fraction, thus, in order to isolate it, the mixture has to be separated in three fractions, as depicted in Figure 2-3.

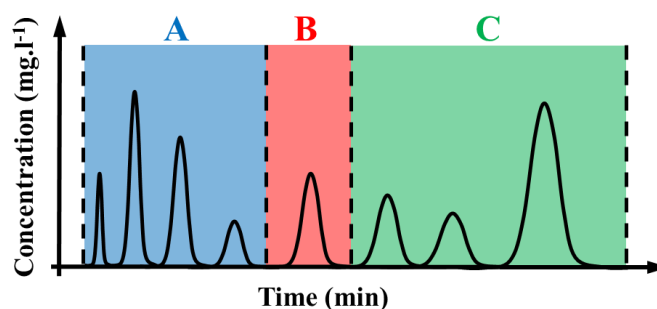


Figure 2-3 - Chromatogram describing a hypothetical mixture composed of 3 fractions. The fraction A is the first eluting one, the intermediary eluting fraction B is the target one and the fraction C is the last one to elute.

Many different SMB variants have been developed for the separation of ternary mixtures. Nicolaos et al. [3] compared different options of cascades with 4 and 5 zone SMB units in the frame of the equilibrium model (Figure 2-4), other authors compared different SMB cascade arrangements for multi-component fractionation [98, 125, 128, 133-136]. Other interesting configurations, such as the 5-zone SMB [3, 118, 137-141] (Figure 2-4 a)), and the 3 column intermittent SMB [142, 143] have also been proposed for ternary and pseudo-ternary separations. Furthermore, dynamic models and optimization algorithms were used for more realistic comparisons between different SMB column arrangements [5, 6, 9, 64, 125, 135, 144-146]. Additionally, many promising semi-continuous configurations, such as the JO (Japan Organo Corp.) or the MCSGP (Multicolumn Countercurrent Solvent Gradient Purification) processes have also been proposed and thoroughly analyzed for performing center-cut separations [9, 144, 145, 147-156].

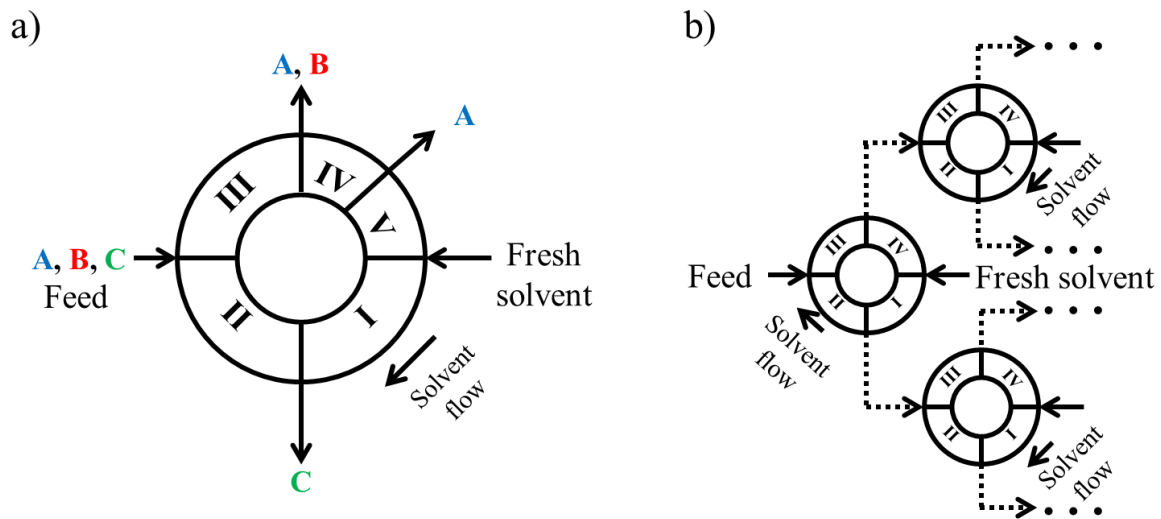


Figure 2-4 – Different Simulated Moving Bed variants proposed for center-cut separations. a) Simulated Moving Bed with 5 zones b) Cascades of independently operated 4-zone Simulated Moving Bed units [3]. These different SMB configurations are shown without discrete columns, since they can be implemented with any number of columns per zone.

2.5. Integrated 8-zone Simulated Moving Bed

Taking as an example the mixture composed of 3 fractions eluting in sequence A, B and C, as the one shown by the chromatogram depicted in the Figure 2-3, the most straightforward approach to employ the SMB process to isolate the intermediary eluting solute in fraction B is to use two independently operated 4-zone SMB units in sequence in such a way that the first unit separates the solute in the elution series that stands between the intermediary eluting solute B and one of the extremes of the elution series. The feed entering the second unit then contains the intermediary eluting solute in either the first or the last position of the elution series, making it possible to separate it from the other contaminations in the second unit. As shown in Figure 2-5, this can be achieved by recycling the extract fraction from the first unit to the second or, alternatively, as shown in Figure 2-6, by recycling the raffinate stream.

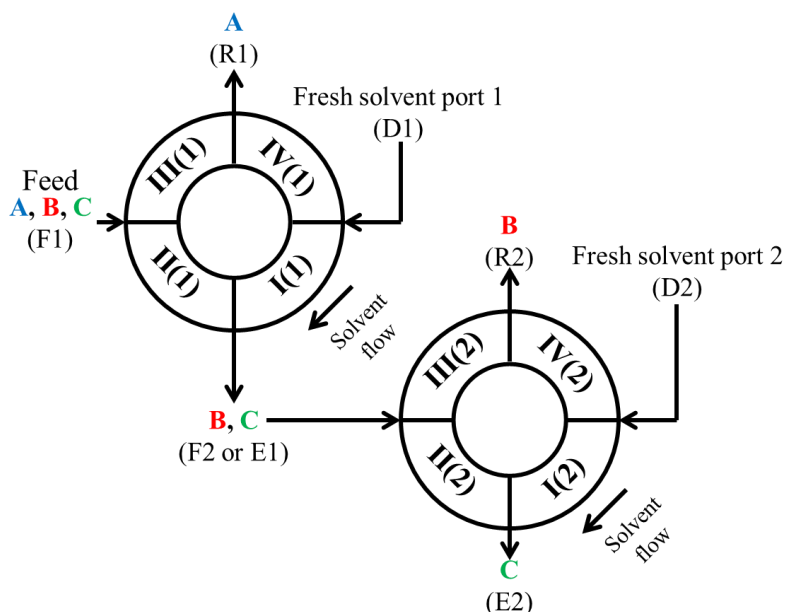


Figure 2-5 – Cascade of two independently operated 4-zone SMB units connected by the extract stream, shown without discrete columns, since they can be implemented with any number of columns per zone. The first unit splits the feed into two fractions, A and B+C, A being the solute (or series of solutes) with lower affinity to the adsorbent than the target solute (fraction B). The second unit splits the feed into two new fractions, B and C, C being the solute (or series of solutes) with higher affinity to the adsorbent than the target solute in fraction B.

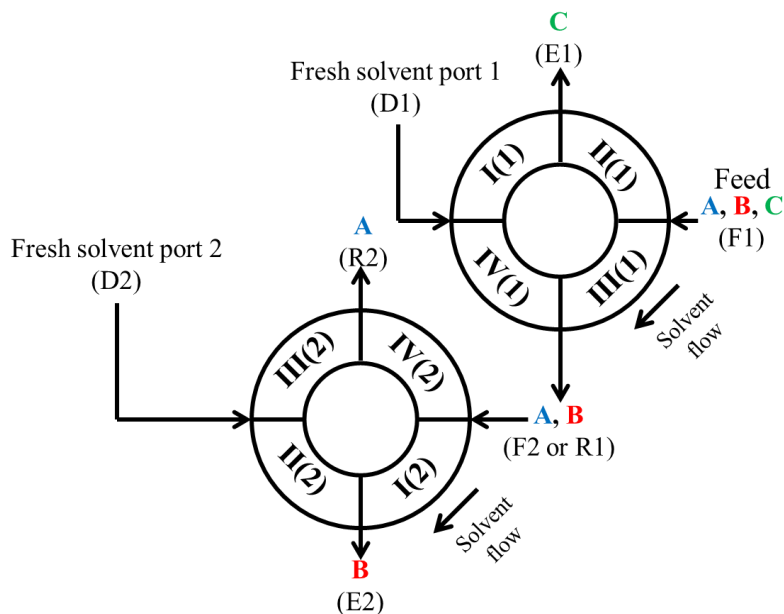


Figure 2-6 – Cascade of two independently operated 4-zone SMB units connected by the raffinate stream, shown without discrete columns, since they can be implemented with any number of columns per zone. The first unit splits the feed into two fractions, A+B and C, C being the solute (or series of solutes) with higher affinity to the adsorbent than the target solute (fraction B). The second unit splits the feed into two new fractions, A and B, A being the solute (or series of solutes) with lower affinity to the adsorbent than the target solute in fraction B.

One interesting variation of this process is to merge two 4-zone SMB units into a larger integrated SMB unit with 8-zones (shown in Figure 2-7 and Figure 2-8) and one switching interval, as originally proposed by A.S.T Chiang, in 1998 [4] and further studied by A. Nicolaos et al. [3], L. C. Kessler and A. Seidel-Morgenstern [7], J. Nowak et al. [8, 9], D. Kiwala et al. [10] and G. Agrawal et al. [5, 6].

There are two ways of doing this coupling, either by recycling the extract from the first subunit into the second subunit (Figure 2-7) or the raffinate (Figure 2-8). The difference being which side of the elution series (the least or the most retained solutes, respectively) is separated first [4, 9].

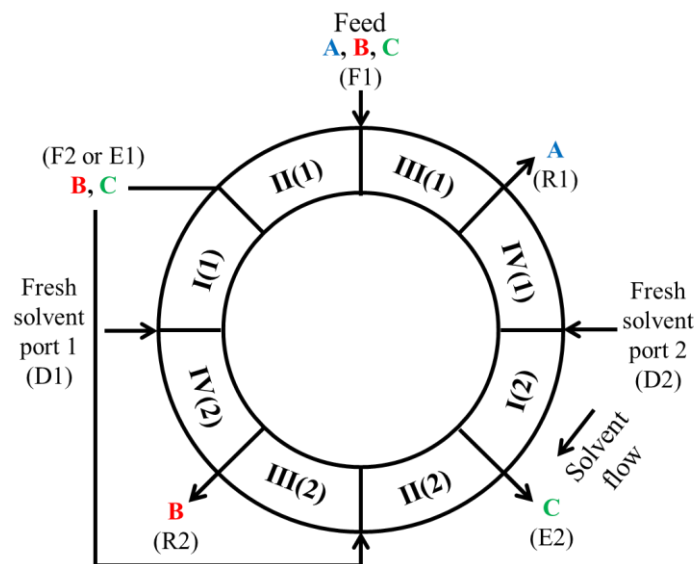


Figure 2-7 – Integrated 8-zone simulated moving bed chromatography with extract recycle, shown without discrete columns, since it can be implemented with any number of columns per zone. It works in an analogous way as a cascade of two SMBs connected by the extract stream of the first subunit, with the difference that after one complete cycle the column(s) in the position I(1) moves to position IV(2) instead of IV(1) and the column(s) in the position I(2) move to position IV(1) instead of IV(2).

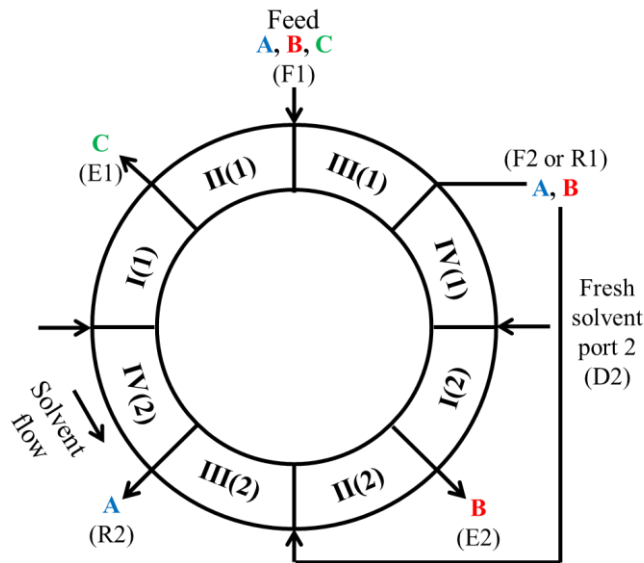


Figure 2-8 – Integrated 8-zone simulated moving bed chromatography with raffinate recycle, shown without discrete columns, since it can also be implemented with any number of columns per zone. In this system the stream recycled to the second subunit is the raffinate stream. This means that the most adsorbed fraction C is separated from the target solute (B) and from the least adsorbed solute(s) in fraction A before the separation of the fractions A and B takes place in the second subunit.

2.6. Summary

In this chapter, the basic principles of chromatographic separation and its core components were described. It was shown that differential retention is its main separation mechanism, which can often be mathematically described by adsorption isotherms. Furthermore, in order to circumvent the main limitation of preparative scale chromatography for industrial application, i.e. high costs, the concept of continuous countercurrent chromatography was introduced, with emphasis on the Simulated Moving Bed (SMB) concept, the main focus of this thesis. Finally, 8-zone SMB was introduced as an interesting option for allowing center-cut separations using SMB. Though this chapter is not, by any means, a comprehensive collection of all aspects of preparative chromatography (for that, the reader is directed to the references: [2, 76, 81]), it hopefully provided the necessary background for a fruitful discussion of this dissertation's results. In the next chapter, the mathematical modeling of chromatography will be explored in greater detail.

3. Mathematical modeling of chromatography

In the following sections, the mathematical modeling tools used in this dissertation are introduced. First, in section 3.1, the mathematical modeling of chromatography is described, starting with the transport dispersive model followed by the concept of geometric equivalence between TMB and SMB in section 3.2, which is used for the application of the classical triangle theory for estimating operating regions. Subsequently, a mixing cell model for simulating non-ideal (dispersed) flow in SMB (section 3.3) and in TMB (section 3.4) units is described. Lastly, in section 3.5, important economic concepts used in this dissertation are described, which are required for the discussion of the results later described in chapter 5.

3.1. Solute mass balance in a chromatographic column

As explained in section 2.1, a chromatographic separation is, at its core, composed of three elements: The adsorbing solutes being separated, the solvent that carries the solutes through the packed bed and an adsorbent having differential affinities for the solutes. As the solutes are carried across the chromatographic column, they are selectively slowed down by the adsorbent and migrate at different velocities, which eventually causes them to exit the system at different times, allowing them to be collected separately. The energy for the separation is constantly supplied by the pumping unit, which pushes the solvent against the pressure drop of the packed bed.

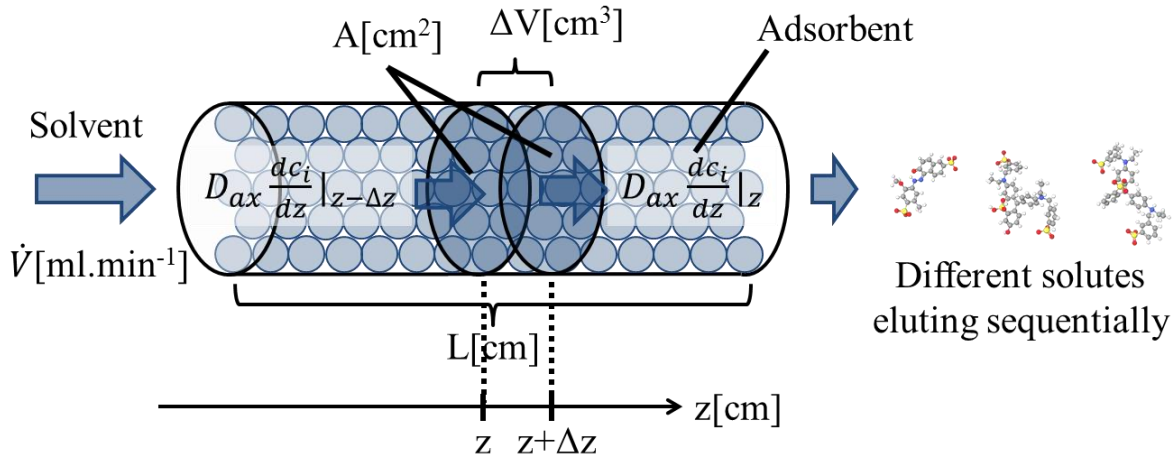


Figure 3-1 – Chromatographic separation abstracted to its core components. The solvent carries the different solutes in the positive direction of the z -axis at a flow rate \dot{V} through a column of cross sectional area A . As the adsorbent has different levels of affinity for the different solutes, their movement is slowed down to different velocities, which, over the length L , causes them to leave the packed bed at different times. By collecting them sequentially, they can be separated from each other. The energy for the separation is provided by the deceleration of the flow caused by the pressure drop of the adsorbent packed bed, which is supplied by the pumping system employed. A highlighted cylindrical section of the chromatographic column with volume ΔV is defined as a control volume for the deduction of the mass balance of the solutes.

If the temperature, specific solvent density and pressure of the chromatographic system shown in Figure 3-1 are constant, an initial mass balance to describe the system can be deduced.

Considering a column of volume V_c , homogeneously packed with arbitrarily small adsorbent particles occupying a fraction $(1 - \varepsilon)$ of the total column volume, a constant and unidimensional solvent flow \dot{V} in the positive direction of the z axis and a solute i , whose concentration (loading) in the adsorbent is described by $q_i(c_i)$, as a function of its concentration in the solvent c_i , the integral mass balance of the solute i in the liquid fraction of a cylindrical section of the chromatographic column with volume ΔV over a period of time Δt can be expressed as:

$$\varepsilon \Delta V [c_i(z, t + \Delta t) - c_i(z, t)] \quad 3-1$$

The integral convectonal mass flow of the solute i in this control volume with width Δz is given by:

$$\dot{V} c_i(z - \Delta z, t) \Delta t - \dot{V} c_i(z, t) \Delta t \quad 3-2$$

Due to the adsorption of part of the solute i in the adsorbent, the variation of its total amount in the control volume is added of:

$$-(1 - \varepsilon) \Delta V [q_i(z, t + \Delta t) - q_i(z, t)] \quad 3-3$$

The integral flow of the solute i over the time period Δt caused by the concentration gradient at the border areas of the control volume is described by Fick diffusion according to:

$$\varepsilon A \Delta t D_{ax} \frac{dc_i}{dz} \Big|_z - \varepsilon A \Delta t D_{ax} \frac{dc_i}{dz} \Big|_{z-\Delta z} \quad 3-4$$

where D_{ax} represents the diffusion coefficient of the solute i in the solvent considered, and A is the cross-sectional area of the column.

Since the volume of the cylindrical fraction ΔV is equivalent to the product of its width Δz and the cross-sectional area A of the column, the complete integral mass balance of the solute i in the solvent fraction of the control volume can be expressed as:

$$\frac{[c_i(z,t+\Delta t) - c_i(z,t)]}{\Delta t} = \frac{V[c_i(z-\Delta z,t) - c_i(z,t)]}{\varepsilon A \Delta z} - \frac{(1-\varepsilon)[q_i(z,t+\Delta t) - q_i(z,t)]}{\Delta t} + \frac{D_{ax}}{\Delta z} \left[\frac{dc_i}{dz} \Big|_z - \frac{dc_i}{dz} \Big|_{z-\Delta z} \right] \quad 3-5$$

By setting Δz and Δt arbitrarily small, the local mass balance of the vanishing cross-section of a chromatographic column can be expressed as:

$$\frac{\partial c_i}{\partial t} + \frac{(1-\varepsilon)}{\varepsilon} \frac{\partial q_i(c_i)}{\partial t} + \frac{v}{\varepsilon A} \frac{\partial c_i}{\partial z} = D_{ax} \frac{\partial^2 c_i}{\partial z^2} \quad 3-6$$

Since the solvent cannot flow through the solid adsorbent, the term $\frac{v}{\varepsilon A}$ is equivalent to its average linear velocity v in the packed bed. Therefore, equation 3-6 can be rewritten as:

$$\frac{\partial c_i}{\partial t} + \frac{(1-\varepsilon)}{\varepsilon} \frac{\partial q_i(c_i)}{\partial t} + v \frac{\partial c_i}{\partial z} = D_{ax} \frac{\partial^2 c_i}{\partial z^2} \quad 3-7$$

This equation, also known as the *equilibrium-dispersive model*, is one of the most widely applied mathematical descriptions of a chromatographic column due to its relative reliability for explaining concentration profiles in finely packed beds, where solute diffusivity can be simplified to a unidimensional process.

For efficient columns, the integration of equation 3-7 is normally performed using the boundary conditions derived by Danckwerts, which consider an inlet concentration profile described by $c_{in,i}(t)$, and no diffusion at the column outlet [76]:

$$\begin{cases} c_i(z=0, t) = c_{in,i}(t) \\ \frac{\partial c_i(z=L, t)}{\partial z} = 0 \end{cases} \quad 3-8$$

The function described by $c_{in,i}(t)$ can be set so as to best describe the concentration profile at the column inlet.

If the chromatographic column is infinitely efficient, i.e. Fick diffusion does not take place and the solvent movement can be well described by a plug flow, the diffusion coefficient D_{ax} tends to zero and equation 3-7 becomes:

$$\frac{\partial c_i}{\partial t} \left(1 + \frac{1-\varepsilon}{\varepsilon} q_i(c_i) \right) + v \frac{\partial c_i}{\partial z} = 0 \quad 3-9$$

which is also known as the *equilibrium model* of chromatography.

Considering a linear correlation between q_i and c_i , (as the adsorption Henry coefficient defined in equation 2-1) equation 3-9 can be simplified to:

$$\frac{\partial c_i}{\partial t} \left(1 + \frac{1-\varepsilon}{\varepsilon} H_i \right) + v \frac{\partial c_i}{\partial z} = 0 \quad 3-10$$

By rearranging the terms of equation 3-9, the convective velocity v_i of a solute i , as a function of the column's porosity ε , the solvent interstitial velocity v and the adsorption coefficient H_i in the direction of the axis z can be predicted using the method of characteristics proposed by Rhee et al. [157]:

$$v_i = \frac{dz}{dt} = \frac{\partial z}{\partial c_i} \frac{\partial c_i}{\partial t} = \frac{v}{\left(1 + \frac{1-\varepsilon}{\varepsilon} H_i \right)} \quad 3-11$$

Using equation 3-11, it is possible, for example, to visualize the migration profile of a rectangular pulse of solute with a linear adsorption isotherm inside a chromatographic column of length L , injected at the beginning of the column as shown in Figure 3-2.

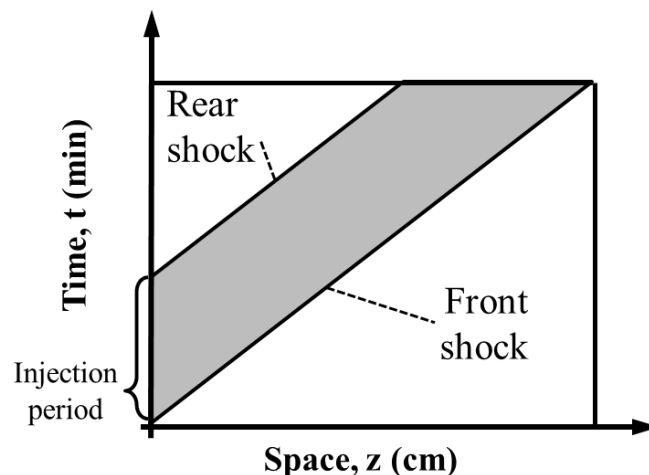


Figure 3-2 – Migration profile of a rectangular pulse injection of a linearly adsorbing solute inside a chromatographic column, which was injected at the beginning of the column during the time period indicated in the left side of the graph. The positions of the front and rear concentration shocks over time are indicated in the figure by the diagonal straight lines (characteristics). The area comprised between the two diagonal lines indicates positions in time and space which contain solute, while the white areas correspond to fully regenerated column sections.

Figure 3-2 shows the position of the front and rear concentration shocks of a solute injected at the beginning of a chromatographic column during the time period indicated. Since it was assumed that the adsorption of this solute is governed by a linear adsorption isotherm, the front and rear shocks are sharp and have a constant velocity (indicated in Figure 3-2 by the diagonal straight lines, also known as *characteristics*, representing the positions of both concentration shocks as a function of time). The shaded region between the two

characteristics represents the sections of the column, which contain solute-rich solvent. Conversely, the white areas show the sections of the column that do not contain solute.

3.2. “Triangle theory” based on the TMB analogy

Using the analogy with a TMB unit, Ruthven and Ching [158] developed an elegant technique to simplify the choice of proper flow rates for operating SMB systems. It assumes the *average* direction the solutes move in each zone of a SMB unit to be the same as those in a similar TMB analog. Extending on this work, Storti et al. [13, 159] demonstrated that a SMB and a TMB are geometrically equivalent if the *net* flow ratio between solvent and adsorbent in each zone k (designated by m_k) are equal, which is expressed by the following relation:

$$m_k = \frac{\dot{V}_{k,SMB}t^* - V_c\varepsilon}{V_c(1-\varepsilon)} = \frac{\dot{V}_{k,TMB}}{\dot{V}_s} \quad 3-12$$

where

$$\dot{V}_s = \frac{V_c(1-\varepsilon)}{t^*} \quad 3-13$$

Applying the method of characteristics proposed by Rhee et al. [157] for solving the equilibrium model, the migration velocity and shape of the solute concentration shocks can be analytically calculated as a function of the solvent velocity, the adsorption isotherms, and, the solutes' concentrations. If the process is operated in the linear range of the adsorption isotherms, the front migration velocity is independent of the concentration and is described as a function of the adsorption Henry coefficient, as explained in section 3.1, by equation 3-11.

If m_k is larger than the adsorption Henry coefficient of a solute, the net direction of its mass flow is the same as the solvent flow since the solute mass flow caused by solvent convection is higher than the adsorbed solute mass flow. Conversely, when the adsorption Henry coefficient is larger than m_k , the net direction of the solute mass flow is the same as the adsorbent flow. When m_k is larger than the adsorption Henry coefficient in one zone and lower in the neighboring one, the solute concentration shock can be effectively “pinched” between these two zones and collected there [133]. Choosing proper combinations of these solvent\adsorbent flow ratios in all zones makes it possible to separate solutes with different Henry coefficients by “pinching” their concentration fronts in different zone interfaces and collecting them pure in the outlet ports.

Considering the dimensionless flow rate m_k , defined in equation 3-12, and using the solution of the equilibrium model of batch chromatography (equation 3-10) explained in the

section 3.1 (equation 3-11), the velocity of the front or rear concentration shocks of a solute i with a linear adsorption isotherm given by the adsorption Henry coefficient H_i , in zone k ($v_{i,k}$), can be expressed as:

$$v_{i,k} = \frac{(Fm_k + 1) L}{(FH_i + 1) t^*} \quad 3-14$$

where L is the length of the column, F is the phase ratio of the column (given by $(1-\varepsilon) \div \varepsilon$), and t^* is the switching interval of the SMB process.

Furthermore, in a real SMB system (in opposition to a TMB system) there are dead volumes between the zones that are caused by the pumps, frits, connections, and, the tubing and valves between the columns [76]. Even in an optimized system, where the dead volumes are reduced, this is still unavoidable. If the dead volumes between the zones are constant and there is no severe back-mixing inside them (which might be a reasonable assumption for capillary tubes) it is possible to account for the delay in the break-through curves caused by the extra volume they must percolate using the method proposed by Katsuo et al. [160] and altered by Nowak et al. [8], which incorporates the extra retention time due to the dead volumes into the adsorption Henry coefficient according to:

$$H_i = H_{i,real} + \frac{V_{dead}}{V_c(1-\varepsilon)} \quad 3-15$$

In order not to cause any confusion with variable labeling, whenever H_i is mentioned in this work, it is the adsorption Henry coefficient adjusted to the dead volume that is meant.

This change of variables is only possible, because it is equivalent to increasing the void fraction of the chromatographic columns to include the dead volumes of the system. This correction is, however, only true as long as linear adsorption isotherms are considered [81].

Taking as an example the separation of the mixture shown in Figure 3-3 c) in an extract fraction (solutes c, d, and e) and in a raffinate fraction (solutes a and b) using a 4-zone SMB unit (Figure 3-3 b)), the dimensionless flow rate in zone I (m_I) has to be high enough to prevent zone IV from being contaminated by adsorbed solutes coming from zone I (in the counterclockwise direction). Therefore, m_I has to be larger than H_e , the largest adsorption Henry coefficient in the mixture. Moreover, in order to prevent carryover of solutes with the solvent recycle from zone IV to zone I, the dimensionless flow rate m_{IV} has to be smaller than the adsorption Henry coefficient of the least adsorbing solute a (H_a), as indicated in the set of inequations 3-16.

In order for the separation between the raffinate and extract fractions to be successful, the directions of the net solute mass flows in zones II and III have to be the ones shown in Figure 3-3 b). The net mass flow direction of the raffinate fraction (solutes a and b) is indicated by the continuous blue arrows, while that of the extract fraction (solutes c, d and e) is indicated by the red dashed lines. As shown in Figure 3-3 b), in zones III and II, the net mass flow directions of the two fractions are expected to have opposite directions, so that the mixture entering the 4-zone SMB unit between zones II and III can be effectively split into the extract and raffinate fractions. Therefore, the dimensionless flow rates m_{II} and m_{III} have to be smaller than H_c and larger than H_b . Since the mixture being separated is fed between zones II and III, the flow rate in zone III is always higher than the one in zone II, as shown by the set of inequations 3-16:

$$\begin{cases} m_I > H_e \\ m_{IV} < H_a \\ H_b < m_{II} < m_{III} < H_c \end{cases} \quad 3-16$$

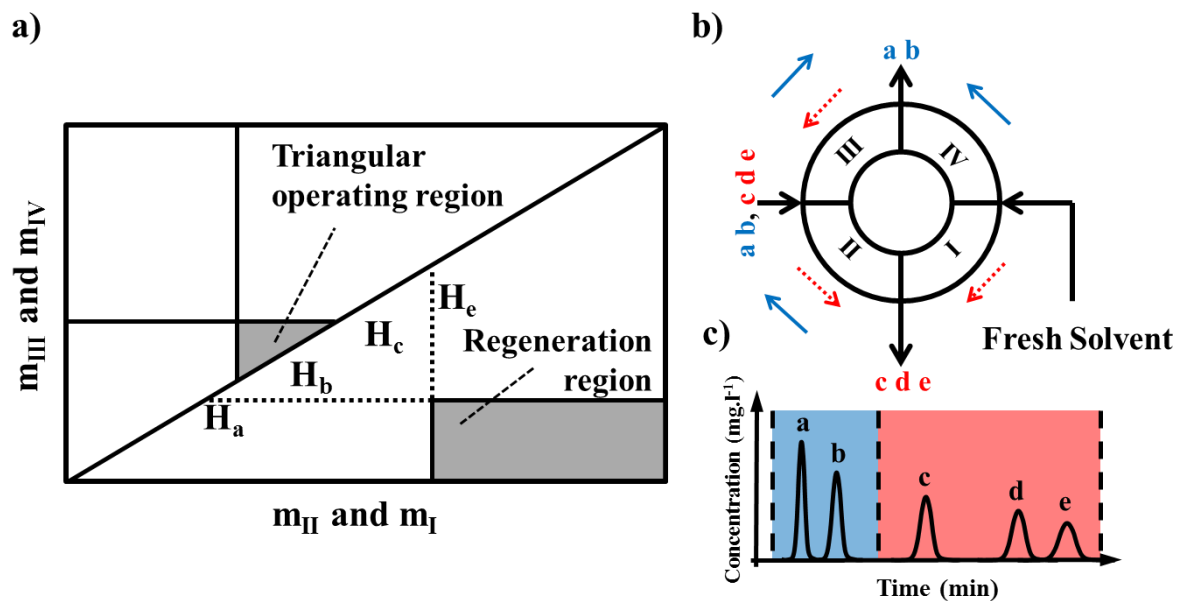


Figure 3-3 a) – Diagram showing the operating ranges of the dimensionless flow rates in a 4-zone SMB unit. The horizontal axis represents, simultaneously, the dimensionless flow rates m_{II} and m_I , while the vertical axis represents the dimensionless flow rates m_{III} and m_{IV} . The grey area indicated as triangular operating region, contains all of the combinations of the dimensionless flow rates m_{II} and m_{III} , which, together with the dimensionless flow rates m_I and m_{IV} inside the grey area indicated as regeneration region, allow a successful separation between the red and blue fractions. The feed contains the solutes a, b, c, d and e and is continuously separated in two streams: The extract fraction (indicated in the diagrams by the red color), which contains the solutes c, d and e; and the raffinate fraction (indicated by the blue color), which contains the solutes a and b. b) Diagram showing the 4-zone SMB, considered in this example. The expected direction of the net flow of both the extract (solutes c, d and e) and the raffinate (solutes a and b) fractions are indicated in each zone, respectively, by the red (dashed) and blue (solid) arrows. c) Chromatogram depicting the elution order of the five solutes (a, b, c, d and e) considered in this example. The two fractions are separated between the solutes b and c.

The diagram shown in Figure 3-3 a) is a practical way of conveying the operating parameter ranges that allow a successful separation between the extract and raffinate fractions using 4-zone SMB. As a result of the triangular shape of the operating region for linear adsorption isotherms, the application of this diagram for predicting dimensionless flow rate ranges for the SMB operation came to be known as triangle theory and was first suggested by Storti et al. in 1993 [13]. This methodology has since proven of great use for the operation of SMB units and has been extended to other variants, different adsorption isotherms and operating conditions [2, 3, 7-9, 12, 161-166].

3.3. Mixing cell model of 8-zone Simulated Moving Bed

High resolution chromatographic columns can be well described by a series of continuous-stirred tanks (CST) [2], as proposed by Martin and Synge [76, 167]. In these CSTs (referred to as cells, from here on) the solvent and adsorbent are in equilibrium and the solvent is pumped from cell to cell as shown in Figure 3-4.

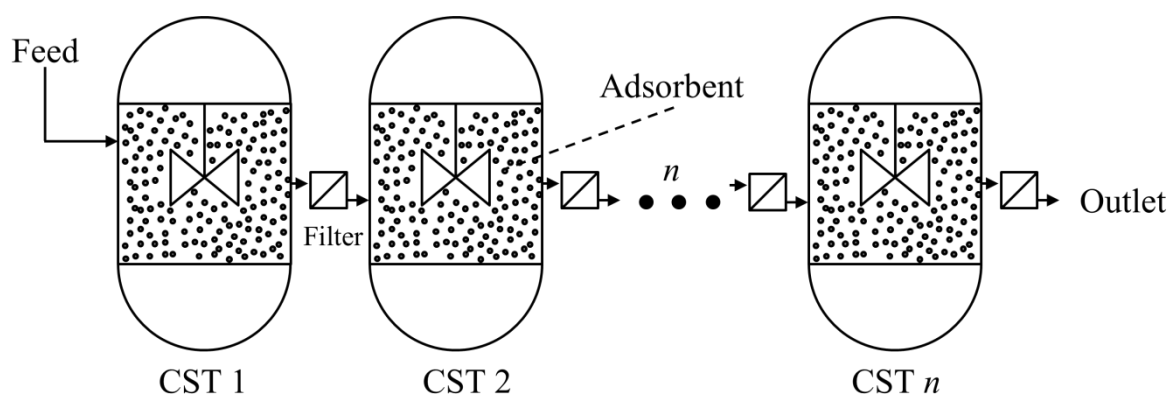


Figure 3-4 – Illustration of a cascade of continuously stirred-tanks (CST) where the adsorbent (grey spheres) and the solvent are in equilibrium. The solvent is pumped downstream (from the left to the right), while the adsorbent remains in its CST, being held back by the filters separating the cells. The separation of different solutes is achieved due to differences in the adsorption isotherms which causes the solutes to break through in the outlet of the cascade at different times.

For systems where adsorption kinetics as well as intra-particle diffusion occurs in a much smaller time-scale compared to other time-dependent processes such as back-mixing and convection, this *cell model* is a fairly good approximation of a chromatographic column [81, 167]. Furthermore, when the number of cells is over 100, there is very little difference between the predictions of the mixing cell model and the equilibrium-dispersive model

explained in section 3.1 [2]. There is, however, a very large difference between the integration time required for the mixing cell and the equilibrium-dispersive models, making the mixing cell model the preferred mathematical model for the validation of the equilibrium model predictions in this work, since, only highly efficient columns were considered.

According to the mixing cell model, the mass balance of one solute i in the j^{th} cell of a zone k can be described by:

$$\varepsilon \frac{V_c}{n} \frac{dc_{i,j}}{dt} + (1 - \varepsilon) \frac{V_c}{n} \frac{dq_{i,j}}{dt} = \dot{V}_k (c_{i,j-1} - c_{i,j}) \quad 3-17$$

When linear isotherms are considered this equation can be simplified to:

$$\varepsilon \frac{V_c}{n} \frac{dc_{i,j}}{dt} + (1 - \varepsilon) H_i \frac{V_c}{n} \frac{dc_{i,j}}{dt} = \dot{V}_k (c_{i,j-1} - c_{i,j}) \quad 3-18$$

where H_i represents the adsorption Henry coefficient of the solute i considered.

Rearranging the terms of 3-18 results in:

$$\frac{V_c}{n} \frac{dc_{i,j}}{dt} \left(1 + \frac{(1-\varepsilon)}{\varepsilon} H_i \right) = \dot{V}_k (c_{i,j-1} - c_{i,j}) \quad 3-19$$

which can be rearranged to:

$$\frac{dc_{i,j}}{dt} = \frac{\dot{V}_k n}{V_c (1 + \frac{(1-\varepsilon)}{\varepsilon} H_i)} (c_{i,j-1} - c_{i,j}) \quad 3-20$$

for $j = 1, n$

which can then be easily integrated.

In the equations above, the subscript j represents the position of the considered cell, starting at the feed port and following the direction of the solvent flow as shown in Figure 3-5. The volumetric solvent flow rate in zone k , given in $\text{l}\cdot\text{min}^{-1}$, is represented by \dot{V}_k , c_j is the concentration of the solute in any given cell, in $\text{mg}\cdot\text{l}^{-1}$, and, the chromatographic column volume is given by V_c , in l . The total number of cells in the columns in each zone is given by n .

It is possible to calculate internal concentration profiles of the 8-zone SMB by integrating equation 3-17 for each of the n cells and periodically changing the boundary conditions of the columns after each cycle [9]. In this dissertation, this was done using ChromWorks™.

For accurately modeling the SMB process, the differential equations of the cells where solvent enters the system (often called nodes) must be modified to take into account either dilution caused by fresh solvent entering the system or concentration caused by injection of the feed stream.

For the 8-zone SMB with extract recycle (see Figure 3-5 and Figure 2-7), the differential equations representing the nodes are:

$$\frac{dc_{i,1}}{dt} = \frac{n\dot{V}_{III(1)}}{V_c\left(1+\frac{(1-\varepsilon)}{\varepsilon}H_i\right)} \left(\frac{1}{\dot{V}_{III(1)}} (\dot{V}_{II(1)}c_{i,8n} + \dot{V}_{F2}c_{i,F2}) - c_{i,1} \right) \quad 3-21$$

$$\frac{dc_{i,2n+1}}{dt} = \frac{n\dot{V}_{I(2)}}{V_c\left(1+\frac{(1-\varepsilon)}{\varepsilon}H_i\right)} \left(\frac{\dot{V}_{IV(1)}}{\dot{V}_{I(2)}} c_{i,2n} - c_{i,2n+1} \right) \quad 3-22$$

$$\frac{dc_{i,4n+1}}{dt} = \frac{n\dot{V}_{III(2)}}{V_c\left(1+\frac{(1-\varepsilon)}{\varepsilon}H_i\right)} \left(\frac{1}{\dot{V}_{III(2)}} (\dot{V}_{II(2)}c_{i,4n} + \dot{V}_{F1}c_{i,7n+1}) - c_{i,4n+1} \right) \quad 3-23$$

$$\frac{dc_{i,6n+1}}{dt} = \frac{n\dot{V}_{I(1)}}{V_c\left(1+\frac{(1-\varepsilon)}{\varepsilon}H_i\right)} \left(\frac{\dot{V}_{IV(2)}}{\dot{V}_{I(1)}} c_{i,6n} - c_{i,6n+1} \right) \quad 3-24$$

For the 8-zone SMB with raffinate recycle (Figure 3-5 and Figure 2-8) these equations are:

$$\frac{dc_{i,1}}{dt} = \frac{n\dot{V}_{III(1)}}{V_c\left(1+\frac{(1-\varepsilon)}{\varepsilon}H_i\right)} \left(\frac{1}{\dot{V}_{III(1)}} (\dot{V}_{II(1)}c_{i,8n} + \dot{V}_{F2}c_{i,5n+1}) - c_{i,1} \right) \quad 3-25$$

$$\frac{dc_{i,2n+1}}{dt} = \frac{n\dot{V}_{I(2)}}{V_c\left(1+\frac{(1-\varepsilon)}{\varepsilon}H_i\right)} \left(\frac{\dot{V}_{IV(1)}}{\dot{V}_{I(2)}} c_{i,2n} - c_{i,2n+1} \right) \quad 3-26$$

$$\frac{dc_{i,4n+1}}{dt} = \frac{n\dot{V}_{III(2)}}{V_c\left(1+\frac{(1-\varepsilon)}{\varepsilon}H_i\right)} \left(\frac{1}{\dot{V}_{III(2)}} (\dot{V}_{II(2)}c_{i,4n} + \dot{V}_{F1}c_{i,F1}) - c_{i,4n+1} \right) \quad 3-27$$

$$\frac{dc_{i,6n+1}}{dt} = \frac{n\dot{V}_{I(1)}}{V_c\left(1+\frac{(1-\varepsilon)}{\varepsilon}H_i\right)} \left(\frac{\dot{V}_{IV(2)}}{\dot{V}_{I(1)}} c_{i,6n} - c_{i,6n+1} \right) \quad 3-28$$

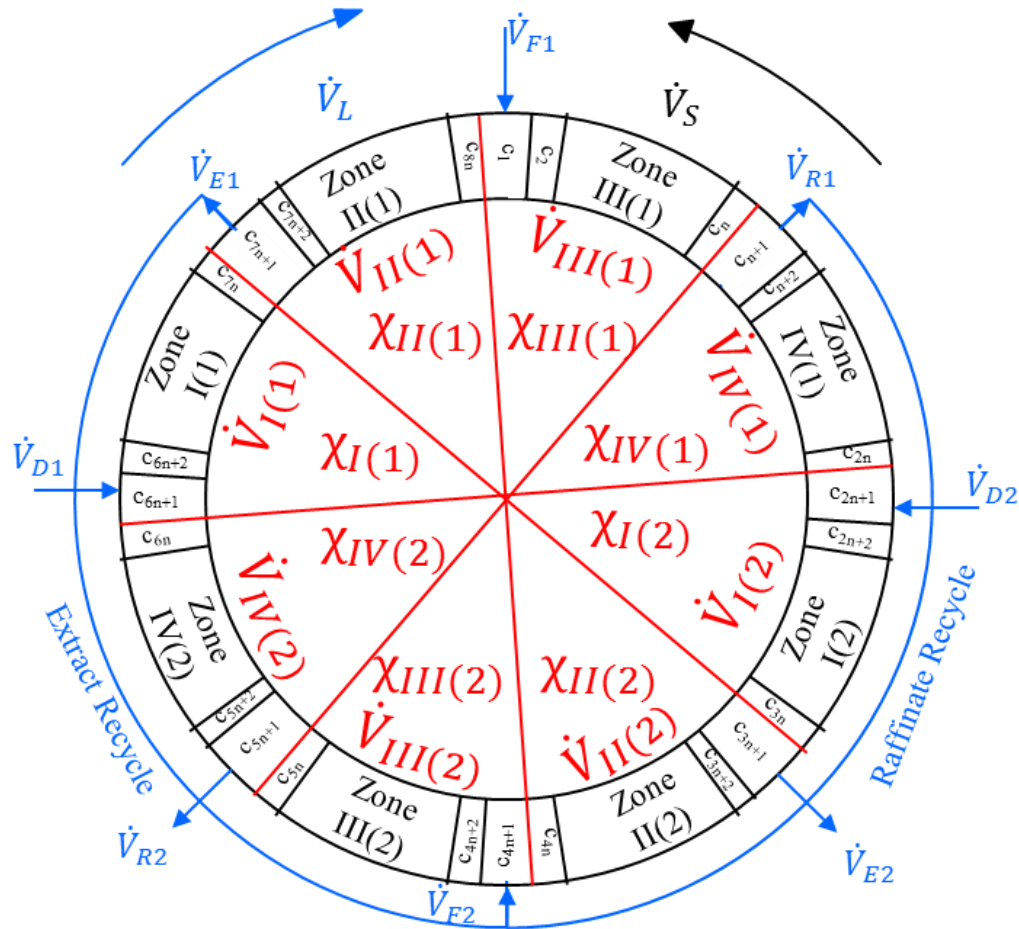


Figure 3-5 – 8-zone TMB or SMB as described by the mixing cell model. The red lines define zones with different flow regimes. The direction of the adsorbent (i.e. of the columns) movement is indicated by the counterclockwise arrow. The blue arrows indicate the direction of the solvent movement for the extract and for the raffinate recycles.

After a certain number of cycles, this system reaches a so-called cyclic steady state [10]. This cyclic steady state is characterized by a repetition of the concentration profiles in the outlet ports during each cycle [83, 168].

3.4. Mixing cell model of 8-zone True Moving Bed

A True Moving Bed (TMB) can also be modeled as a series of perfectly mixed cells. In each of the cells the adsorbent is in equilibrium with the solvent, with the solutes partly adsorbed onto the surface of the adsorbent and partly dissolved in the solvent. The continuous, linear, and, one-dimensional countercurrent flow of the adsorbent carries the adsorbed solutes upstream and the solvent flow carries the dissolved solutes downstream. When adsorption isotherms of the solutes are linear the mass balance of one solute in the j^{th} cell in the k^{th} zone can be expressed as [169]:

$$\dot{V}_k c_{j-1} - \dot{V}_s H_k c_j - \dot{V}_k c_j + \dot{V}_s H_k c_{j+1} = \pm \dot{V}_{out} c_j \quad 3-29$$

In this equation, \dot{V}_s is the volumetric flow of adsorbent in $\text{l} \cdot \text{min}^{-1}$.

The flow rate of the system outlet, \dot{V}_{out} , has positive sign if the flow leaves the system, negative if it enters it, and, zero if the considered cell does not have an outlet connection. The resulting mass balance can be described by:

$$\chi_k c_{j-1} - (1 + \chi_k) c_j + c_{j+1} = 0, \text{ where } \chi_k = \frac{\dot{V}_k}{\dot{V}_s H_k} \quad 3-30$$

for $j = 1, n$

where n represents the number of cells per zone, which can be on the range of thousands, resulting in large and sparse systems of equations, which, in this work, are solved using the LDU (lower upper decomposition) using MATLAB R2015b.

Equation 3-30 is valid for every cell in the 8-zone TMB with the exception of the inlet ports, outlet ports, and, their neighboring cells that need the extra equations shown in Table 3-1 to be properly described.

Extract recycle 8-zone TMB	Raffinate recycle 8-zone TMB
$-(1 + \chi_{III(1)})c_1 + c_2 + \chi_{II(1)}c_{8n} = -\chi_{F1}c_{F1}$	$-(1 + \chi_{III(1)})c_1 + c_2 + \chi_{II(1)}c_{8n} = -\chi_{F1}c_{F1}$
$\chi_{III(1)}c_n - (1 + \chi_{IV(1)} + \chi_{R1})c_{n+1} + c_{n+2} = 0$	$\chi_{III(1)}c_n - (1 + \chi_{IV(1)} + \chi_{R1})c_{n+1} + c_{n+2} = 0$
$\chi_{IV(1)}c_{2n-1} - (1 + \chi_{IV(1)})c_{2n} + c_{2n+1} = 0$	$\chi_{IV(1)}c_{2n-1} - (1 + \chi_{IV(1)})c_{2n} + c_{2n+1} = 0$
$\chi_{IV(1)}c_{2n} - (1 + \chi_{I(2)})c_{2n+1} + c_{2n+2} = 0$	$\chi_{IV(1)}c_{2n} - (1 + \chi_{I(2)})c_{2n+1} + c_{2n+2} = 0$
$\chi_{I(2)}c_{3n} - (1 + \chi_{II(2)} + \chi_{E2})c_{3n+1} + c_{3n+2} = 0$	$\chi_{I(2)}c_{3n} - (1 + \chi_{II(2)} + \chi_{E2})c_{3n+1} + c_{3n+2} = 0$
$\chi_{II(2)}c_{4n-1} - (1 + \chi_{II(2)})c_{4n} + c_{4n+1} = 0$	$\chi_{II(2)}c_{4n-1} - (1 + \chi_{II(2)})c_{4n} + c_{4n+1} = 0$
$\chi_{II(2)}c_{4n} - (1 + \chi_{III(2)})c_{4n+1} + c_{4n+2} + \chi_{F2}c_{7n+1} = 0$	$\chi_{II(2)}c_{4n} - (1 + \chi_{III(2)})c_{4n+1} + c_{4n+2} + \chi_{F2}c_{7n+1} = 0$
$\chi_{III(2)}c_{5n} - (1 + \chi_{IV(2)} + \chi_{R2})c_{5n+1} + c_{5n+2} = 0$	$\chi_{III(2)}c_{5n} - (1 + \chi_{IV(2)} + \chi_{R2})c_{5n+1} + c_{5n+2} = 0$
$\chi_{IV(2)}c_{6n-1} - (1 + \chi_{IV(2)})c_{6n} + c_{6n+1} = 0$	$\chi_{IV(2)}c_{6n-1} - (1 + \chi_{IV(2)})c_{6n} + c_{6n+1} = 0$
$\chi_{IV(2)}c_{6n} - (1 + \chi_{I(1)})c_{6n+1} + c_{6n+2} = 0$	$\chi_{IV(2)}c_{6n} - (1 + \chi_{I(1)})c_{6n+1} + c_{6n+2} = 0$
$\chi_{I(1)}c_{7n} - (1 + \chi_{II(2)} + \chi_{E1})c_{7n+1} + c_{7n+2} = 0$	$\chi_{I(1)}c_{7n} - (1 + \chi_{II(2)} + \chi_{E1})c_{7n+1} + c_{7n+2} = 0$
$\chi_{II(1)}c_{8n-1} - (1 + \chi_{II(1)})c_{8n} + c_1 = 0$	$\chi_{II(1)}c_{8n-1} - (1 + \chi_{II(1)})c_{8n} + c_1 = 0$

Table 3-1 – Cell model mass balance equations for the nodes of an 8-zone True Moving Bed (TMB) with either extract (left side, Figure 3-5) and raffinate (right side, Figure 3-5) recycle.

The subscript represents the position of the cell following the solvent flow direction starting at the feed port, with 1 being the cell that receives crude feed.

Since, depending on the number of cells, the system of equations describing the mixing cell model of TMB can become very large, an efficient solution algorithm is necessary to reduce the calculation times required. If the adsorption isotherms considered are

linear, the algorithm developed by A. Kremser [170] to countercurrent extraction processes and further extended to TMB by D. Beltscheva [169] and C. Kessler [7, 162] can be used to reduce the size of this system of equations to the set of just 28 equations shown in Table 3-2. In this system, only the cells shown in Figure 3-6 are explicitly considered in the actual computation. The Kremser's recursive solution is mathematically equivalent to the solution of the original system of equations using the LDU (as later shown in Figure 5-6 b)), due to the fact that there is no approximation involved. The Kremser's recursive solution, however, simplifies the calculation process by focusing solely on the concentrations in the outlet and inlet ports and its direct neighboring cells, by solving sequential similar equations recursively.

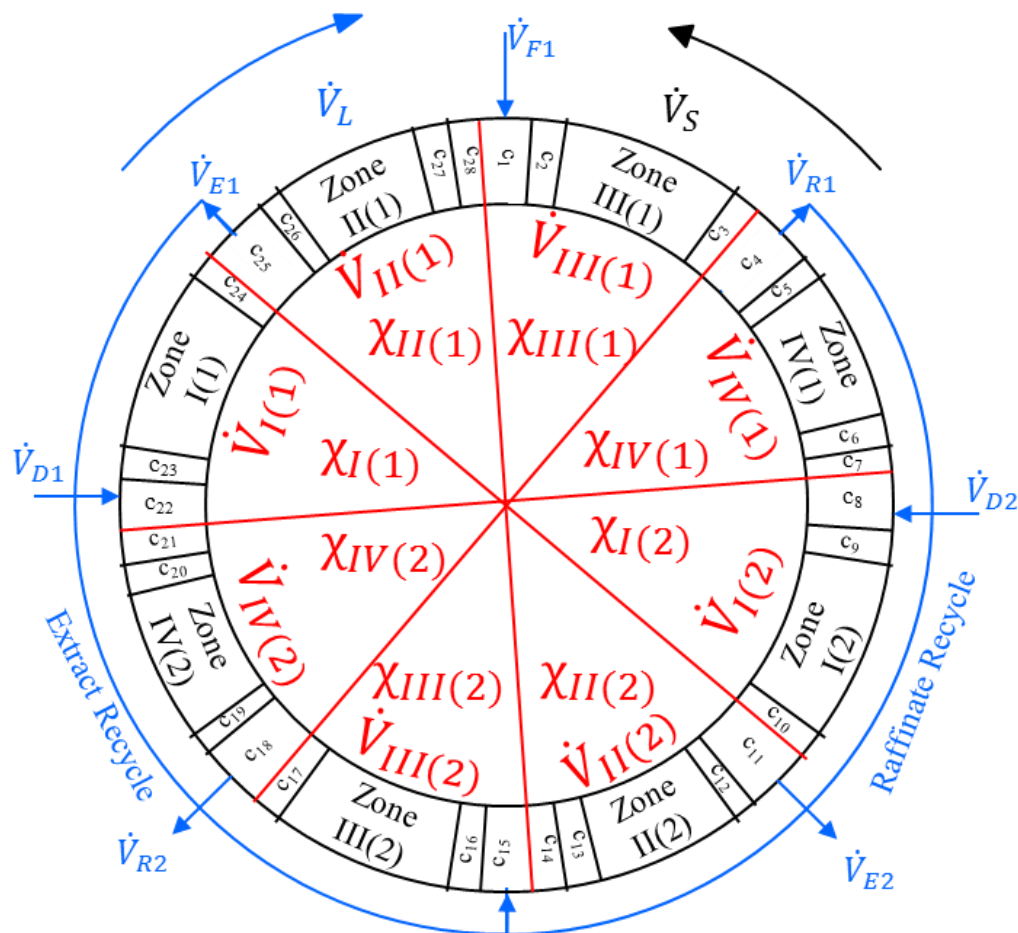


Figure 3-6 – 8-zone TMB as described by the mixing cell model using the Kremser's recursive solution. The direction of the adsorbent (and therefore of the columns) movement is indicated by the counterclockwise arrow. The blue arrows indicate the direction of the solvent movement for the extract and for the raffinate recycles.

Extract recycle 8-zone TMB	Raffinate recycle 8-zone TMB
$\left\{ \begin{array}{l} -(1 + \chi_{III(1)})c_1 + c_2 + \chi_{II(1)}c_{28} = -\chi_{F1}c_{F1} \\ (\gamma_{III(1)} - 1)c_1 - \gamma_{III(1)}c_2 + c_3 = 0 \\ c_2 - \eta_{III(1)}c_3 + (\eta_{III(1)} - 1)c_4 = 0 \\ \chi_{III(1)}c_3 - (1 + \chi_{IV(1)} + \chi_{R1})c_4 + c_5 = 0 \\ (\gamma_{IV(1)} - 1)c_4 - \gamma_{IV(1)}c_5 + c_6 = 0 \\ c_5 - \eta_{IV(1)}c_6 + (\eta_{IV(1)} - 1)c_7 = 0 \\ \chi_{IV(1)}c_6 - (1 + \chi_{IV(1)})c_7 + c_8 = 0 \\ \chi_{IV(1)}c_7 - (1 + \chi_{I(2)})c_8 + c_9 = 0 \\ (\gamma_{I(2)} - 1)c_8 - \gamma_{I(2)}c_9 + c_{10} = 0 \\ c_9 - \eta_{I(2)}c_{10} + (\eta_{I(2)} - 1)c_{11} = 0 \\ \chi_{I(2)}c_{10} - (1 + \chi_{II(2)} + \chi_{E2})c_{11} + c_{12} = 0 \\ (\gamma_{II(2)} - 1)c_{11} - \gamma_{II(2)}c_{12} + c_{13} = 0 \\ c_{12} - \eta_{II(2)}c_{13} + (\eta_{II(2)} - 1)c_{14} = 0 \\ \chi_{II(2)}c_{13} - (1 + \chi_{II(2)})c_{14} + c_{15} = 0 \\ \chi_{II(2)}c_{14} - (1 + \chi_{III(2)})c_{15} + c_{16} + \chi_{F2}c_{25} = 0 \\ (\gamma_{III(2)} - 1)c_{15} - \gamma_{III(2)}c_{16} + c_{17} = 0 \\ c_{16} - \eta_{III(2)}c_{17} + (\eta_{III(2)} - 1)c_{18} = 0 \\ \chi_{III(2)}c_{17} - (1 + \chi_{IV(2)} + \chi_{R2})c_{18} + c_{19} = 0 \\ (\gamma_{IV(2)} - 1)c_{18} - \gamma_{IV(2)}c_{19} + c_{20} = 0 \\ c_{19} - \eta_{IV(2)}c_{20} + (\eta_{IV(2)} - 1)c_{21} = 0 \\ \chi_{IV(2)}c_{20} - (1 + \chi_{IV(2)})c_{21} + c_{22} = 0 \\ \chi_{IV(2)}c_{21} - (1 + \chi_{I(1)})c_{22} + c_{23} = 0 \\ (\gamma_{I(1)} - 1)c_{22} - \gamma_{I(1)}c_{23} + c_{24} = 0 \\ c_{23} - \eta_{I(1)}c_{24} + (\eta_{I(1)} - 1)c_{25} = 0 \\ \chi_{I(1)}c_{24} - (1 + \chi_{II(1)} + \chi_{E1})c_{25} + c_{26} = 0 \\ (\gamma_{II(1)} - 1)c_{25} - \gamma_{II(1)}c_{26} + c_{27} = 0 \\ c_{26} - \eta_{II(1)}c_{27} + (\eta_{II(1)} - 1)c_{28} = 0 \\ c_1 + \chi_{II(1)}c_{27} - (1 + \chi_{II(1)})c_{28} = 0 \end{array} \right.$	$\left\{ \begin{array}{l} -(1 + \chi_{III(1)})c_1 + c_2 + \chi_{II(1)}c_{28} = -\chi_{F1}c_{F1} \\ (\gamma_{III(1)} - 1)c_1 - \gamma_{III(1)}c_2 + c_3 = 0 \\ c_2 - \eta_{III(1)}c_3 + (\eta_{III(1)} - 1)c_4 = 0 \\ \chi_{III(1)}c_3 - (1 + \chi_{IV(1)} + \chi_{R1})c_4 + c_5 = 0 \\ (\gamma_{IV(1)} - 1)c_4 - \gamma_{IV(1)}c_5 + c_6 = 0 \\ c_5 - \eta_{IV(1)}c_6 + (\eta_{IV(1)} - 1)c_7 = 0 \\ \chi_{IV(1)}c_6 - (1 + \chi_{IV(1)})c_7 + c_8 = 0 \\ \chi_{IV(1)}c_7 - (1 + \chi_{I(2)})c_8 + c_9 = 0 \\ (\gamma_{I(2)} - 1)c_8 - \gamma_{I(2)}c_9 + c_{10} = 0 \\ c_9 - \eta_{I(2)}c_{10} + (\eta_{I(2)} - 1)c_{11} = 0 \\ \chi_{I(2)}c_{10} - (1 + \chi_{II(2)} + \chi_{E2})c_{11} + c_{12} = 0 \\ (\gamma_{II(2)} - 1)c_{11} - \gamma_{II(2)}c_{12} + c_{13} = 0 \\ c_{12} - \eta_{II(2)}c_{13} + (\eta_{II(2)} - 1)c_{14} = 0 \\ \chi_{II(2)}c_{13} - (1 + \chi_{II(2)})c_{14} + c_{15} = 0 \\ \chi_{II(2)}c_{14} - (1 + \chi_{III(2)})c_{15} + c_{16} + \chi_{F2}c_4 = 0 \\ (\gamma_{III(2)} - 1)c_{15} - \gamma_{III(2)}c_{16} + c_{17} = 0 \\ c_{16} - \eta_{III(2)}c_{17} + (\eta_{III(2)} - 1)c_{18} = 0 \\ \chi_{III(2)}c_{17} - (1 + \chi_{IV(2)} + \chi_{R2})c_{18} + c_{19} = 0 \\ (\gamma_{IV(2)} - 1)c_{18} - \gamma_{IV(2)}c_{19} + c_{20} = 0 \\ c_{19} - \eta_{IV(2)}c_{20} + (\eta_{IV(2)} - 1)c_{21} = 0 \\ \chi_{IV(2)}c_{20} - (1 + \chi_{IV(2)})c_{21} + c_{22} = 0 \\ \chi_{IV(2)}c_{21} - (1 + \chi_{I(1)})c_{22} + c_{23} = 0 \\ (\gamma_{I(1)} - 1)c_{22} - \gamma_{I(1)}c_{23} + c_{24} = 0 \\ c_{23} - \eta_{I(1)}c_{24} + (\eta_{I(1)} - 1)c_{25} = 0 \\ \chi_{I(1)}c_{24} - (1 + \chi_{II(1)} + \chi_{E1})c_{25} + c_{26} = 0 \\ (\gamma_{II(1)} - 1)c_{25} - \gamma_{II(1)}c_{26} + c_{27} = 0 \\ c_{26} - \eta_{II(1)}c_{27} + (\eta_{II(1)} - 1)c_{28} = 0 \\ c_1 + \chi_{II(1)}c_{27} - (1 + \chi_{II(1)})c_{28} = 0 \end{array} \right.$

Table 3-2 – Cell model mass balance equations for the 8-zone True Moving Bed (TMB) with either extract (left side) or raffinate (right side) recycle simplified by the recursive solution developed by A. Kremser [170] and further extended by D. Beltscheva [169] and C. Kessler [7, 162] to TMB with linear adsorption isotherms to a set of just 28 linear equations with 28 unknown variables.

$$\gamma_k = \frac{\chi_k^{n-1}-1}{\chi_k^{-1}}, \text{ for } k = \text{I(1), III(1), I(2), and, III(2)} \quad 3-31$$

$$\eta_k = \frac{\chi_k^{-n+1}-1}{\chi_k^{-1}-1}, \text{ for } k = \text{I(1), III(1), I(2), and, III(2)} \quad 3-32$$

$$\gamma_k = \frac{\chi_k^{n-2}-1}{\chi_k^{-1}}, \text{ for } k = \text{II(1), IV(1), II(2), and, IV(2)} \quad 3-33$$

$$\eta_k = \frac{\chi_k^{-n+2}-1}{\chi_k^{-1}-1}, \text{ for } k = \text{II(1), IV(1), II(2), and, IV(2)} \quad 3-34$$

The ratio between the adsorption Henry coefficients (defined in equation 2-1) of two solutes a and b is given by the selectivity factor:

$$\alpha_{a,b} = \frac{H_b}{H_a} \quad 3-35$$

The use of the Kremser's recursive solution significantly reduces the computational costs of the solution of the mass balances [92, 162, 169, 170]. This can be seen by evaluating the time used by a standard personal computer to solve the system of equations as a function of the number of cells per zone. As shown in Figure 3-7. The resolution time using the Kremser's recursive solution is approximately independent from the number of cells, whereas the time needed for solving the system of equations using LDU grows in direct proportion to it.

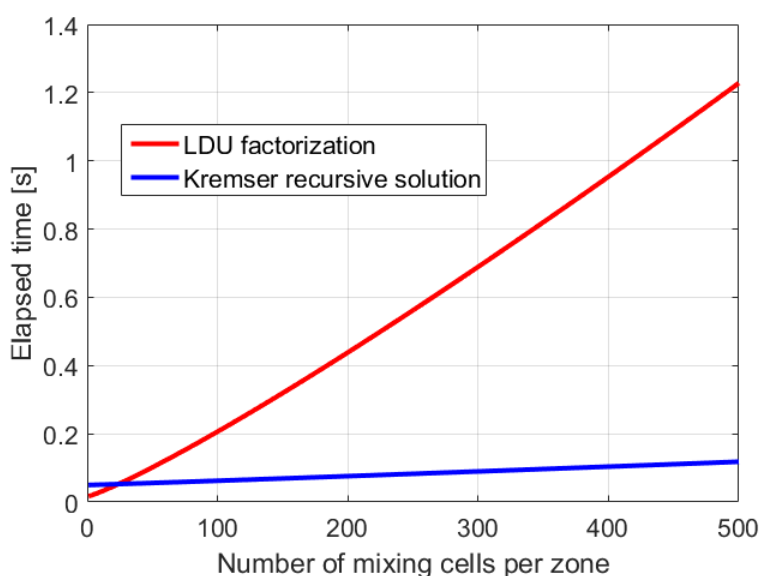


Figure 3-7 – Comparison of the computing time of the solution using LDU and using the Kremser's recursive solution plotted as a function of the number of cells per zone.

3.5. Performance evaluation of continuous chromatography

Among the several different possibilities for assembling and improving chromatographic separations, there are, on one side, the physicochemical aspects, such as the composition of the solvent and adsorbent, temperature, pressure and many others. On the other side, there is the process layout choice, which includes questions about the operation, such as: continuous vs. batch operation; column dimensions; flow rates; system configuration, etc. The optimization of chromatographic separations is seldom a matter of improving only one of these aspects, instead, all of them have to be considered together in order to increase the profitability of the whole process. An optimization workflow can be roughly divided in:

1. Identification of the controllable variables;
2. Choice of the performance indicators;
3. Identification of constraints;
4. Choice of the optimization strategies.

1. Identification of the controllable variables

Considering the 8-zone SMB system studied in this dissertation (later described in the section 7.2.5), only solvent flow rates, switching times (i.e. the solid flow rate) and the configuration (extract or raffinate recycle) can be controlled. Therefore, the physicochemical parameters of the process (such as the adsorption isotherms, temperature, pressure, adsorbent composition and feed concentration), many of the most common process design parameters (such as column dimensions, pump capacities, dead volumes and particle sizes) as well as the economic parameters of the production process were considered uncontrollable variables.

2. Choice of performance indicators

In this dissertation, the main purpose is assumed to be the maximization of an objective function defined as the profit (P) of the production process:

$$P = \frac{(\text{money earned} - \text{money invested})}{\text{time interval}} \quad 3-36$$

This function represents the balance between the amount of money that is produced by the separation process discounted of the amount of money that needs to be invested during its operation over a given time interval without considering initial investment costs. Many other definitions of the objective function have been suggested for evaluating the performance of chromatographic separations (many interesting examples can be found in: [2, 5, 6, 9, 10, 81, 145, 171, 172]). They are, however, beyond the scope of the present work, since the definition considered here (equation 3-36) was found to be an interesting approach for evaluating the performance of 8-zone SMB separations.

3. Identification of constraints

In order to find the best operating conditions of the 8-zone SMB operation, the constraints associated with the process operation and performance requirements must be considered. Constraints are usually categorized according to their application as controllable variables or performance variables.

The controllable variables are usually constrained by the physical limitations of the system. The maximal flow rate, for example, is usually limited by the mechanical strength of the packed beds, which may yield under too high pressure drops. Furthermore, reversed flow direction might damage the packing of the adsorbent beds, therefore, in this work, only unidirectional flow was accepted as a solution. The purity, a performance parameter, was constrained, in chapter 5, to values above 99%, in order to account for product quality requirements.

4. Choice of optimizing strategies

Much work has already been done on the development and application of different tools for optimizing continuous chromatographic processes [2, 76, 81, 173]. Kiwala et al. [10], for example, used a modified Nelder-Mead method to find the operating conditions that maximize their objective function for an 8-zone SMB process with internal solvent recycle. Nowak et al. [9] as well as Kawajiri and Biegler [171] used genetic algorithms to find the best trade-off between productivity and solvent consumption for pseudo-ternary separations considering different multi-column processes. Furthermore, Kawajiri et al. [171, 172] as well as Palacios et al. [145] have developed an interesting super-structure-based methodology for the optimization of different configurations of continuous countercurrent chromatography aimed at center-cut separations. In the present work, a simplified model of 8-zone SMB and economic parameters of the production process were used to provide an initial estimative of its profitability.

3.6. Summary

In this chapter the mathematical foundations of the theoretical work developed in this dissertation were established. First, the classical equilibrium-dispersive model of chromatography was deduced and simplified to the equilibrium model, whose solution based on the method of characteristics developed by Rhee et al. [157] was then demonstrated. This will be the groundwork of the research described in chapter 6. Subsequently, the deduction of the triangle theory, as originally described by Storti et al. [13, 159], was presented, which will be extended to the 8-zone TMB process in chapter 5. Afterwards, the mixing cell model was introduced as an efficient tool for simulating both the SMB (section 3.3) and the TMB (section 3.4) processes, which will be employed throughout chapters 5, 6 and 7. Last but not

least, the general concepts of preparative chromatography optimization were introduced in section 3.5. In the following chapter, the concepts and mathematical tools used in the experimental part of the research described in in chapter 7 will be explained.

4. Theoretical background of the experimental methods used

This chapter describes the theory necessary for the execution and interpretation of the experiments described in chapter 7. In section 4.1, the methods for estimating adsorption isotherms are introduced, with emphasis on frontal analysis, the method of choice in this dissertation. Afterwards, in section 4.2, the estimation of the concentration of solutes in samples using High Performance Liquid Chromatography (HPLC) is introduced and, finally, in section 4.3, the basics of spectrophotometry are explained.

4.1. Experimental estimation of adsorption isotherms

The starting point for SMB simulation is the estimation of the adsorption isotherms. Without it, the mass balance of the chromatographic columns cannot be solved. Therefore, many different experimental techniques have been proposed over the years for this purpose. A comprehensive review of many possible experimental methods can be found in [76, 174].

Adsorption isotherm estimation methods can be categorized as dynamic or static. The former includes methods based on overall mass balances. These methods are usually less precise than dynamic methods. They are, however, easier and cheaper, which simplifies the implementation of large scale screenings of solvents and adsorbents. In many cases, such methods can be used as an initial step for the selection of solvents and adsorbents, when very precise information is less relevant. Static methods include, for example, the batch method, the adsorption-desorption method and the circulation method.

Dynamic methods are, on the other hand, more complex and require more sophisticated equipment and software. However, the experimental setup more closely resembles the chromatographic system that is being modeled, which increases the reliability of the results. Examples of this category are: the peak fitting method; the perturbation method; the elution by characteristic point method; the peak maximum method; and the frontal analysis, described below.

The adsorption isotherms in this work were estimated using the frontal analysis [2, 76]. Frontal analysis is typically more accurate than other dynamic methods, since only equilibrium states are evaluated, which minimizes the interference of kinetic effects. However, the amount of solute and solvent necessary for single experiments are relatively

large and hydrodynamic effects might interfere with the shape of the concentration shock fronts. Furthermore, High Performance Liquid Chromatography (HPLC) systems, such as the one used in this work, are not optimized for frontal analysis (being normally commercialized for analysis of samples), which means that much of the experimental protocol had to be performed manually (as later described in the chapter 7), without making much use of automation.

Frontal analysis consists of pumping a concentration step increase into a previously equilibrated chromatographic column. The adsorbent is initially in thermodynamic equilibrium with the solute-free solvent and, as the solute-rich solvent is pumped into the column at constant flow rate, temperature and pressure, a new thermodynamic equilibrium builds up and is reached when the outlet solute concentration is the same as the inlet solute concentration.

Based on the retention time of the concentration step increase (Δc) in the column outlet, the loading step increase (Δq) can be calculated using the integral two-phase mass balance of the chromatographic column:

$$V_{fl}\Delta c + V_{ads}\Delta q(c) = \dot{V} \int_0^{\infty} \Delta c_{in}(t)dt - \dot{V} \int_0^{\infty} \Delta c_{out}(t)dt \quad 4-1$$

Where the average solute concentration increase in the solvent inside the column is described by the term Δc ; the volume of solvent inside the column is represented by the term V_{fl} ; the volume of adsorbent inside the column is represented by the term V_{ads} ; the loading step increase (mass of solute per volume of adsorbent) inside the column is defined by the term $\Delta q(c)$; the term \dot{V} represents the constant solvent flow rate percolating the column during the experiment; the solute concentration increase in the inlet of the column is described by the term Δc_{in} ; the solute increase at the column outlet is described by Δc_{out} .

The integration is performed from the time zero (the moment of the step inlet concentration increase) until the solute outlet concentration reaches the inlet concentration value. At this moment, the column is equilibrated with the feed concentration of the solute.

The first integral in equation 4-1 can be well approximated by the area before the vertical dashed line drawn in Figure 4-1, as long as this line is drawn at the mean value of the concentration front, i.e., as long as the two shaded areas (before and after the dashed line) are the same. At this point:

$$V_{fl}\Delta c + V_{ads}\Delta q(c) = \dot{V}\Delta c_{in}t_b \quad 4-2$$

Rearranging the terms of equation 4-2 yields:

$$\frac{V_{fl}}{\dot{V}} + \frac{V_{ads}\Delta q(c)}{\dot{V}\Delta c} = \frac{\Delta c_{in}t_b}{\Delta c}$$

4-3

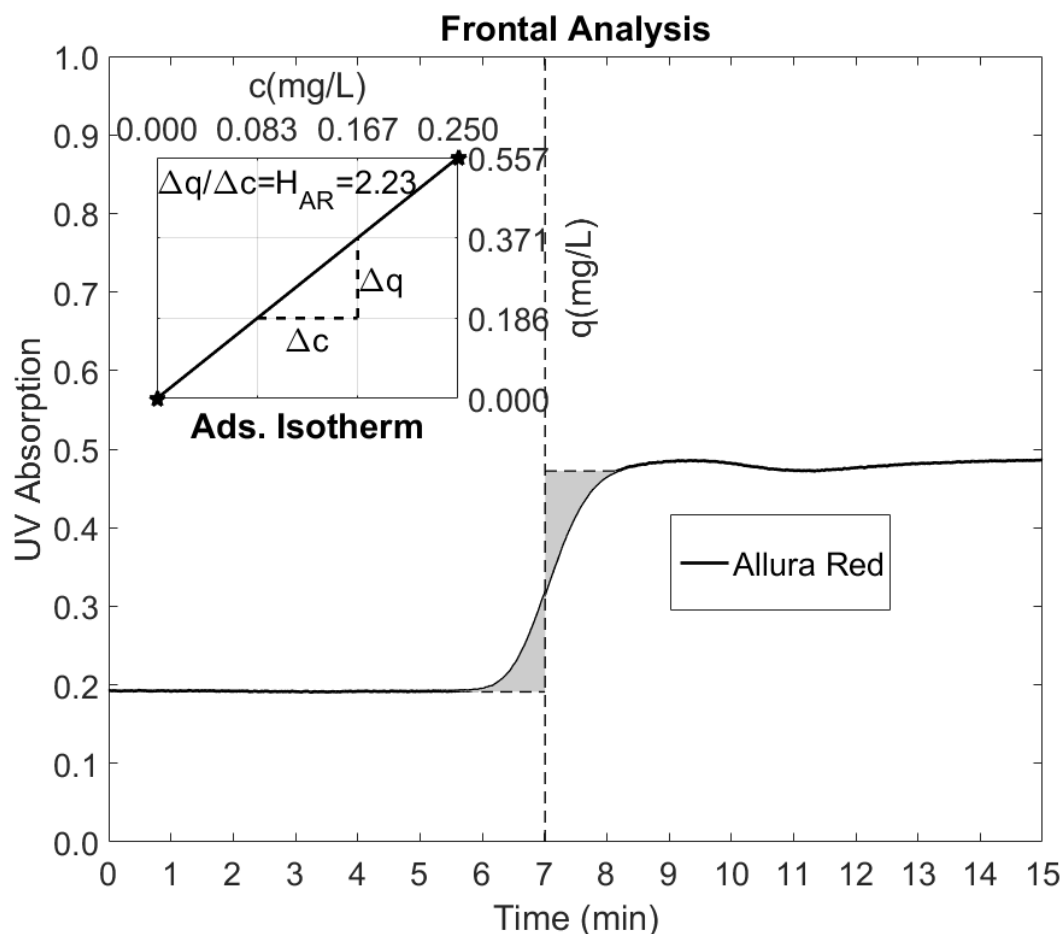


Figure 4-1 – Chromatogram (translated to the left in order to account for the dead time (t_{dead}) of the HPLC system) depicting one loading step of the food dye Allura Red (0.25 mg.l^{-1}) in LiChroprep® RP-18 (particle size: 25-40 μm) using 15/85 (v/v) ethanol / 70mM acetic acid in water as solvent (2 ml.min^{-1}) at room temperature. The vertical axis represents the UV absorbance (254 nm) signal in arbitrary units. The vertical dashed line corresponds approximately to the break through time of the loading step. The subplot on the upper left corner shows the value of the concentration plateau of the loading step (horizontal axis) and the corresponding equilibrium adsorbed load on the solid phase (vertical axis). The inclination of this line allows the estimation of the adsorption isotherm.

Since, by the time the concentration front leaves the system, the column is fully equilibrated at the second concentration plateau concentration, $\Delta c = \Delta c_{in}$. Considering that the liquid fraction of the column volume (V_{fl}) divided by the solvent flow rate is equal to the column dead time (t_0) and that the volume of adsorbent inside the column divided by the liquid fraction of the column volume is equal to the phase ratio (F), equation 4-3 can be rearranged to:

$$\Delta q(\Delta c) = \frac{1}{F} \left(\frac{t_b}{t_0} - 1 \right) \Delta c$$

4-4

Thus, allowing the calculation of the loading of the adsorbent (q_i) as a function of the concentration (c_i). The adsorption isotherm can then be estimated by plotting the loading of solute in the adsorbent as a function of the solute concentration in the solvent as shown in the subplot of Figure 4-1.

4.2. Measurement of solute concentrations using HPLC

One of the most widely employed analytical techniques for the quantification of solutes in samples is the High Performance Liquid Chromatography (HPLC). The universality of its applicability and its practicality have contributed to its current position as a staple technique in most modern analytical chemistry laboratories around the world. In the last decades, advances in data acquisition, storage and processing have considerably simplified the experimental analysis of large numbers of samples. Furthermore, the automation of sample injection has turned HPLC into an attractive technique for laboratories where a large number of samples is analyzed on a regular basis. Finally, in part as a result of the growing popularity of HPLC analysis (and, in part as its cause), different specialized stationary phases have been developed, thus widening the field of its potential applications [80].

The first step in the analysis of a solution is the injection of a, typically small, sample into the hydraulic path of an HPLC unit, as the one shown in Figure 3-1. The constant solvent flow generated by a high precision pump upstream of the chromatographic column insures the migration of the solutes through the packed bed. As explained in section 2.1, the different adsorbent affinities of the solutes cause their retention times to differ, and, therefore they separate in discrete bands that elute sequentially in the column's outlet as exemplified in Figure 4-2 a). Different separation principles can be used for the separation of solutes using HPLC, the most commonly used are normal-phase chromatography, reversed-phase, ion-exchange, chiral selectivity, size-exclusion and hydrophobic interaction chromatography [175].

Detectors are typically placed at the outlet of the chromatographic column and their output is typically sent to a computer as an electric signal, which is proportional to the solute concentration. Due to Fick diffusion, the solute bands normally appear downstream of the column in the detector as Gaussian peaks. By comparing the retention time of these peaks to that of known standards, it is possible to identify the solutes they correspond to. The variable measured by the detector normally corresponds to a characteristic of the solution that changes

according to the concentration of the solutes being analyzed, such as light absorbance, conductivity, refraction index or the polarization angle. The detector signal is recorded and plotted on a time axis, thus generating a chromatogram, as the one shown in Figure 4-2 a).

The mid-height width of a peak can be used to estimate the *efficiency* of a chromatographic column as a function of its equivalent number of theoretical plates (NTP), which is approximately equivalent to n in the cell model described in sections 3.3 and 3.4 [76]:

$$NTP = 5.54 \left(\frac{t_R}{w_{1/2}} \right)^2 \quad 4-5$$

Where t_R is the first moment (or the retention time) of a single pulse peak of the solute, $w_{1/2}$ is the width of the peak at mid-height and NTP is the number of theoretical plates of the chromatographic column.

The number of theoretical plates in a chromatographic column can often be correlated to the solvent flow rate using the Van Deemter correlation [2]:

$$NTP = \frac{L}{\left(A + \frac{B}{v} + Cv\right)} \quad 4-6$$

Where L is the length of the column, A , B and C are experimental coefficients and v is the average linear velocity of the solvent going through the column.

As depicted in Figure 4-2 a), the chromatogram can be used for evaluating which solutes are present in the sample. Without supplementary information, however, it cannot provide quantitative information about the concentration of the solutes. For that, it is necessary to convert the y-axis to a concentration basis and the x-axis to a volumetric basis. The conversion of the horizontal axis from time to volume is done by simply multiplying the abscissa of the gauged points by the flow rate. The resulting chromatogram shows the detector signal profile according to the collected outlet volume.

In order to convert the units of the vertical axis to concentration, information about the correlation between the detector's signal and the solute concentration is necessary. This information is normally expressed as a calibration curve that, at low concentrations, approaches a straight line, which can be then expressed by a coefficient. This coefficient can be obtained by correlating the intensity of the detector's response (a_i) to each solute i concentration in a series of increasing concentration plateaus. Finally, the conversion of the detector signal can be done by dividing the recorded signal by the linear coefficient of the calibration curve b_i , as shown in Figure 4-2 b).

If the calibration curve is not linear, a polynomial expression representing the correlation between the concentration of the solutes and the detector signal can be used for transforming the signal into concentration. This, however, is not a trivial task in case the solute peaks are not completely separated in the chromatogram.

The total mass of the solute M_i can be obtained by integrating the area under its concentration (c_i) peak over the band volume according to equation 4-7.

$$M_i = \int_{V_t}^{V_{t+\Delta t}} c_i(V) dV \quad 4-7$$

The solute concentration in the original sample $c_{i,sample}$ is given by dividing its total mass M_i in the sample by the injected volume V_{inj} .

$$c_{i,sample} = \frac{M_i}{V_{inj}} \quad 4-8$$

Alternatively, since at low concentrations, the detector signal is linearly correlated to the solute concentration, it is possible to build a calibration curve by injecting pulses of single solute samples with different concentrations and recording the peaks generated. As long as the solvent flow rates and the injection volumes are kept constant, the areas under the peaks are directly proportional to the solute concentration in each sample according to equation 4-9:

$$c_{i,sample} = \frac{\dot{V}}{V_{inj} b_i} \int_t^{t+\Delta t} a_i(t) dt \quad 4-9$$

By injecting standard samples of increasing concentrations, the coefficient b_i can be approximated and later used for estimating the solute concentration.

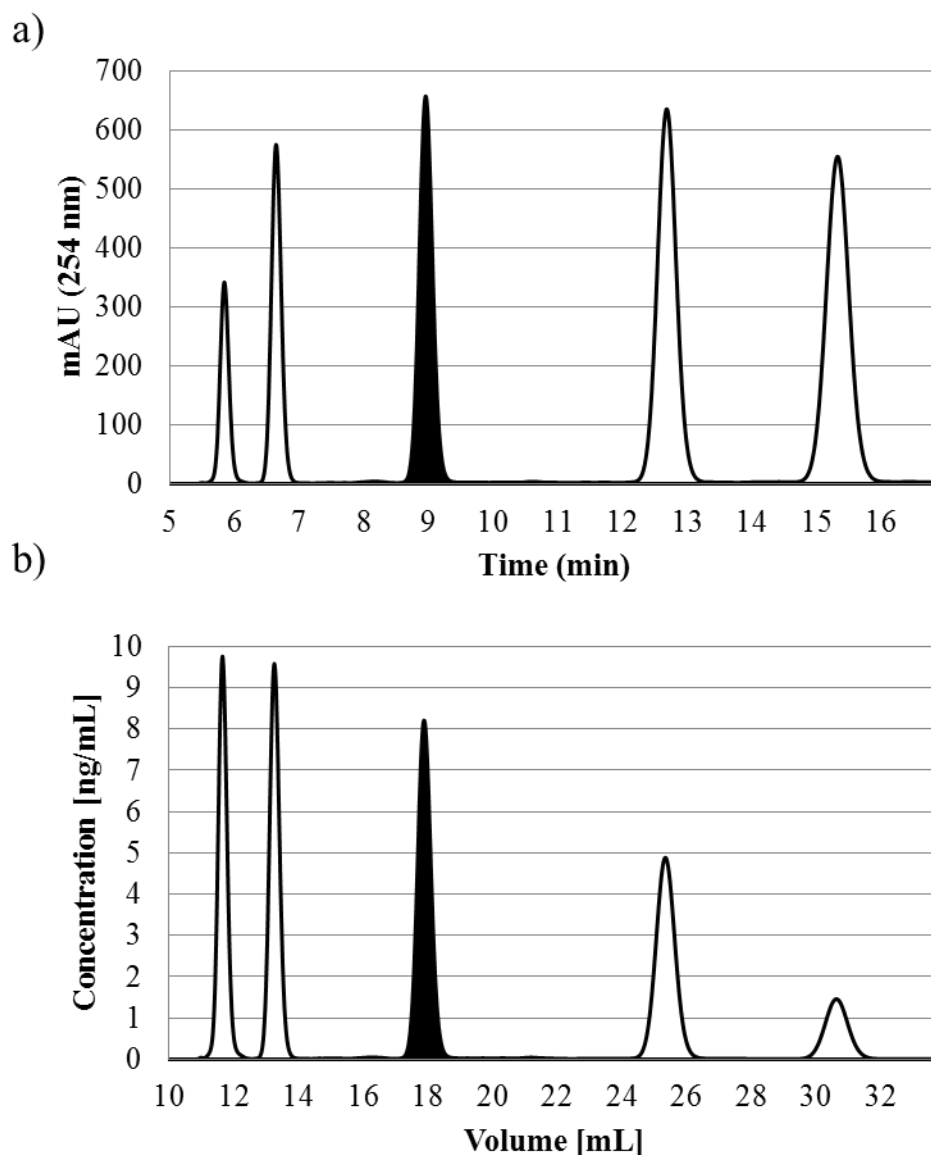


Figure 4-2 – a) Chromatogram showing the outlet UV (254 nm) absorbance signal, as a function of time, generated by a pulse injection of 100 μ L of sample containing Tartrazine (0.05 mg.l⁻¹, first peak), Sunset Yellow (0.05 mg.l⁻¹, second peak), Allura Red (0.05 mg.l⁻¹, third peak), Crystal Ponceau (0.05 mg.l⁻¹, fourth peak) and Fast Green (0.015 mg.l⁻¹, last peak) separated using a Luna C18 column (Phenomenex®, USA) with 15/85 (v/v) ethanol / 70mM acetic acid in water at 2 ml.min⁻¹ at room temperature. In order to estimate the concentration of the solutes, the chromatogram has to be converted from a time basis into a volumetric one by multiplying the x-coordinates of the gauged points by the flow rate used. Furthermore, the y-axis has to be converted from a detector signal (UV absorbance) basis into a concentration one by dividing the ordinate of the points in each peak of the chromatogram by the specific correlation coefficient of the solute they correspond to. The resulting chromatogram is shown in b). If, for example, the purpose of the experiment is to estimate the concentration of the third solute to elute in the sample, the black area under the central peak has to be estimated by numerically integrating the curve in this region. The total solute mass obtained by the peak integration divided by the injected volume of the sample is approximately equivalent to the concentration of this solute in the original sample.

4.3. Measurement of absorbance spectra

Spectrophotometry is a general term describing the study of the interaction between materials and electromagnetic waves. In the scope of this text, though, spectrophotometry refers to the estimation of solute concentrations in solution and to the prediction of their apparent color based on the quantitative measurement of light absorbance spectra. The correlation between the amount of light absorbed by a solution and the concentration of its solutes is based on the classical works of the French mathematician Lambert and the German physicist Beer, which laid the foundations of spectrophotometry.

Assuming that all measurements are performed using the same spectrophotometer and sample cell, the light path length is constant and, therefore, according to the *Lambert-Beer law* [176], the light absorbance of the solution in the λ wavelength is directly proportional to the concentration of the solute i in solution and to a proportionality constant $b_{i,\lambda}$, according to:

$$a_{i,\lambda} = b_{i,\lambda}c_i \quad 4-10$$

As long as there are no interactions between the different solutes in solution, the additive property of the Lambert-Beer law implies that the total absorbance at a wavelength $a_{\lambda,Total}$ of the mixture can be expressed as the sum of all m individual contributions of each of the solutes (equation 4-11).

$$a_{\lambda,Total} = \sum_{i=1}^m b_{i,\lambda}c_i \quad 4-11$$

$$i = 1, m$$

If the light absorbance of the mixture at different wavelengths is simultaneously measured, it is possible to express the absorbance spectrum as a sum of the individual contributions of each of the solutes. The resulting system of equations can be expressed in matrix form as shown in equation 4-12.

$$BC = A \quad 4-12$$

Where A represents the vector of light absorbance values of the mixture at different wavelengths, B represents the matrix of absorbance coefficients of each solute at each wavelength measured and C represents the vector of concentrations of each solute.

After measuring the light absorbance spectra of the mixture, the term A in equation 4-12 is known. Each term of B is obtained by successively measuring the light absorbance spectra of single solute solutions at different concentrations and using the minimum square method to find the inclination of the lines that best fit the experimental points.

The precision of the estimated concentrations can be improved if several wavelengths are analyzed simultaneously, which can be especially helpful in case the absorbance spectra of the different solutes are very similar. However, if more wavelengths than solutes are considered, the system of equations 4-12 becomes over-determined and a numerical technique (such as the partial least squares method, the principal component regression method or the multiple least squares method) needs to be used for the calculation of the solute concentrations.

The relative error of the concentration estimation is typically divided into three categories: background noise of the light source; background noise of the photomultiplier or photodiode and background noise caused by stray light reaching the detector. While the relative interference of the background noise of the light source on the precision of the concentration estimation does not change significantly as a function of the percentage of light being absorbed by the solution, the background noise of the photomultiplier and the one caused by stray light does. Since the concentration estimation error caused by these sources is additive, the overall precision of the concentration estimation is a complex function of the solution absorbance. Typically, the minimal concentration estimation error is found around 0.7 AU, therefore, the samples are normally diluted to this point, where precision is maximal.

Solutes that absorb light in the visible range (400 nm – 750 nm) are expected to imbue solutions with an apparent color, which is a function of their absorbance spectrum, since the light that is not absorbed by the solute, scatters through the solvent and determines its color under white light. Therefore, the apparent color of a solution will mostly correspond to the wavelengths that are not absorbed, which can be predicted by plotting each point of the absorbance spectrum on the opposite side of the Derrigton-Krauskopf-Lennie (DKL) color wheel, as shown in Figure 4-3. [177].

It is important to notice that the transformation of the light absorbance spectrum into the apparent color wheel, as shown in Figure 4-3, is not isometric, since the wheel is divided into 6 sections, each having its own metric. These different metrics are a rough representation of the different sensitivity of the human eye to different light wavelengths. For example, the angular distance between 480 nm and 560 nm is $\pi/3$ radians, which means that, in this section, the mapping scale is $\pi/240 \text{ rad.nm}^{-1}$, meanwhile the angular distance between 400 nm and 430 nm, which is also represented by $\pi/3$ radians, has a mapping scale of $\pi/90 \text{ rad.nm}^{-1}$, 2.67 times larger. This distinction can be explained by the fact that the absorbance spectrum section between 400 nm and 430 nm maps on the opposite side of the color wheel as apparent

was introduced and the correlation between the visible light absorbance spectra of solutions and their apparent color was shown.

Here ends the theoretical background part of this dissertation. In the next three chapters, the contributions of the present research work will be described, starting with studies based on the TMB analogy, followed by the adjustment of the triangle theory to the 8-zone SMB process and finishing with an experimental study using food dyes.

5. Operating regions and analysis of 8-zone TMB

In this chapter, the analogy with the True Moving Bed (TMB) is used as a tool for predicting suitable operating conditions for 8-zone Simulated Moving Bed (SMB) using the equilibrium model and for predicting the internal concentration profiles of the system. These profiles are calculated using a recursive solution of the mixing cell model and are the basis of newly developed analytical expressions of the ideal 8-zone TMB product concentrations, which are later used in combination with an economic description of the process components to suggest a new strategy for finding its maximal profitability. Finally, the comparison of the best achievable performances of each configuration (extract and raffinate recycle) is used to derive explicit criteria for the selection of the best separation order. The results described in this section were peer-reviewed and published in the Journal of Chromatography A [12].

5.1. Operating regions of 8-zone TMB with extract recycle

The operation of the 8-zone TMB is characterized by the following dimensionless flow rate balances:

$$\left\{ \begin{array}{l} m_{I(2)} - m_{II(2)} = m_{E2} \\ m_{III(2)} - m_{IV(2)} = m_{R2} \\ m_{I(1)} - m_{IV(2)} = m_{D1} \\ m_{III(1)} - m_{II(1)} = m_{F1} \\ m_{I(1)} - m_{II(1)} = m_{E1} \\ m_{III(1)} - m_{IV(1)} = m_{R1} \\ m_{I(2)} - m_{IV(1)} = m_{D2} \\ m_{III(2)} - m_{II(2)} = m_{F2} \end{array} \right. \quad 5-1$$

In the case of the 8-zone TMB with extract recycle $m_{F2} = m_{E1}$ and, therefore:

$$\left\{ \begin{array}{l} m_{I(2)} - m_{II(2)} = m_{E2} \\ m_{III(2)} - m_{IV(2)} = m_{R2} \\ m_{I(1)} - m_{IV(2)} = m_{D1} \\ m_{III(1)} - m_{II(1)} = m_{F1} \\ m_{III(1)} - m_{IV(1)} = m_{R1} \\ m_{I(2)} - m_{IV(1)} = m_{D2} \\ m_{I(1)} = m_{III(2)} + m_{II(1)} - m_{II(2)} \end{array} \right. \quad 5-2$$

Considering a hypothetical mixture composed of three fractions A, B and C shown in Figure 5-1 (with the arbitrary adsorption Henry coefficients listed in Table 5-1) according to

the equilibrium model (as explained in section 3.2 [13, 158, 178]) the dimensionless flow rates that allow obtaining pure fraction B should respect the following inequations:

$$\left\{ \begin{array}{l} m_{IV(2)} < H_B \\ m_{IV(1)} < H_A \\ m_{I(2)} > H_C \\ m_{I(1)} > H_C \\ H_B < m_{III(2)} < H_C \\ H_A < m_{II(1)} < H_B \end{array} \right. \quad 5-3$$

Because of the solvent mass balance in the recycled stream, the zone II(2) cannot prevent the intermediary eluting fraction from leaking out in the second extract port without causing either zones I(1), II(1), or, III(2) to fail at their functions (which would compromise the purity of the target fraction), as already shown elsewhere [3, 7].

In the scope of this work, the recovery yield (Rec) is defined as:

$$Rec = \frac{\dot{V}_{Outlet} c_{Product}}{\dot{V}_{Feed} c_{Feed}} \quad 5-4$$

The productivity (*Pr*) is given by:

$$Pr = \frac{\dot{V}_{Outlet} (1 - \varepsilon_{Total}) c_{Product}}{\dot{V}_S \varepsilon_{Total} c_{Feed}} \quad 5-5$$

The productivity definition used in this work is dimensionless in order to consider the scale of the TMB process and to allow an objective comparison of different process operating conditions. It is normalized by the solid flow rate and porosity, since increasing the volumetric adsorbent flow rate causes the product output to increase without changing its relation to solvent consumption, product concentration and recovery yield. Furthermore, the productivity also needs to be normalized by the feed concentration, because, in this work, only linear adsorption isotherms were considered, increased product concentrations can be directly obtained by increasing feed concentrations without adding any extra information to the analysis of the process operation.

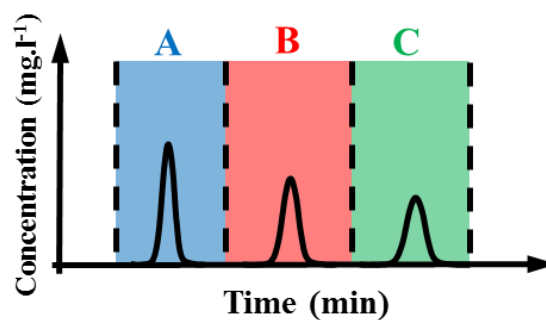


Figure 5-1 – Chromatogram of a hypothetical mixture of 3 solutes. The fraction A is the first eluting one, the fraction B is the target one and the fraction C is the last one to elute. In this chapter, the solutes A (blue), B (red) and C (green) in each of these fractions have the arbitrary adsorption Henry coefficients shown in Table 5-1 for illustrating some of the theoretical results.

Solute	Adsorption Henry coefficient (H_i)
A	1.00
B	1.50
C	2.25

Table 5-1 – Arbitrary adsorption Henry coefficients of the solutes A (blue), B (red) and C (green), shown in Figure 5-1, which are used throughout this chapter for illustrating some of the theoretical results.

An useful way to convey process parameters while showing performance indicators is to plot $m_{II(x)}$, and, $m_{III(x)}$ in the same plot according to the triangle theory explained in section 3.2 [3, 13]. Figure 5-2 and Figure 5-3 show the region in this plot where the dimensionless flow rates allow pure fraction B to be obtained.

The dimensionless flow rates $m_{I(x)}$, and, $m_{IV(x)}$, can be easily determined from inequations 5-2 simply by choosing values for $m_{I(x)}$ larger than H_C , a value for $m_{IV(2)}$ that is smaller than H_B and a value for $m_{IV(1)}$ that is smaller than H_A , so these points are not shown in Figure 5-2 and in Figure 5-3. A safety margin is necessary in order to account for the product contamination caused by dispersion effects.

The solid lines in Figure 5-2 and Figure 5-3 correspond to the arbitrary adsorption Henry coefficients from Table 5-1. The colored regions were calculated by setting either $(m_{II(1)}; m_{III(1)})$ (Figure 5-2) or $(m_{II(2)}; m_{III(2)})$ (Figure 5-3) and then using the Kremser's recursive solution of the equilibrium cell model (Table 3-2 and equations 3-31 to 3-34) for every possible combination of the remaining pair of dimensionless flow rates that results in a product purity over 99%. The calculations were performed considering 200 cells per zone in MATLAB R2015b.

The very good agreement between the area in the parameter space where pure fraction B is expected to be obtained in the outlet port predicted by the equilibrium model and the one found by the scanning algorithm shows the robustness of the equilibrium model as a design tool for systems with relatively high plate numbers.

Because of the recycle, the choice of the parameter $m_{II(1)}$ limits the region where the pair $(m_{II(2)}; m_{III(2)})$ can be chosen [3]. In Figure 5-2 a) this restriction is shown by the diagonal line with equation:

$$m_{III(2)} = m_{II(2)} + H_C - m_{II(1)} \quad 5-6$$

As shown in Figure 5-2, increasing $m_{II(1)}$ increases the achievable recovery as well as the size of the region where $m_{II(2)}$ and $m_{III(2)}$ can be chosen, but it causes the achievable

productivity to decrease because of the reduction in the feed flow rate. The values of the dimensionless flow rates $m_{II(2)}$ and $m_{III(2)}$ must be above the line described by equation 5-6 otherwise $m_{I(1)}$ is smaller than H_C , and pure fraction B is not obtained in the outlet port.

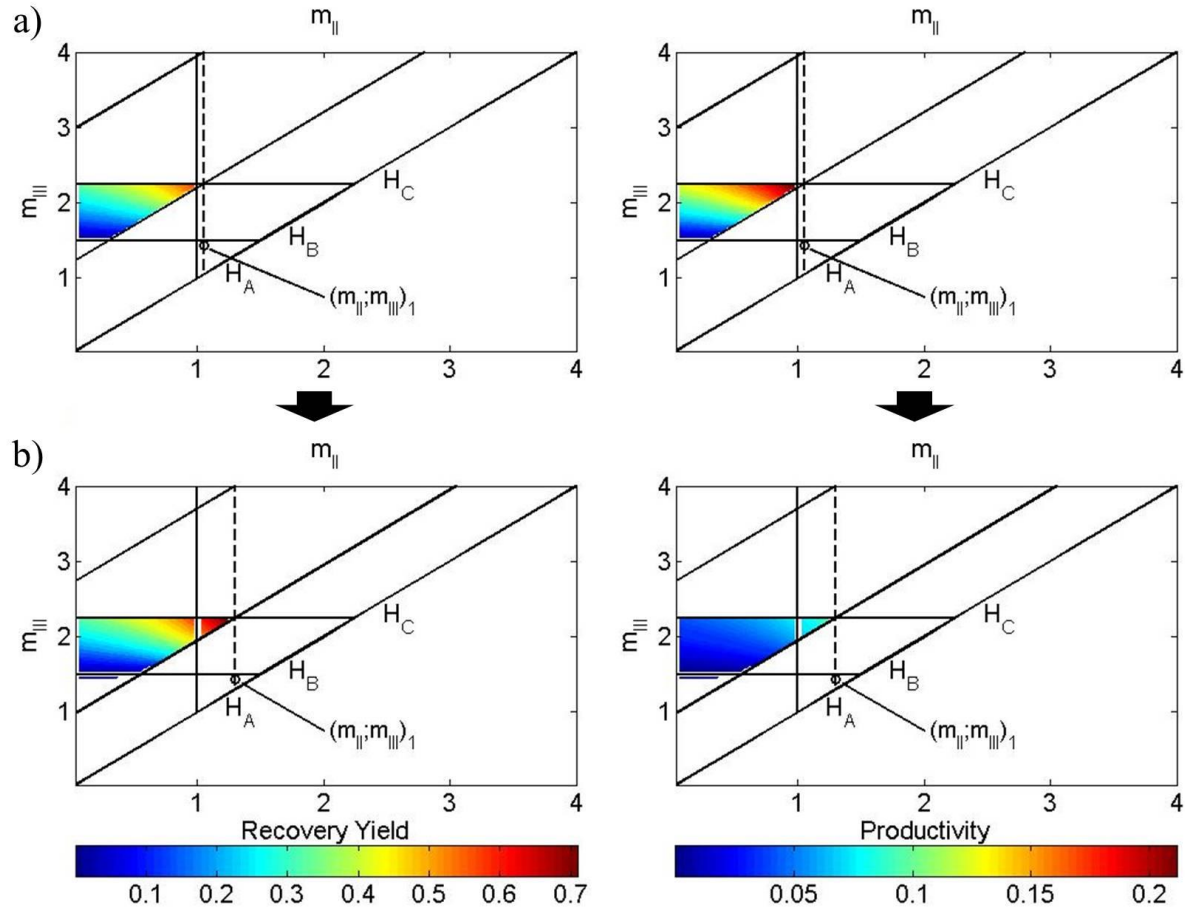


Figure 5-2 a) – Productivity and recovery when the dimensionless flow rates $m_{II(1)}$ and $m_{III(1)}$ are chosen as shown. b) – Increased recovery yield and decreased productivity obtained with increased $m_{II(1)}$. The values were calculated using the Kremser's recursive solution of the equilibrium cell model (Table 3-2 and equations 3-31 to 3-34) for every possible combination of the remaining pair of dimensionless flow rates $(m_{II(2)}; m_{III(2)})$ that results in a product purity over 99%. The calculations were performed considering 200 cells per zone and the adsorption Henry coefficients listed in Table 5-1 using MATLAB R2015b.

In this example, the maximal dimensionless flow rate in any zone was arbitrarily chosen to be 4, which limits the region where the values for $m_{II(2)}$ and $m_{III(2)}$ can be chosen to the space below the line with equation $m_{III(2)} = m_{II(2)} - m_{II(1)} + 4$.

The choice of the parameters $m_{II(2)}$ and $m_{III(2)}$ can also limit the region where $m_{II(1)}$ and $m_{III(1)}$ can be chosen. This restriction is shown in Figure 5-3 a) by the diagonal line with equation:

$$m_{III(2)} = m_{II(2)} + H_C - H_A$$

When the pair $(m_{II(2)}; m_{III(2)})$ is above this line, there is no extra limitation for the choice of $m_{II(1)}$ (besides its need to be between H_A and H_B). However, when $(m_{II(2)}; m_{III(2)})$ is below this line, either the value of $m_{II(1)}$ must be smaller than H_C (in which case the fraction C contaminates the product port) or the region where $m_{II(1)}$ and $m_{III(1)}$ can be chosen shrinks as shown in Figure 5-3 b). This reduction in the area can be shown by the displacement of the vertical dashed line with equation:

$$m_{II(1)} = m_{II(2)} - m_{III(2)} + H_C \tag{5-8}$$

to the right, where $H_A < m_{II(2)} - m_{III(2)} + H_C$. Thus adding a new left border to the region where $m_{II(1)}$ and $m_{III(1)}$ can be chosen.

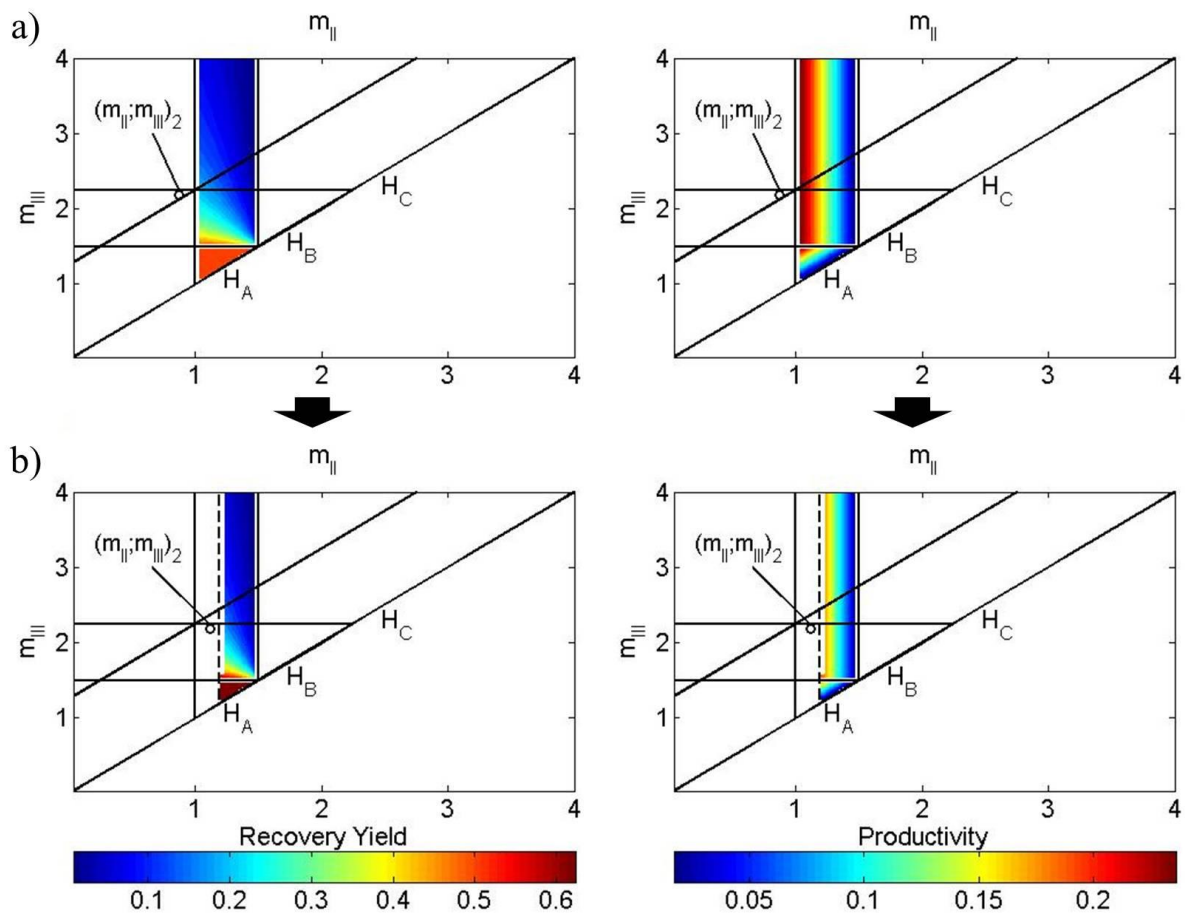


Figure 5-3 a) – Productivity and recovery when the dimensionless flow rates $m_{II(2)}$ and $m_{III(2)}$ are chosen as shown. b) – Increased recovery yield and decreased productivity obtained with increased $m_{II(2)}$. The values were calculated in the same way as in Figure 5-2 considering the adsorption Henry coefficients listed in Table 5-1, for every possible combination of the remaining pair of dimensionless flow rates $(m_{II(1)}; m_{III(1)})$ that results in a product purity over 99%.

In Figure 5-2 a) and b) it can be seen that both productivity and recovery yield increase when $m_{III(2)}$ approaches H_C from below, without surpassing it (where the purity of fraction B in the outlet port is compromised). Similarly, both recovery yield and productivity

increase as $m_{II(2)}$ approaches H_A as shown in Figure 5-2 a). If $m_{II(2)}$ is further increased, the recovery yield achieves even higher values, but the productivity is penalized due to the decrease in the feed flow. Therefore, it is possible to define a point of *highest productivity* (HP point), where the flow rates $m_{II(2)}$ and $m_{III(2)}$ lead to the maximal achievable productivity without compromising the purity. In the limiting case of an infinitely large number of cells, this point is $(m_{II(2)}; m_{III(2)})_{HP} = (H_A; H_C)$.

Figure 5-3 a) (left side) shows that the productivity increases when $m_{II(1)}$ is reduced, but remains larger than H_A . It can also be seen that the productivity will increase as $m_{III(1)}$ is increased towards H_B but will then remain constant. Therefore the optimal value, in terms of productivity, for the point $m_{II(1)}$ vs. $m_{III(1)}$ has the coordinates $(m_{II(1)}; m_{III(1)})_{HP} = (H_A; H_B)$, since further increasing $m_{III(1)}$ will not increase neither recovery yield nor productivity, just solvent consumption. It has been proposed that a continuous flow reduction of the recycled stream with concentration of the solutes could allow higher recoveries without loss of productivity and, therefore, better performances for the 8-zone TMB [7], but this will not be considered here for simplicity sake.

If $m_{II(2)}$ is increased beyond the HP point, it is possible to maximize the recovery yield. The point of *highest recovery* yield (HR point) is reached at $(m_{II(2)}; m_{III(2)})_{HR} = (H_B; H_C)$. At this point, complete recovery yield is achieved in the limiting case of an ideal system with an infinitely large number of cells, since this point belongs to the triangle defined by H_B and H_C . Based on the position of the HR point for the dimensionless flow rates $m_{II(2)}$ and $m_{III(2)}$ the coordinates of the HR point for $(m_{II(1)}; m_{III(1)})_{HR}$ are $(H_B; H_B)$, showing that this point is only a theoretical limit, with a feed flow rate equal to zero.

Since solvent consumption is minimized by choosing optimal values for $m_{I(x)}$, and, $m_{IV(x)}$ (which are defined by the adsorption Henry coefficients) and the product dilution decreases the closer $m_{II(x)}$, and, $m_{III(x)}$ are to the borders of the operating regions (see section 5.3), the optimal operating conditions for 8-zone TMB depend only on the importance of recovery and productivity to the process economics. Hence, for an ideal system, the optimal operating point is necessarily between the HP and the HR point. Since the coordinates of $m_{III(1)}$ and $m_{III(2)}$ are independent from each other, and, for an infinitely large number of cells, $m_{II(2)}$ can be equal to $m_{II(1)}$, this optimal economic point can be defined in terms of a single dimensionless variable M_E (larger than H_A and smaller than H_B) such that:

$$(m_{II(2)}; m_{III(2)}) = (M_E; H_C) \quad \text{and} \quad (m_{II(1)}; m_{III(1)}) = (M_E; H_B) \quad 5-9$$

which will be used in section 5.4 for the profit maximization.

Raffinate recycle 8-zone TMB will be studied in a similar way in the following section

5.2. Operating regions of 8-zone TMB with raffinate recycle

The analysis performed in section 5.1 can be extended for the raffinate recycle. Since, in the case of the 8-zone TMB with raffinate recycle $m_{F2} = m_{R1}$, the equation 5-1 simplifies to:

$$\left\{ \begin{array}{l} m_{I(2)} - m_{II(2)} = m_{E2} \\ m_{III(2)} - m_{IV(2)} = m_{R2} \\ m_{I(1)} - m_{IV(2)} = m_{D1} \\ m_{I(1)} - m_{II(1)} = m_{E1} \\ m_{III(1)} - m_{II(1)} = m_{F1} \\ m_{I(2)} - m_{IV(1)} = m_{D2} \\ m_{IV(1)} = m_{II(2)} + m_{III(1)} - m_{III(2)} \end{array} \right. \quad 5-10$$

In this case, zone III(2) cannot fulfill its function because of the mass balance. Since for reaching the necessary flow rate in zone III(2), either zone III(1), IV(1), or, II(2) cannot have the proper flow rates. This means that if the fraction B is to be collected pure, the second raffinate port will always be contaminated with the fraction B [3, 7].

Based on the equilibrium model [13, 158, 178], in order to obtain pure fraction B from the hypothetical mixture Figure 5-1, the flow rates in each zone must respect the following inequations:

$$\left\{ \begin{array}{l} m_{IV(2)} < H_A \\ m_{IV(1)} < H_A \\ m_{I(2)} > H_B \\ m_{I(1)} > H_C \\ H_A < m_{II(2)} < H_B \\ H_B < m_{III(1)} < H_C \end{array} \right. \quad 5-11$$

Suitable values for $m_{I(2)}$, $m_{IV(2)}$, and, $m_{I(1)}$ can be deduced from the system of inequations 5-11, i.e. $m_{I(2)}$ must be larger than H_B , $m_{IV(2)}$ must be smaller than H_A and $m_{I(1)}$ must be higher than H_C .

The region where the remaining flow rates allow pure fraction B in the outlet port is shown in Figure 5-4 and in Figure 5-5.

Similarly to what happens in the 8-zone TMB with extract recycle, the choice of the dimensionless flow rate in zone III(1) shrinks the region where the dimensionless flow rates $m_{II(2)}$ and $m_{III(2)}$ leading to a pure fraction B can be chosen. In Figure 5-4 a) this restriction is shown by the diagonal line with equation:

$$m_{III(2)} = m_{II(2)} + m_{III(1)} - H_A \quad 5-12$$

For the 8-zone TMB with raffinate recycle, an extra restriction comes from the fact that the flow rate in zone IV(1) cannot be smaller than zero. Therefore the region in the parameter space where $m_{II(2)}$ and $m_{III(2)}$ can be chosen is further shrunk to the region below the line:

$$m_{III(2)} = m_{II(2)} + m_{III(1)} \quad 5-13$$

By decreasing $m_{III(1)}$, as shown in Figure 5-4, the region where the dimensionless flow rates $m_{II(2)}$ and $m_{III(2)}$ can be chosen moves down and the maximum achievable recovery yield increases, but the achievable productivity decreases.

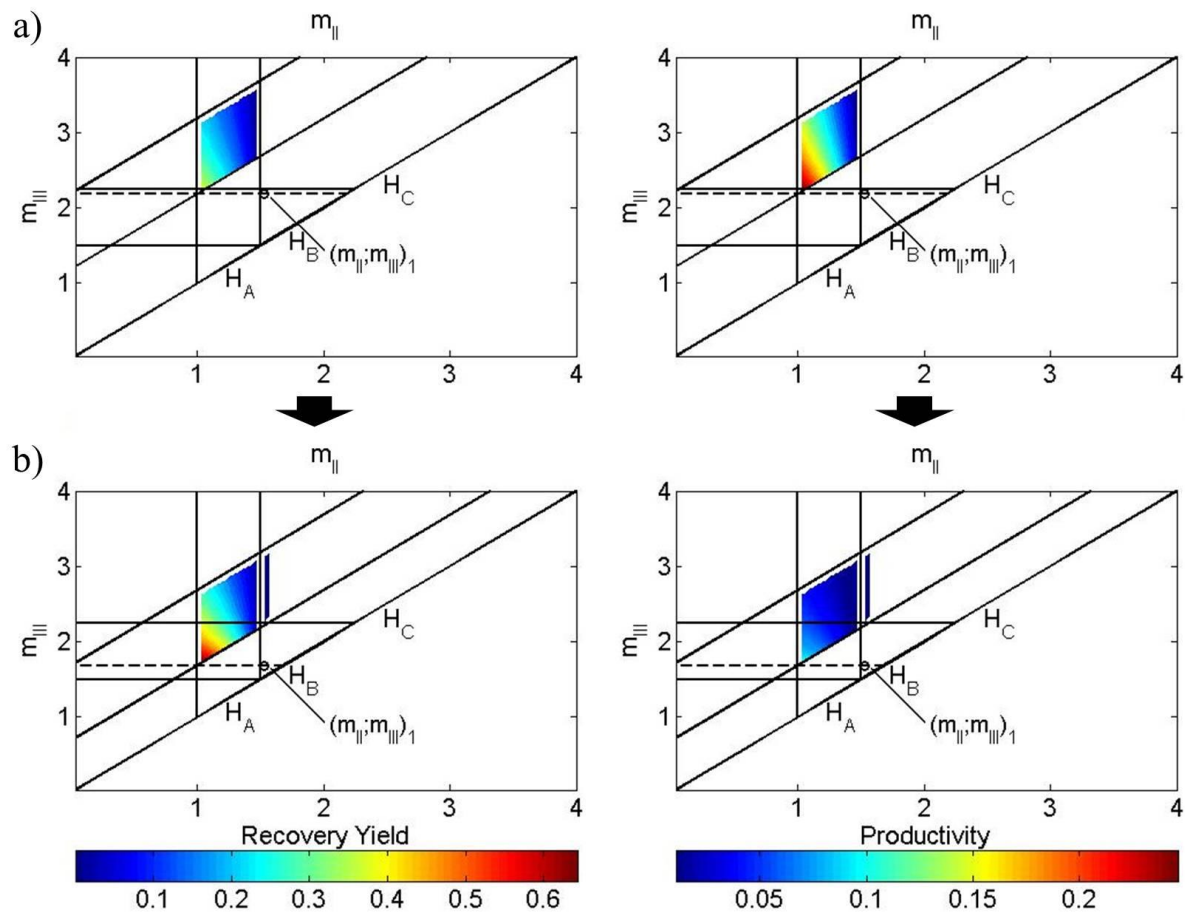


Figure 5-4 a) – Productivity and recovery when dimensionless flow rates $m_{II(1)}$ and $m_{III(1)}$ are chosen as shown. b) – Increased recovery yield and decreased productivity obtained with increased $m_{II(1)}$. The values were calculated in the same way as in Figure 5-2 considering the adsorption Henry coefficients listed in Table 5-1, for every possible combination of the remaining pair of dimensionless flow rates $(m_{II(2)}; m_{III(2)})$ that results in a product purity over 99%.

The value of the parameters $m_{II(2)}$ and $m_{III(2)}$ can also introduce a restriction to the region in the parameter space where $m_{II(1)}$ and $m_{III(1)}$ can be chosen. This is represented in Figure 5-5 a) by the diagonal line with equation:

$$m_{III(2)} = m_{II(2)} + H_C - H_A \quad 5-14$$

As long as the values chosen for $m_{II(2)}$ and $m_{III(2)}$ are above this line, the value of $m_{IV(1)}$ is smaller than H_A and, therefore, the region in the parameter space where $m_{II(1)}$ vs. $m_{III(1)}$ remains at its original size. As shown in Figure 5-5 b), if the point chosen for $m_{II(2)}$ vs. $m_{III(2)}$ lies below this line, in order to keep $m_{IV(1)}$ smaller than H_A (and the product pure) the region where $m_{II(1)}$ vs. $m_{III(1)}$ can be chosen is limited to the region below the horizontal dashed line described by equation:

$$m_{III(1)} = m_{III(2)} - m_{II(2)} + H_A \tag{5-15}$$

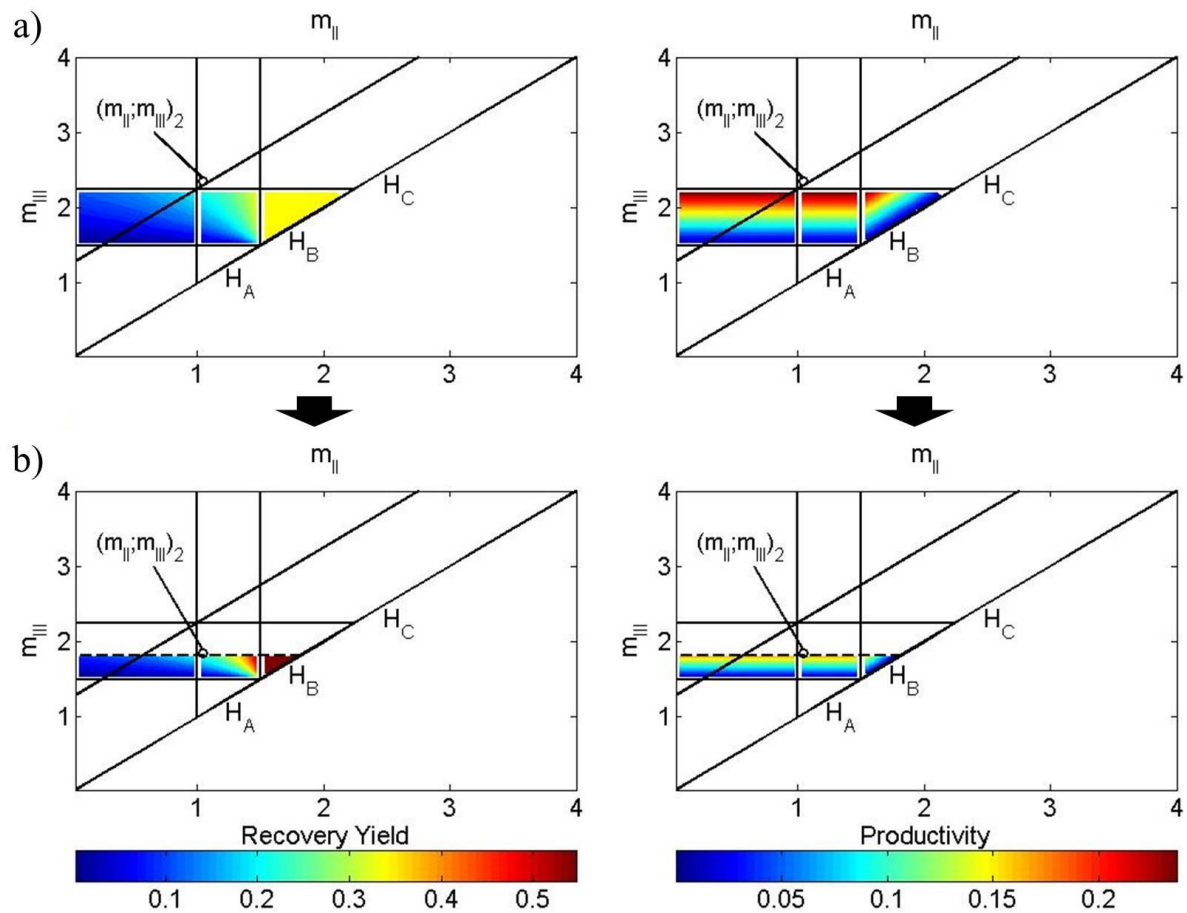


Figure 5-5 a) – Productivity and recovery when dimensionless flow rates $m_{II(2)}$ and $m_{III(2)}$ are chosen as shown. b) – Increased recovery yield and decreased productivity obtained with increased $m_{II(2)}$. The values were calculated in the same way as in Figure 5-2 considering the adsorption Henry coefficients listed in Table 5-1, for every possible combination of the remaining pair of dimensionless flow rates $(m_{II(1)}; m_{III(1)})$ that results in a product purity over 99%.

It is possible to conclude from Figure 5-4 a) that as $m_{II(2)}$ decreases towards H_A (but remains larger than it) and $m_{III(2)}$ decreases towards H_C , both recovery yield and productivity increase. However, due to the recycle mass balance, it is not possible to decrease the value of $m_{III(2)}$ below H_C without adding an extra restriction on the value of $m_{III(1)}$. Although, as shown

in Figure 5-4 b), this increases recovery yield it also decreases the productivity of the process, since it decreases the feed flow rate. Therefore, the coordinates of the highest productivity point (HP point) in terms of $m_{II(2)}$ and $m_{III(2)}$ for the limiting case of an infinitely large number of cells are $(m_{II(2)}; m_{III(2)})_{HP} = (H_A; H_C)$.

The analysis of Figure 5-5 a) (left side) shows that as long as the values chosen for $m_{II(1)}$ and $m_{III(1)}$ are inside the triangle defined by the adsorption Henry coefficients H_B and H_C , the recovery yield is at its highest value. Figure 5-5 b) (right side) shows that inside this triangle the productivity reaches its maximum when $m_{III(1)}$ tends towards H_C and $m_{II(1)}$ tends towards H_B . This is the HP point defined in terms of $m_{II(1)}$ and $m_{III(1)}$, and, at the limiting case of an infinitely large number of cells, has the coordinates $(m_{II(1)}; m_{III(1)})_{HP} = (H_B; H_C)$.

It is also possible to define the point of highest recovery yield (HR point), where, in the limiting case of an infinitely large number of cells, complete recovery yield is obtained, $(m_{II(2)}; m_{III(2)})_{HR} = (H_A; H_B)$. The coordinates of $m_{II(1)}$ and $m_{III(1)}$ at the HR point are $(m_{II(1)}; m_{III(1)})_{HR} = (H_B; H_B)$. Showing that, at the HR point, productivity is zero.

The dimensionless variable M_R (between H_B and H_C) represents both $m_{III(2)}$ and $m_{III(1)}$ at the point (between the HP and the HR points) where, depending on the relative importance of recovery and productivity on the process economics, 8-zone TMB with raffinate recycle performs at its highest profitability. When the number of cells is infinitely large, the point of optimal economic operation of the process is:

$$(m_{II(2)}; m_{III(2)}) = (H_A; M_R) \quad \text{and} \quad (m_{II(1)}; m_{III(1)}) = (H_B; M_R) \quad 5-16$$

which will be used in section 5.4 for the profit maximization.

5.3. Estimation of 8-zone TMB outlet concentrations

In the following example, the flow rates of extract recycle 8-zone TMB were set close to the HP point. This generated the solute concentration profiles in the system shown in Figure 5-6 a), which shows that for a very high number of cells (700 cells per zone, in this case), the difference between the concentration of the target fraction in the recycled stream and in the outlet stream is very small. This difference is caused by band broadening of the solute plateaus.

This band broadening effect becomes more significant as the dimensionless flow rates are set closer to the borders of the operating regions defined by the equilibrium model, thus constraining the achievable purity. If the number of cells is large, high purity fraction B can

be obtained much closer to these borders, which allows higher product concentrations to be obtained because the recycled and outlet port stream concentrations converge. This is shown in Figure 5-6 b), where the concentration in the outlet port (X) asymptotically increases towards the concentration of product in the recycled stream (horizontal dashed lines) as the number of cells per zone (n) increases, keeping purity requirements constant and setting dimensionless flow rates closer to the borders of the operating regions. When the number of cells is infinitely large, these two concentrations become equal.

In many of small and medium scale applications of preparative chromatography the number of cells is very high (reaching hundreds or even thousands of theoretical plates per column). This means that such systems behave very close to ideality.

If the number of cells is infinitely large, $m_{III(2)}=H_C$ for the 8-zone TMB with extract recycle and $m_{II(2)}=H_A$ for the raffinate recycle configuration. Then it is possible to calculate the concentration of fraction B in the outlet stream based on the mass balance of the first subunit in a similar way as described by Zhong and Guiochon [179].

From the mass balance of fraction B in the 8-zone TMB with extract recycle:

$$c_{B,F1}(\dot{V}_{III(1)} - \dot{V}_{II(1)}) = c_{B,E1}(\dot{V}_{I(1)} - \dot{V}_{II(1)}) \quad 5-17$$

Since ideal behavior is assumed ($c_{B,R2} = c_{B,E1}$) it follows that:

$$\frac{c_{B,R2}}{c_{B,F1}} = \frac{(m_{III(1)} - M_E)}{(m_{I(1)} - M_E)} = \frac{(H_B - M_E)}{(H_C - M_E)} \quad 5-18$$

Using the mass balance of fraction B in the 8-zone TMB with raffinate recycle:

$$c_{B,F1}(\dot{V}_{III(1)} - \dot{V}_{II(1)}) = c_{B,R1}(\dot{V}_{III(1)} - \dot{V}_{IV(1)}) \quad 5-19$$

Therefore:

$$\frac{c_{B,E2}}{c_{B,F1}} = \frac{(M_R - m_{II(1)})}{(M_R - m_{IV(1)})} = \frac{(M_R - H_B)}{(M_R - H_A)} \quad 5-20$$

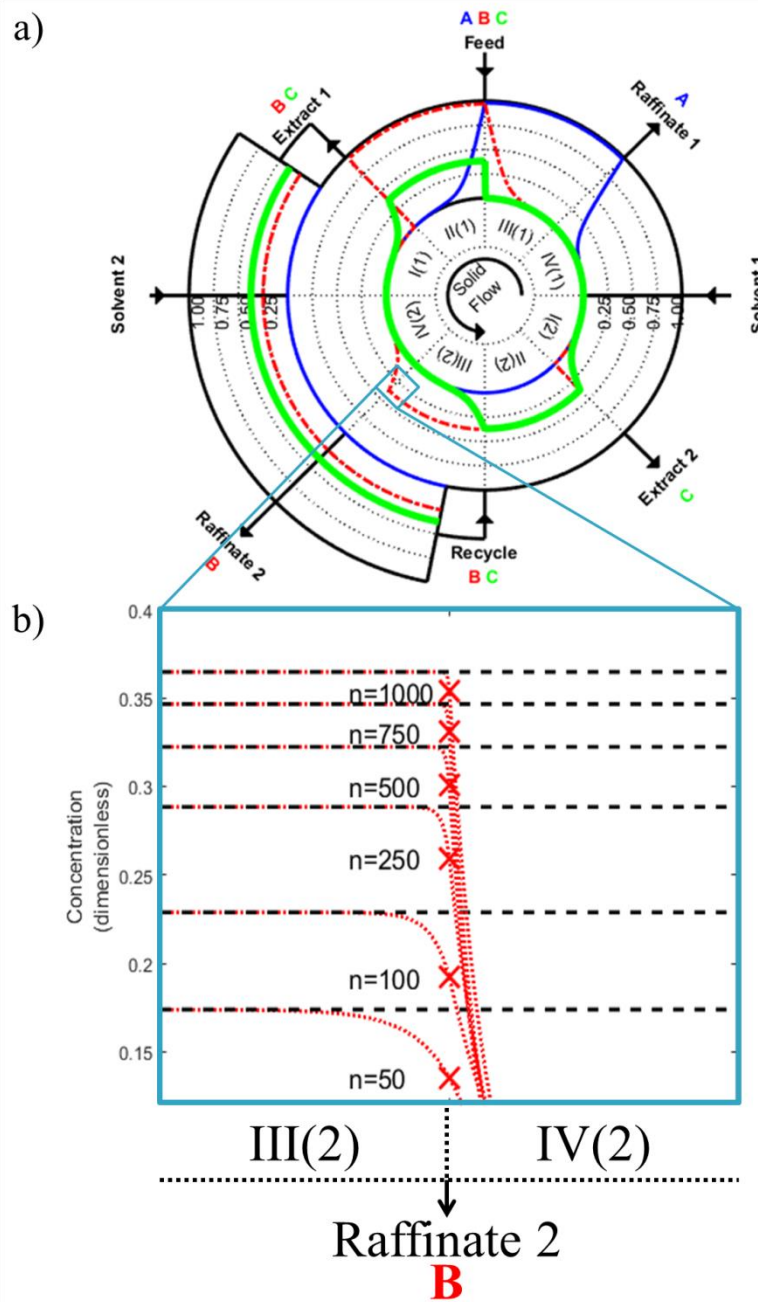


Figure 5-6 – a) Dimensionless concentration (divided by feed concentration) profiles of the fractions A (blue), B (red), and C (green) inside the 8-zone TMB with extract recycle operated close to the HP point calculated using LDU solution of the cell model mass balance (continuous lines) in MATLAB R2015b considering $n=700$, the adsorption Henry coefficients listed in Table 5-1 and $m_{I(2)}=2.273$, $m_{II(2)}=0.965$, $m_{III(2)}=2.228$, $m_{IV(2)}=1.485$, $m_{I(1)}=2.273$, $m_{II(1)}=1.01$, $m_{III(1)}=1.485$, $m_{IV(1)}=0.99$. The external section of the circle represents the solute concentrations inside the recycle stream. b) Closer look at the dimensionless internal concentration profile of the product around the first raffinate port obtained at different separation efficiencies keeping a minimum purity requirement of 99%. As the number of cells increases from 50 to 1000, the concentration of fraction B in the outlet port (X) becomes progressively higher and closer to the concentration in the recycled stream (horizontal dashed lines).

5.4. Economic performance of 8-zone TMB

Based on the discussion presented in sections 5.1 and in 5.2 it was shown that in the ideal case, an optimal point in terms of process economics can be found for 8-zone TMB between the HP and HR points. This makes the decision between the two configurations more challenging than it is for a cascade of two independently operated 4-zone TMB units (where the global optimal is simply the HP point), since the maximization of different performance indicators converges to different operating points depending on the specific cost contributions of each process component to the overall profitability. Therefore, in the next section, the contribution of each performance indicator to the process economy will be analyzed.

5.4.1. Economic analysis

The performance of 8-zone TMB or SMB may vary according to productivity, recovery yield, product concentration and solvent consumption as a function of the configuration and operating conditions chosen. Considering the effect that each of these performance indicators has on the total process profitability, equation 5-21 was derived to describe the profit P (defined in equation 3-36), as the financial balance of the entire production process. In this function, each of the coefficients (PSP , SCo , $SRCo$, and, FCo) can be further broken down into different gains and expenses (as show in Table 5-2) without loss of generality. Therefore, each of the coefficients in equation 5-21 can be interpreted as a non-exhaustive list of costs belonging to each of the categories shown in Table 5-2.

$$P = \dot{V}_S c_{Feed} \frac{\varepsilon_{Total}}{1 - \varepsilon_{Total}} \times Pr \times PSP - SC \times SCo - \dot{V}_{Outlet} \times SRCo - c_{Feed} \dot{V}_{Feed} \times FCo \quad 5-21$$

The first term in this function ($\dot{V}_S c_{Feed} \frac{\varepsilon_{Total}}{1 - \varepsilon_{Total}} \times Pr \times PSP$) has a positive sign and represents the income generated by the sales of the product. This number is proportional to the amount of purified solute produced over a unit of time and to the product selling price (PSP , in Table 5-2), which represents the adjusted profit margin of the product sales per unit of mass. The actual selling price of the product must be discounted of the operating costs of the whole production (such as salaries, taxes, and other business related costs, as well as the costs associated with further processing of the product *after its purification*) before it can be multiplied by the amount of pure product generated. This correction is necessary, since a

financial analysis of the whole production is important before a realistic evaluation of the profitability of the separation process can be made.

The second term in this function ($SC \times SCo$) has a negative sign and represents the amount of money that needs to be invested over unit of time in fresh solvent. This term is directly proportional to the total solvent consumption (SC) as well as to the solvent costs (SCo) (which is further broken down in Table 5-2).

The last term in the profit function ($c_{Feed} \dot{V}_{Feed} \times FCo$) also has a negative sign and corresponds to the investment associated with the production of the feed that is to be separated. It accounts for monetary losses associated with a low recovery yield of the product, since it is directly proportional to the amount of crude feed ($c_{Feed} \dot{V}_{Feed}$) consumed by the separation process. The term FCo (crude feed purchase costs) includes not only the spending associated with the production and pretreatment of the crude feed itself, but also the original feedstock and its potential transportation costs.

It is important to highlight that Kawajiri and Biegler [171] as well as Nicoud [81] have suggested similar expressions to the one proposed in this work for the profit rate. However, there is an extra term in equation 5-21 compared to the function suggested by Kawajiri and Biegler [171]. This term ($\dot{V}_{Outlet} \times SRCo$) represents the costs of removing the solvent from the purified product stream and is directly proportional to the product outlet volumetric flow rate (\dot{V}_{Outlet}). That is an important contribution, since, depending on the nature of the process, these costs might be substantial. Solvent removal processes such as distillation, evaporation and ultra-filtration, for example, might increase the operating costs associated with product dilution substantially in the form of energy consumption.

Product selling price (PSP) ¹	Solvent costs (SCo) ²	Solvent removal costs ($SRCo$) ²	Crude feed purchase costs (FCo) ¹
+ Final product price	+ Solvent purchase price	+ Costs of solvent recovery	+ Costs of crude feed production (raw materials, energy, etc.)
- Costs of polishing operations after separation	+ Costs of energy consumption due to pumping	+ Costs of solvent disposal	+ Costs of crude feed pre-separation (filtration, extraction, distillation, etc.)
- Costs of packaging, transportation, and, other general post production costs	+ Costs of solvent storage	+ Costs of solvent drying energy	+ Costs of crude feed transportation (shipping, pumping, etc.)
- Other costs (salaries, taxes, bills, etc.)	+ ...	+ ...	+ ...
- ...			

Table 5-2 – Cost contributions to the profit of preparative chromatography [76, 180-182] with their corresponding sign. ¹Per gram of the final product. ²Per liter.

To simplify the economic evaluation process, by reducing the size of the equations used, it is useful to define a dimensionless profit function (DP) by dividing equation 5-5 by $\dot{V}_S c_{Feed} \frac{\varepsilon_{Total}}{1-\varepsilon_{Total}} \times PSP$, which yields:

$$DP = Pr - SCR \times DSC - SRCR \times DOFR - FCR \times DFFR \quad 5-22$$

Where DSC is the dimensionless (divided by \dot{V}_S) total solvent consumption, $DOFR$ is the dimensionless outlet flow rate of the product stream (divided by \dot{V}_S), $DFFR$ is the dimensionless feed flow rate (divided by \dot{V}_S), and, the new coefficients are defined as follows:

$$SCR \text{ (solvent costs ratio)} = \frac{SCo[\$/l]}{c_{Feed}[g/l] \times PSP[\$/mg]} \quad 5-23$$

$$SRCR \text{ (solvent removal costs ratio)} = \frac{SRCo[\$/l]}{c_{Feed}[mg/l] \times PSP[\$/mg]} \quad 5-24$$

$$FCR \text{ (crude feed purchase costs ratio)} = \frac{FCo[\$/mg]}{PSP[\$/mg]} \quad 5-25$$

5.4.2. Evaluation of extract recycle 8-zone TMB

For the 8-zone TMB with extract recycle, the point between the HP and HR points at which, the economics of the process is optimal can be found in terms of M_E . The dimensionless productivity at this point is equal to:

$$Pr = (m_{III(2)} - m_{IV(2)}) \frac{(1 - \varepsilon_{Total}) c_{B,R2}}{\varepsilon_{Total} c_{B,F1}} = (H_C - H_B) \frac{(1 - \varepsilon_{Total}) c_{B,R2}}{\varepsilon_{Total} c_{B,F1}} \quad 5-26$$

Substituting equation 5-18 in equation 5-26 yields

$$Pr = \frac{(1 - \varepsilon_{Total}) (H_C - H_B) (H_B - M_E)}{\varepsilon_{Total} (H_C - M_E)} \quad 5-27$$

The dimensionless solvent consumption (DSC) is equal to:

$$DSC = m_{I(2)} - m_{IV(1)} + m_{I(1)} - m_{IV(2)} + m_{III(1)} - m_{II(1)} = 2H_C - H_A - M_E \quad 5-28$$

The dimensionless outlet flow rate ($DOFR$) is:

$$DOFR = m_{III(2)} - m_{IV(2)} = H_C - H_B \quad 5-29$$

and the dimensionless feed flow rate ($DFFR$) is equal to:

$$DFFR = m_{III(1)} - m_{II(1)} = H_B - M_E \quad 5-30$$

Substituting equations 5-27, 5-28, 5-29, and, 5-30 in the expression for dimensionless profit (5-22) and then differentiating it in terms of M_E yields:

$$\frac{d(DP)}{dM_E} = SCR + FCR - \left(\frac{H_C - H_B}{M_E - H_C} \right)^2 \quad 5-31$$

As postulated above, there is a value for M_E between H_A and H_B where this derivative is equal to zero. This is the point of maximal profit for 8-zone TMB with extract recycle:

$$M_E = H_C - \frac{H_C - H_B}{\sqrt{SCR + FCR}} \quad 5-32$$

The function found for M_E is only valid between H_A and H_B , and, therefore, there are some restrictions for its validity. The first one is that $SCR+FCR$ cannot be larger than 1, otherwise M_E becomes larger than H_B and the feed flow rate becomes negative. In reality, such flow rates would not be chosen, but if $SCR+FCR$ is equal or larger than 1, the final product is too cheap compared to the costs of solvent added to crude feed and that 8-zone TMB is not the best alternative for this separation.

The second restriction for the proper use of the function found for M_E comes from the fact that reducing M_E below H_A does not lead to higher productivities (as an initial analysis of equation 5-32 would indicate). The reason why is that $m_{II(2)}$ can be reduced below H_A , but $m_{II(1)}$ cannot (as shown by the set of inequations 5-3), otherwise there is contamination of the second raffinate port with fraction A.

Equating the function 5-32 to H_A allows the definition of a lower limit for $\sqrt{SCR + FCR}$ below which, for a process in which the economy is strongly biased by the productivity, the HP point should be chosen instead of the point indicated by equation 5-32. This limit is:

$$\sqrt{SCR + FCR} = \frac{(\alpha_{B,C} - 1)}{(\alpha_{B,C} - \frac{1}{\alpha_{A,B}})} \quad 5-33$$

5.4.3. Evaluation of raffinate recycle 8-zone TMB

For the 8-zone TMB with raffinate recycle, the dimensionless productivity of the point between the HR and HP points where the profit rate is maximal is given by:

$$Pr = (m_{I(2)} - m_{II(2)}) \frac{(1 - \varepsilon_{Total})}{\varepsilon_{Total}} \frac{c_{B,E2}}{c_{B,F1}} = (H_B - H_A) \frac{(1 - \varepsilon_{Total})}{\varepsilon_{Total}} \frac{c_{B,E2}}{c_{B,F1}} \quad 5-34$$

Substituting equation 5-20 in equation 5-34, yields:

$$Pr = \frac{(1 - \varepsilon_{Total}) (H_B - H_A) (M_R - H_B)}{\varepsilon_{Total} (M_R - H_A)} \quad 5-35$$

The dimensionless solvent consumption at this point is:

$$DSC = m_{I(2)} - m_{IV(1)} + m_{I(1)} - m_{IV(2)} + m_{III(1)} - m_{II(1)} = H_C - 2H_A + M_R \quad 5-36$$

The dimensionless outlet flow rate is:

$$DOFR = m_{I(2)} - m_{II(2)} = H_B - H_A \quad 5-37$$

and the dimensionless feed flow rate is:

$$DFFR = m_{III(1)} - m_{II(1)} = M_R - H_B \quad 5-38$$

It is possible to find the point between the HR and HP points of maximal profit by substituting equations 5-35, 5-36, 5-37, and, 5-38 in equation 5-22 and differentiating it in M_R :

$$\frac{d(DP)}{dM_R} = \left(\frac{H_A - H_B}{M_R - H_A} \right)^2 - SCR - FCR \quad 5-39$$

which can be equated to zero and solved for M_R between H_B and H_C , which gives:

$$M_R = H_A + \frac{H_B - H_A}{\sqrt{SCR + FCR}} \quad 5-40$$

Once more, $SCR+FCR$ cannot be larger than 1, otherwise M_R becomes smaller than H_B and the feed flow rate becomes negative and using 8-zone TMB does not make sense economically.

The lower limit for $\sqrt{SCR + FCR}$ can be found by equating the function 5-40 to H_C . The result is the following condition:

$$\sqrt{SCR + FCR} = \frac{\left(1 - \frac{1}{\alpha_{A,B}}\right)}{\left(\alpha_{B,C} - \frac{1}{\alpha_{A,B}}\right)} \quad 5-41$$

If $\sqrt{SCR + FCR}$ is even smaller, the optimal value for M_R found by equation 5-40 is higher than H_C . At such point, the assumption that $m_{III(2)} = m_{III(1)}$ is not valid anymore, since $m_{III(2)}$ can be increased beyond H_C , but $m_{III(1)}$ cannot, otherwise fraction C contaminates the final product. This means that at this point equation 5-40 is not valid, and productivity actually decreases with increasing $m_{III(2)}$ (as shown in Figure 5-4 a), right side). Hence, when $\sqrt{SCR + FCR}$ is smaller than the value of equation 5-41, $M_R=H_C$ (that is, the HP point) should be chosen instead of the value calculated by equation 5-40.

5.4.4. Highest productivity point

So far, it has been assumed that the optimal economic point is somewhere between the HR and the HP points. However, this is not necessarily true, if

$$\sqrt{SCR + FCR} < \frac{\left(1 - \frac{1}{\alpha_{A,B}}\right)}{\left(\alpha_{B,C} - \frac{1}{\alpha_{A,B}}\right)} \quad \text{and} \quad \sqrt{SCR + FCR} < \frac{(\alpha_{B,C} - 1)}{\left(\alpha_{B,C} - \frac{1}{\alpha_{A,B}}\right)} \quad 5-42$$

equations 5-32 and 5-40 are not valid, and the HP points should be chosen instead. At these points $M_E=H_A$ and $M_R=H_C$. Therefore, from equation 5-27, the dimensionless concentration of the fraction B in the outlet port of 8-zone TMB with extract recycle becomes:

$$\frac{c_{B,R2}}{c_{B,F1}} = \frac{(1 - \frac{1}{\alpha_{A,B}})}{(\alpha_{B,C} - \frac{1}{\alpha_{A,B}})} \quad 5-43$$

From equation 5-35, at the HP point, the dimensionless concentration of fraction B in the outlet port of 8-zone TMB with raffinate recycle is

$$\frac{c_{B,E2}}{c_{B,F1}} = \frac{(\alpha_{B,C} - 1)}{(\alpha_{B,C} - \frac{1}{\alpha_{A,B}})} \quad 5-44$$

It is then possible to compare the concentrations of fraction B in the outlet port obtained at the HP point for the two system configurations by plotting them together for a wide range of selectivity factors as shown in Figure 5-7.

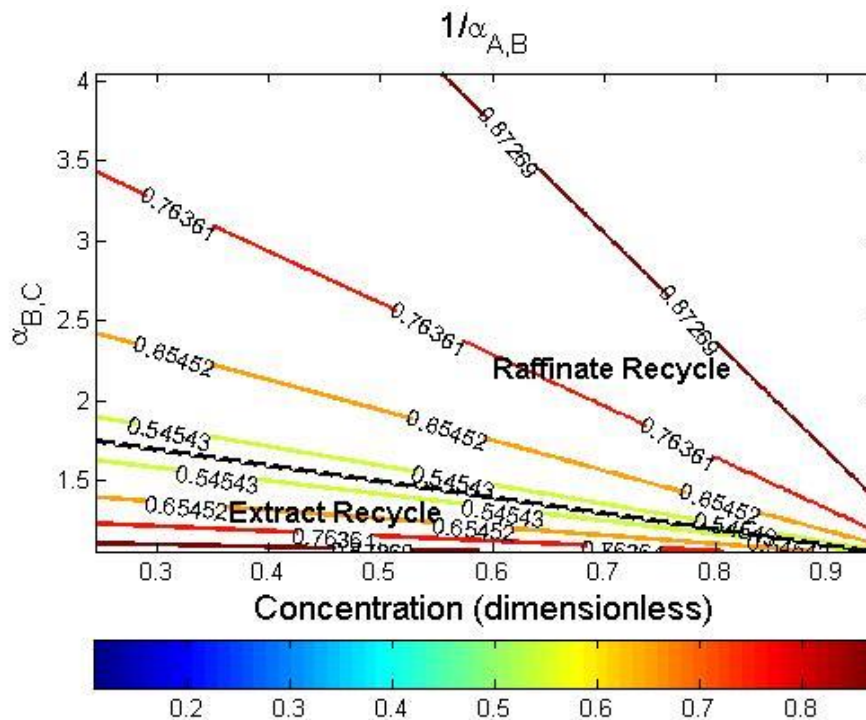


Figure 5-7 – Dimensionless concentration (divided by feed concentration) of product in the outlet port of 8-zone TMB with extract recycle and with raffinate recycle at their HP points. The plot was generated by comparing the concentrations of fraction B in the outlet port obtained by raffinate and extract recycle 8-zone TMB operated at their HP points for every selectivity factor in the given space calculated using equations 5-43 and 5-44. When the concentration is higher for one configuration than for the other, only the highest one is shown. The dashed line is defined by equation 5-45 and separates the region where raffinate recycle outperforms extract recycle and vice-versa.

The dashed line dividing the region in the plot where extract recycle outperforms raffinate recycle in terms of product concentration can be analytically calculated based on equations 5-27 and 5-35. This line is defined by selectivity factors that lead to the same product concentrations at the HP point for both system configurations, therefore:

$$\frac{(1 - \frac{1}{\alpha_{A,B}})}{(\alpha_{B,C} - \frac{1}{\alpha_{A,B}})} = \frac{(\alpha_{B,C} - 1)}{(\alpha_{B,C} - \frac{1}{\alpha_{A,B}})} \quad \therefore \quad \alpha_{B,C} = 2 - \frac{1}{\alpha_{A,B}} \quad 5-45$$

Using equations 5-18 and 5-20 it is possible to calculate the recovery yield (Rec) of the fraction B in the product port at the HP point for any selectivity factor. For the 8-zone TMB with extract recycle:

$$Rec = \frac{(m_{III(2)} - m_{IV(2)})c_{B,R2}}{(m_{III(1)} - m_{II(1)})c_{B,F1}} = \frac{(\alpha_{B,C} - 1)c_{B,R2}}{(1 - \frac{1}{\alpha_{A,B}})c_{B,F1}} = \frac{(\alpha_{B,C} - 1)}{(\alpha_{B,C} - \frac{1}{\alpha_{A,B}})} \quad 5-46$$

The recovery of the fraction B in 8-zone TMB with raffinate recycle operated at the HP point can be calculated in a similar way:

$$Rec = \frac{(m_{I(2)} - m_{II(2)})c_{B,E2}}{(m_{III(1)} - m_{II(1)})c_{B,F1}} = \frac{(1 - \frac{1}{\alpha_{A,B}})c_{B,E2}}{(\alpha_{B,C} - 1)c_{B,F1}} = \frac{(1 - \frac{1}{\alpha_{A,B}})}{(\alpha_{B,C} - \frac{1}{\alpha_{A,B}})} \quad 5-47$$

It is then possible to compare the recovery of the fraction B in the product port operated at the HP point of the two system configurations. A mirror image reflected around the line defined by equation 5-45 of the plot shown in Figure 5-7 is obtained (as shown in Figure 5-8).

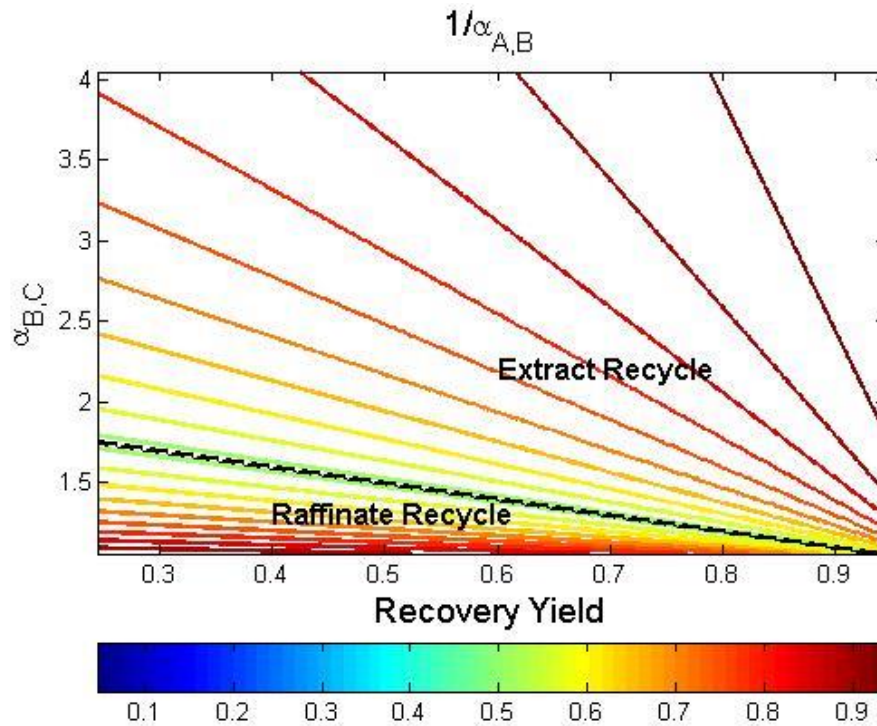


Figure 5-8 – Recovery yield of 8-zone TMB with extract or raffinate recycle. The plot was generated by comparing the recovery yield obtained by either raffinate or extract recycle 8-zone TMB for every selectivity factor in the given space at the HP point calculated using equations 5-46 and 5-47. When one outperforms the other, the highest one is plotted following the color code and vice-versa. The straight line separating the region where raffinate recycle outperforms extract recycle is the line defined by equation 5-45.

The productivity of either system configuration at the HP point can also be analytically calculated. For the 8-zone TMB with extract recycle:

$$Pr = m_{R2} \frac{(1 - \varepsilon_{Total}) c_{B,R2}}{\varepsilon_{Total} c_{B,F1}} = H_B \frac{(1 - \frac{1}{\alpha_{A,B}})(\alpha_{B,C} - 1)}{(\alpha_{B,C} - \frac{1}{\alpha_{A,B}})} \frac{(1 - \varepsilon_{Total})}{\varepsilon_{Total}} \quad 5-48$$

For the 8-zone TMB with raffinate recycle:

$$Pr = m_{E2} \frac{(1 - \varepsilon_{Total}) c_{B,E2}}{\varepsilon_{Total} c_{B,F1}} = H_B \frac{(\alpha_{B,C} - 1)(1 - \frac{1}{\alpha_{A,B}})}{(\alpha_{B,C} - \frac{1}{\alpha_{A,B}})} \frac{(1 - \varepsilon_{Total})}{\varepsilon_{Total}} \quad 5-49$$

Thus demonstrating that, at the HP point, both system configurations perform equally well in terms of productivity.

Equation 5-49 is plotted against a range of different selectivity factors in Figure 5-9. It is possible to see that higher H_B values lead to higher productivities and the higher the selectivity factors are the higher the productivity is.

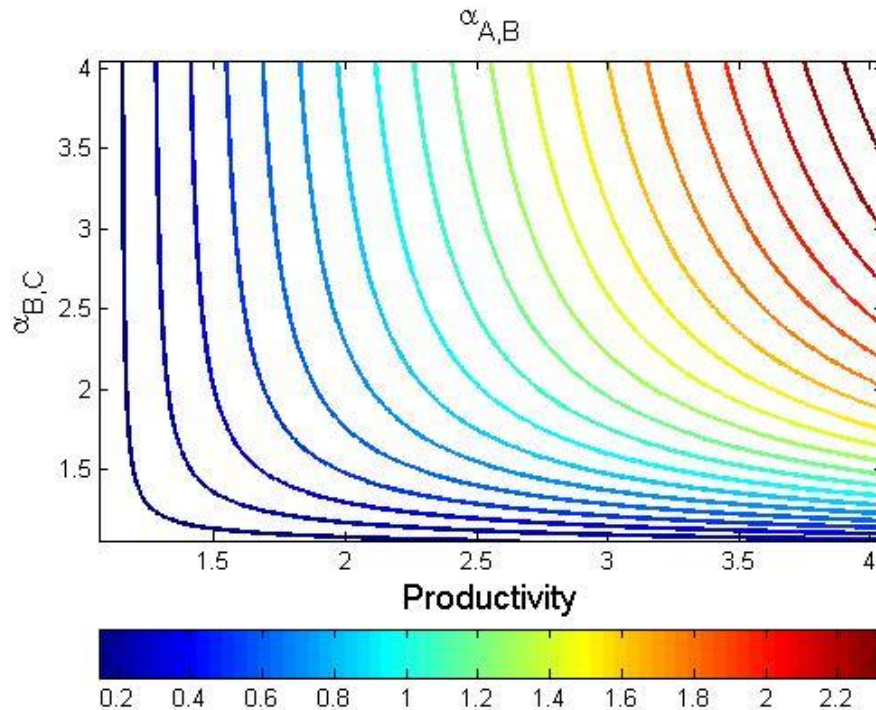


Figure 5-9 – 8-zone TMB Productivity at the HP point calculated using equation 5-49. It can be seen that the higher the selectivity factors and H_B are, the higher the productivity becomes.

For the 8-zone TMB with extract recycle, the total specific solvent consumption (TSSC) is equal to:

$$TSSC = SC_E = \dot{V}_s(m_{I(2)} - m_{IV(1)} + m_{I(1)} - m_{IV(2)} + m_{III(1)} - m_{II(1)}) = \dot{V}_s(2H_C - 2H_A) \quad 5-50$$

and, for the 8-zone TMB with raffinate recycle, it is:

$$TSSC = SC_R = \dot{V}_S(m_{I(2)} - m_{IV(1)} + m_{I(1)} - m_{IV(2)} + m_{III(1)} - m_{II(1)}) = \dot{V}_S(2H_C - 2H_A) \quad 5-51$$

Showing that, at their HP points, solvent consumption is also the same for both configurations.

When 8-zone TMB with raffinate and extract recycle are operated at their HP points, the total solvent consumption is the same, as shown in Figure 5-10. This shows that, at the HP point, productivity is strictly correlated to the total solvent consumption.

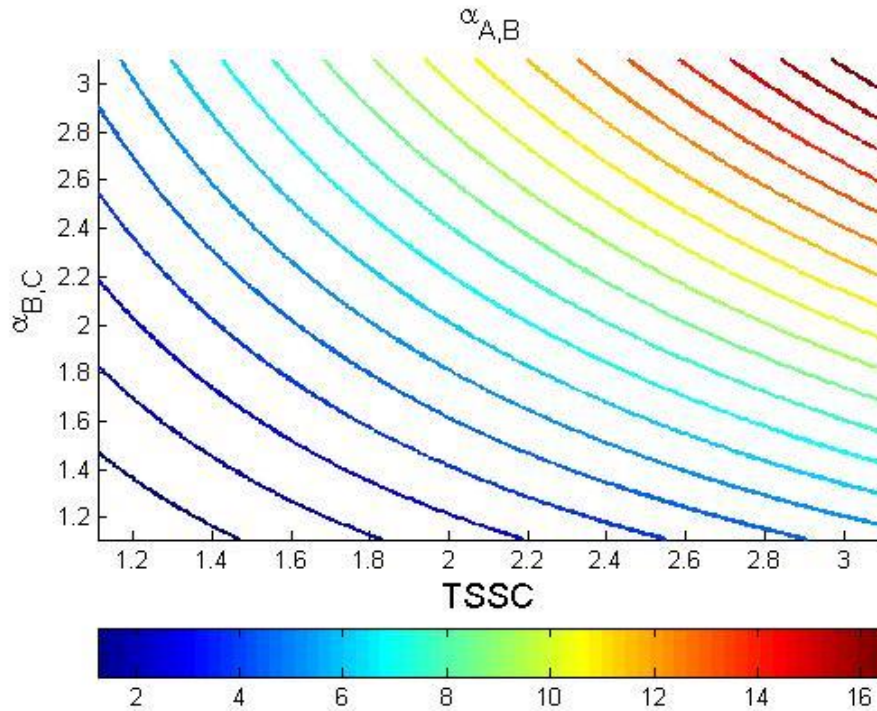


Figure 5-10 – Total specific solvent consumption for 8-zone TMB at the HP point. The plot was generated using equation 5-51. The larger the selectivity factors and H_B are, the larger the solvent consumption is.

5.5. Operating guidelines for 8-zone TMB

With the solutions found in section 5.4, it is possible to find the operating point between the HR and the HP points for both 8-zone TMB with extract and raffinate recycle, which corresponds to the highest profit rate, as a function of the adsorption Henry coefficients and the cost factors of the process. With this information at hand, it is possible to compare extract and raffinate recycle in order to decide which one is more profitable. For that, a useful concept is the profit differential, which is analogous to the differential cost concept commonly used in Economy for the comparison of different investment options. It is

defined here as the sign of the difference between the profit achievable by 8-zone TMB with extract recycle and its raffinate recycle counterpart:

$$\text{sgn}(\Delta_{profit}) = \text{sgn}(P_{Extract\ recycle} - P_{Raffinate\ recycle}) = \begin{cases} +1 & \text{if } \Delta_{profit} > 0 \\ 0 & \text{if } \Delta_{profit} = 0 \\ -1 & \text{if } \Delta_{profit} < 0 \end{cases} \quad 5-52$$

This allows the removal of all fixed costs as well as the process scale factors from the comparison, since they are the same for both system configurations.

Since profit was already defined in equation 5-22, all of its variables were defined by equations 5-27 to 5-29, and, 5-35 to 5-38, and, all constants were defined in equations 5-23 to 5-25 and in Table 5-2, it is possible to analyze the sign of the profit differential as a function of selectivity factors and cost contributions.

By doing the proper substitutions, equation 5-52 becomes:

$$\begin{aligned} \text{sgn}(\Delta_{profit}) = \text{sgn} & \left(\frac{(H_C - H_B)(H_B - M_E)}{(H_C - M_E)} - \frac{(H_B - H_A)(M_R - H_B)}{(M_R - H_A)} \right. \\ & + \text{SCR}(M_R + M_E - H_C - H_A) + \text{SRCR}(2H_B - H_C - H_A) \\ & \left. + \text{FCR}(M_R + M_E - 2H_B) \right) \end{aligned} \quad 5-53$$

Using equations 5-32 and 5-40 to define optimal values for M_E and M_R , respectively, yields:

$$\begin{aligned} \text{sgn}(\Delta_{profit}) = \text{sgn} & \left(\frac{(H_C - H_B) \left(H_B - H_C + \frac{(H_C - H_B)}{\sqrt{\text{SCR} + \text{FCR}}} \right)}{\left(H_C - H_C + \frac{(H_C - H_B)}{\sqrt{\text{SCR} + \text{FCR}}} \right)} \right. \\ & - \frac{(H_B - H_A) \left(H_A + \frac{(H_B - H_A)}{\sqrt{\text{SCR} + \text{FCR}}} - H_B \right)}{\left(H_A + \frac{(H_B - H_A)}{\sqrt{\text{SCR} + \text{FCR}}} - H_A \right)} \\ & + \text{SCR} \left(H_A + \frac{(H_B - H_A)}{\sqrt{\text{SCR} + \text{FCR}}} + H_C - \frac{(H_C - H_B)}{\sqrt{\text{SCR} + \text{FCR}}} - H_C - H_A \right) \\ & + \text{SRCR}(2H_B - H_C - H_A) \\ & \left. + \text{FCR} \left(H_A + \frac{(H_B - H_A)}{\sqrt{\text{SCR} + \text{FCR}}} + H_C - \frac{(H_C - H_B)}{\sqrt{\text{SCR} + \text{FCR}}} - 2H_B \right) \right) \end{aligned} \quad 5-54$$

After all the necessary algebra, equation 5-54 can be rewritten as:

$$\text{sgn}(\Delta_{profit}) = \text{sgn} \left((2H_B - H_A - H_C) \left(1 - \frac{(\sqrt{\text{SCR} + \text{FCR}} - 1)^2}{\text{SCR} + \text{SRCR}} \right) \right) \quad 5-55$$

which can be divided by $H_A\alpha_{A,B}$ (with no change of sign, since $H_A\alpha_{A,B}$ is always a positive number) and rearranged to yield:

$$\text{sgn}(\Delta_{\text{profit}}) = \text{sgn}\left(2 - \frac{1}{\alpha_{A,B}} - \alpha_{B,C}\right) \times \text{sgn}\left(1 - \frac{1 + FCR - SRCR}{2\sqrt{SCR + FCR}}\right) \quad 5-56$$

This expression shows the dependency of the sign of the profit differential on five dimensionless constants. These constants can be grouped in two categories:

1. Two thermodynamic constants (that is, the selectivity factors) that depend solely on the physicochemical characteristics of the process, (such as the solvent and solid phase composition, temperature, and, pressure).

2. Three economic factors (SCR , FCR and $SRCR$) that lump all cost contributions to the economics of the process.

It is possible to analyze the sign of each of the two factors in the left side of this expression separately and conclude, from the sign operation, when the profit differential is positive, negative or zero.

If inequations 5-42 are true, the HP point is chosen for both system configurations and the profit differential can also be used to compare the profit achievable by 8-zone TMB with extract and with raffinate recycle.

At this point $M_E=H_A$ and $M_R=H_C$ and equation 5-53 becomes:

$$\text{sgn}(\Delta_{\text{profit}}) = \text{sgn}\left(2 - \frac{1}{\alpha_{A,B}} - \alpha_{B,C}\right) \times \text{sgn}\left(1 - \frac{FCR}{SRCR}\right) \quad 5-57$$

As expected, this expression does not depend on product and solvent prices, since at the HP point, both productivity and solvent consumption are the same for the two system configurations (as shown in section 5.4). It is also separated into two factors, one which sign is dependent on the selectivity factors and another one which sign depends on the cost contributions.

The decision tree shown in Figure 5-11 comprehensively organizes all the information gathered so far to help direct the choice between the two configurations.

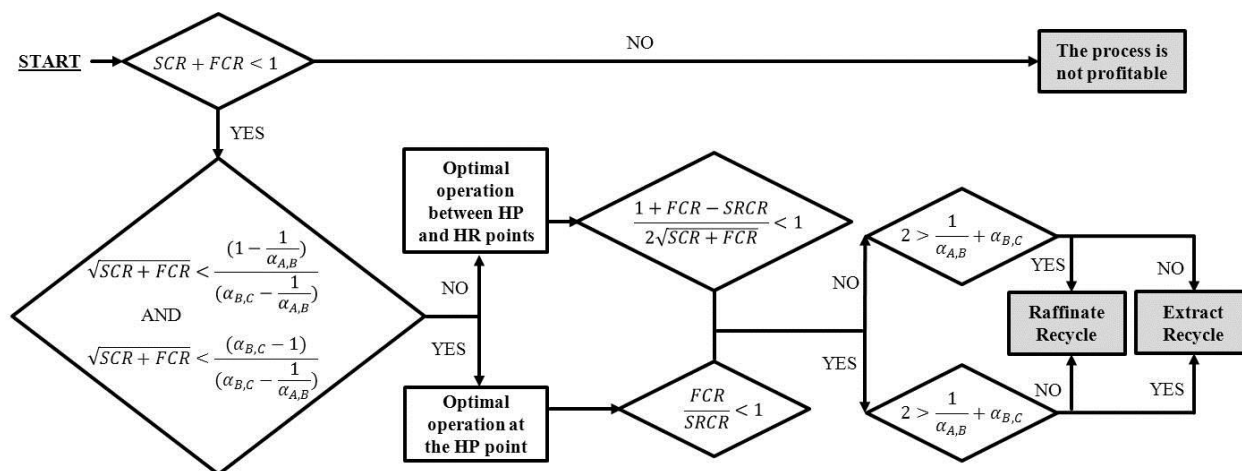


Figure 5-11 – Decision tree for the 8-zone TMB configuration. Initially, it is evaluated whether the separation is profitable or not by comparing the product price to the added costs of crude feed and fresh solvent. Then, inequations 5-42 (in the largest rhombus) are used to evaluate if the optimal operating point is at the HP (highest productivity) point or not, in order to choose which expression for the profit differential (5-56 or 5-57) is the most appropriate. In order for the optimal operating point to be between the HP and the HR points, both expressions shown in the largest rhombus have to be violated, and for it to be at the HP point, both have to be respected. The last two steps consist in calculating the sign of the profit differential to decide which of the two configurations is the most profitable.

5.6. Discussion and outlook

The results presented in Figure 5-11 show that for 8-zone TMB operated at the HP point, when solvent removal costs have a higher impact on the economics of the process than crude feed costs, the choice between raffinate and extract recycle is done on the basis of product concentration (Figure 5-7), while at the opposite situation, the choice between the two system configurations is done on the basis of recovery yield. When these two cost contributions are the same, both configurations perform equally well in terms of economics for any selectivity factors, because profit gains from increased recoveries are compensated by profit losses in increased product dilution and the other way around for any selectivity factors. In a similar way, when the difference between H_C and H_B and between H_B and H_A is the same, Δ_{profit} is also zero. This means that, in this case, none of the cost contributions plays any role in the choice of system configuration because they perform equally well.

For points between the HR and HP points and when $1/\alpha_{A,B} + \alpha_{B,C} < 2$ increased solvent costs generally make extract recycle a better option, since, in this case, solvent consumption is different for the two configurations. When these costs are reduced, the recycle of raffinate becomes the most favorable option. Conversely, these conclusions are inverted when $1/\alpha_{A,B} + \alpha_{B,C} > 2$.

Regardless if the best economic performances are found at the HP point or not, when costs associated with removal of solvent are high and $1/\alpha_{A,B} + \alpha_{B,C} < 2$, extract recycle is generally a better option. The opposite is true when $1/\alpha_{A,B} + \alpha_{B,C} > 2$.

In any case, the relative position of the selectivity factors with relation to the line defined by $\alpha_{B,C} = 2 - 1/\alpha_{A,B}$ is a critical element for the decision of which separation should be performed in the first subunit. This is mathematically equivalent to the comparison between $(H_C - H_B)$ and $(H_B - H_A)$ suggested by Nicolaos et al. [3] for other TMB configurations also aiming at ternary separations. However, in the case of the 8-zone TMB, the classic heuristics: “It is better to perform the easier separation first” is oversimplifying, since the ideal split sequence is just as much a function of process economics as it is of the adsorption Henry coefficients, as already reported by Kessler and Seidel-Morgenstern [7]. In effect, if, for example, crude feed costs dominate the process economics and solvent purchase and removal costs can be neglected (which might apply for natural extracts and products of expensive reactions, for example), recovery yield and productivity outweigh solvent consumption and product dilution as performance indicators. This causes the second factor in expressions 5-56 and 5-57 to simplify to functions that can only assume negative values, which means that, in this case, the hardest separation ought to be performed first.

Figure 5-11 covers nearly all possible separation problems; however, there is a space that has been neglected so far. When either

$$\frac{(1 - \frac{1}{\alpha_{A,B}})}{(\alpha_{B,C} - \frac{1}{\alpha_{A,B}})} < \sqrt{SCR + FCR} < \frac{(\alpha_{B,C} - 1)}{(\alpha_{B,C} - \frac{1}{\alpha_{A,B}})} \quad \text{or} \quad \frac{(\alpha_{B,C} - 1)}{(\alpha_{B,C} - \frac{1}{\alpha_{A,B}})} < \sqrt{SCR + FCR} < \frac{(1 - \frac{1}{\alpha_{A,B}})}{(\alpha_{B,C} - \frac{1}{\alpha_{A,B}})} \quad 5-58$$

The decision tree shown in Figure 5-11 does not apply. However, the decision between raffinate and extract recycle based on equation 5-53 is still valid. This means that the sign of the profit differential can still be used for this purpose. Unfortunately, in this space, equation 5-53 cannot be factorized into two factors (comprising respectively cost contributions and selectivity factors) as was done in section 5.5. Therefore, equation 5-53 must be solved on a case by case basis in order to determine which of the two system configurations performs the best.

Finally, as already argued in section 5.4, when $SCR + FCR > 1$ the whole economics of the process is in trouble. When this sum is larger than one, the specific product selling price is lower than the sum of the specific costs of crude feed and solvent. This means that the sign of the profit function is negative.

Although the results obtained in this section apply, by definition, to TMB, and not necessarily to an equivalent SMB process, TMB and SMB share many similarities [179, 183, 184]. Thus, the decision tree shown in Figure 5-11 can be, if not an ultimate guide for the question of which separation to perform first, at least a reasonable first guess. This is especially true if $(H_C - H_B)$ and $(H_B - H_A)$ do not have similar values. Lastly, it is important to highlight that the decision about which separation to perform first, the easy or the harder one, is also encountered in other continuous equilibrium staged separations such as extraction, crystallization and distillation [185, 186].

5.7. Conclusions

The results obtained in this chapter were derived using the True Moving Bed analogy as a framework for predicting the operating parameter space of 8-zone SMB and for calculating its outlet concentrations. Novel analytical expressions were developed for the estimation of outlet concentrations (equations 5-18 and 5-20), which were then combined with economic information to find the best operating conditions of the process and to maximize its profitability. Subsequently, by comparing the potential profitability of the competing extract and raffinate recycle configurations, it was possible to create a decision tree (Figure 5-11) for the selection of the configuration, which was published in the Journal of Chromatography A [172]. It has been, however, observed that the 8-zone SMB process is not always well described by its geometrically equivalent TMB [3, 6]. Therefore, in the next chapter, a detailed study of the cyclic steady state of 8-zone SMB applying the method of characteristics will be used to more accurately predict its operating regions.

6. Operating regions of 8-zone SMB

In chapter 5 it was assumed that the performance of the physically feasible integrated 8-zone Simulated Moving Bed (SMB) can be well approximated by a theoretical 8-zone True Moving Bed (TMB) analog. There have been, however, indications that the performance of these two processes can, in some cases, significantly differ [5, 9]. In this chapter, the method of characteristics [157] was used to predict the cyclic steady state of both 8-zone SMB with extract and raffinate recycle to demonstrate how dynamic effects cause product recovery yields to be higher than what is expected using the TMB analogy. The goal was to derive more accurate predictions of the 8-zone SMB operating limits, which should ultimately help to highlight the differences between the performance of an integrated 8-zone SMB and that of two independently operated 4-zone SMB units.

6.1. Operating regions of 8-zone SMB with 8 columns

As explained in session 3.2, as long as the net adsorbent and solvent flow rates of a SMB and of a similar TMB unit are the same, i.e. equation 3-12 is satisfied in all of the zones, the net mass flow directions of the solutes should be the same. Therefore, it should be possible to predict the operating parameter spaces (or triangles) of the dimensionless flow rates in a SMB unit using the much simpler TMB analog, as first suggested by Storti et al. [13]. In chapter 5, the TMB analogy was used for predicting the operating parameter spaces of 8-zone SMB with raffinate and with extract recycle considering linear adsorption isotherms, in order to extend on the work of Nicolaos et al. [3]. It has been, however, noticed in the works of J. Nowak et al. [8, 9] and G. Agrawal et al. [5, 6] that the separation performance of 8-zone SMB is, often, better than what would be expected based on the triangle theory. This difference, however, has neither been explained nor modeled.

The TMB has historically been assumed to have a higher separation driving force than a similar SMB, since the solvent and the adsorbent are in true countercurrent movement with respect to each other. The SMB, on the other hand, does not provide a real countercurrent flow between the liquid and the solid phases (albeit a simulated one does take place). The result of that is that the quality of the separation provided by a TMB system with a given

number of plates is normally expected to be higher than the one provided by a SMB [83] and, therefore, TMB has usually been considered an idealized version of SMB. This difference, however, tends to disappear as the number of plates is very high.

Based on simulation studies using the mixing cell model, it will be shown, in this chapter, that the target solute recovery yield is, rather counterintuitively, lower in an 8-zone TMB than in an 8-zone SMB unit operated with the same dimensionless flow rates (m_k). Hence, the application of the triangle theory results in a consistent underestimation of the achievable performance of 8-zone SMB, since the operating parameter spaces are predicted based on the TMB analog.

In the present chapter, the difference between the outlet concentrations of the target solute predicted for an 8-zone TMB unit (with *continuous* adsorbent flow) and for an 8-zone SMB unit (with *discontinuous* adsorbent flow) operated with the same dimensionless flow rates is explained using the method of characteristics [157].

In the case of the SMB process, the dimensionless flow rates (m_k) can be calculated by reformulating equation 3-12, according to [13]:

$$m_k = \frac{\varepsilon}{1 - \varepsilon} \left(\frac{v_k t^*}{L} - 1 \right) \quad 6-1$$

Where L is the length of the column, v_k is the velocity of a non-retained solute or solvent and t^* is the switch time interval.

6.1.1. Extract recycle 8-zone SMB with 8 columns

As a starting point, the dimensionless flow rate operating ranges of an 8-zone TMB unit necessary for isolating the target intermediary eluting solute c from a mixture containing the five solutes a , b , c , d , and e (such as the one shown in Figure 6-1), where all of them adsorb according to linear adsorption isotherms (and $H_a < H_b < H_c < H_d < H_e$, as shown in Table 6-1), are predicted using the TMB analogy. Since all of the adsorption isotherms considered in this chapter are linear, their migration velocities are independent of the concentrations and, thus, the operating ranges are only defined by the first and last solutes in each fraction. Therefore, there could be more solutes eluting between the solutes a and b (in fraction A) and between the solutes d and e (in fraction C), without changing the operating ranges of the dimensionless flow rates.

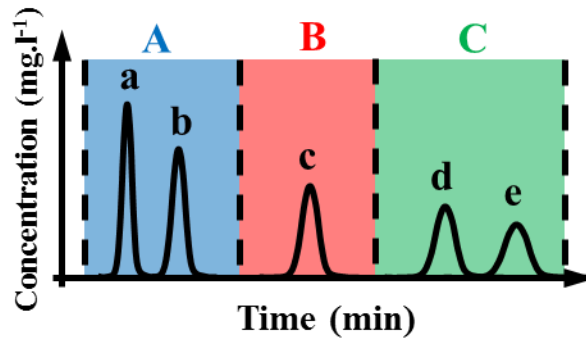


Figure 6-1 - Chromatogram of a hypothetical mixture composed of 3 fractions. The fraction A (solutes a and b, blue) is the first eluting one, the fraction B (the target solute c, red) is the intermediary eluting one and the fraction C (solutes d and e, green) is the last one to elute. Fractions A and C were defined here as having only two solutes, however, since the adsorption isotherms of all solutes in this example are considered to be linear, it is possible to conceive more solutes eluting between the solutes a and b (in fraction A) and between the solutes d and e (in fraction C), without loss of generality of the tools developed in this chapter.

Solute	Adsorption Henry coefficient (H_i)
a	1.000
b	1.050
c	1.837
d	2.297
e	2.412

Table 6-1 – Arbitrary adsorption Henry coefficients of the solutes “a” and “b” (blue), “c” (red), “d” and “e” (green), shown in Figure 6-1, which are used in this section for illustrating the theoretical results.

According to the triangle theory described in section 3.2, if the ratio of adsorbed and dissolved solute (given by its adsorption Henry coefficient H_i) is higher than the dimensionless flow rate (m_k), the solute net flow rate has the direction of the adsorbent flow, and the other way around, when $H_i < m_k$. Therefore, in order to obtain the pure solute c from the mixture shown in Figure 6-1 using 8-zone TMB with extract recycle (Figure 2-7), the following dimensionless flow rate constraints must be respected:

$$\left\{ \begin{array}{l} m_{IV(2)} < H_c \\ m_{IV(1)} < H_a \\ m_{I(2)} > H_e \\ m_{I(1)} > H_e \\ H_c < m_{II(2)} < m_{III(2)} < H_d \\ H_b < m_{II(1)} < m_{III(1)} < H_c \end{array} \right. \quad 6-2$$

Since the first extract stream is completely recycled into the second subunit, it follows that:

$$m_{II(2)} = m_{III(2)} + m_{II(1)} - m_{I(1)} \quad 6-3$$

However, as explained in the section 5.1, since $m_{III(2)} > H_c$, $m_{II(1)} < H_c$, and, $m_{I(1)} > H_c$, there is no way $m_{II(2)}$ can be larger than H_c , so in order for solute c to be pure in the second raffinate port, $m_{II(2)}$ has to be smaller than H_c and solute c should be lost in the second extract port.

If the second subunit were an independently operated 4-zone SMB (but with the same switching interval as the first one), that would mean that it is not possible to obtain pure raffinate from it. However, inside an 8-zone SMB, the recycled stream is directly fed into the second subunit and, since the solutes being recycled have different retention times, they enter the second subunit “pre-separated”, which facilitates the separation in the second subunit. That means that the solute c is not fed to the second subunit during the entire switching interval, as it would be the case of a second independently operated 4-zone SMB unit, where the feed composition would be constant.

It is possible to use the type of plot shown in Figure 3-2, to visualize the characteristics [157] of the solutes inside the system as a function of the process parameters. Figure 6-2 shows the cyclic steady state positions of the characteristics of an extract recycle 8-zone SMB unit with one column per zone operated at the dimensionless flow rates and the porosity listed in Table 6-2 considering the adsorption Henry coefficients listed in Table 6-1, for illustration

$m_{I(2)}$	$m_{II(2)}$	$m_{III(2)}$	$m_{IV(2)}$	$m_{I(1)}$	$m_{II(1)}$	$m_{III(1)}$	$m_{IV(1)}$	ε
2.653	1.2	2.15	1.67	2.6	1.65	1.75	0.909	0.6

Table 6-2 – Dimensionless flow rates and porosity considered in this section for illustrating the theoretical results

As shown in Figure 6-2, after the valves switch, the rear concentration shock of the solute c enters zone III(2) in the second subunit after a time delay (t_c). After the rear concentration shock of the solute c entered the second subunit, it still has the time left in the switch interval ($t^* - t_c$) to move through the column in zone III(2) before this column is shifted to zone II(2). Therefore, after the next valve switch, the rear concentration shock will already have traveled a distance Δ_{z2} in the column, and it only needs to go through the remaining distance ($L - \Delta_{z2}$, where L is the length of the column), during the whole next switch interval in order to be completely eluted from the column in zone II(2). As long as the rear concentration shock of the solute c coming from zone II(2) enters zone III(2) before, or

at least at the same time as, the rear concentration shock of the solute c coming from zone I(1), a stable cyclic steady state condition can be created. If, however, the rear concentration shock of the solute c coming from zone II(2) enters zone III(2) after the one coming from zone I(1), there would still be solute c left inside the column in zone II(2) at the switch time, which would cause the solute c to be lost as a contamination in the second extract port.

The minimum dimensionless flow rate necessary to wash the solute c from zone II(2) will be represented by $m_{II(2)min}$ and, in order to find it, it is first necessary to find the cyclic steady state conditions. So that the cyclic steady state can exist, the positions of the front and rear concentration shocks of any solute in the end of a switch interval must be the same as the positions where they start the next switch interval shifted one zone to the left, so that after one more switch interval they can be again in the same starting positions.

Although, in theory, starting with a SMB unit equilibrated with pure solvent, it would take an infinite time to reach a perfect cyclic steady state, after a dozen cycles or so, the approximate positions of characteristics differ so little from the cyclic steady state ones, that they can be considered at cyclic steady state.

For the solute c , this means that the distance between its rear concentration shock and the end of zone II(1) (Δ_{z1}) in the end of a switch interval must be the same as its distance to the end of zone I(1) in the beginning of the next switch interval. Analogous conditions can also be defined for the concentration shocks of all other solutes in the other zones, but since they are already well understood they will not be discussed here (for a more detailed description, the reader is invited to refer to the work of A. Rajendran [187]).

The rear concentration shock of the solute c enters zone II(1) at a time t_c that allows these two distances to be equal. Therefore, this distance is defined by:

$$\frac{L - \Delta_{z1}}{v_{c,II(1)}} = t^* - \frac{\Delta_{z1}}{v_{c,I(1)}} \quad 6-4$$

where $v_{c,I(1)}$ and $v_{c,II(1)}$ are the velocities of the rear concentration shocks of the solute c in zone I(1) and in zone II(1), respectively, and t_c is given by:

$$t_c = \frac{\Delta_{z1}}{v_{c,I(1)}} \quad 6-5$$

The cyclic steady state is defined by one more condition, i.e., it is necessary that the rear concentration shock of the solute c entering zone III(2) come from zone II(2) in a time equal or smaller than t_c , otherwise solute c will accumulate in zone II(2) and contaminate the extract port.

Since the lowest allowable flow rate in zone II(2) is defined, at the limiting case, when the value chosen for $m_{II(2)}$ causes the rear concentration shock of solute c coming from zone II(2) to enter zone III(2) at exactly the same time as the rear concentration shock of solute c coming from the recycle line, any $m_{II(2)}$ larger than that will also allow a complete recovery yield of the solute c.

Based on the flow rate in zone III(2) and on t_c , Δz_2 can be found:

$$\Delta z_2 = v_{c,III(2)}(t^* - t_c) \quad 6-6$$

and the corresponding minimum $v_{c,II(2)}$ is:

$$v_{c,II(2),min} = \frac{L - \Delta z_2}{t_c} \quad 6-7$$

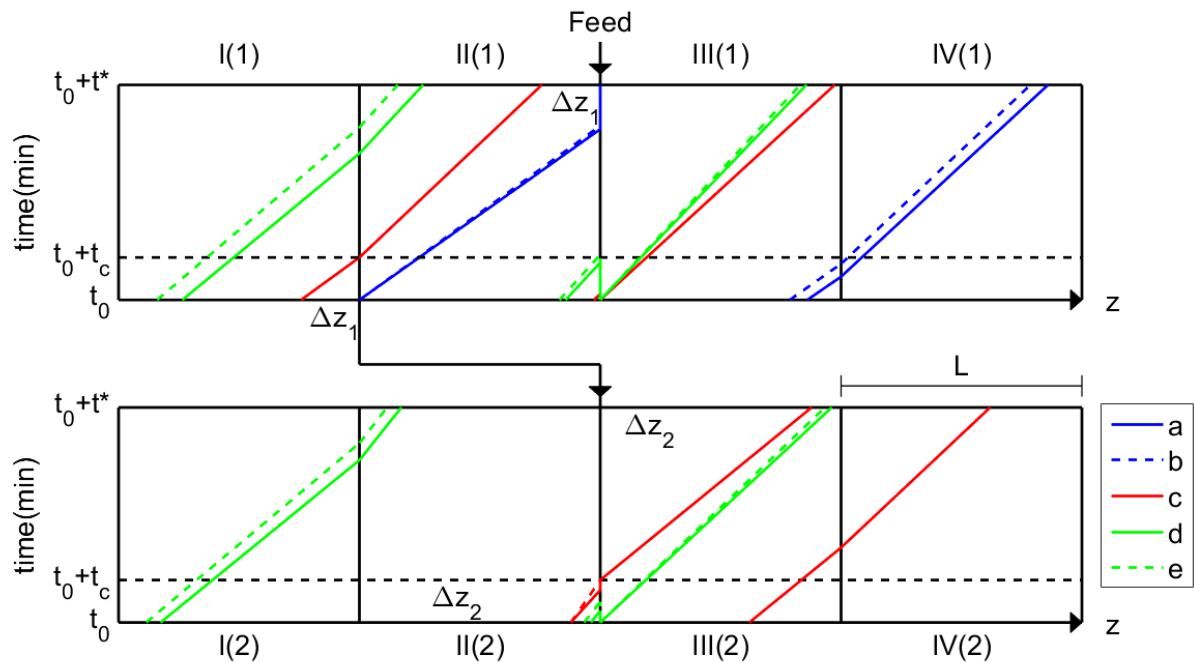


Figure 6-2 – Positions of the front and rear concentration shocks (characteristics) of the solutes a, b, c, d, and, e inside an extract recycle 8-zone SMB with one column per zone after the cyclic steady state is reached. The calculations were performed using MATLAB R2015b considering the adsorption Henry coefficients listed in Table 6-1 and the dimensionless flow rates and porosity listed in Table 6-2. The red dashed lines represents the limiting case of $m_{II(2)} = m_{II(2),min}$. The continuous red lines show the characteristics obtained considering the given $m_{II(2)}$.

From equations 6-5, 6-6 and 6-7, the derivation of the minimum $m_{II(2)}$ was done using the expression for the velocity of the rear and front concentration shocks of the solute c (equation 6-1):

$$m_{II(2),min} = m_{III(2)} - \frac{(m_{I(1)} - m_{II(1)})(m_{III(2)} - H_c)}{(H_c - m_{II(1)})} \quad 6-8$$

and, since $m_{III(2)} = m_{I(1)} + m_{II(2)} - m_{II(1)}$,

$$m_{II(2),min} = 2H_c - m_{I(1)} \tag{6-9}$$

Hence, the left border of the triangle referring to the operation of the second subunit is defined by equation 6-9, not by H_c , as previously considered in the TMB analogy (shown in the set of inequations 6-2).

Since $m_{I(1)}$ needs to be larger than H_e for a successful isolation of the target solute c (see the set of inequations 6-2) and, by definition, H_e is larger than H_c , the value of $m_{II(2),min}$ is always smaller than H_c . Therefore, the parameter space of the second subunit of an 8-zone SMB unit with extract recycle is always larger than that of an equivalent 8-zone TMB.

Furthermore, since $m_{II(2)}$ cannot be smaller than $2H_c + m_{I(1)}$, it follows that $m_{III(2)} - m_{I(1)} + m_{II(1)}$ also cannot be smaller than that. Rearranging the terms, it follows that:

$$m_{II(1),min} = 2H_c - m_{III(2)} \tag{6-10}$$

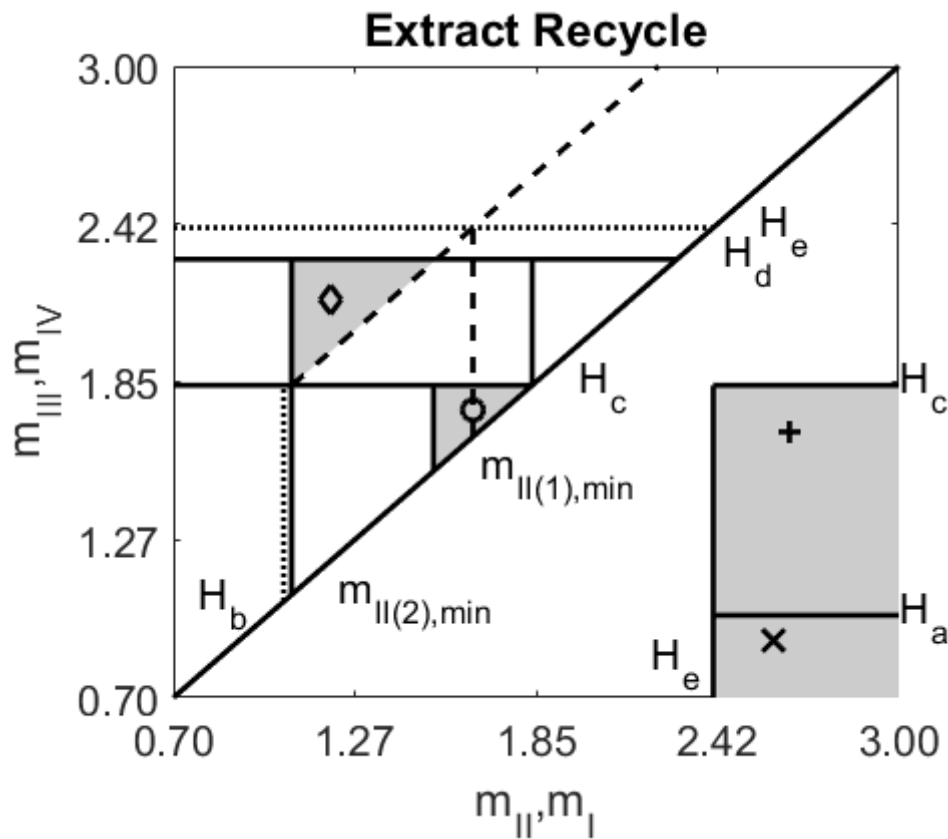


Figure 6-3 – Operating regions (grey areas) for the first and second subunits of 8-zone SMB with extract recycle where complete recovery yield of the solute c is expected. The vertical dotted line shows the potential left border for the first subunit’s triangle (H_b), which (in this case) is ignored, since $2H_c - m_{III(2)} > H_b$. The coordinates of $(m_{II(2)}, m_{III(2)})$ are given by the diamond, the coordinates of $(m_{II(1)}, m_{III(1)})$ are given by the circle, the coordinates of $(m_{I(1)}, m_{IV(1)})$ are given by the “x”, and, the coordinates of $(m_{I(2)}, m_{IV(2)})$ are given by the cross. The calculations were performed using MATLAB R2015b considering the adsorption Henry coefficients listed in Table 6-1 and the dimensionless flow rates and porosity listed in Table 6-2.

Thus, the left border of the triangle referring to the operation of the first subunit must also be redefined. This is only necessary, of course, only in case $2H_c - m_{III(2)}$ is larger than H_b (the original left border of this triangle), otherwise, the original definition of the left border supersedes the new one and is, therefore, kept.

Considering the arbitrary adsorption Henry coefficients listed in Table 6-1 and the dimensionless flow rates and porosity listed in Table 6-2, the operating ranges of 8-zone SMB with extract recycle predicted using the set of inequations 6-2 corrected by the equations 6-9 and 6-10 are shown in Figure 6-3.

Figure 6-4 a) shows the dimensionless internal concentration profiles of the solutes in an 8-zone TMB with extract recycle operated at the points indicated in Figure 6-3 calculated using the mixing cell model described in section 3.4 considering 1000 mixing cells per zone. Figure 6-4 b) shows the dimensionless internal concentration profiles of the equivalent extract recycle 8-zone SMB with one column per zone averaged over one cycle after cyclic steady state was reached, also operated at the points indicated in Figure 6-3, calculated using the mixing cell model described in section 3.3, using ChromWorksTM 2015 considering 1000 mixing cells per column.

Since the concentration shocks in a SMB system are in constant movement, in order to more clearly compare them to the static TMB concentration profiles, the solute concentrations at each coordinate shown in Figure 6-4 b) were averaged over one switching interval after cyclic steady state was reached. Thereby, the comparison is made easier, since, it is possible to see in the 8-zone SMB plot the regions in the system where the solutes spend most of their residence time.

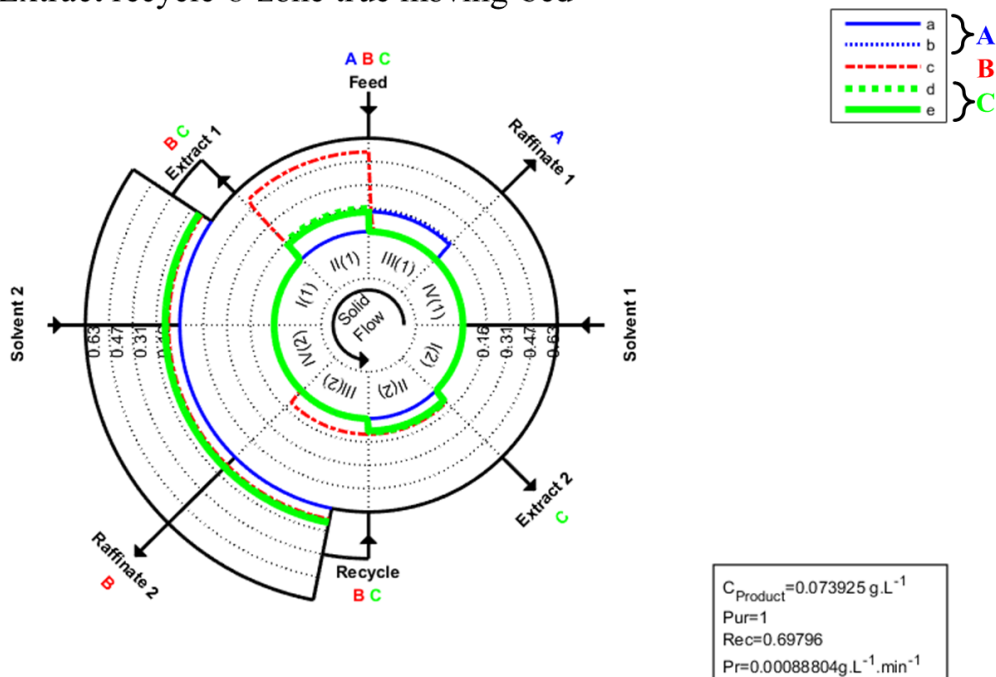
When compared to the TMB, the averaged concentration profiles in an SMB unit are typically bulged in the middle of the zones, since most of the back and forth shifting of the concentration shocks happen on the regions between neighboring zones. However, the average solute concentrations in the outlet ports of the SMB and TMB tend to be very similar, especially if the number of plates in both systems is very high.

It is worth noting by how much the performances of both systems differ, even though the dimensionless flow rates used for both systems are the same and respect the geometric similarity criteria (equation 3-12) explained in section 3.2. The main difference is the recovery yield of the solute c, which, in the case of the TMB is approximately 30% lower than that obtained from the equivalent SMB simulation.

Unlike the average internal concentration profiles in the first subunits of SMB and TMB, which are very similar, the internal concentration plateau of the solute c in the second subunit of the SMB system is much more concentrated in zone II(2) than in the corresponding zone of the second subunit of the 8-zone TMB. The reason for this difference can be seen in Figure 6-2, which shows that, due to the discontinuous feed of solute c into the second subunit through the recycle, the presence of solute c in zone III(2) of the SMB is much smaller than in the TMB scenario, where the second subunit is continuously fed with solute c .

In both the 8-zone SMB and TMB simulations shown in Figure 6-4, $m_{II(2)} = 1.2$, which is smaller than H_c (1.837). Therefore, as shown in Figure 6-4 a), the 8-zone TMB simulation predicts a partial recovery yield (of approximately 70%), which is in agreement with the fact that $m_{II(2)}$ is smaller than H_c and demonstrates the validity of the set of inequations 6-2 for predicting the operating ranges of 8-zone TMB. However, as shown in Figure 6-4 b), the same $m_{II(2)}$ value, when applied to the extract recycle 8-zone SMB with one column per zone, results in a recovery yield of approximately 100%, since this value is larger than the $m_{II(2),min}$ of 1.075, predicted by equation 6-9. Thus, confirming the accuracy of equations 6-9 and 6-10 for predicting the operating ranges of $m_{II(2)}$ and $m_{II(1)}$, respectively, in an 8-zone SMB with extract recycle.

a) Extract recycle 8-zone true moving bed



b) Extract recycle 8-zone simulated moving bed (Cycle 21/Step 1)

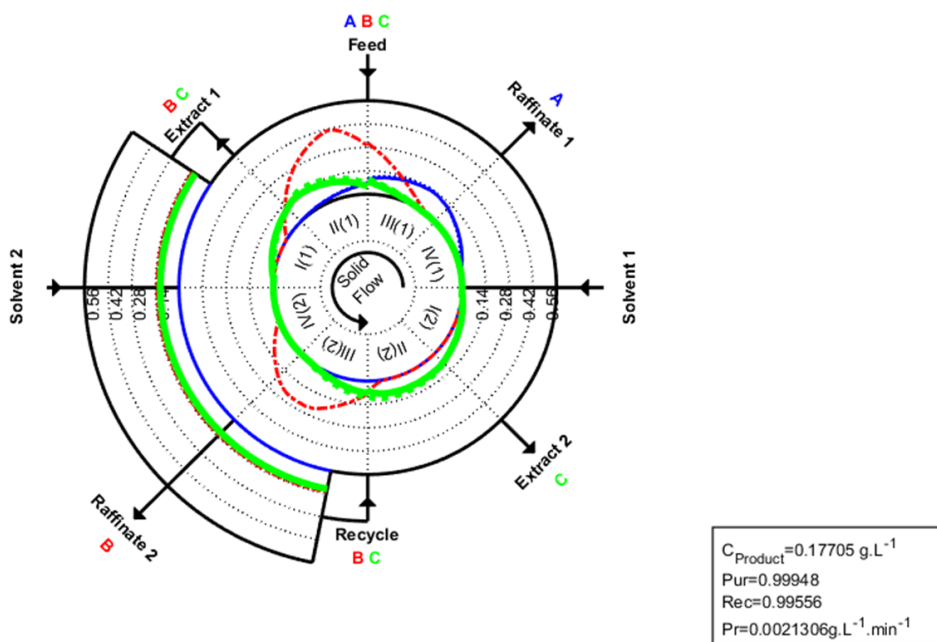


Figure 6-4 - a) Dimensionless concentration (divided by feed concentration) profiles of the solutes a, b, c, d, and, e inside 8-zone TMB with extract recycle calculated using LDU of the mixing cell model performed using MATLAB R2015b. b) Dimensionless concentration profiles inside extract recycle 8-zone SMB with one column per zone averaged over one switch interval after cyclic steady state is reached calculated using ChromWorks™ 2015 considering the mixing cell model. The external section of the circle in both diagrams represents the solute concentrations inside the recycle stream. In both cases, 1000 mixing cells per zone were considered. The adsorption Henry coefficients listed in Table 6-1 and the dimensionless flow rates and porosity listed in Table 6-2 were considered.

The potential interference of diffusion in the comparison between the 8-zone SMB and TMB performances was minimized by using adsorbent beds with a very high plate number in the simulations. In both cases, 1000 mixing cells per zone were considered, which, as far as simulated preparative chromatography is concerned, can be considered nearly ideal adsorbent packed beds [2, 12]. In the absence of any other potentially confounding factors, the difference between the performances predicted by 8-zone SMB with extract recycle and 8-zone TMB with extract recycle can only be well explained by the recycle of a partially pre-separated stream from the first into the second subunit, as explained in this section.

6.1.2. Raffinate recycle 8-zone SMB with 8 columns

In a similar way as described in the section 5.2, according to the triangle theory, in order to obtain pure solute c from the mixture of solutes a, b, c, d, and, e from the mixture containing five solutes shown in Figure 6-1, employing the 8-zone TMB with raffinate recycle (Figure 2-8), the following restrictions on the dimensionless flow rates must be respected:

$$\left\{ \begin{array}{l} m_{IV(2)} < H_a \\ m_{IV(1)} < H_a \\ m_{I(2)} > H_c \\ m_{I(1)} > H_e \\ H_b < m_{II(2)} < m_{III(2)} < H_c \\ H_c < m_{II(1)} < m_{III(1)} < H_d \end{array} \right. \quad 6-11$$

Since the adsorbent flow rate is the same for both subunits, and the feed in the second subunit is the raffinate stream of the first subunit, it follows that:

$$m_{II(2)} = m_{III(2)} + m_{II(1)} - m_{I(1)} \quad 6-12$$

Typically, in an 8-zone SMB with raffinate recycle, $m_{III(2)}$ is larger than H_c , and, therefore, it would not be expected that the raffinate stream would be pure based on the TMB analogy (as explained in section 5.2). This would be true if the second subunit were an independently operated 4-zone SMB, for example. However, as shown in Figure 6-5 for example, a cyclic steady state condition where the target solute c is not lost in the second raffinate port can be achieved in a raffinate recycle 8-zone SMB unit with one column per zone operated at the dimensionless flow rates and the porosity listed in Table 6-4 considering the adsorption Henry coefficients listed in Table 6-3.

Solute	Adsorption Henry coefficient (H_i)
a	1.000
b	1.050
c	1.575
d	2.362
e	2.481

Table 6-3 – Arbitrary adsorption Henry coefficients of the solutes “a” and “b” (blue), “c” (red), “d” and “e” (green), shown in Figure 6-1, which are used in this section for illustrating the theoretical results.

$m_{I(2)}$	$m_{II(2)}$	$m_{III(2)}$	$m_{IV(2)}$	$m_{I(1)}$	$m_{II(1)}$	$m_{III(1)}$	$m_{IV(1)}$	ε
1.732	1.15	2.2	0.909	2.729	1.7	1.9	0.85	0.6

Table 6-4 – Dimensionless flow rates and porosity considered in this section for illustrating the theoretical results

In the first subunit, when cyclic steady state is reached, the distance between the front concentration shock of the solute c and the beginning of zone IV(1) (Δ_{z1}) in the end of the switch interval must be the same as the distance between the beginning of zone III(1) and the front concentration shock of the solute c in the start of the next switch interval. The distance Δ_{z1} is defined such that:

$$\frac{L - \Delta_{z1}}{v_{c,III(1)}} = t^* - \frac{\Delta_{z1}}{v_{c,IV(1)}} \quad 6-13$$

In the second subunit, when cyclic steady state is reached, the distance Δ_{z2} between the front concentration shock of solute c and the end of zone III(2) in the end of one switch interval is the same as the distance between where this front concentration shock starts the next switch interval and the end of zone II(2).

As shown in Figure 6-5, in an 8-zone SMB with raffinate recycle, the front concentration shock of solute c coming from the recycle line does not enter zone III(2) immediately at the beginning of the switch interval. Instead it only enters after a delay time t_c , given by:

$$t_c = \frac{L - \Delta_{z1}}{v_{c,III(1)}} \quad 6-14$$

The condition for no accumulation of solute c in zone III(2) (and, therefore, pure raffinate) is that $m_{III(2)}$ is such that the front concentration shock of solute c coming from zone II(2) does not enter zone III(2) before the time t_c (when the front concentration shock of solute c coming from the recycle line enters zone III(2)). Any $m_{III(2)}$ lower than that will also allow a pure raffinate stream.

In order to find the maximum $m_{III(2)}$ that allows this to happen, the distance Δz_2 that the front concentration shock of solute c needs to percolate until the end of zone II(2) at cyclic steady state must be found:

$$\Delta z_2 = v_{c,II(2)} t_c \quad 6-15$$

This distance must also be the distance left for the front concentration shock of solute c to reach the end of zone III(2) in the end of a switch interval. This allows the determination of the maximum $v_{c,III(2)}$ that makes it possible:

$$v_{c,III(2),max} = \frac{L - \Delta z_2}{t^* - t_c} \quad 6-16$$

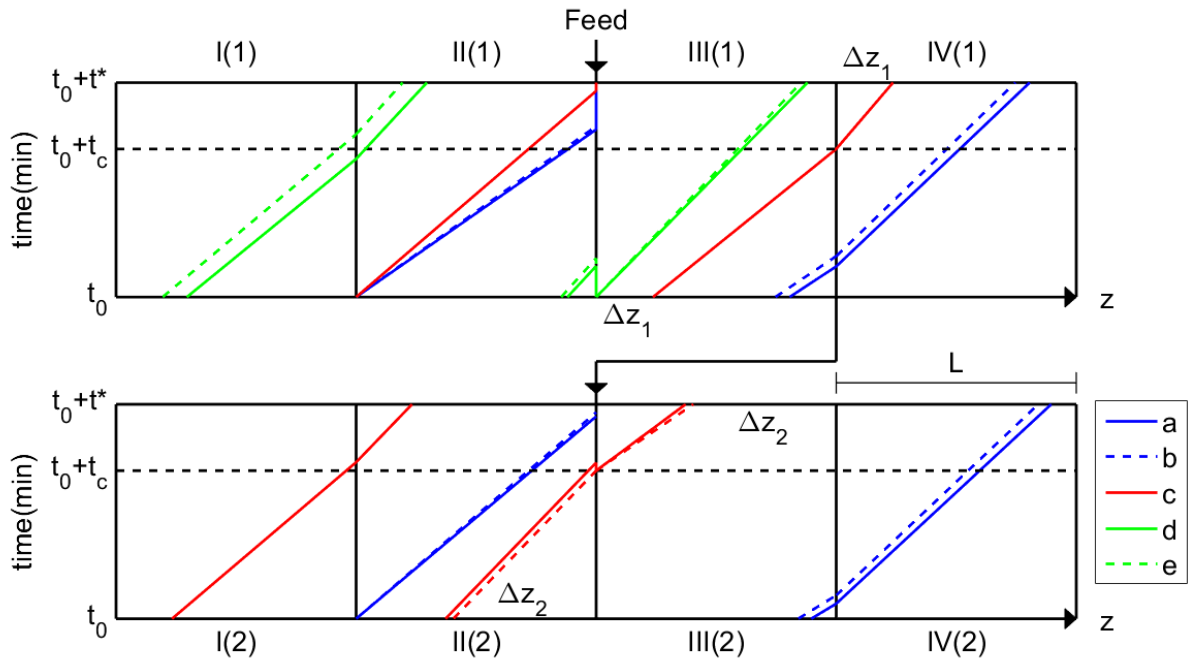


Figure 6-5 – Positions of the front and rear concentration shocks (characteristics) of the solutes a, b, c, d, and, e inside an raffinate recycle 8-zone SMB with one column per zone after the cyclic steady state is reached. The calculations were performed using MATLAB R2015b considering the adsorption Henry coefficients listed in Table 6-3 and the dimensionless flow rates and porosity listed in Table 6-4. The red dashed lines represents the limiting case of $m_{III(2)} = m_{III(2),max}$. The continuous red lines show the characteristics obtained considering the given $m_{III(2)}$.

From which, the determination of the maximum $m_{III(2)}$ follows:

$$m_{III(2),max} = \frac{H_c(m_{III(1)} - m_{IV(1)}) + m_{II(2)}(m_{IV(1)} - H_c)}{(m_{III(1)} - H_c)} \quad 6-17$$

and, since $m_{II(2)} = m_{III(2)} - m_{III(1)} + m_{IV(1)}$,

$$m_{III(2),max} = 2H_c - m_{IV(1)} \quad 6-18$$

Equation 6-18 defines a new upper border for the triangle referring to the operation of the second subunit of 8-zone SMB with raffinate recycle to replace the TMB analogy prediction (H_c), based on the set of inequations 6-11. It is interesting to notice that, since $m_{IV(1)}$ must be smaller than H_a (as shown by the set of inequations 6-11), $m_{III(2),max}$, as defined by equation 6-18, is always larger than H_c , which means that the operating range of $m_{III(2)}$ is effectively larger in an 8-zone SMB compared to that of a similar 8-zone TMB.

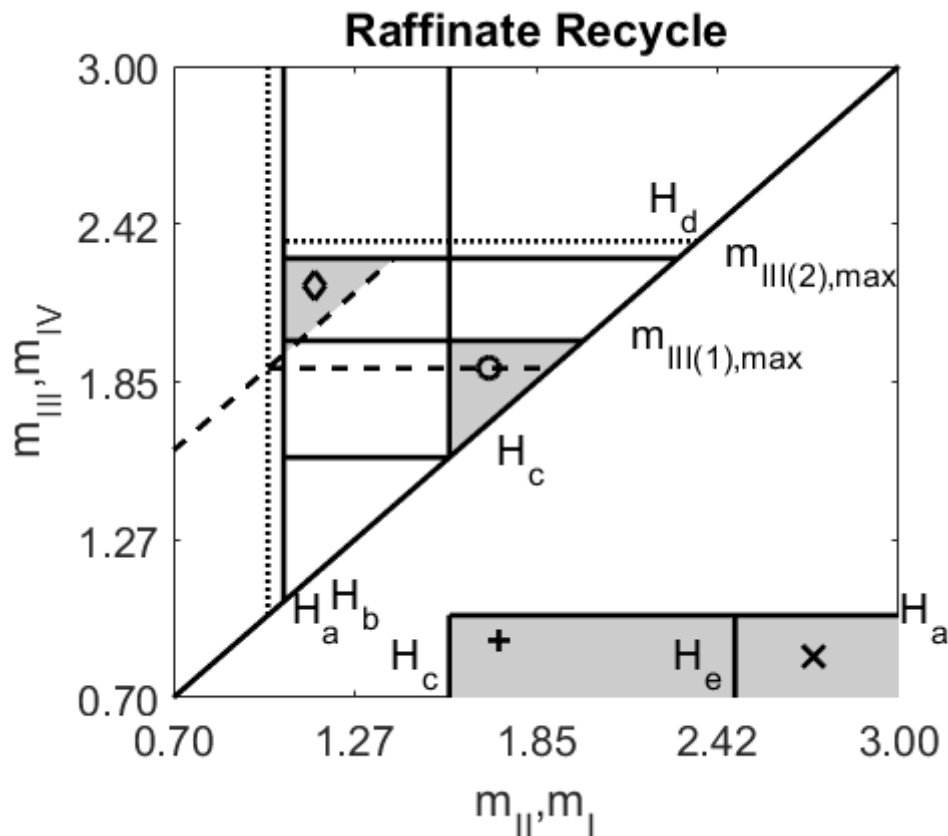


Figure 6-6 – Operating regions (grey areas) for the first and second subunits of 8-zone SMB with raffinate recycle where complete recovery yield of the solute c is expected. The dotted horizontal line shows the potential upper border for the first subunit's triangle (H_d), which (in this case) is ignored, since $2H_c - m_{II(2)} < H_d$. The coordinates of $(m_{II(2)}, m_{III(2)})$ are given by the diamond, the coordinates of $(m_{II(1)}, m_{III(1)})$ are given by the circle, the coordinates of $(m_{I(1)}, m_{IV(1)})$ are given by the "x", and, the coordinates of $(m_{I(2)}, m_{IV(2)})$ are given by the cross. The calculations were performed using MATLAB R2015b considering the adsorption Henry coefficients listed in Table 6-3 and the dimensionless flow rates and porosity listed in Table 6-4.

Since $m_{III(2)} = m_{II(2)} + m_{III(1)} - m_{IV(1)}$, the term $m_{II(2)} + m_{III(1)} - m_{IV(1)}$ also cannot be larger than $2H_c - m_{II(2)}$, which means that the upper border of the triangle defining the operating region of the first subunit also needs to be redefined.

Rearranging the terms yields:

$$m_{III(1),max} = 2H_c - m_{II(2)}$$

Which only needs to be considered when $2H_c - m_{III(2)}$ is smaller than H_d (the *a priori* upper border of the triangle). When that is not the case, it is enough to consider H_d to be the maximum allowed value for $m_{III(1)}$.

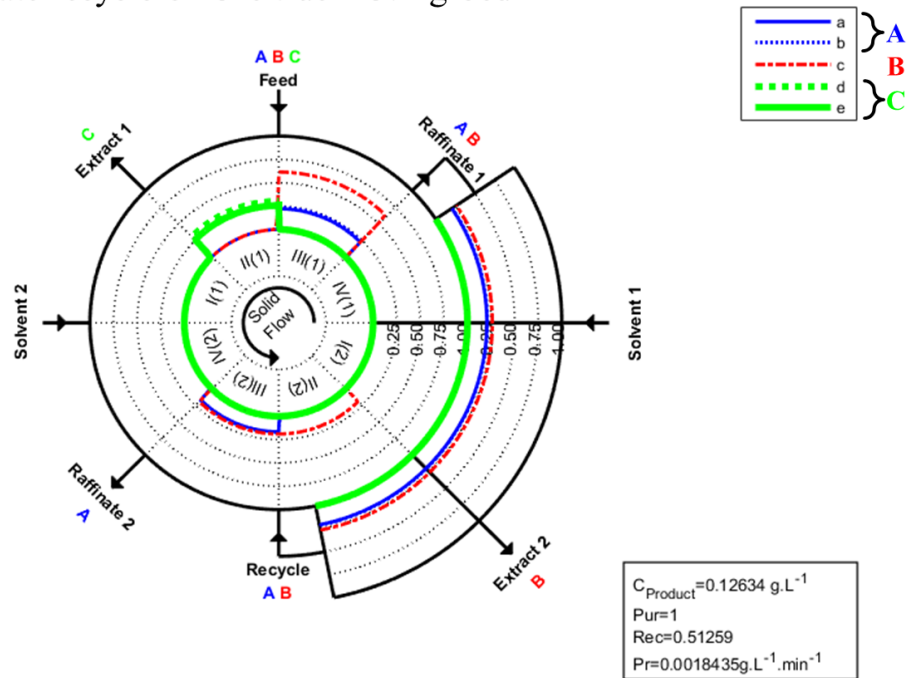
Figure 6-6 shows the operating regions predicted using the set of inequations 6-11 as well as the newly developed equations 6-18 and 6-19 considering the adsorption Henry coefficients listed in Table 6-3 and the dimensionless flow rates and porosity listed in Table 6-4, in order to illustrate the methodology developed.

The dimensionless internal concentration profiles of the solutes a, b, c, d and e are shown in Figure 6-7 a) for the 8-zone TMB with raffinate recycle operated at the points indicated in Figure 6-6 calculated using the mixing cell model described in section 3.4 considering 1000 mixing cells per zone. Figure 6-7 b) shows the dimensionless internal concentration profiles of the equivalent raffinate recycle 8-zone SMB with one column per zone averaged over one cycle after cyclic steady state was reached, also operated at the points indicated in Figure 6-6, calculated using the mixing cell model described in section 3.3, using ChromWorks™ 2015 considering 1000 mixing cells per column.

An analysis of Figure 6-7 a) and b) shows that after cyclic steady state was reached, in the second case, the solute c is much more concentrated in zone II(2) than in the first case, which causes its concentration in the second extract stream to be much higher than in the equivalent 8-zone TMB. This can be interpreted according to Figure 6-5, which shows that the front concentration shock of the solute c does not percolate the column in zone III(2) very far, before this column moves back to zone II(2). This causes the recovery of the target solute c that can be obtained from the 8-zone SMB to be much higher than the one that can be obtained from the TMB. Nonetheless, the performance of the first subunits is, as expected, essentially the same in both the 8-zone TMB and SMB cases.

As shown in Figure 6-7 b), the value chosen for $m_{III(2)}$, 2.2, is smaller than the $m_{III(2),max}$ of 2.3, predicted by equation 6-18. Consequently, the recovery yield predicted by the raffinate recycle 8-zone SMB with one column per zone simulation is approximately 100%. However, when this $m_{III(2)}$ value is applied to the 8-zone TMB (as shown in Figure 6-7a)) the simulation predicts a partial recovery yield of only 51%, which is in agreement with the fact that $m_{III(2)}$ is larger than H_c (around 1.6) and demonstrates the validity of the set of inequations 6-11 for predicting the operating ranges of 8-zone TMB. Additionally, the equations 6-18 and 6-19 are more accurate for predicting the operating ranges of raffinate recycle 8-zone SMB, than the set of inequations 6-11 alone.

a) Raffinate recycle 8-zone true moving bed



b) Raffinate recycle 8-zone simulated moving bed (Cycle 21/Step 1)

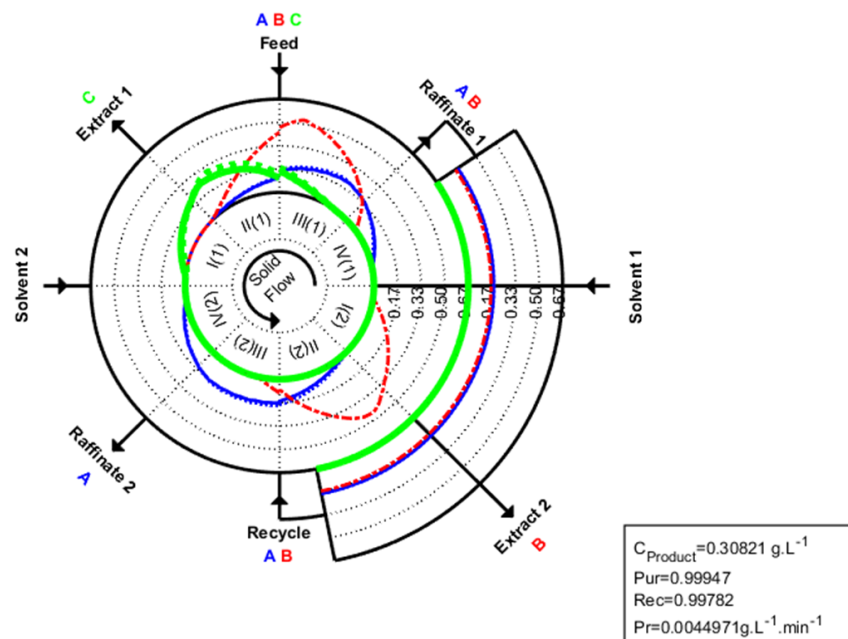


Figure 6-7 – a) Dimensionless concentration (divided by feed concentration) profiles of the solutes a, b, c, d, and e inside 8-zone TMB with raffinate recycle calculated using LDU of the mixing cell model performed using MATLAB R2015b. b) Dimensionless concentration profiles inside 8-zone SMB with raffinate recycle averaged over one switch interval after cyclic steady state is reached calculated using ChromWorks™ 2015 considering the mixing cell model. The external section of the circle in both diagrams represents the solute concentrations inside the recycle stream. In both cases, 1000 mixing cells per zone were considered. The adsorption Henry coefficients listed in Table 6-3 and the dimensionless flow rates and porosity listed in Table 6-4 were considered.

In the examples shown in Figure 6-4 and in Figure 6-7, the number of mixing cells per zone considered for both the 8-zone TMB and the 8-zone SMB simulations was 1000, which can be considered an essentially ideal performance from the adsorbent columns [2, 12]. That said, the difference between the separation performance obtained from the 8-zone TMB and the one obtained from the 8-zone SMB operated at the same flow rate ratios is still very large.

The recovery yield of the solute *c* obtained from the 8-zone SMB was much higher than the one obtained from the 8-zone TMB, both in the case of the extract and raffinate recycle configurations, notwithstanding the fact that the number of theoretical equilibrium plates in the TMB system for the same number of mixing cells per zone is expected to be higher. Given that, in both cases, the packing of the adsorbent beds considered was nearly ideal, the difference between the recovery yield of the target solute *c* obtained from the 8-zone SMB and the one obtained from the 8-zone TMB can only be well justified by the pre-separation of the recycled stream taking place in the first subunit of the 8-zone SMB.

6.2. 8-zone SMB vs. two independent 4-zone SMB units

The main difference between an integrated 8-zone SMB (Figure 2-7 and Figure 2-8) and the competing configuration of a cascade of two independently operated 4-zone SMB units (as the ones shown in Figure 2-6 and in Figure 2-5) is the discontinuity of the feed of the second subunit of the 8-zone SMB. In a cascade of two independently operated 4-zone SMB units, the feed of the second SMB unit is expected to be completely homogeneous, since a buffer tank is normally necessary between both SMB units in order to compensate for the asynchronous switching of the chromatography columns in the two units.

6.2.1. Extract recycle

Considering a 4-zone SMB connected to a second 4-zone SMB by the extract stream shown in Figure 2-5, the first unit can only successfully separate the fraction containing the solutes *c*, *d* and *e* from the hypothetical mixture shown in Figure 6-1, as long as the dimensionless flowrates respect the following inequations:

$$\left\{ \begin{array}{l} m_{IV(1)} < H_a \\ m_{I(1)} > H_e \\ H_b < m_{II(1)} < m_{III(1)} < H_c \end{array} \right. \quad 6-20$$

The optimum operating point of the first unit can be readily identified as the lowest solvent consumption point (LSC) defined by A. Nicolaos et al. [3]. This point lays exactly at the operating limits of the SMB process as explained by the triangle theory: $m_{I(1)} = H_e$, $m_{IV(1)} = H_a$, $m_{II(1)} = H_b$, $m_{III(1)} = H_c$. Under these conditions, the feed flow rate \dot{V}_{F1} can be calculated in a similar way as described by G. Zhong and G. Guiochon [179, 184].

$$\dot{V}_{F1} = \dot{V}_{I(1)} \left(\frac{H_c}{H_e} - \frac{H_b}{H_e} \right) \quad 6-21$$

Since the flow rate in zone I(1) is given by $\dot{V}_{I(1)} = \dot{V}_{S1} H_e$, the adsorbent flow rate \dot{V}_{S1} in the first 4-zone SMB unit can be expressed as a function of the feed flow rate and the adsorption Henry coefficients of the solutes c and b, according to:

$$\dot{V}_{S1} = \frac{\dot{V}_{F1}}{(H_c - H_b)} \quad 6-22$$

In order for the second 4-zone SMB unit to completely separate the target solute c from the fraction containing the solutes d and e without loss or contamination, the dimensionless flow rates must respect the following inequations:

$$\begin{cases} m_{IV(2)} < H_c \\ m_{I(2)} > H_e \\ H_c < m_{II(2)} < m_{III(2)} < H_d \end{cases} \quad 6-23$$

Following a similar logic as the one described for the first 4-zone SMB unit, the adsorbent flow rate of the second unit, at the LSC point, is given by:

$$\dot{V}_{S2} = \frac{\dot{V}_{F2}}{(H_d - H_c)} \quad 6-24$$

Since the feed of the second 4-zone SMB is the extract stream of the first 4-zone SMB unit, which is given by:

$$\dot{V}_{E1} = \frac{\dot{V}_{F1}(H_e - H_b)}{(H_c - H_b)} \quad 6-25$$

the adsorbent flow rate in the second 4-zone SMB unit can be expressed as a function of the feed flow rate of the first unit according to:

$$\dot{V}_{S2} = \frac{\dot{V}_{F1}(H_e - H_b)}{(H_d - H_c)(H_c - H_b)} \quad 6-26$$

and therefore,

$$\dot{V}_{S2} = \dot{V}_{S1} \frac{(H_e - H_b)}{(H_d - H_c)} \quad 6-27$$

Since $H_e > H_d$ and $H_b < H_c$ (Figure 6-1), the adsorbent slow rate in the second 4-zone SMB unit is always larger than the adsorbent flow rate in the first unit. Which means that, as long as the SMB cascade is running at optimal conditions (and assuming that the adsorbent columns have the same size in both units), the two 4-zone SMB units are not operated with the same switching interval.

Considering Figure 6-2, it is possible to visualize that if the switching time of both SMB units is not synchronized, the rear concentration shock of the solute c coming from zone I(1) through the recycle does not enter the second unit in every switching interval with the same time delay after the columns of the second 4-zone SMB unit switched position. Instead, since the switching interval of the second 4-zone SMB unit is shorter than that of the first unit, after every new column switch, the rear concentration shock of the solute c coming from zone I(1) enters zone III(2) later than in the previous switching interval. Therefore, during the operation of the process, if complete recovery of the target solute c is to be guaranteed, the minimum allowable dimensionless flow rate in zone $m_{II(2)}$ needs to be H_c , and not $2H_c - m_{I(1)}$, as in the case of the 8-zone SMB with extract recycle.

6.2.2. Raffinate recycle

In the case of a 4-zone SMB connected to a second 4-zone SMB by the raffinate stream, as shown in Figure 2-6, the first unit can only successfully separate the fraction containing the solutes a, b and c from the contaminating solutes d and e, shown in the hypothetical mixture depicted in Figure 6-1, if the dimensionless flowrates respect the following inequations:

$$\begin{cases} m_{IV(1)} < H_a \\ m_{I(1)} > H_e \\ H_c < m_{II(1)} < m_{III(1)} < H_d \end{cases} \quad 6-28$$

The optimum operating point of the first unit is again defined by the LSC point, where $m_{I(1)} = H_e$, $m_{IV(1)} = H_a$, $m_{II(1)} = H_c$, $m_{III(1)} = H_d$. Once more using the strategy suggested by G. Zhong and G. Guiochon [179, 184], the feed flow rate \dot{V}_{F1} can be expressed by:

$$\dot{V}_{F1} = \dot{V}_{I(1)} \left(\frac{H_d}{H_e} - \frac{H_c}{H_e} \right) \quad 6-29$$

The flow rate in zone I(1) at the LSC point is given by $\dot{V}_{I(1)} = \dot{V}_{S1} H_e$, therefore, the adsorbent flow rate \dot{V}_{S1} can be expressed as a function of the feed flow rate and the adsorption Henry coefficients of the solutes c and d,

$$\dot{V}_{S1} = \frac{\dot{V}_{F1}}{(H_d - H_c)} \quad 6-30$$

The second 4-zone SMB unit can only completely separate the target solute c from the contaminating fraction containing the solutes a and b without loss or contamination, if the dimensionless flow rates respect the following inequations:

$$\begin{cases} m_{IV(2)} < H_a \\ m_{I(2)} > H_c \\ H_b < m_{II(2)} < m_{III(2)} < H_c \end{cases} \quad 6-31$$

Therefore, the adsorbent flow rate of the second 4-zone SMB unit, at the LSC point, is given by:

$$\dot{V}_{S2} = \frac{\dot{V}_{F2}}{(H_c - H_b)} \quad 6-32$$

The raffinate stream of the first 4-zone SMB unit, is given by:

$$\dot{V}_{R1} = \frac{\dot{V}_{F1}(H_d - H_a)}{(H_d - H_c)} \quad 6-33$$

which has the same flow rate as the second 4-zone SMB unit feed. Hence, the adsorbent flow rate in the second 4-zone SMB unit can be expressed as a function of the feed flow rate of the first unit according to:

$$\dot{V}_{S2} = \frac{\dot{V}_{F1}(H_d - H_a)}{(H_d - H_c)(H_c - H_b)} \quad 6-34$$

and therefore,

$$\dot{V}_{S2} = \dot{V}_{S1} \frac{(H_d - H_a)}{(H_c - H_b)} \quad 6-35$$

Since, by definition, $H_d > H_c$ and $H_a < H_b$ (Figure 6-1), the adsorbent flow rate in the second 4-zone SMB unit must also be larger than the adsorbent flow rate in the first unit in the case of the 4-zone SMB cascade connected by the first raffinate stream. Therefore, at optimal operating conditions, it is not possible to operate both 4-zone SMB units with the same switching interval in either configuration. This is a result of the fact that the outlets of the first subunit are always more diluted than the original feed, so the second subunit needs to process a higher feed flow rate and, therefore, operate at shorter switching intervals than the first 4-zone SMB unit.

Similarly, in the case of two 4-zone SMB units connected by the raffinate stream, it can be visualized in Figure 6-5 that, when the switching interval of the second SMB unit is shorter than that of the first unit (in case both SMB units are operated at the LSC point), the

front concentration shock of the solute c coming from zone II(1) through the recycle enters zone III(2) every cycle later than in the previous one. This trend proceeds until it skips an entire switching interval of the second 4-zone SMB unit and enters at the beginning of the next one. When this happens, the distance A_{z2} becomes very large (tending to L) thus decreasing $m_{III(2),max}$ to H_c , instead of $2H_c - m_{IV(1)}$, as in the case of 8-zone SMB.

Therefore, two SMB units in a cascade cannot be operated at optimal conditions and, at the same time, have a pre-separated feed entering the second unit, regardless of the presence of a buffer tank between both units (which would only make the separation in the second unit more difficult, due to the insertion of a mixing unit between them). In order to circumvent this limitation, it is possible to equalize the switching intervals of both units, in order to synchronize them and increase the operating region of the second unit. This would, however, remove one degree of freedom from the process operating parameters and make the operation of the cascade of two 4-zone SMB units mathematically indistinguishable from that of an integrated 8-zone SMB.

Another option to increase the performance of the cascade of two independently operated 4-zone SMB units, by pre-separating the second unit feed, is to use broader columns in the second unit, so that the switching times can be kept constant, even though the adsorbent flow rate is still larger in the second subunit. This might be an interesting option for separation processes that do not change over long periods of time, which could justify the extra investment demanded by specially shaped chromatographic columns. However, for most applications, that is not the case, since it is not a very practical solution and lacks flexibility to adapt to different separating conditions.

Lastly, it is conceivable to try to synchronize the concentration shock of the solute c coming from the first SMB unit with the one coming from the relevant adjacent zone in the second subunit so that some degree of recycled feed pre-separation can be achieved. This is possible if the switching interval of the second SMB unit can be represented as a rational fraction of the first SMB unit switching interval. The smaller the nominator and denominator of this fraction are, the larger the pre-separation degree of the recycled feed that can be achieved will become (reaching a maximum when this fraction is 1, and both switching intervals are the same). This is a potentially interesting option, since it incorporates some pre-separation of the recycled feed, while keeping an extra degree of freedom in the operation of the separation system. However, due to the complexity of developing a universal

mathematical description of how to implement such strategy, it will not be further explored in this work.

6.3. Operating regions of 8-zone SMB with 16 columns

As already established in sections 6.1.1 and 6.1.2, the reason for the different performances of 8-zone SMB and 8-zone TMB is the periodic shifting of the columns in the former in opposition to the continuous movement of the adsorbent in the latter. Therefore, it could, on a first analysis, be expected that increasing the number of columns per zone in an 8-zone SMB unit would cause the difference in its performance with that of an 8-zone TMB to disappear as the stepwise movement of the adsorbent approaches a continuous movement. However, as it will be shown, for systems where no dispersion takes place, that is not the true.

6.3.1. Extract recycle 8-zone SMB with 16 columns

It is possible to use the same strategy explained in the section 6.1.1 to predict the positions of the front and rear concentration shocks of the solutes in an extract recycle 8-zone SMB unit with two columns per zone after cyclic steady state is reached. Figure 6-8 shows the characteristics of the solutes inside an extract recycle 8-zone SMB unit with two columns per zone over two switching intervals. The same adsorption Henry coefficients (Table 6-1) and dimensionless flow rates (Table 6-2) considered in the example shown in section 6.1.1 were applied.

As it can be seen in Figure 6-8, the only difference between the strategy used for predicting the cyclic-steady state conditions of an 8-zone SMB with two columns per zone and the one used for an unit with only one column per zone (Figure 6-2) is that, in the case of the system with two columns per zone, the front and rear concentration shocks are separated in different columns instead of being in the same one.

Considering that both the system with one and the system with two columns per zone have columns with the same dimensions and that the same adsorbent and solvent flow rates were used, it remains true that a stable cyclic steady state condition where no solute c is lost in the second extract port is only possible if the time when the rear concentration shock of the solute c coming from zone II(2) enters zone III(2) before or at least at the same time as the rear concentration shock of the solute c coming from zone I(1) through the recycle. If this

condition is not fulfilled, the rear concentration shock of the solute c coming from zone II(2) reaches the end of the first column in zone III(2) with a delay, which causes the second extract port to be contaminated with solute c, in the same way as in the 8-zone SMB with one column per zone.

As shown in Figure 6-8, as long as the dimensionless flow rate in zone II(2) is larger than the lower limit imposed by equation 6-9, the rear concentration shock of the target solute c already traveled a distance Δz_2 in the column at the beginning of a switching interval, and, therefore, it only needs to go through the remaining distance $L - \Delta z_2$, during the next switch interval in order to be completely eluted from the column in zone II(2) before this column moves into zone I(2).

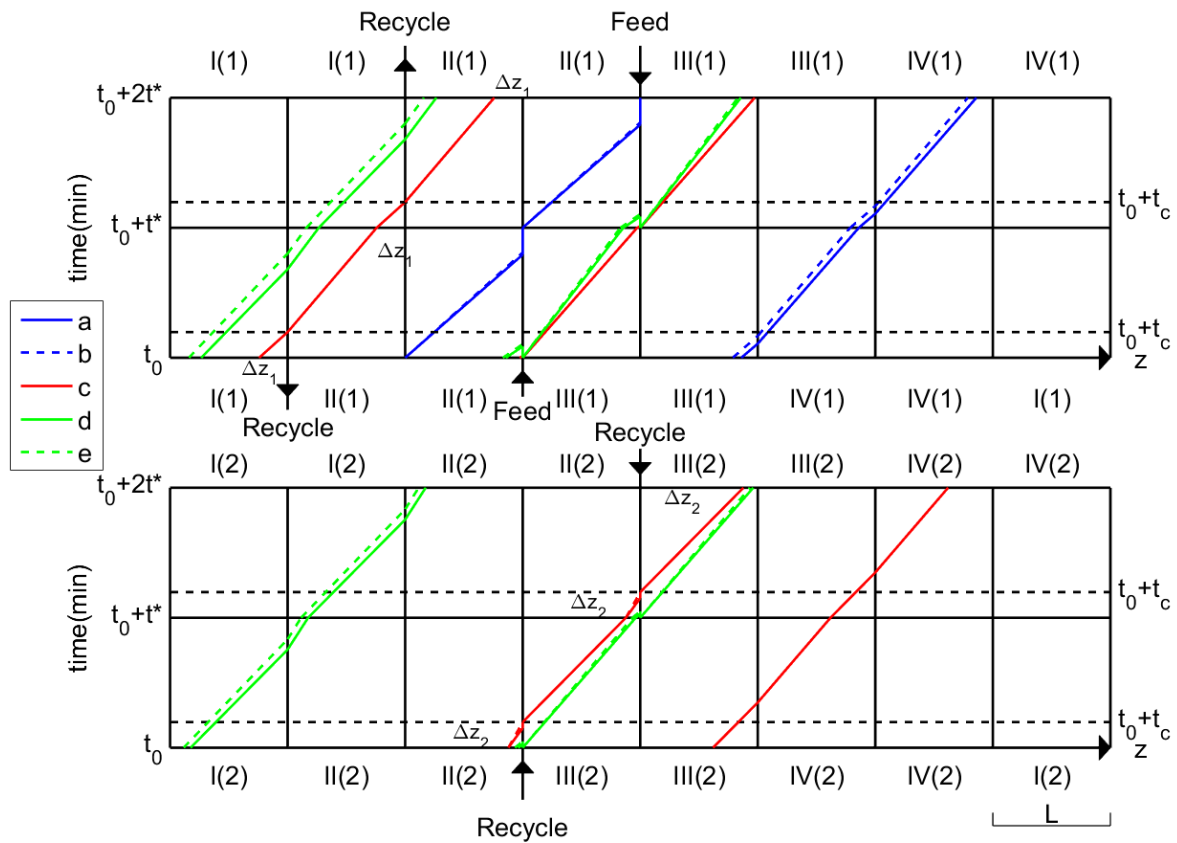


Figure 6-8 – Positions of the front and rear concentration shocks (characteristics) of the solutes a, b, c, d, and, e inside an extract recycle 8-zone SMB with two columns per zone after the cyclic steady state is reached. The calculations were performed using MATLAB R2015b considering the adsorption Henry coefficients listed in Table 6-1 and the dimensionless flow rates and porosity listed in Table 6-2. The red dashed lines represents the limiting case of $m_{II(2)} = m_{II(2),min}$. The continuous red lines show the characteristics obtained considering the given $m_{II(2)}$.

Since the distance $L - \Delta z_2$ is calculated using equations 6-1 and 6-6, and the length of the columns (L) as well as the switching interval (t^*) are the same, the delay time t_c also remains constant, regardless of the number of columns. Therefore, the lower limits of $m_{II(2)}$ and $m_{III(1)}$ (given, respectively, by equations 6-9 and 6-10), which are calculated based on t_c and t^* and on the equation 6-7, also do not change and, thus, the operating regions remain the same as in an extract recycle 8-zone SMB unit with only one column per zone.

It is interesting to highlight that, although the operating regions do not change, Figure 6-8 shows that zones I(1), I(2), IV(1) and IV(2) can function with only one column each, regardless of the number of columns in zones II(1), II(2), III(1) and III(2), since only the last column in zone I and the first column in zone IV are actually used.

When the number of columns in the 8-zone SMB is increased to three or more columns per zone, while maintaining the same column lengths, switching intervals and solvent velocities, the same logic can be applied to show that the lower limits of $m_{II(2)}$ and $m_{III(1)}$ remain the same. Therefore, it can be extrapolated that the difference between 8-zone SMB and 8-zone TMB does not tend to disappear if the zones are further subdivided into more columns, since the concentration shocks always move on a smaller time scale than the upstream movement of the columns.

Therefore, the operating regions of 8-zone SMB with extract recycle (shown in Figure 6-3) can always be calculated using the set of inequations 6-2 corrected by the equations 6-9 and 6-10, independently of how many columns are employed in the system.

6.3.2. Raffinate recycle 8-zone SMB with 16 columns

An 8-zone SMB with raffinate recycle unit can also be built using two chromatographic columns per zone and the strategy explained in the section 6.1.2 can then be applied to predict the cyclic steady state positions of the front and rear concentration shocks of the solutes. Figure 6-9 shows the characteristics of the solutes inside a raffinate recycle 8-zone SMB unit with two columns per zone over two switching intervals. The same adsorption Henry coefficients (Table 6-3) and dimensionless flow rates (Table 6-4) used in the example shown in section 6.1.2 were considered.

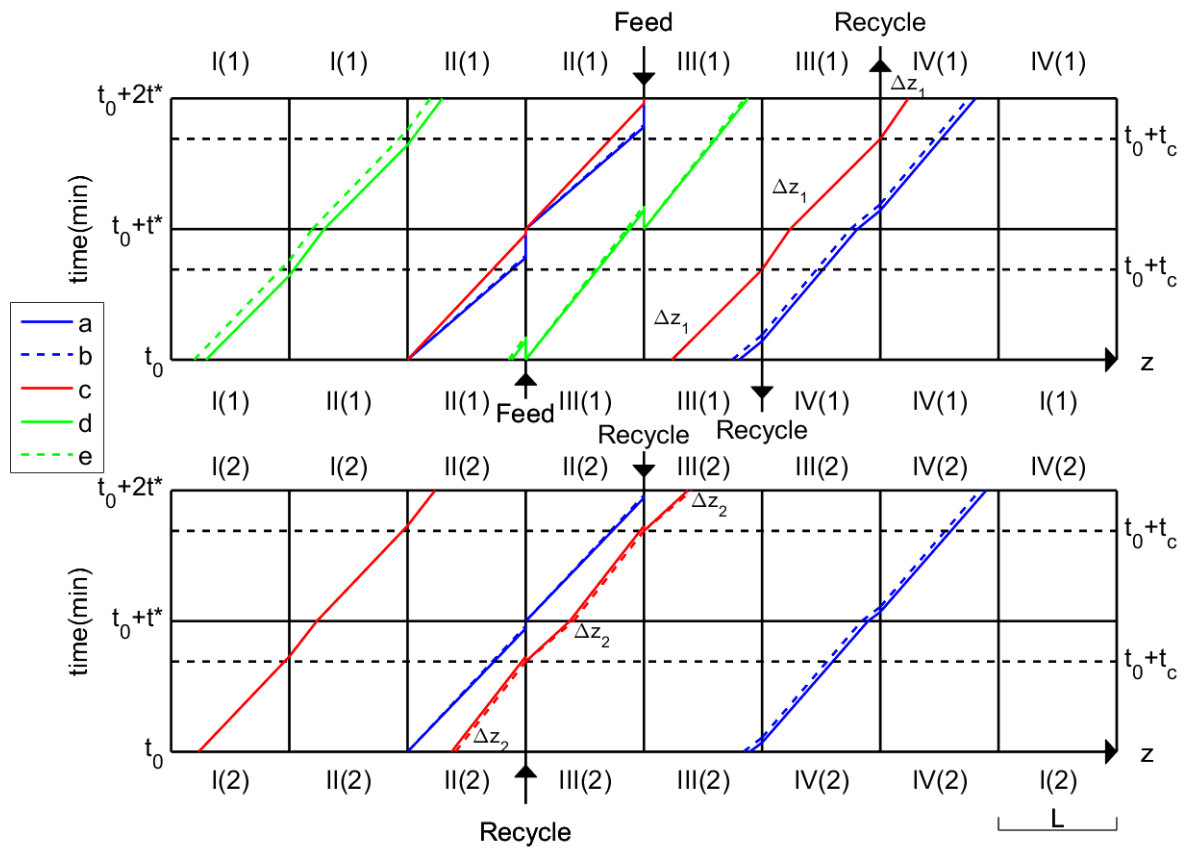


Figure 6-9 – Positions of the front and rear concentration shocks (characteristics) of the solutes a, b, c, d, and, e inside an raffinate recycle 8-zone SMB with two columns per zone after the cyclic steady state is reached. The calculations were performed using MATLAB R2015b considering the adsorption Henry coefficients listed in Table 6-3 and the dimensionless flow rates and porosity listed in Table 6-4. The red dashed lines represents the limiting case of $m_{III(2)} = m_{III(2),max}$. The continuous red lines show the characteristics obtained considering the given $m_{III(2)}$.

The position of the concentration shock front of solute c in the first raffinate port can be used to predict the delay time t_c after which the concentration shock front of solute c enters the second subunit through the recycle stream. It can be seen in Figure 6-9 that a stable cyclic steady state condition where the target solute c is obtained pure in the second extract port can only be achieved if its front concentration shock coming from zone II(2) enters zone III(2) after (or at least the same time) as the one coming from zone III(1) though the recycle stream. The delay time t_c of the solute c front concentration shock remains the same, since it is calculated using equation 6-14, and all variables (column lengths, switching intervals, porosities and dimensionless flow rates) are kept constant. Therefore, the maximum dimensionless flow rate in zone III(2) (calculated using equation 6-18) remains unchanged, and the shape of the operating regions is kept constant. This reasoning can be easily extended

to 8-zone SMB units with raffinate recycle composed of more than two columns per zone and, therefore, in much the same way as the 8-zone SMB with extract recycle, they do not approximate the behavior of an 8-zone TMB as the zones are further subdivided into more beds.

Hence, the operating regions of raffinate recycle (Figure 6-6) can always be calculated using the set of inequations 6-11 corrected with the newly developed equations 6-18 and 6-19, as explained in section 6.1.2, regardless of the number of columns used.

6.4. Limitations of 8-zone SMB

It is possible to completely separate the target solute c from the pseudo-ternary mixture depicted in Figure 6-1 using an integrated 8-zone SMB, as long as the dimensionless flow rate restrictions deduced in sections 6.1.1 and 6.1.2 are respected. Therefore, based on the comparison between the integrated 8-zone SMB and the cascade of two 4-zone SMB units described in the section 6.2, it can be concluded that 8-zone SMB can provide a better performance than the cascade of two independently operated 4-zone SMB units. While the cascade of two independently operated 4-zone SMB units is also able to completely recover the solute c from the feed, its second 4-zone SMB unit must have a higher adsorbent flow rate than the first one, in order to be operating at optimal conditions (as explained in section 6.2). Furthermore, since the dimensionless flow rates $m_{I(1)}$, $m_{I(2)}$, $m_{IV(1)}$ and $m_{IV(2)}$ are the same for both the SMB cascade and the 8-zone SMB, it follows that the SMB cascade must have a higher specific solvent consumption than the 8-zone SMB, while the achievable recovery yield and purity are the same (100%).

The integrated 8-zone SMB is, however, not always superior to the SMB cascade. The main difference between the two configurations is given by the fact that, in principle, there are no limitations for the adsorption Henry coefficients of the solutes being separated using the 4-zone SMB cascade. This is a reflection of the extra operating degree of freedom that the cascade of two independently operated 4-zone SMB units has when compared to the integrated 8-zone SMB.

Analyzing the set of inequations 6-2 and the equations 6-9 and 6-10, it is possible to conclude that not all possible combinations of adsorption Henry coefficients will allow for a complete separation of the target solute c from the feed using an integrated 8-zone SMB with extract recycle.

When $H_d + H_c - H_e < -F^I$, the dashed line defining the diagonal side of the operating region of the second subunit (given by $m_{III(2)} = m_{II(2)} - m_{II(1)} + H_e$) does not allow $m_{III(2)} < H_d$ and $m_{III(2)} > -F^I$ at the same time. Therefore, in this case, there are no allowable flow rates that can result in a completely pure solute c, since dimensionless flow rates smaller than $-F^I$ correspond to negative flow rates, which were not accepted solutions in the scope of this work, due to the technical limitations of most chromatographic systems (as explained in section 3.5). In other words, if the adsorption Henry coefficient of the strongest adsorbing solute (H_e) is too large, the flow rate necessary to completely regenerate the adsorbent in zone I(1) would result in the flow rate in zone III(2) to be too high to prevent solute d from reaching the second raffinate port and contaminating the product stream.

A similar analysis can be performed for 8-zone SMB with raffinate recycle. However, it does not yield any theoretical limitations for which solutes' adsorption Henry coefficients can allow a successful purification of the target solute c. This results from the fact that, regardless of how large the difference between H_a and H_c is, $m_{III(2),max}$ is never too large, since there is no theoretical upper limit to how high dimensionless flow rates can be.

6.5. Discussion and outlook

The difference between the performances of the integrated 8-zone SMB with extract recycle and raffinate recycle and their respective 8-zone TMB geometrical equivalents exemplified, respectively, in Figure 6-4 and in Figure 6-7 was explained by the periodic movement of the adsorbent in SMB that causes the second subunit to receive a pre-separated feed, which can be much more easily separated than a homogeneous feed. The 8-zone TMB, on the other hand, receives a feed with constant composition from the first subunit, since the movement of the adsorbent is fully continuous. Furthermore, as explained in section 6.3, this difference does not tend to disappear if the zones are further divided into more beds, since the concentration shocks move on a smaller time scale than the upstream movement of the columns, regardless of the total number of beds.

The performance of a cascade of two independently operated 4-zone SMB units is limited in the same way as that of an 8-zone TMB, i.e., as discussed in section 6.2, the feed of the second SMB unit is normally homogeneous. While it is conceivable to try to circumvent this limitation by increasing the size of the columns in the second SMB unit or by partially synchronizing the switching intervals of both SMB units, these are, however, not very practical and universal solutions for improving the performance of the 4-zone SMB cascade.

On the other hand, as discussed in the section 6.4, 8-zone SMB does not always correspond to a superior performance when compared to a cascade of two independently operated 4-zone SMB units. Typically, if the difference between the largest adsorption Henry coefficient and the adsorption Henry coefficient of the target solute is too large, 8-zone SMB with extract recycle is not expected to provide a complete (100%) recovery of the target solute. In contrast, in the case of the 4-zone SMB cascade, it is always possible (at least in theory) to scale up the throughput of the second subunit by decreasing the switching interval so that solutes with any adsorption Henry coefficients can be successfully separated. This is a reflection of the extra degree of freedom that the operation of the cascade of two independently operated 4-zone SMB units allows.

In this chapter, the operating regions of 8-zone SMB were predicted for linear adsorption isotherms, due to the relative simplicity of the calculations involved. The use of preparative chromatography in general, and SMB, in specific, is, however, only pertinent if the purpose is to achieve higher profit margins, therefore, performing a preparative chromatography-based separation on the linear range of the solutes' adsorption isotherms is neither very common, nor desirable. Thus, the prediction of the operating regions of 8-zone SMB should be extended for nonlinear adsorption isotherms and the strategy suggested in sections 6.1.1 and 6.1.2 is a good starting point.

It is important to highlight that the difference between the equilibrium model SMB-based predictions and the TMB-based ones does not take place in the case of systems that do not have internal recycle streams, such as the classical 4-zone SMB process. There are, however, other important SMB variants, such as the 9-zone SMB [3] and, most notably, the commercial Sorbex® process family (Parex®, Olex®, Molex®, Sarex®, Cresex® and Cymex®) [1, 188-190] (UOP Honeywell, USA) which do incorporate internal recycle streams. Consequently, important insight into the dynamics of these systems can be gained by using the characteristics-based strategy for predicting the operating regions proposed in sections 6.1.1 and 6.1.2.

6.6. Conclusions

The work described in this chapter used the equilibrium theory and the method of characteristics to estimate the internal concentration profiles of the integrated 8-zone SMB with extract and raffinate recycle at cyclic steady state, which showed that its outlet concentrations can significantly differ from those of a geometrically equivalent 8-zone TMB

process. This motivated the adjustment of the triangle theory to better describe the 8-zone SMB, demonstrating that, contrary to its TMB analog, it may be able to completely recover the target solute. Moreover, it was possible to more accurately compare the 8-zone SMB with a cascade of two independently operated 4-zone SMB units and to conclude that the difference with the 8-zone TMB process does not tend to disappear as the number of columns per zone is increased. In order to consolidate and validate the theoretical results described in this chapter, a solution of several food dyes was chosen as a model mixture to demonstrate an 8-zone SMB separation. The experimental results will be reported in the next chapter.

7. Experimental validation

The purpose of the work described in this chapter was the experimental demonstration of a continuous center-cut separation using the 8-zone SMB process carried out in a Modified Prochrom® ICLC-16-10 unit. For that, a model mixture of food dyes was selected and analyzed. A suitable solvent composition was identified and, using the strategy described in chapter 6, the operating parameter space was predicted. Based on it, adequate flow rates and switching times were chosen and theoretically validated using simulations. Finally, two pilot scale experimental separation runs were performed and, while not completely successful, resulted in instructive insight into the experimental system and process concept.

7.1. Chromatographic separation of food dyes

In order to validate the model described in chapter 6, it was necessary to choose an experimental system. This includes adsorbent, solutes to be separated, the solvent used for the elution, and the simulated moving bed facility. Since the main goal of the experimental part of this dissertation was the demonstration of the validity of the mathematical tools developed in chapter 6, the experimental system does not need to involve any real separation problem in need to be solved. Instead, emphasis was given to practicality and, therefore, the starting point was the use of the Modified Prochrom® ICLC-16-10 Research Scale Continuous Chromatograph SMB (Prochrom, Nancy, France) for the demonstration of the 8-zone SMB separation, since this system was available at the Max Planck Institute Magdeburg and was used by J. Nowak [8, 9] and D. Kiwala [10] in previous work. This facility, however, limits the separation to the conditions shown in Table 7-1.

Parameter	Limitation
Solvent state	Liquid
Pressure and temperature	Uncontrolled
Maximal column length	15 cm
Maximal pressure drop of the columns	200 bar
Material	Vulnerable to corrosion (Stainless steel)

Table 7-1 – Experimental limitations of the Modified Prochrom® ICLC-16-10 Research Scale Continuous Chromatograph SMB (Prochrom, Nancy, France).

In addition to the limitations shown in Table 7-1, the solutes and solvents used should ideally be nontoxic, nonflammable, cheap and readily available. Furthermore, the concentration of the solutes chosen should be easily, quickly and precisely estimable. Additionally, the technique chosen for the concentration measurement should be able to estimate the concentrations of each solute without interference from the others. Therefore, solutes with a concentration that can be estimated using spectrophotometric methods have the most potential, due to their practicality, availability, low price and reliability. Moreover, spectrophotometric methods have the potential to allow the estimation of the outlet solute concentrations during the experimental runs.

Many organic compounds absorb light in the near UV range (190-280nm), however, due to the narrowness of this range, the discrimination of different compounds based solely on the UV absorbance spectra is not possible using most conventional spectrophotometers. Therefore, a prior separation would be necessary before analyzing the absorbance spectra of the samples in this range, which would decrease the efficiency of the experimental protocol. Consequently, an interesting option is the identification of solutes based on the visible light (Vis) absorbance spectra. The visible light range is considerably wider than the near UV, starting at around 400nm and extending to 750nm or 800nm [177], and has the added advantage of allowing eye-based estimations of concentrations and compositions, which can minimize the chance of experimental errors and potentially save time that could otherwise be consumed analyzing samples of visibly failed experiments.

Colorants can easily be differentiated based on their absorbance spectra on the visible light range and are, therefore, promising candidates for model solutes and *food* colorants, in especial, are non-toxic, cheap and readily available. Furthermore, they are chemically similar to each other, which should simplify the selection of the chromatographic separation method. Moreover, the estimation of their concentrations can be done based on the deconvolution of their visible light absorbance spectra [176], i.e., by estimating the specific contributions of

each one to the overall spectra based on their different specific contributions at different wavelengths.

Food colorants are compounds that impart color to foods or drinks. Contrary to what their name might suggest, food colorants are not only used for commercial products with nutritional value, being also widely applied in the cosmetics and pharmaceutical industries. Food colorants can either be naturally sourced from living organisms (such as plants, fungi, animals or bacteria, as in the case of the natural colorants Carmine, Lycopene and Turmeric), or artificially synthesized from organic precursors (as Allura Red, Sunset Yellow and Brilliant Blue). Food colorants can also be produced by mixed routes, being the result of chemical alterations to natural molecules (caramel, for example, is the product of the oxidization of carbohydrates).

Most importantly for this work, though, is the distinction between pigments and dyes. Pigments are usually finely ground insoluble powders that convey color to suspensions. Dyes, on the other hand, are completely miscible liquids or solids [191, 192]. Since, in this work, a model mixture had to be chosen for demonstrating an adsorption-based separation of a homogeneous solution, the food colorants chosen were dyes.

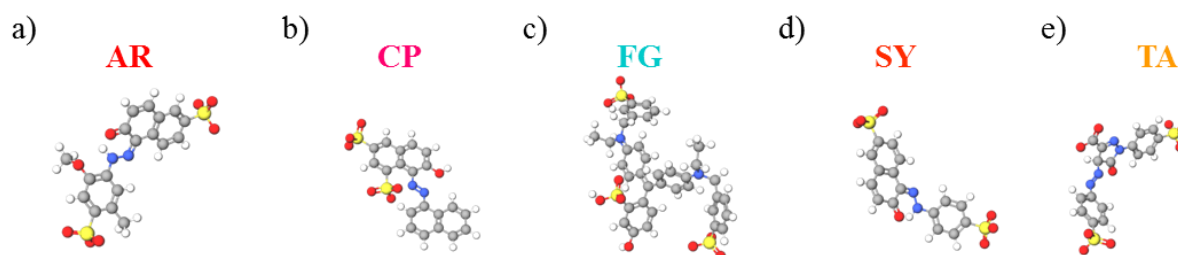


Figure 7-1 – The food dyes selected for this work. a) Allura Red AC b) Crystal Ponceau 6R c) Fast Green FCF d) Sunset Yellow FCF e) Tartrazine. The grey beads represent carbon atoms, the white beads represent hydrogen atoms, the yellow beads represent sulfur atoms, the blue beads represent nitrogen atoms and the red beads represent oxygen atoms.

As shown in Figure 7-1, four synthetic azo dyes were selected: Allura Red AC (a.k.a. Food Red 17, C.I. 16035, and FD&C Red 40), Crystal Ponceau 6R (a.k.a. Ponceau 6R, Crystal scarlet, Brilliant crystal scarlet 6R, Acid Red 44, or C.I. 16250), Sunset Yellow FCF (a.k.a. Orange Yellow S, or C.I. 15985) and Tartrazine (a.k.a. E102, C.I. 19140, FD&C Yellow 5, Acid Yellow 23, or Food Yellow 4). Additionally, one synthetic triarylmethane dye, Fast Green FCF (a.k.a. Food green 3, FD&C Green No. 3, Green 1724, Solid Green

FCF, and C.I. 42053), was chosen. Some of these dyes were also used in an application note published by Agilent Technologies (USA) [193] that partially motivated the experimental section of this dissertation.

In the work previously performed by J. Nowak at the Max Planck Institute Magdeburg, 10 semi-preparative columns 10 cm long have been packed with LiChroprep® RP-18 [8, 10]. These columns were successfully tested in the modified Prochrom ICLC-16-10 unit (Prochrom, Champigneulle, France) and their pressure drop does not exceed the capabilities of the facility's connections and pumps. Furthermore, the separation of food colorants using octadecyl-grafted (C18) silica particles chromatographic columns has already been described in the literature [193, 194].

7.1.1. Adsorption mechanism of food dyes onto C18 silica

Since dyes are often particularly difficult to remove waste water contaminants from the food and cosmetics industry, much of the research available on the thermodynamics of their adsorption has focused on cheap and easily available natural adsorbents, such as porous carbon, chitosan, diatomaceous earth and chitin [195-211].

As a result of the lack of practical application, the adsorption mechanism of food dyes onto octadecyl-grafted (C18) silica particles has been even less researched. Furthermore, several different isotherm models have been applied for the description of their adsorption onto the aforementioned adsorbents: Langmuir, Freundlich, BET, Toth, Temkin, Redlich–Peterson, Sips, Frumkin, Harkins–Jura, Halsey, Henderson and Dubinin–Radushkevich, being just a few [210]; which highlights the lack of theoretical understanding of the mechanism behind the retention of food dyes. However, some relevant aspects of their adsorption mechanism can be predicted based on their functional groups. The food dyes used in this work (Figure 7-1), are relatively large organic molecules containing electronegative and ionizable groups, which can, therefore, be separated using C18 silica columns with aqueous-organic solvents added of ionic additives [212].

According to Gritti, F. and Guiochon, G. [213], the first widely accepted interpretation of the retention mechanism of solutes on C18 silica chromatographic columns was the solvophobic theory suggested by Horvath C. [214], which describes the retention mechanism as a liquid-liquid partition between the bulk solvent and the layer of hydrophobic alkyl chains that coat the surface of the stationary phase (Figure 7-2). This model explains the common observation that the retention times of many solutes is reduced by the presence of

organic modifiers in the mobile phase [215]. It was, however, not able to predict well the retention behavior of the solutes when the silica was modified with different groups. Therefore, it was suggested by Dill, K.A. [216] that adsorption instead of partition must be the main retention mechanism.

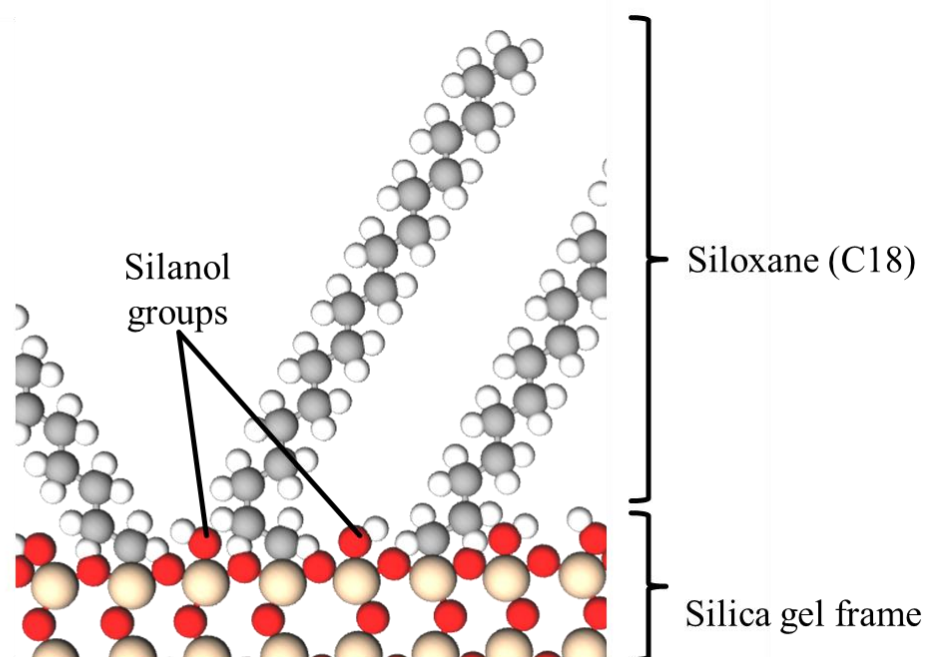


Figure 7-2 – Octadecyl-grafted (C18) silica surface [217]. Though most of the adsorption takes place on the siloxane layer, the exposed silanol groups may also participate in the adsorption mechanism. The grey beads represent carbon atoms, the white beads represent hydrogen atoms, the beige beads represent silicon atoms and the red beads represent oxygen atoms.

Several different mechanisms also contribute to the retention of solutes in C18-silica packed beds. For instance, it has been shown via Monte-Carlo calculations that small molecules can penetrate deeper onto the silanol-grafted phase, which effectively increases its adsorption capacity for smaller molecules relative to larger ones [213]. Additionally, if charged solutes have a higher affinity for the silanol groups than water, they can displace the adsorbed water molecules [213]. Furthermore, it is also possible that the hydrophobic layer, primarily composed of organic solvent modifier that forms on the surface of the bound siloxane phase, influences the retention of partially hydrophobic molecules. This phase adds an extra liquid-liquid partition between the bulk and the adsorbent to the overall retention mechanism.

The heterogeneity of the C18 silica surface has made it difficult to develop a general model to explain its adsorption mechanism, since, polar silanol groups, hydrophobic siloxane groups and charged metal impurities can contribute to the retention of ionic solutes. Moreover, the different energy of these adsorption sites can influence the overall retention behavior of the solutes [2]. Furthermore, due to the presence of metal cation contaminations, the average surface charge of C18 silica is typically positive, however, at higher pH, silanol groups dissociate and become negatively charged resulting in complex surface charge distributions [212].

The presence of charged groups in the solutes adds an extra layer of complexity to the C18 silica retention mechanism. The resulting adsorption is the result of the combined effects of the weak interaction of the undissociated species onto the large number of siloxane adsorption sites and the strong affinity of the dissociated ones onto the few high-energy silanol sites [218]. Since the concentration of ionic solutes at the surface of the adsorbent may increase to levels above the buffering capacity of the solvent, their local dissociation ratio may increase as well, which results in a stronger affinity for the exposed silanol groups [80]. Since the silanol adsorption sites are greatly outnumbered by the siloxane groups, the hydrophilic groups are easily overloaded compared to the hydrophobic sites. Therefore, at relatively high concentrations, the charged species migrate faster than the neutral ones, which causes the peaks to appear anti-Langmuirian in the resulting chromatograms, despite the fact that the difference in the retention times of dissociated and undissociated species cannot be detected at the end of the column (since they are at dynamic equilibrium) [213]. At higher feed concentrations, the adsorption isotherms might even look S shaped as the hydrophobic adsorption sites also become overloaded. However, it is recognized by Gritti, F. and Guiochon, G. that the deformation of chromatographic peaks might also be explained by the repulsion of charged adsorbed solutes [219].

Charged species might also be unable to diffuse into the pores of the adsorbent due to ion-exclusion, which is related to the effective molecular size of charged molecules in aqueous solution. Contrary to neutral solutes, charged molecules create a double shell of coordinated water molecules around them, since the dipole moment of water molecules causes their alignment with electric fields. The resulting shell of coordinated water molecules is relatively stable and moves with the solute within, effectively increasing its diameter in solution and altering its diffusivity [219]. Moreover, the presence of charged groups in the silica surface generates zeta potential and the resulting electric double-layer of coordinated

water molecules reduces the effective size of the pores of the silica scaffold. The presence of buffering agents in the solvent partially suppresses the silanol ionization and decreases the width of the coordinated double-layer due to the increased ionic strength [212]. Furthermore, it also stabilizes the dissociation ratio of ionic solutes, which contributes to the robustness of the separation method.

In summary, the adsorption of charged solutes, such as food dyes, onto octadecyl-coated silica particles is a very complex and not fully understood process. It is influenced by several different mechanisms, including liquid-liquid partition, dissociation of the adsorbent silanol groups and ion-exclusion, among other effects. Therefore, the successful development of a protocol for the chromatographic separation of food dyes requires reliance on experimental work, which is described next.

7.2. Experimental protocols

In this section, the experimental protocols used in this dissertation are described. The high performance liquid chromatographic experiments were performed using the Agilent Infinity 1260 Quaternary LC (Figure 7-3, Agilent Technologies, USA) HPLC system. This system consists of a low pressure quaternary pump, a vacuum degasser, an autosampler and a UV-Vis diode array light absorbance detector. The experiments performed in this system included the estimation of the adsorption isotherms using frontal analysis and the analysis of the fractions generated by the Modified Prochrom® ICLC-16-10 Research Scale Continuous Chromatograph (Prochrom, Nancy, France).

The measurement of the absorbance spectra of the food dyes were performed with the spectrophotometer Genesys 6 (Thermo Fisher Scientific, Germany) and 10 mm light path glass precision cells from Hellma Gruppe (Germany).

The Modified Prochrom® ICLC-16-10 Research Scale Continuous Chromatograph unit (Prochrom, Nancy, France) at the Max Planck Institute Magdeburg was used for the 8-zone SMB experimental runs. The pumps connected to this system were six Agilent 1200 Series binary pumps (Agilent Technologies, USA), and one Agilent 1200 Series (Agilent Technologies, USA) quaternary pump, controlled by an Agilent 1200 Series instant pilot (Agilent Technologies, USA) monitor.

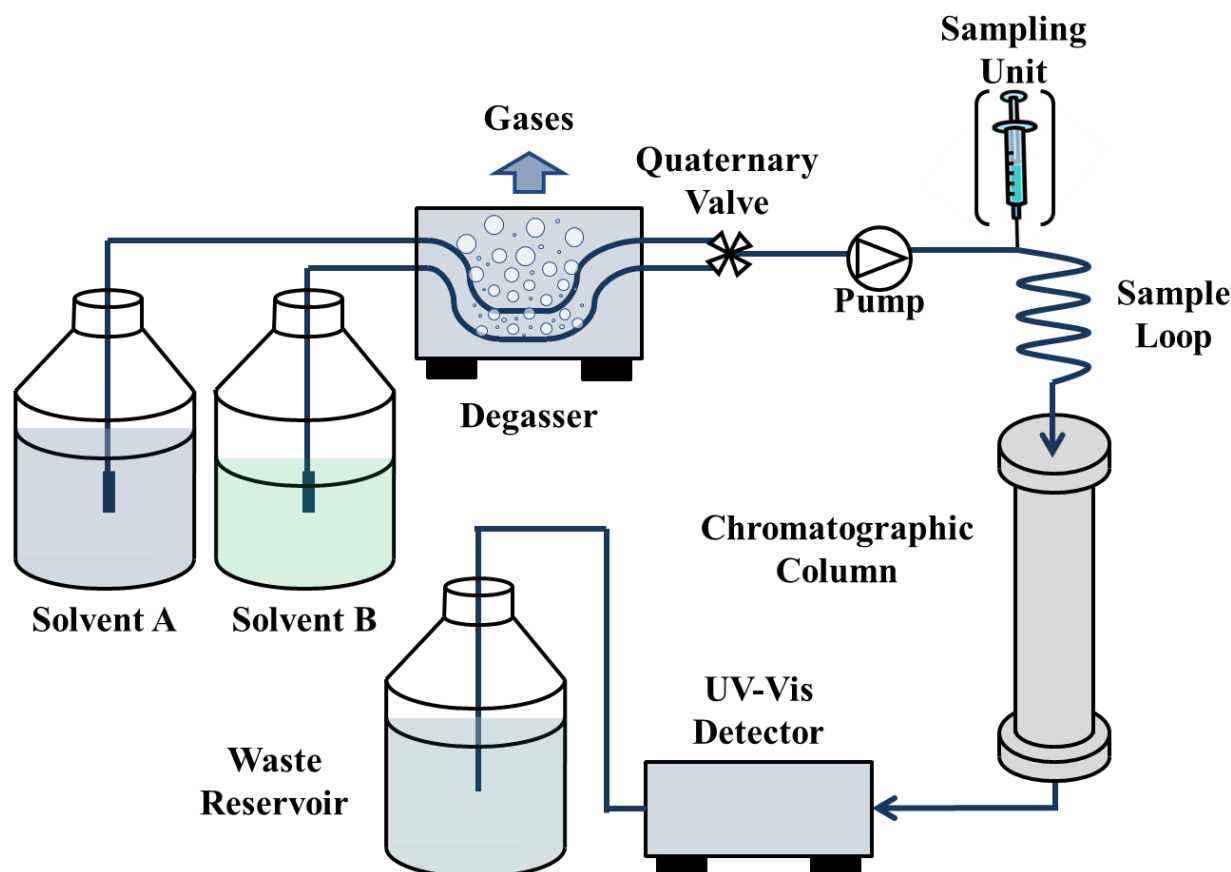


Figure 7-3 – Agilent Infinity 1260 LC system (Agilent Technologies, USA). The solvents used in this work always went through the degasser before entering the system, so that no bubbles could form inside the capillary tubes or in the chromatographic column. The quaternary valve can be connected to up to four different reservoirs, which allows different proportions of the solvents to be mixed and used for the elution process, a feature that was used for the creation of the concentration steps in the frontal analysis experiments. Since there is only one possibility for the hydraulic path of the solvent between the quaternary valve and the waste reservoir, the dead volume of the frontal analysis experiments is the total volume between the quaternary valve and the UV-Vis detector, i.e. 2.224 ml.

7.2.1. High performance liquid chromatography

The samples generated from the 8-zone SMB experiments were analyzed using a 25 cm long Luna C18 column with a particle size of 10 μm and an inner diameter (i.d.) of 0.5 cm (Phenomenex®, USA) in the Agilent Infinity 1260 (Agilent Technologies, USA) shown in Figure 7-3. The method used consisted of equilibrating the chromatographic column with 15/85 (v/v) ethanol / 70mM acetic acid in water at 2 $\text{ml}\cdot\text{min}^{-1}$ and room temperature followed by the injection of 100 μl of each sample using the autosampler device built in the system. The separation always took less than 20 minutes for each sample.

This method was able to generate baseline separation of Tartrazine, Sunset Yellow, Allura Red, Crystal Ponceau and Fast Green and could resolve them over a reasonable

amount of time. According to the data analysis method explained in section 4.2, the absorbance calibration curve of each food dye was used to first transform the chromatograms from absorbance-based (mAU in the vertical axis) to concentration-based ($\text{mg}\cdot\text{l}^{-1}$ in the vertical axis). The horizontal coordinates of the points of the chromatogram were converted from a time basis [min] into a volume one [ml] by multiplying them by the flow rate used ($2\text{ ml}\cdot\text{min}^{-1}$). The peaks in the resulting chromatograms were integrated and their areas represented the total amount of dye in the sample [76]. After dividing each area by the volume of sample injected, the concentration of each different food dye could be estimated.

Figures A-1 to A-5 and Figure 7-14 show the chromatograms of each outlet port for every cycle of the two 8-zone SMB experimental runs. The estimated concentrations of each food dye in each outlet port for every cycle of the first and second 8-zone SMB experimental runs are shown in Tables A-1 to A-6. The concentrations in each sample were estimated according to the methodology explained in section 4.2 using the software ChromeleonTM (Thermo Fisher Scientific, Germany) and, therefore, the intermediary calculation data is not shown here. The calibration curves were approximated using the concentration steps from the frontal analysis experiments from section 7.2.3.

7.2.2. Characterization of the 8-zone SMB columns

In order to account for the delay of the concentration shocks caused by the capillaries and valves before and after the chromatographic column, the breakthrough times of the concentration shocks fronts (t_b), as well as the dead times of the columns (t_0), were corrected for the dead time of the system. The dead volume of the Agilent Infinity 1260 HPLC unit (the volume between the quaternary valve and the UV-Vis detector, shown in Figure 7-3), was estimated to be 2.224 ml, using a $0.1\text{ g}\cdot\text{l}^{-1}$ solution of Blue Dextran (Sigma-Aldrich, Sweden) in 15/85 (v/v) ethanol / 70mM acetic acid in water as solvent.

Blue Dextran is a macromolecule obtained from Dextran, which is itself a polymer composed of 95% α -1,6-linked glucose residues in the main chain and α -1,3-linked glucose residues in the side branches. The light absorbance of Dextran in the UV range is increased by the addition of the chromophore group Reactive Blue 2, which is covalently bound to the hydroxyl groups of the glucose residues, creating Blue Dextran.

The phase ratio (F) was also calculated from the retention time (t_0) of a $0.1\text{ g}\cdot\text{l}^{-1}$ solution of Blue Dextran (Sigma-Aldrich, Sweden) in 15/85 (v/v) ethanol / 70mM acetic acid in water as solvent. The Blue Dextran used in this work has a molecular weight of around

2×10^6 Da, and, therefore, it was not expected to be able to enter the pores of the LiChrorep® RP-18 (25-40 μm) adsorbent particles, which have an average pore size of approximately 10 nm. The porosity estimated using Blue Dextran was, therefore, the external (inter-particle) porosity [76].

The estimation of the adsorption isotherms, as well as the 8-zone SMB simulations, was performed considering only the external porosity, in order to guarantee $q \geq 0 \text{ mg.l}^{-1}$. Since it was noticed that some of the food dyes tested had, at higher ethanol concentrations, retention volumes smaller than the dead volumes of the columns estimated using the smaller tracer molecule Uracil (data not shown). This was, most likely, caused by size exclusion of these food dyes from the internal volume of the adsorbent particles, since the molecular diameter of the food dyes used in this work was in the same size range as the average LiChrorep® RP-18 particle pore size, i.e. around 10 nm.

Therefore, the adsorption Henry coefficients estimated in the next section are better described as being dimensionless retention coefficients instead of adsorption isotherms, since they represent the combined effects of the actual adsorption process and the breakthrough delay caused by the void fraction of the chromatographic columns.

The average porosity of the eight LiChrorep® RP-18 columns used in this work, estimated using the retention time of Blue Dextran, was 0.3157, which can be explained by the relatively wide size distribution of LiChrorep® RP-18 adsorbent particles (that range from 25 μm to 40 μm) and by the fact that only the external porosity was measured.

The number of plates of the LiChrorep® RP-18 columns (inner diameter: 1 cm, length: 10 cm) was estimated for three different cycloketones (cyclopentanone, cyclohexanone and cycloheptanone) using equation 4-5 by J. Nowak in her PhD dissertation [8]. The solvent used was a mixture of methanol and water. It was found that the NTP of the 8 LiChrorep® RP-18 columns showed only a very small variability (under 1%) and could be well explained by the Van Deemter correlation (equation 4-6).

The NTP of all of the LiChrorep® RP-18 columns was between 1000 and 2000, when operated between 0.1 ml.min^{-1} and 5.0 ml.min^{-1} . Since the same flow rate range and the same columns were used in this work, the same NTP values were considered. However, in J. Nowak's work [8], it was also noticed that the relatively large dead volumes between the chromatographic columns in the Modified Prochrom® ICLC-16-10 Research Scale Continuous Chromatograph and, specially, inside the recycle stream, significantly decreased the efficiency of chromatographic columns during the operation of the 8-zone SMB.

In this work, the lower limit of 1000 mixing cells were used for the 8-zone SMB simulations. However, in reality, the plate number of the chromatographic columns operated in the Modified Prochrom® unit is probably lower than that, due to the large dead volumes of the system. Nonetheless, the actual plate number of the chromatographic columns is not very important for the prediction of the SMB performance when it is on the range of two to three digits [2, 83], since the retention of the concentration shocks caused by adsorption plays a much more important role on the separation of the solutes.

The average pressure drop caused by the eight 10 cm long and 1 cm i.d. LiChrorep® RP-18 columns was also measured using the Agilent Infinity 1260 Quaternary LC (Agilent Technologies, USA) HPLC system. As shown in Figure 7-4, after discounting the pressure drop caused by the HPLC system without column (14.07 bar) no significant pressure drop could be detected at flow rates under 0.5 ml.min⁻¹. Furthermore, at 5 ml.min⁻¹ the pressure drop was still safely under the 200 bar limit of the Modified Prochrom® ICLC-16-10 Research Scale Continuous Chromatograph (Table 7-1). Therefore, the LiChrorep® RP-18 columns could safely be used for the experimental 8-zone SMB runs using the ethanol / 70mM acetic acid in water mixture as solvent.

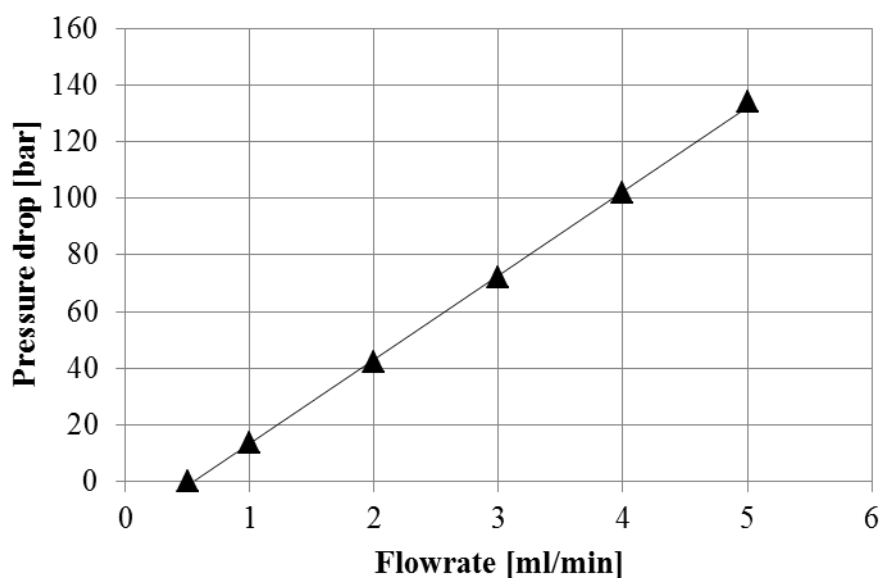


Figure 7-4 – Pressure drop of the LiChrorep® RP-18 (particle size: 25-40 µm, i.d. 1 cm, length: 10 cm) columns measured with the Agilent Infinity 1260 HPLC (Agilent Technologies, USA) using 15/85 (v/v) ethanol / 70mM acetic acid in water as solvent at room temperature. The pressure drop of the HPLC system measured without column was 14.07 bar.

7.2.3. Adsorption isotherm estimation using frontal analysis

The application note published by Agilent Technologies (USA) [193], which served as starting point for this section, suggested a mixture of 75/25 (v/v) methanol / 10mM acetic acid in water as a solvent for the separation of Tartrazine, New red, Amaranth, Indigo Carmine, Ponceau 4R, Sunset Yellow, Red 33, Allura Red, Erioglucine, Azophloxine and Erythrosine using an Agilent Poroshell 120 EC-C18 3.0 x 100 mm, 2.7 μ m particles. However, here, ethanol was used instead of methanol, due to its reduced toxicity and similar elution characteristics. Therefore, the adsorption isotherms of Allura Red (1 mg.l⁻¹), Crystal Ponceau (1 mg.l⁻¹), Fast Green (1 mg.l⁻¹), Sunset Yellow (1 mg.l⁻¹) and Tartrazine (1 mg.l⁻¹) in LiChroprep® RP-18 (particle size: 25-40 μ m) were estimated using 15% – 30% (v/v) ethanol complemented with 70mM acetic acid in water as solvent at a flowrate of 2 ml.min⁻¹ using the Agilent Infinity 1260 Quaternary LC (Figure 7-3, Agilent Technologies, USA) HPLC system, at room temperature.

Before any adsorption isotherm estimation experiment, however, the HPLC system was equilibrated with the solute-free solvent being tested including the chromatographic column on the hydraulic path by pumping it from bottle A through the quaternary pump (Figure 7-3). Subsequently, the solvent containing solute was pumped from bottle B through the quaternary pump, to guarantee that the capillaries connecting the bottle to the pump were filled with solvent containing only the solute being tested and at the correct concentration. Nonetheless, before equilibrating the quaternary pump with the solute-rich solvent, the chromatographic column always had to be removed from the hydraulic path and replaced by a zero-volume connector, since the HPLC unit used in this work does not allow the bypass of the chromatographic column, as shown in Figure 7-3. The next step was the re-equilibration of the HPLC system (still without the column) with the solute-free solvent followed by the installation of the chromatographic column and its re-equilibration using the same solvent. This protocol was always performed immediately before any frontal analysis experiment (including the case of sequential replicates) and it was found to be the best procedure to guarantee reproducibility and sharpness of the concentration shock fronts.

The concentration shock fronts must percolate the dead volume between the quaternary valve and the detector, since both the solute-rich and solute-free solvents are pumped through the same pump. This configuration is not optimal for frontal analyses due to the relatively large dead volume, which increased the dispersion of the concentration shock

fronts. However, for the estimation of the adsorption isotherms in this work, this configuration was found to perform well enough, since the retention volume of the concentration shocks was the only factor being measured.

To increase the amount of information obtained from each experiment, the frontal analyses were performed as a series of increasing concentration steps followed by the same number of decreasing steps. The decreasing concentration steps improve the chance that any unusual retention behavior (which could correspond to nonlinear adsorption isotherms) would be perceived. Nonlinear adsorption isotherms usually break the symmetry of the concentration steps in the outlet profiles.

Each concentration step was equally spaced and the number of concentration steps in each experiment was four, due to limitation of the operating system of the Agilent Infinity 1260 LC used in this work, the ChromeleonTM (Thermo Fisher Scientific, Germany). Each concentration step was held during a time long enough for a stable plateau to be reached; 20 minutes at 2 ml.min⁻¹ was found to be more than enough for this purpose.

The increasing concentration steps were used to measure the breakthrough time of each concentration shock front and the retention time of the decreasing concentration steps were used to double-check the linearity of the adsorption isotherms. The resulting chromatograms were translated to the left by discounting the dead time of the HPLC system so that only the retention time caused by adsorption was considered in the estimation of the adsorption isotherms.

Since the retention volume of the solutes is correlated to the course of their adsorption isotherms, the precise estimation of the dead volumes of the system was fundamental for guaranteeing consistency of the results obtained in the experimental part of this work. The dead volume of the HPLC system, as well as the porosity of the packed chromatographic columns, was estimated following the exact same procedure as the frontal analysis (with the exception that when the dead volume of the system was being estimated, the column was replaced by a zero volume connector).

The concentration steps from the frontal analysis protocol used in this work allow any retention caused by an unexpected adsorption of the tracer molecule to the adsorbent to be seen as a break in the symmetry of the chromatograms. The tracer molecule used for estimation of the dead volumes was Blue Dextran. The flow rate was set to 2 ml.min⁻¹, all experiments were performed at room temperature and the solute-rich solvent was stored in the solvent reservoir B (Figure 7-3).

7.2.4. Measurement of absorbance spectra

In order to facilitate sample analysis and allow the visual monitoring of the SMB experimental runs, the absorbance spectra of Allura Red, Crystal Ponceau, Fast Green, Sunset Yellow and Tartrazine were measured in the visible light range (400 – 800 nm) using the different solvent compositions tested throughout this work. All measurements were performed with the spectrophotometer Genesys 6 (Thermo Fisher Scientific, Germany) and 10 mm light path glass precision cells from Hellma Gruppe (Germany), the wavelength resolution was set to 1 nm and the exposure time to 0.3 s for each wavelength step. The light absorbance spectra were corrected in order to account for the light absorbance of pure solvent [220].

The concentration used for the measurements was 0.01g.l^{-1} , which resulted in absorbance peaks under 2 absorbance units (AU) for all of the food dyes tested. Above 2 AU, the detector signal is expected to become saturated, which increases the concentration estimation error.

7.2.5. Simulated moving bed chromatography with 8 zones

The 8-zone SMB unit used in this work was the Modified Prochrom® ICLC-16-10 Research Scale Continuous Chromatograph SMB (Prochrom, Nancy, France) available at the Max Planck Institute Magdeburg, schematized in Figure 7-5. The pumps used in this system were six Agilent 1200 Series binary pumps (Agilent Technologies, USA), with the exception of the feed pump Q1, which was an Agilent 1200 Series (Agilent Technologies, USA) *quaternary* pump. All pumps could supply a flowrate ranging from 0.001 to 5.000 ml.min^{-1} to 1% accuracy as long as the pressure drop was kept under 200 bar. The pumps were controlled by an Agilent 1200 Series instant pilot (Agilent Technologies, USA) monitor. Flow restrictors were installed between the outlet pump outlets and the environment, so that the pumps would work against a pressure gradient (according to their original design purpose), thus helping to ensure the precision of the flowrates.

The outlet and inlet ports were connected to the columns by 16 dead-end path multiport valves (VICI, Valco Instruments Co. Inc., USA) controlled by air-actuators. Each inlet or outlet port was connected to a specific multiport valve as shown in Figure 7-5, and could be connected to each, and only one, of the 16 columns (indicated by one of the 16 positions, as shown in Figure 7-5) at any given moment. The flow of solvent in the unit

shown in Figure 7-5 is unidirectional and clockwise, which was guaranteed by the one-way valves (Upchurch Scientific, USA) installed between the columns (represented by the small white valve symbols in Figure 7-5). The 4-way valve (4WV) connected to the internal recycle was manually switched back and forth from the raffinate to the extract recycle positions.

The positions of the multiport valves were controlled by the PROCHROM software, which was programmed by the Max Planck Institute Magdeburg electrical workshop. The actuation of the valves was done via a PCI 20482 interface (Intelligent Instrumentation Inc., USA). The switching of the valves could be performed either manually or automatically. It was done automatically during experimental runs and manually, during the cleaning and equilibration of the unit.

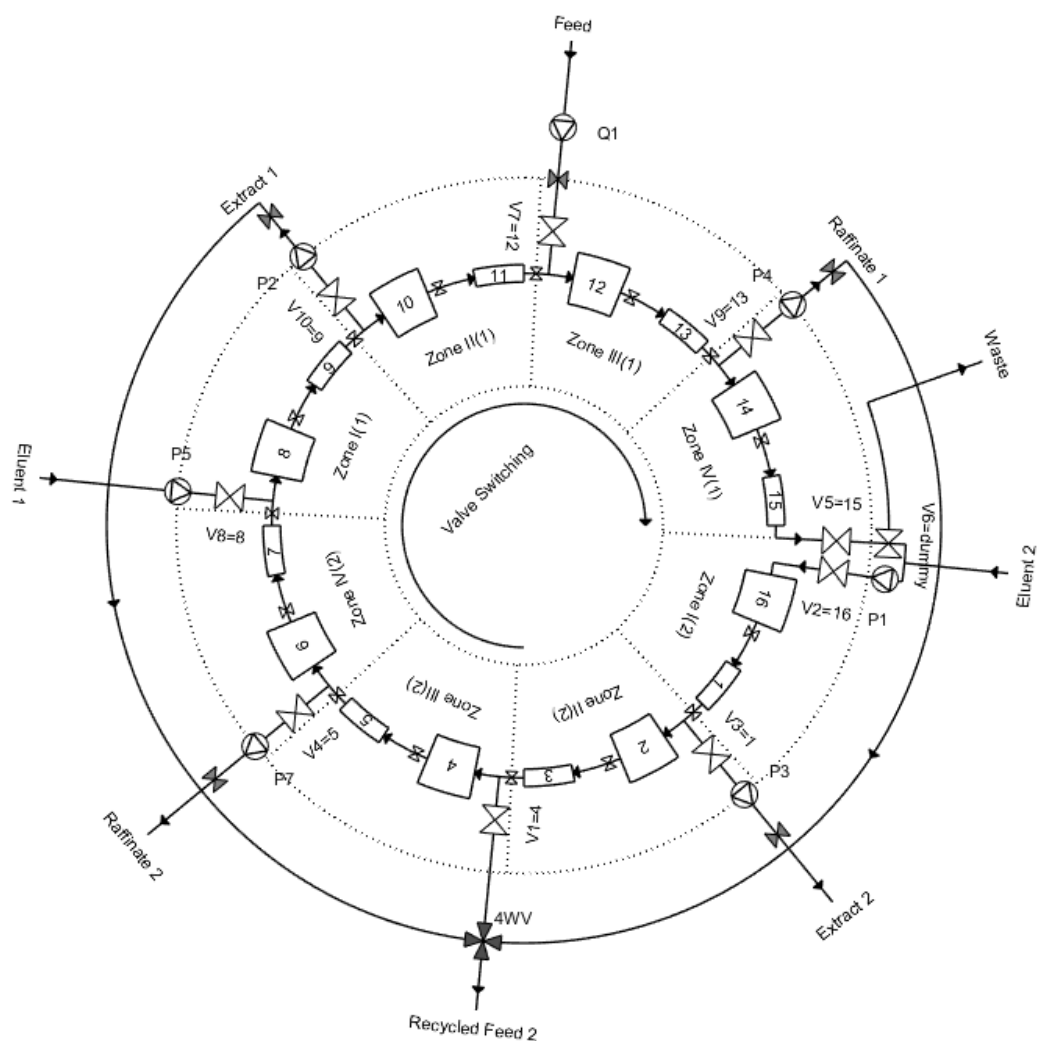


Figure 7-5 – Illustration of the Modified Prochrom® ICLC-16-10 Research Scale Continuous Chromatograph (Prochrom, Nancy, France). The positions where the chromatographic columns were installed are indicated by the larger rectangles, the smaller rectangles indicate the connectors that fill in the positions that were not used in this configuration and the numbers inside them indicate their positions thereof. The multiport valves are indicated by the white symbols and the letter V (the first number indicating the valve and the second number indicating the current position of said valve in this illustration), the small white symbols represent the one-way valves, the dark grey symbols represent the back-pressure regulator valves and the 4-way valve (4WV) is represented by the black symbol. Multiport valve V6 does not change position; therefore it is a dummy valve. The pumps (and their flow direction) are indicated by the triangles circumscribed by the circles and the letter P. The external reservoirs are indicated in the outer rim of the illustration and the SMB zones are indicated in the inner rim of the illustration. As indicated by the inner arrow in this illustration, the positions of the valves shift clockwise, which shifts the positions of the zones, without moving the actual chromatographic columns.

7.2.6. Estimation of the Prochrom® ICLC-16-10 dead volumes

The layout of the piping in the Modified Prochrom® ICLC-16-10 Research Scale Continuous Chromatograph SMB (Prochrom, Nancy, France) unit is not optimized, which causes the dead volumes between the chromatographic columns to be relatively large, compared to the volume of the columns [8]. Therefore, before the modeling of the 8-zone SMB, the precise dead volumes of the system had to be estimated. This was done by disconnecting the capillaries in chosen points inside the loop, replacing the feed for a dye solution and then measuring the time necessary for the color to reach the opening of the loop. When carefully choosing the opening points, the dead volumes between the columns could be estimated precisely. A particularly useful detail to improve the precision of this technique was to carefully insert a small air bubble between the dye solution and the colorless solvent, in order to prevent diffusion of the dye and facilitate the timing of the concentration shock.

The average dead volume between the columns was estimated to be 0.75 ml, and the dead volume between each consecutive column was approximately the same, since the piping layout is symmetric. The only exception was the dead volume between the valves V5 and V2, i.e. the volume between zones IV(1) and I(2), which was estimated to be 6.5 ml. This, however, should not interfere with the separation, since the solvent recycled between these two zones should be free of solutes. The dead volume of the recycle stream, however, was 3.75 ml, which should negatively interfere with the performance of the second subunit.

7.3. Experimental results and analysis thereof

7.3.1. Measurement of the absorbance spectra

The visible light absorbance spectra of Allura Red, Crystal Ponceau, Fast Green, Sunset Yellow and Tartrazine are plotted in Figure 7-6. They were normalized in order to account for the fact that, despite all measurements being performed at the same concentration (0.01 g.l⁻¹), the different food dyes used in this work have absorbance maxima of different intensities. In particular, Fast Green has an absorbance maximum five times higher than any other of the solutes tested, which resulted in its stronger apparent color intensity. There was, however, no measurable difference between the absorbance spectra of the food dyes in any of the different solvent compositions tested.

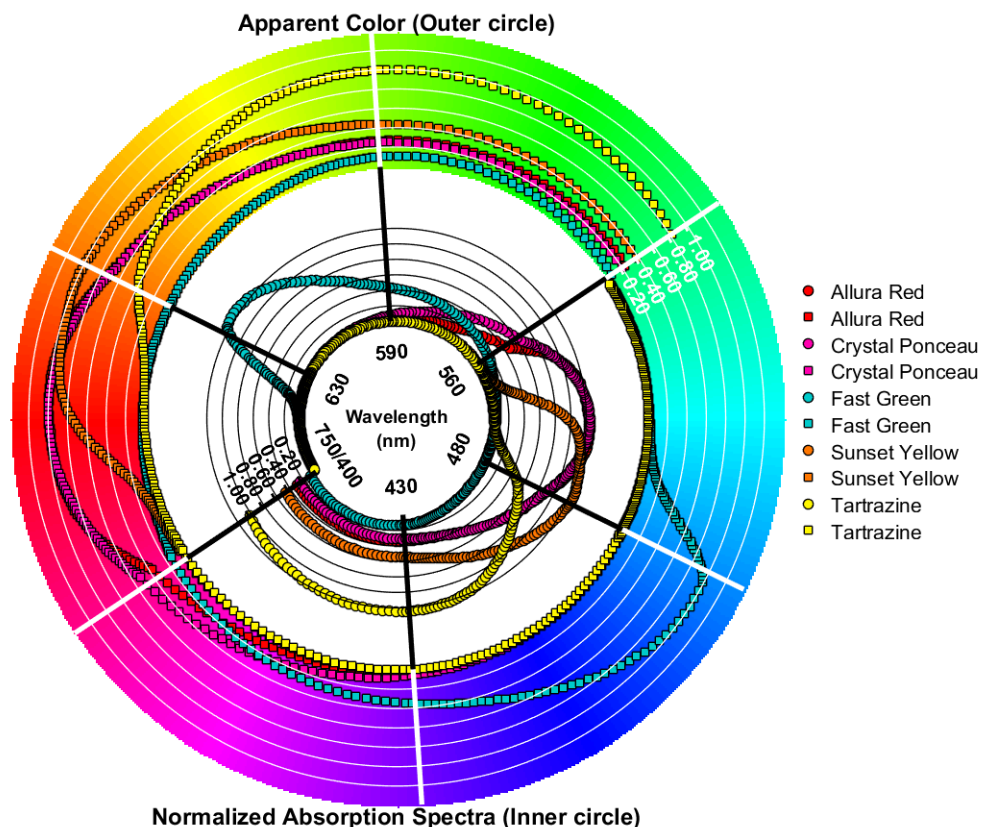


Figure 7-6 – Adsorption spectra of Allura Red, Crystal Ponceau, Fast Green, Sunset Yellow and Tartrazine in the visible light range (400 nm – 750 nm) at 0.01g.l^{-1} . The circular dots plotted in the inner circle show the normalized light adsorption intensity at different wavelengths for each of the solutes tested. The squared dots plotted onto the outer circle show the corresponding expected apparent color plotted in the Derrington-Krauskopf-Lennie (DKL) space based on the light absorbance spectra.

Due to the different molecular structures of the food dyes, the shapes of their light absorbance spectra varied considerably. While Crystal Ponceau has a very broad absorbance band ranging from 370 nm to almost 590 nm, Fast Green absorbance ranges from only 550 nm to 670 nm. Additionally, it can be seen in Figure 7-6 that Crystal Ponceau and Allura Red have very similar absorbance spectra, which makes them very hard to distinguish using spectrophotometric methods. It is interesting to notice, however, that the human eye can easily tell them apart, Allura Red having a deeper red hue, while Crystal Ponceau is perceptively pinkish. This can be justified by the fact that Crystal Ponceau absorbs more light in the long wavelength region than Allura Red.

Fast Green absorbed light intensively at wavelengths higher than 590 nm, which makes it one of the easiest food dyes to distinguish from the others, since it is the only one detectable at the very wide wavelength extreme of the visible light spectrum. Tartrazine had

an absorbance peak around 430 nm, where no strong competition with the other food dyes occurs, it has however, the lowest absorbance maximum from all the food dyes tested, which was also visibly noticeable in its very pale yellowish hue. Sunset Yellow's absorbance band stretches from 350 nm all the way to 550 nm which makes it relatively hard to distinguish in solution from Tartrazine, Allura Red and Crystal Ponceau using spectrophotometric methods.

As explained in section 4.3, the area of the color wheel, in the outer ring of Figure 7-6, mostly covered by the reflected absorbance spectrum approximately corresponds to the apparent color of the solute in solution. The apparent colors predicted in Figure 7-6 corresponded well to the actual colors of the food dyes. Tartrazine, for example, has indeed a pale yellow hue with a hint of green; Sunset Yellow is the most orange of the food dyes tested; Allura Red is red with a touch of orange and Fast Green is indeed more blue than green. Crystal Ponceau is, however, pinker than what would be expected based on Figure 7-6. This can be explained by the underestimation of the sensitivity to pink hues associated with an overestimation of the sensitivity human eye to red in the transformation metrics used in Figure 7-6, which is a result of the coarse resolution of the metrics used in this work (only 6 degrees of sensitivity were considered). However, given the inherent high variability of sensitivity to colors expressed by the human population, working on a very fine and, at the same time, accurate transformation metrics that can be agreed upon by a majority of observers is, in most likelihood, a hopeless task. Therefore, it was found that the transformation metrics used in this work resulted, still, on the best correlation between prediction and observation compared to the other metrics tested [177].

7.3.2. Deconvolution of absorbance spectra

As demonstrated in Figure 7-6, the identification of different food dyes in solution can be relatively challenging if there are large absorbance spectra overlaps. However, if the absorbance spectra measurements are performed at low concentrations, where linear correlations between light absorbance intensity and concentrations are expected [176], it is possible to unequivocally quantify different food dyes in mixed solutions. This can be done via spectra deconvolution as explained in section 4.3 and exemplified below, in Figure 7-7 [176].

Figure 7-7 shows an example of the spectra deconvolution. The visible light absorbance spectrum of a mixture of Crystal Ponceau (CP) 0.01 g.l^{-1} , Fast Green (FG) 0.006 g.l^{-1} , Sunset Yellow (SY) 0.01 g.l^{-1} and Tartrazine (TA) 0.01 g.l^{-1} in 15/85 (v/v) ethanol /

70mM acetic acid in water was measured. The resulting spectrum was deconvoluted by solving the system of equations 4-12 using the multiple least squares method, as explained in section 4.3, using MATLAB R2015b. Since 400 different wavelengths were evaluated, and four food dye concentrations were estimated, the system of equations had a large degree of redundancy, which reflected in the high accuracy of the estimations.

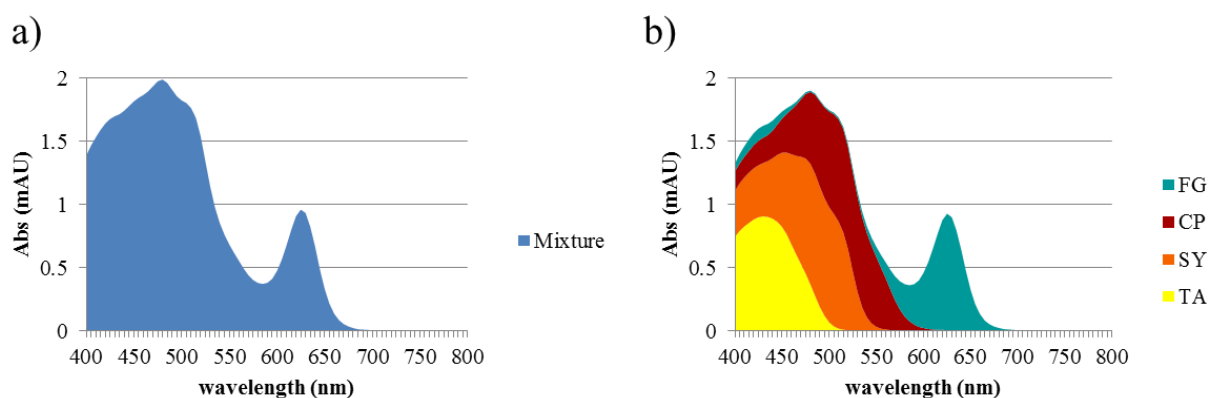


Figure 7-7 – a) Adsorption spectrum of a mixture of Crystal Ponceau (CP) 0.01 g.l^{-1} , Fast Green (FG) 0.006 g.l^{-1} , Sunset Yellow (SY) 0.01 g.l^{-1} and Tartrazine (TA) 0.01 g.l^{-1} in the visible light range (400 nm – 800 nm) in (15/85 (v/v) ethanol / 70mM acetic acid in water. b) Deconvoluted absorbance spectra obtained by solving the system of equations 4-12 in order to predict the concentrations of the food dyes; the resulting concentration vector was multiplied by the matrix of absorbance coefficients of each wavelength tested (B) for each solute and the resulting single-solute spectra were added to generate the predicted complete mixture spectrum. The relative difference between the predicted and the actual concentrations of each of the food dyes was around 3%.

The resulting concentrations obtained from the deconvolution of the visible light absorbance spectrum of the mixture shown in Figure 7-7 a) were multiplied by the absorbance coefficient vector of each of the food dyes, resulting on the estimated individual absorbance spectra of each solute. The resulting spectra were added, in order to simulate the complete absorbance spectrum of the mixture, shown in Figure 7-7 b).

Comparing the absorbance spectra shown in Figure 7-7 a) and b), it is possible to visualize that, on the linear range of the light absorbance/concentration correlation, the individual spectra add together and faithfully recreate the complete absorbance spectrum of the mixture. The relative error in the estimation of the food dyes' concentrations was under 3%.

7.3.3. Estimation of the adsorption isotherms

Using the experimental protocol described in section 7.2.2, the retention times of each concentration step of Allura Red, Crystal Ponceau, Fast Green, Sunset Yellow and Tartrazine were measured. The experimental retention times were then used for the calculation of the loading step (Δq) of the chromatographic column at each concentration step using equation 4-4, introduced in section 4.1. The loading of the column was calculated for each concentration step by progressively adding each loading step, starting from zero (the fully regenerated column). Each loading value was plotted against the corresponding plateau value of the concentration step and an adsorption isotherm function to describe their correlation was found (as demonstrated in Figure 7-8). This procedure was repeated for each dye used and for each different solvent composition tested.

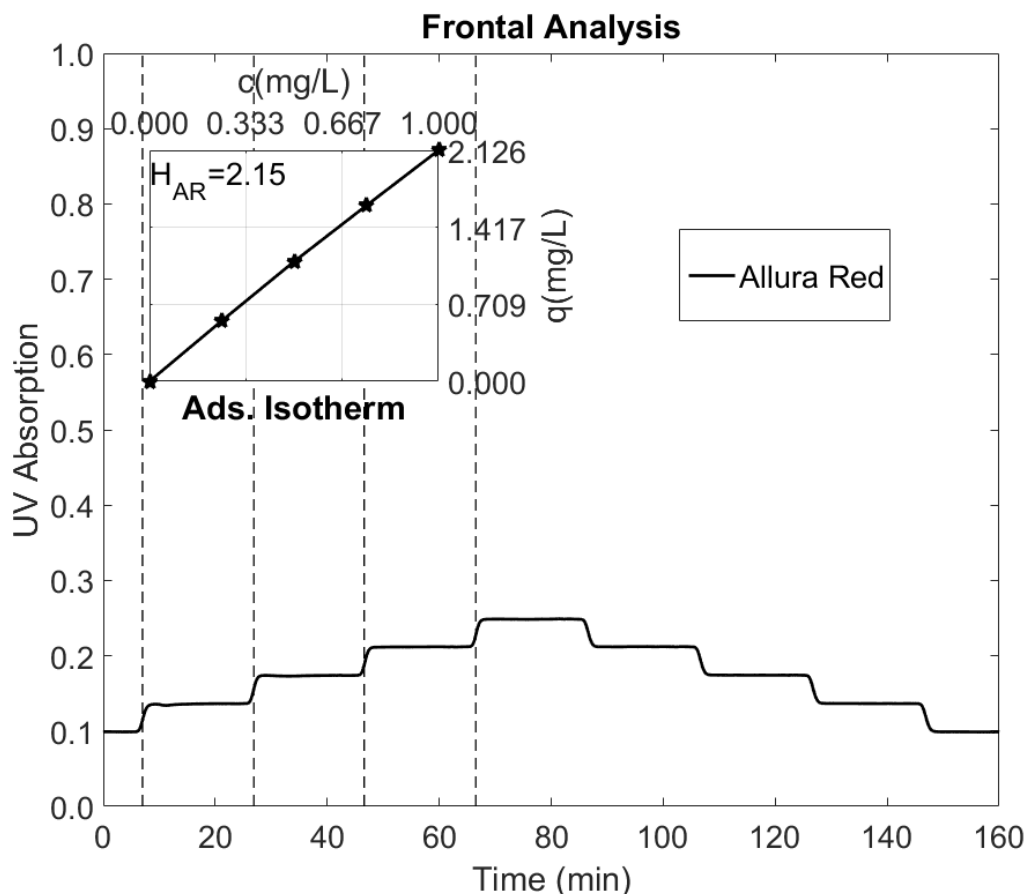


Figure 7-8 – Chromatogram (translated to the left in order to account for the dead time (t_{dead}) of the HPLC system) depicting four loading and four eluting 20 min long steps of Allura Red (1 mg.l^{-1}) in LiChroprep® RP-18 (particle size: 25-40 μm) using 15/85 (v/v) ethanol / 70mM acetic acid in water as solvent (2 ml.min^{-1}) at room temperature. The vertical axis represents the UV absorbance (254 nm) signal in arbitrary units. The vertical dashed lines correspond to the break through times of each concentration shock front. The subplot on the upper left corner shows the value of the concentration plateau of each loading step (horizontal axis) and the corresponding equilibrium adsorbed load on the solid phase (vertical axis). The inclination of this line is the adsorption Henry coefficient.

The concentrations of solutes used in this work were kept relatively low (under 1 mg.l^{-1}) due to the strong absorbance of visible light caused by the food dyes used. When higher concentrations were used, the signal of the UV-Vis diode array detector was overloaded, preventing an adequate measurement of the retention times of the concentration shock fronts. As a result, all of the adsorption isotherms obtained in this work were linear and could be described by adsorption Henry coefficients, which were correlated to the concentration of ethanol in the solvent using the Soczewinski equation [142, 221]. As illustrated in Figure 7-9, the higher the concentration of ethanol in the solvent was, the shorter the retention time became, which is in agreement with the theory described in section 7.1 [213].

The determination of a suitable solvent composition for the 8-zone SMB experiments was done based on the heuristics of maximizing the separation between the solutes, while keeping the adsorption Henry coefficient of the strongest adsorbing solute under the somewhat arbitrary value of 10 (i.e., inside the purple shaded area in Figure 7-9).

There is no strong theoretical reason preventing the largest Henry coefficient involved in the separation to exceed exactly 10. However, due to the upper limit of the solvent flow rates in the modified Prochrom ICLC-16-10 unit (5 ml.min^{-1}) used for the 8-zone SMB experiments, Henry coefficients much larger than 10 require cycle times in the range of hours, which increase the necessary time to reach cyclic steady state to impractically long periods. Furthermore, as explained in the section 6.4, an 8-zone SMB separation with high recovery is more likely to be achieved if the largest Henry coefficient involved in the separation is not unreasonably larger than the Henry coefficient of the target solute.

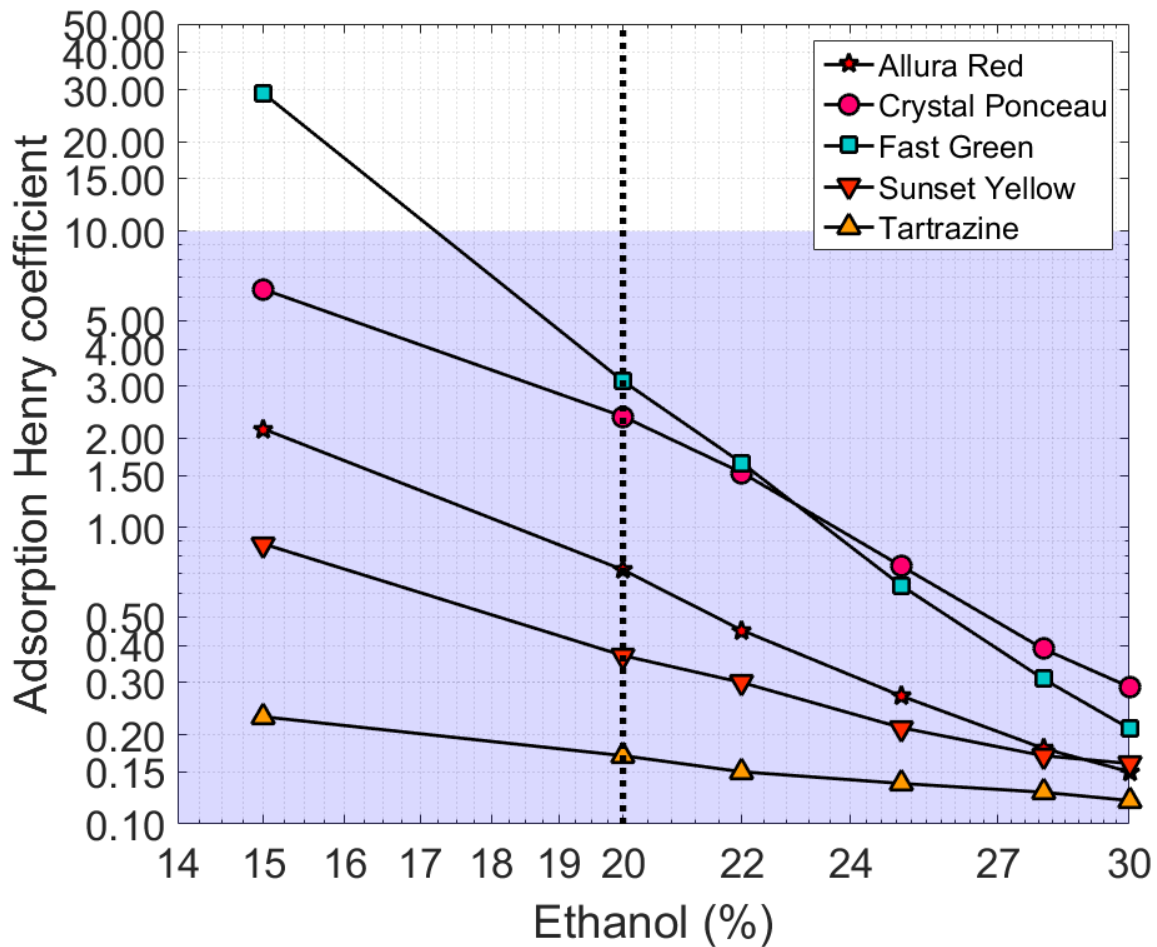


Figure 7-9 – Effect of the solvent composition on the adsorption Henry coefficients of Allura Red (star, 1 mg.l^{-1}), Crystal Ponceau (circle, 1 mg.l^{-1}), Fast Green (square, 1 mg.l^{-1}), Sunset Yellow (downward pointing arrow, 1 mg.l^{-1}) and Tartrazine (upward pointing arrow, 1 mg.l^{-1}) in LiChroprep® RP-18 (particle size: $25\text{-}40 \mu\text{m}$) using 15% - 30% (v/v) ethanol / 70mM acetic acid in water as solvent (2 ml.min^{-1}) shown in a log-log plot according to the Soczewinski equation [221]. Each solute is represented by its respective color and the purple shaded area represents the range of adsorption Henry coefficients desirable for an 8-zone SMB separation.

As shown in Figure 7-9, the ethanol composition (indicated by the vertical dashed line) of 20% (v/v) resulted in the largest separation between the food dyes, while the adsorption Henry coefficient of Fast Green did not exceed 10. Figure 7-10 shows the superposed frontal analysis experiments of Allura Red, Crystal Ponceau, Fast Green, Sunset Yellow and Tartrazine at the selected ethanol concentration in order to illustrate their separation.

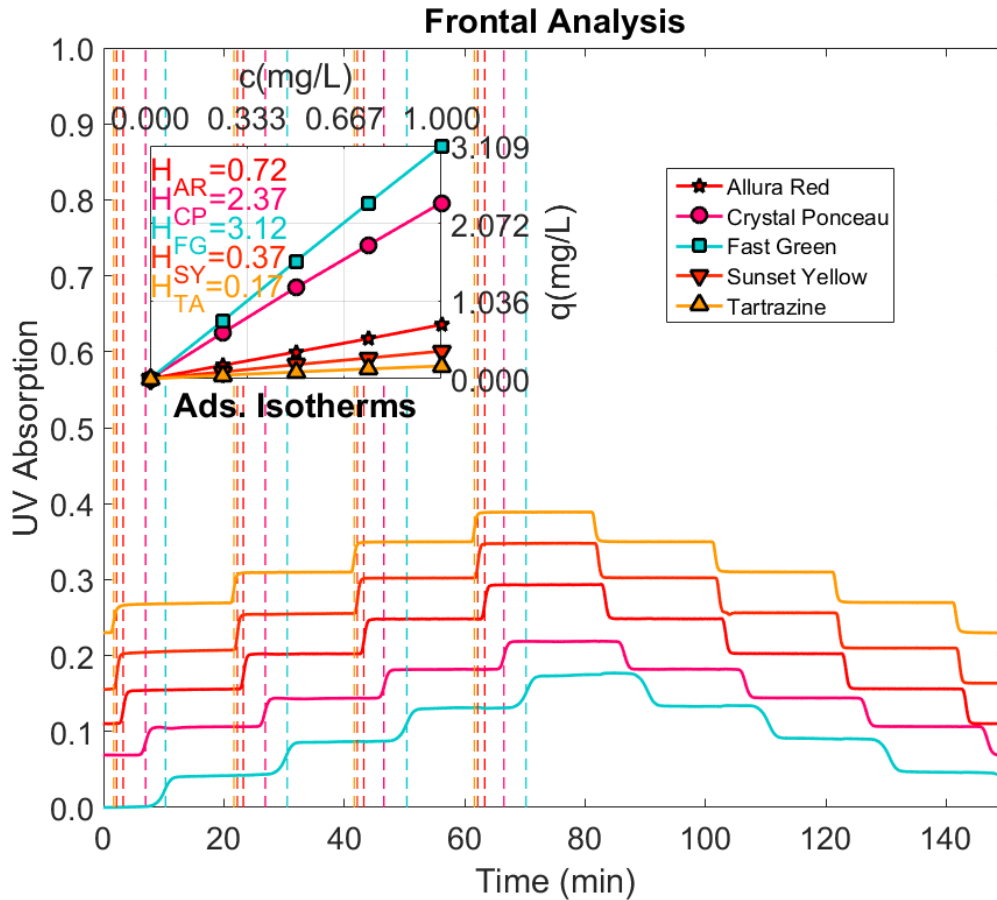


Figure 7-10 – Chromatogram (translated to the left in order to account for the dead time (t_{dead}) of the HPLC system) depicting four loading and four eluting 20 min long steps of Allura Red (AR, 1 mg.l^{-1}), Crystal Ponceau (CP, 1 mg.l^{-1}), Fast Green (FG, 1 mg.l^{-1}), Sunset Yellow (SY, 1 mg.l^{-1}) and Tartrazine (TA, 1 mg.l^{-1}) in LiChroprep® RP-18 (particle size: 25-40 μm) using 20/80 (v/v) ethanol / 70mM acetic acid in water as solvent (2 ml.min^{-1}) at room temperature. The vertical axis represents the UV absorbance (254 nm) signal in arbitrary units. The baselines of each experiment are shifted vertically in order to facilitate the visualization. The dashed lines correspond to the break through times of each concentration shock front and each color represents a different solute. The subplot on the upper left corner shows the value of the concentration plateau of each loading step (horizontal axis) and the corresponding equilibrium adsorbed load on the solid phase (vertical axis) for each solute. The inclination of each line is the adsorption Henry coefficient of each solute.

7.4. Simulation of 8-zone SMB separation of food dyes

To demonstrate the designing process of an 8-zone SMB separation of Allura Red from a mixture containing Crystal Ponceau, Fast Green, Sunset Yellow and Tartrazine using the selected solvent composition from section 7.3.1 (20/80 (v/v) ethanol / 70mM acetic acid in water), the operating regions of 8-zone SMB with extract and raffinate recycle were drawn using the methodology explained in the chapter 6. The letters (a), (b), (c), (d) and (e) were added, from here on, after each food dye, in order to highlight their correspondence with the fictitious solutes used in the theory developed in chapter 6.

In order to account for average the dead volume of 0.75 ml between the columns in the Modified Prochrom® ICLC-16-10 Research Scale Continuous Chromatograph SMB (Prochrom, Nancy, France), the method proposed by Katsuo et al. [160] and modified by Nowak et al. [9] was used to alter the adsorption Henry coefficients, so that the increased retention time of the concentration shock fronts could be considered when predicting the operating regions. Considering the average porosity of the columns used, the adsorption Henry coefficients were increased by a factor of 0.14 using equation 3-15, resulting in the adjusted adsorption Henry coefficients shown in Table 7-2.

Solute	Adsorption Henry coefficient	Adjusted adsorption Henry coefficient (H_i)
Tartrazine – TA (a)	0.17	0.31
Sunset Yellow – SY (b)	0.37	0.51
Allura Red – AR (c)	0.72	0.86
Crystal Ponceau – CP (d)	2.37	2.51
Fast Green – FG (e)	3.12	3.26

Table 7-2 – Adsorption Henry coefficients of Allura Red (AR), Crystal Ponceau (CP), Fast Green (FG), Sunset Yellow (SY) and Tartrazine (TA) in LiChroprep® RP-18 (particle size: 25-40 μm) using 20/80 (v/v) ethanol / 70mM acetic acid in water as solvent at room temperature and the corresponding adjusted adsorption Henry coefficients correct by a factor 0.14 in order to account for the average dead volume of 0.75 ml per zone in the Modified Prochrom® ICLC-16-10 Research Scale Continuous Chromatograph SMB (Prochrom, Nancy, France) unit, considering $\varepsilon = 0.31567$.

Considering the operating regions drawn for 8-zone SMB with extract (Figure 2-7) and raffinate recycle (Figure 2-8), different operating conditions were chosen and simulated using the mixing cell model as described in section 3.3 in the ChromWorks™ 2016 platform as an additional validation step, so that the simulated process performances could be compared to the equilibrium model-based predictions from sections 6.1.1 and 6.1.2. The main purpose of the validation study was to double-check the flow rates and switching intervals chosen based on the operating regions predicted by the method of characteristics (as explained in sections 6.1.1 and 6.1.2). The second objective of the simulation study was to evaluate how the 8-zone SMB unit would respond to inadequate operating conditions so that the experimental results could be more easily interpreted.

7.4.1. Parametric study: 8-zone SMB with extract recycle

Figure 7-11 shows the operating regions of 8-zone SMB with extract recycle (Figure 2-7) drawn considering the adsorption Henry coefficients shown in Figure 7-10 increased by

0.14 in order to account for the average extra dead volume of 0.75 ml for each column in the 8-zone SMB unit. The borders of the plot were drawn considering the smallest allowable values that the dimensionless flow rates can reach, $m = -0.46$, since values smaller than that correspond to negative flow rates.

The operating region of the central zones of the first subunit ($m_{II(1)}$, $m_{III(1)}$) was defined by the adjusted adsorption Henry coefficients of Sunset Yellow (b) and Allura Red (c), since its function was to separate the weakly adsorbing dyes Sunset Yellow (b) and Tartrazine (a) from the stronger adsorbing Allura Red (c), Crystal Ponceau (d) and Fast Green (e). The operating point inside the operating region indicated by the circle in Figure 7-11, represents the dimensionless flow rates chosen for zones II(1) and III(1).

In order for the column coming from zone I(1) to be completely regenerated before it moves to zone IV(2), $m_{I(1)}$ has to be larger than the adjusted adsorption Henry coefficient of Fast Green (e). Moreover, in order for the solvent coming from the first subunit and recycled into zone I(2) to be pure, the dimensionless flow rate in zone IV(1) cannot be larger than the adjusted adsorption Henry coefficient of Tartrazine (a). An operating point ($m_{I(1)}$, $m_{IV(1)}$) that respects these restrictions was chosen and is indicated in Figure 7-11 by the cross.

The purpose of the second subunit was to separate Allura Red (c) from Crystal Ponceau (d) and the stronger adsorbing Fast Green (e), therefore the maximal value for $m_{III(2)}$ was the adjusted adsorption Henry coefficient of Crystal Ponceau (d). As it can be inferred from the plot shown in Figure 7-11, the lowest limit of $m_{II(2)}$ is outside the plot area (its value is smaller than -0.46). Hence, the constraint defined by equation 6-10 is irrelevant, and $m_{III(2)}$ can be set arbitrarily small (as long as $v_{II(2)} \geq 0$ ml.min⁻¹), while complete recovery of Allura Red (c) is still expected. That is only possible because any flow rate in zone III(2) that respects the restriction $H_{AR} < m_{III(2)} < H_{CP}$ (d) is also high enough to completely elute Allura Red (c) from the column before it moves to zone II(2). Consequently, the flow rate in zone II(2) is irrelevant for the recovery of Allura Red (c). The operating point of the central zones of the second subunit ($m_{I(2)}$, $m_{IV(2)}$) is indicated in Figure 7-11 by the “x” and has to be inside the region defined by the minimum $m_{I(2)}$ necessary for the complete regeneration of the adsorbent in zone I(2) (given by the adjusted adsorption Henry coefficient of Fast Green (e)), and the maximum dimensionless flow rate in zone IV(2) that still allows the stream recycled into zone I(1) to be solute-free (defined by H_{AR}).

Since there is no value $m_{III(2)}$ can reach, where Allura Red (c) is expected to be lost in the second extract port, the following parametric study focused on the contamination of the

target solute Allura Red (c) by Crystal Ponceau (d) and Fast Green (e) in the second raffinate port when the second subunit is operated outside of its ideal operating region.

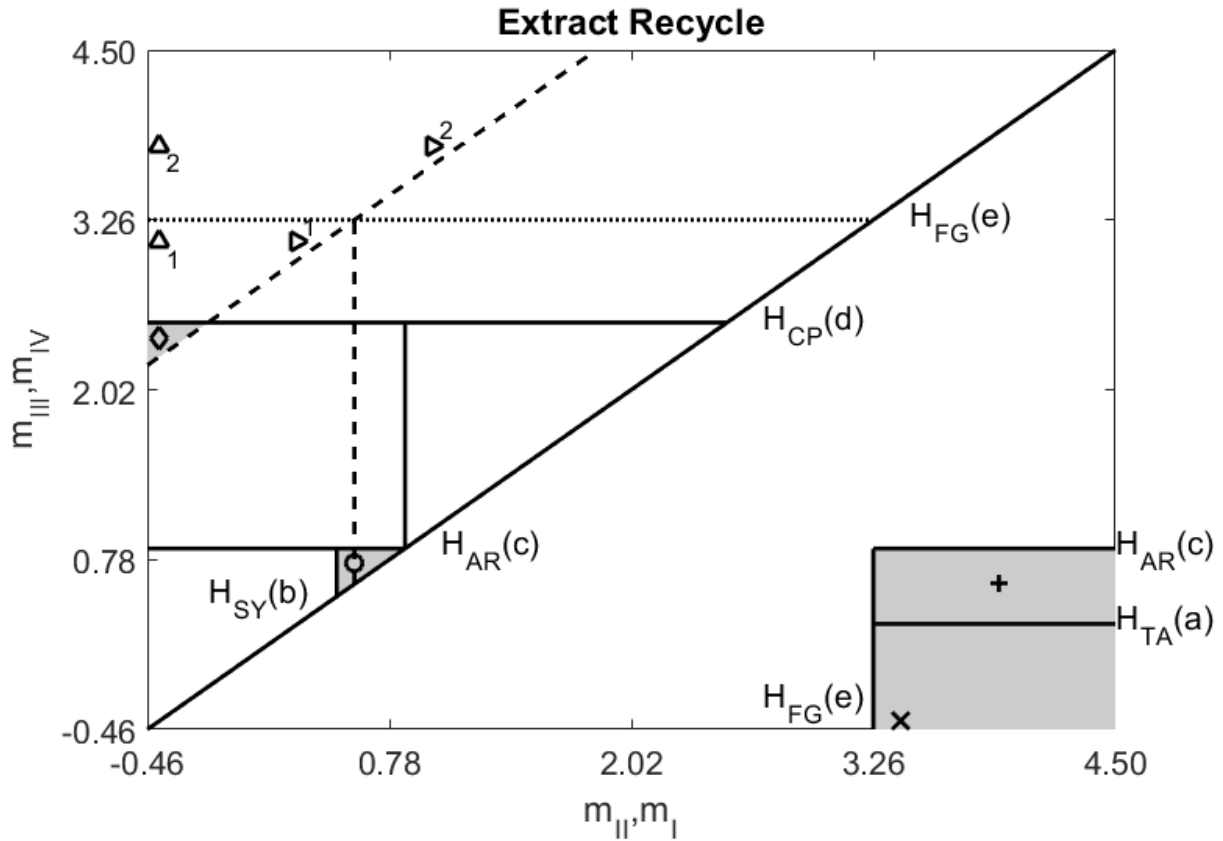


Figure 7-11 – Operating regions (grey areas) for the first and second subunits of 8-zone SMB with extract recycle where complete recovery yield of Allura Red (c) (AR) is expected considering the adsorption Henry coefficients shown in Table 7-2. The lowest borders of the plot are the smallest possible values for the dimensionless flow rates (m , where $v=0 \text{ ml}\cdot\text{min}^{-1}$, considering $\varepsilon = 0.31567$). The coordinates of $(m_{II(1)}, m_{III(1)})$ are given by the circle, the coordinates of $(m_{I(1)}, m_{IV(1)})$ are given by the “x”, and, the coordinates of $(m_{I(2)}, m_{IV(2)})$ are given by the cross. $m_{I(2)}=3.9$, $m_{IV(2)}=0.6$, $m_{I(1)}=3.4$, $m_{IV(1)}=-0.4$, $m_{II(1)}=0.6$ and $m_{III(1)}=0.75$. The coordinates of $(m_{II(2)}=-0.4, m_{III(2)}=2.4)$ where complete recovery and 100% purity of the target solute are expected are given by the diamond. The upward and leftward pointing triangles show the other coordinates tested for the second subunit $(m_{II(2)}, m_{III(2)})$. The performances calculated using ChromWorks™ 2016 are shown in Table 7-3. The calculations were performed using MATLAB R2015b.

As shown in Table 7-3, the performance of the separation process changes as the dimensionless flow rate in zone $m_{III(2)}$ is altered. Since the operating conditions of the first subunit were kept constant, and the dimensionless flow rates in zones II(1) and III(1) were within the first subunit's triangle, no contamination of the product stream with either Sunset Yellow (b) or Tartrazine (a) was expected. However, as shown in Table 7-3, as the dimensionless flow rate in zone III(2) is increased to values larger than H_{CP} (d), the second raffinate stream became contaminated with Crystal Ponceau (d). Remarkably, the recovery of Allura Red (c) remained at 100%, regardless of the flow rate in zones II(2) and III(2), which

further corroborates the hypothesis that, as long as $m_{II(2)}$ is larger than a minimum limit set by equation 6-10, no Allura Red (c) should be lost in the second extract outlet. Furthermore, only when $m_{III(2)}$ is smaller than H_{CP} (d), pure Allura Red (c) can be obtained in the second raffinate outlet.

$(m_{III(2)}, m_{II(2)})$	Symbol	Purity of AR (c)	Recovery Yield of AR (c)
$(m_{II(2)}=-0.4, m_{III(2)}=2.4)$	Diamond	99.9%	99.9%
$(m_{II(2)}=-0.4, m_{III(2)}=3.1)$	Upward pointing arrow 1	95.6%	99.9%
$(m_{II(2)}=-0.4, m_{III(2)}=3.8)$	Upward pointing arrow 2	65.6%	99.8%
$(m_{II(2)}=0.3, m_{III(2)}=3.1)$	Leftward pointing arrow 1	95.4%	99.9%
$(m_{II(2)}=1, m_{III(2)}=3.8)$	Leftward pointing arrow 2	63.2%	99.7%

Table 7-3 – Average performance after 50 cycles of the simulated 8-zone SMB with extract recycle calculated using ChromWorks™ 2016, considering the mixing cell model and 1000 mixing cells per column and the adsorption Henry coefficients shown in Table 7-2, $V_c=7.854$ ml and $t^*=4.7$ min.

The simulations confirmed that when the 8-zone SMB with extract recycle unit is operated at the flow rates shown in the Figure 7-11 and the operating point chosen for $m_{III(2)}$ and $m_{II(2)}$ is the one indicated by the diamond, Allura Red (c) should be obtained with high purity and recovery.

7.4.2. Parametric study: 8-zone SMB with raffinate recycle

The operating regions of 8-zone SMB with raffinate recycle (Figure 2-8) are shown in Figure 7-12. The adsorption Henry coefficients considered are shown in Table 7-2 and dimensionless flow rates smaller than -0.46 correspond to negative flow rates, and were, therefore, not considered. The operating region of the central zones of the first subunit (II(1) and III(1)) was defined by the adjusted adsorption Henry coefficient of Allura Red (c) and the equation 6-19, so that $m_{III(2)}$ can be inside the operating region defined by the equation 6-18. The point indicated by the circle in Figure 7-12, represents the value chosen for $m_{II(1)}$ and $m_{III(1)}$.

Since the function of the first subunit was to separate the more strongly adsorbing food dyes Crystal Ponceau (d) and Fast Green (e) from the weaker adsorbing Allura Red (c), Sunset Yellow (b) and Tartrazine (a) and the dimensionless flow rates ($m_{II(1)}$, $m_{III(1)}$) of the first subunit were not changed during the parametric study, the target solute (Allura Red (c)) was not expected to be contaminated by neither Crystal Ponceau (d) and Fast Green (e).

For a successful separation of Allura Red (c) from the mixture, the column coming from zone I(1) needed to be completely regenerated before moving to zone IV(2), therefore $m_{I(1)}$ had to be larger than the adjusted adsorption Henry coefficient of Fast Green (e). Moreover, the solvent coming from the first subunit and recycled into zone I(2) needed to be completely pure, therefore the dimensionless flow rate in zone IV(1) should not be larger than the adjusted adsorption Henry coefficient of Tartrazine (a). The operating point ($m_{I(1)}$, $m_{IV(1)}$) chosen for the simulation of the separation process is indicated in Figure 7-12 by the cross.

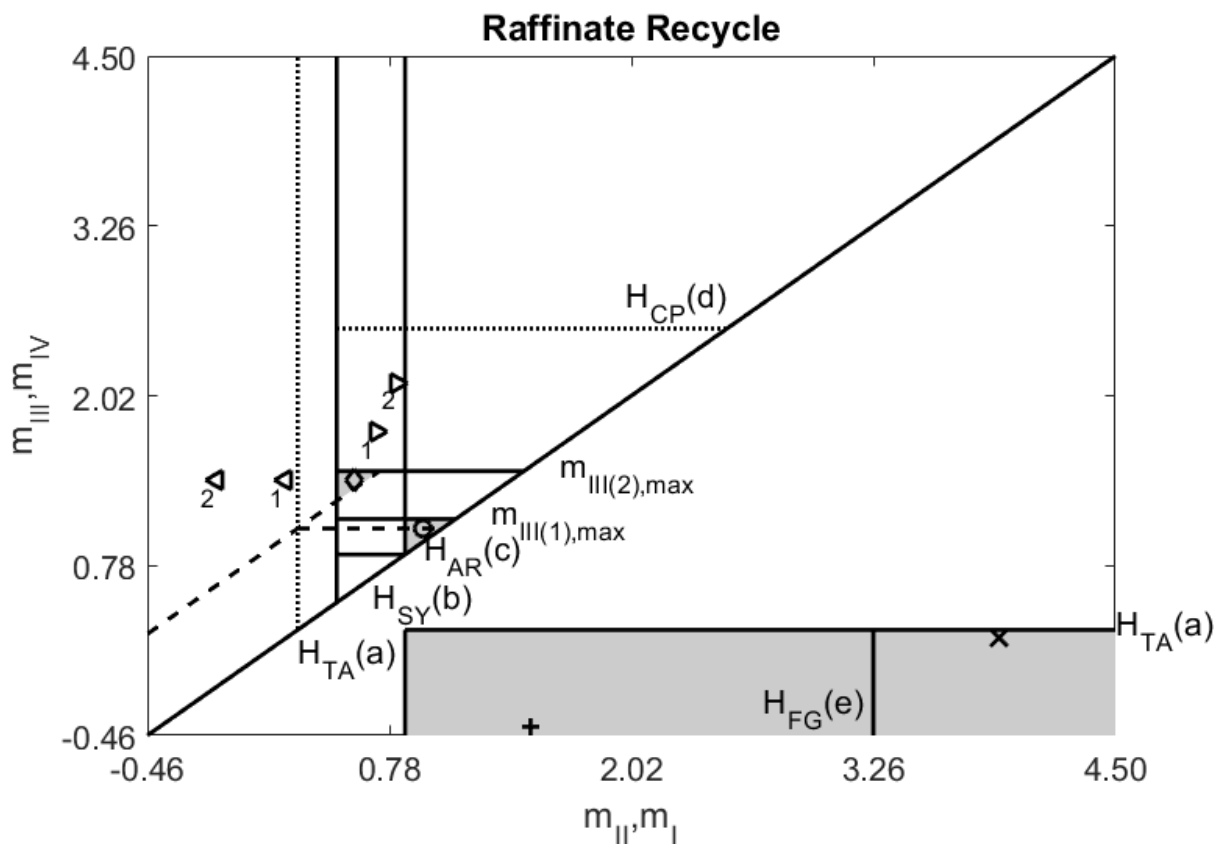


Figure 7-12 – Operating regions (grey areas) for the first and second subunits of 8-zone SMB with raffinate recycle where complete recovery yield of Allura Red (c) (AR) is expected considering the adsorption Henry coefficients shown in Table 7-2. The lowest borders of the plot are the smallest possible values for the dimensionless flow rates (m , where $v=0 \text{ ml}\cdot\text{min}^{-1}$, considering $\varepsilon = 0.31567$). The coordinates of ($m_{I(1)}$, $m_{III(1)}$) are given by the circle, the coordinates of ($m_{I(1)}$, $m_{IV(1)}$) are given by the “x”, and, the coordinates of ($m_{I(2)}$, $m_{IV(2)}$) are given by the cross. $m_{I(2)}=1.5$, $m_{IV(2)}=-0.4$, $m_{I(1)}=3.9$, $m_{IV(1)}=0.25$, $m_{II(1)}=0.95$ and $m_{III(1)}=1.05$. The coordinates of ($m_{II(2)}=0.6$, $m_{III(2)}=1.4$) where complete recovery and 100% purity of the target solute are expected are given by the diamond. The rightward and leftward pointing triangles show the other coordinates tested for the second subunit ($m_{II(2)}$, $m_{III(2)}$). The calculations were performed using MATLAB R2015b.

The purpose of the second subunit was the separation of Allura Red (c) from the more weakly adsorbing food dyes Tartrazine (a) and Sunset Yellow (b). Therefore, the lower limit

for $m_{II(2)}$ was the adjusted Henry coefficient of Sunset Yellow (b). The operating point ($m_{I(2)}$, $m_{IV(2)}$) is indicated in Figure 7-12 by the “x” and was defined inside the region delimited by the minimum $m_{I(2)}$ necessary for the complete regeneration of the column in zone I(2) (the adjusted adsorption Henry coefficient of Allura Red (c)), and the maximum dimensionless flow rate in zone IV(2) that allows the complete retention of Tartrazine (a) before recycling the solvent into zone I(1) (given by H_{TA} (a)).

$(m_{III(2)}, m_{II(2)})$	Symbol	Purity of AR (c)	Recovery Yield of AR (c)
$(m_{II(2)}=0.6, m_{III(2)}=1.4)$	Diamond	100%	99.7%
$(m_{II(2)}=0.71, m_{III(2)}=1.76)$	Rightward pointing arrow 1	100%	83%
$(m_{II(2)}=0.82, m_{III(2)}=2.11)$	Rightward pointing arrow 2	100%	27.5%
$(m_{II(2)}=0.25, m_{III(2)}=1.4)$	Leftward pointing arrow 1	62.8%	99.9%
$(m_{II(2)}=-0.11, m_{III(2)}=1.4)$	Leftward pointing arrow 2	39%	99.9%

Table 7-4 – Average performance after 50 cycles of the simulated 8-zone SMB with raffinate recycle calculated using ChromWorks™ 2016, considering the mixing cell model and 1000 mixing cells per column and the adsorption Henry coefficients shown in Table 7-2, $V_c=7.854$ ml and $t^*=4.7$ min.

The upper limit for $m_{III(2)}$ is given by equation 6-18, therefore, the operating points in Figure 7-12 found above this line (that is, the rightward pointing arrows) result in only partial recovery yields of the target solute Allura Red (c). As shown in Table 7-4, the higher $m_{III(2)}$ is, the lower the recovery yield of Allura Red (c) becomes. When the second subunit of the 8-zone SMB with raffinate recycle was operated at the point indicated by the diamond, the recovery yield reached approximately 100%, even though $m_{III(2)}$ was much higher than H_{AR} (c), thus confirming the strategy proposed in section 6.1.2 for the definition of the operating regions of 8-zone SMB with raffinate recycle.

The operation of 8-zone SMB with raffinate recycle with $m_{II(2)}$ values smaller than the lowest bound (given by H_{SY} (b)) is expected to compromise the purity of the Allura Red (c) fraction in the second extract port. This can be seen in Table 7-4, as the operating conditions represented by the leftward pointing arrows result in the contamination of the product with both Tartrazine (a) and Sunset Yellow (b). However, as both operating points share the same $m_{III(2)}$ coordinate (1.4), which is under the upper limit given by equation 6-18, they still result in approximately 100% recovery of Allura Red (c) in the second extract port.

Therefore, operation the Modified Prochrom® ICLC-16-10 Research Scale Continuous Chromatograph SMB (Prochrom, Nancy, France) at the dimensionless flow rates

shown in Figure 7-12 by the “x”, the cross, the circle and the diamond should result in a pure Allura Red (c) fraction, without any losses in the second raffinate port.

7.5. Food dye separation using raffinate recycle 8-zone SMB

An experimental isolation of Allura Red (c) using the Modified Prochrom® ICLC-16-10 Research Scale Continuous Chromatograph (Prochrom, Nancy, France) with recycle of the raffinate stream was performed using a mixture composed of 0.05 mg.l⁻¹ of Tartrazine (a), Sunset Yellow (b), Crystal Ponceau (d), and the target solute, Allura Red (c), as well as 0.015 mg.l⁻¹ of Fast Green (e) using a mixture of 20/80 (v/v) ethanol / 70mM acetic acid in water as solvent. The dimensionless flow rates indicated in Figure 7-12 by the “x”, the cross, the circle and the diamond were used for the operation of the system. The switching interval chosen was 4.7 min, so that none of the resulting solvent flow rates were higher than 5 ml.min⁻¹. The flow rates used were $v_{I(2)}=2.243$ ml.min⁻¹, $v_{II(2)}=1.214$ ml.min⁻¹, $v_{III(2)}=2.128$ ml.min⁻¹, $v_{IV(2)}=0.070$ ml.min⁻¹, $v_{I(1)}=4.987$ ml.min⁻¹, $v_{II(1)}=1.614$ ml.min⁻¹, $v_{III(1)}=1.728$ ml.min⁻¹, $v_{IV(1)}=0.8139$ ml.min⁻¹, $v_{D2}=1.429$ ml.min⁻¹, $v_{E2}=1.029$ ml.min⁻¹, $v_{F2}=0.915$ ml.min⁻¹, $v_{R2}=2.058$ ml.min⁻¹, $v_{D1}=4.917$ ml.min⁻¹, $v_{E1}=3.374$ ml.min⁻¹, $v_{F1}=0.114$ ml.min⁻¹ and $v_{R1}=0.915$ ml.min⁻¹.

The complete volume of every outlet stream was collected separately over each cycle, which corresponded to 16 valve switches, the time period necessary for the multiport valves to reach their starting positions. Each fraction was homogenized and 100 µL samples were taken from them and analyzed using a Luna C18 column (Phenomenex®, USA) in the Agilent Infinity 1260 (Agilent Technologies, USA) according to the analysis protocol described in section 7.2.1. Figure 7-14 shows the stacked chromatograms of the pooled fractions from the first extract outlet stream from each cycle of the first experimental run, the chromatograms of the other outlet stream are shown in the Appendix A, in Figures A-1 to A-2 for every cycle and the corresponding concentrations are listed in Tables A-1 to A-3.

The outlet course of each food dye concentration is shown in Figure 7-13 and the performance of the separation is shown in Table 7-5. It can be seen in Figure 7-13 and in Figure 7-15, that after approximately five complete cycles of continuous uninterrupted operation, the outlet concentrations became approximately constant.

During the first experimental run, as shown in Figure 7-13, the feed pump was switched off two times, first at the fifth and then at the eighth cycle. This was an automatic response of the system caused by sudden pressure spikes measured at the feed pump Q1

(Figure 7-5), whose origin could not be precisely determined. Nevertheless, in order to collect as much data as possible, the experiment proceeded until a stable cyclic steady state was again achieved. It is possible to see in Figure 7-13 that five cycles after the second time the feed pump was switched off, the outlet concentrations achieved a stable cyclic steady state.

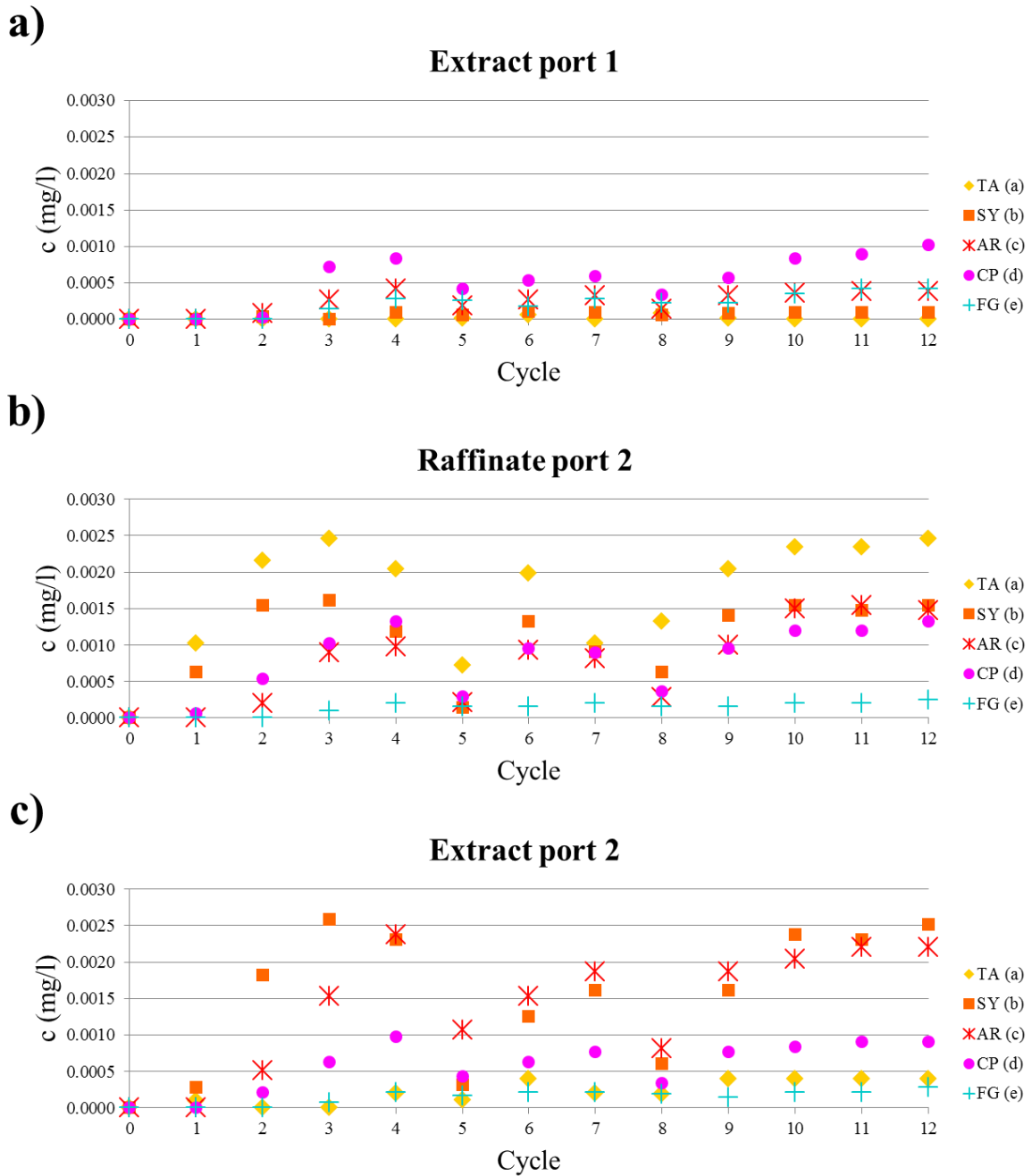


Figure 7-13 – Outlet concentrations averaged over each cycle of the first experimental run of 8-zone SMB with raffinate recycle. a) Extract Port 1 (3.374 ml.min⁻¹), b) Raffinate Port 2 (2.058 ml.min⁻¹), c) Extract Port 2 (1.029 ml.min⁻¹).

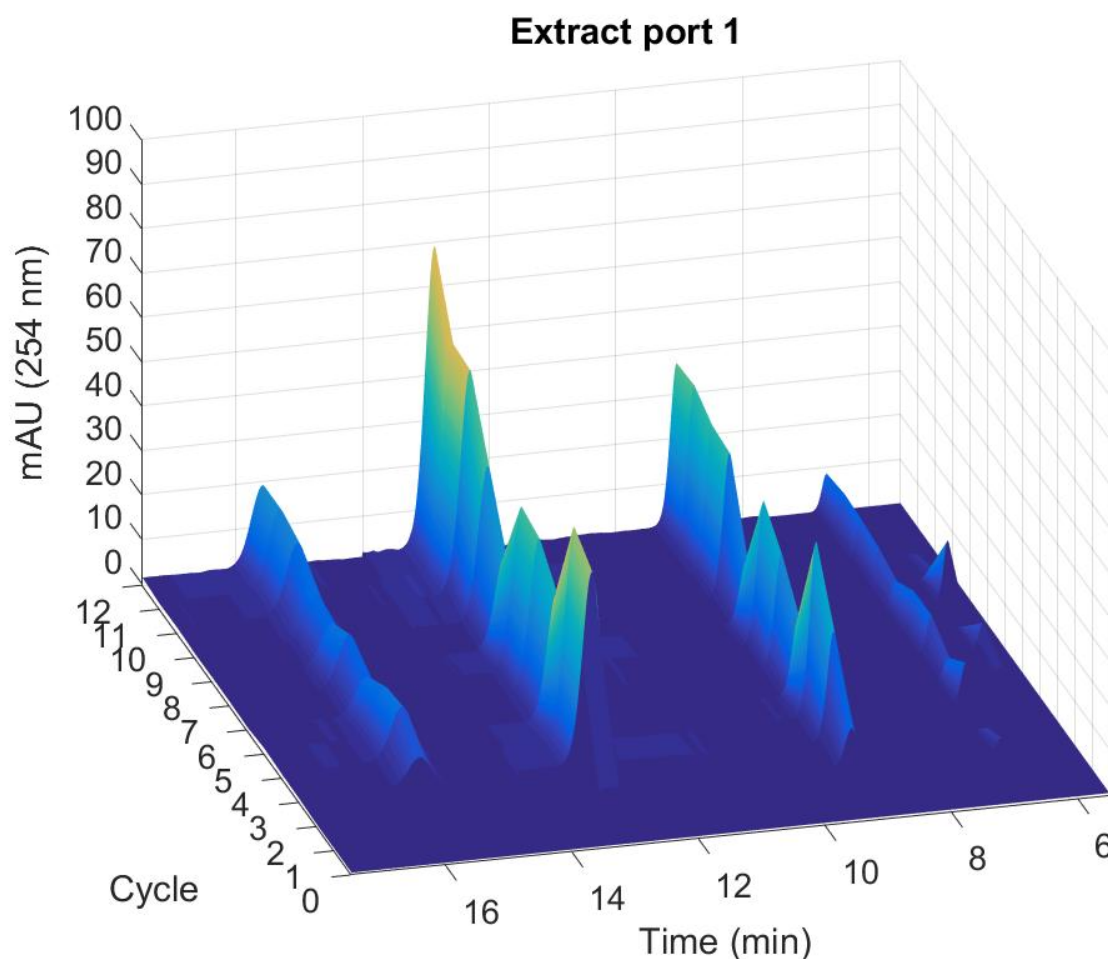


Figure 7-14 – First experimental run of the 8-zone SMB with raffinate recycle - Chromatograms showing the composition of the pooled fractions from the first extract port of each of the 12 cycles. The time axis shows the chromatogram of each sample obtained using the HPLC method described in section 7.2.1. The “cycle” axis indicates from which cycle each sample was obtained from. The vertical axis shows the absorbance signal from the chromatograms at 254 nm. The first peak corresponds to Tartrazine (a), the second, to Sunset Yellow (b), the third, to Allura Red (c), the fourth, to Crystal Ponceau (d) and the fifth, to Fast Green (e).

It can be seen in Table 7-5 that the target solute Allura Red (c) was only obtained at 36.22% of purity. Furthermore, the recovery yield obtained was also very low, at about 27.12%. As shown in Figure 7-13 c), the product fraction was mostly contaminated with Sunset Yellow (b), although significant amounts of Crystal Ponceau (d), Fast Green (e) and traces of Tartrazine (a) could also be found in it.

The weakly adsorbing fraction A, composed of Tartrazine (a) and Sunset Yellow (b), was expected to be obtained pure in the second raffinate port. However, only 41.91% Sunset Yellow (b) could be recovered in that stream and, while Tartrazine (a) could mostly be recovered in the expected outlet port (at 65.89% of recovery yield), fraction A was still

heavily contaminated with Allura Red (c), Crystal Ponceau (d) and Fast Green (e), as shown in Figure 7-13 b).

Moreover, the first subunit did not successfully purify the stronger adsorbing fraction C, since relatively large amounts of Allura Red (c) could be found contaminating it. It can be seen in Table 7-5 that the recovery yield of Fast Green (e) was around 45.77% and only 33.62% of Crystal Ponceau (d) could be recovered in the first extract port.

	TA (a)	SY (b)	AR (c)	CP (d)	FG (e)
Recovery Yield (%)	65.89%	41.91%	27.12%	33.62%	45.77%
Purity (%)	38.05%	24.20%	36.22%	49.29%	20.14%

Table 7-5 – Performance of the first experimental run of 8-zone SMB with raffinate recycle.

7.6. Repetition of the food dye separation using 8-zone SMB

Due to the feed disruptions in the first experimental run, a second one was performed using the same mixture (composed of 0.05 mg.l⁻¹ of Tartrazine (a), Sunset Yellow (b), Crystal Ponceau (d) and Fast Green (e) and 0.015 mg.l⁻¹ of Allura Red (c)) and the same flow rates and switching intervals (shown in Figure 7-12). The outlet streams of the 8-zone SMB unit with raffinate recycle were once more collected over each complete cycle and 100 µL samples of each of them were analyzed using the HPLC method described in section 7.2.1. The chromatograms are depicted in Figures A-3 to A-5 and the Tables A-4 to A-6 show the corresponding concentrations. The performance of the separation, however, did not change very significantly.

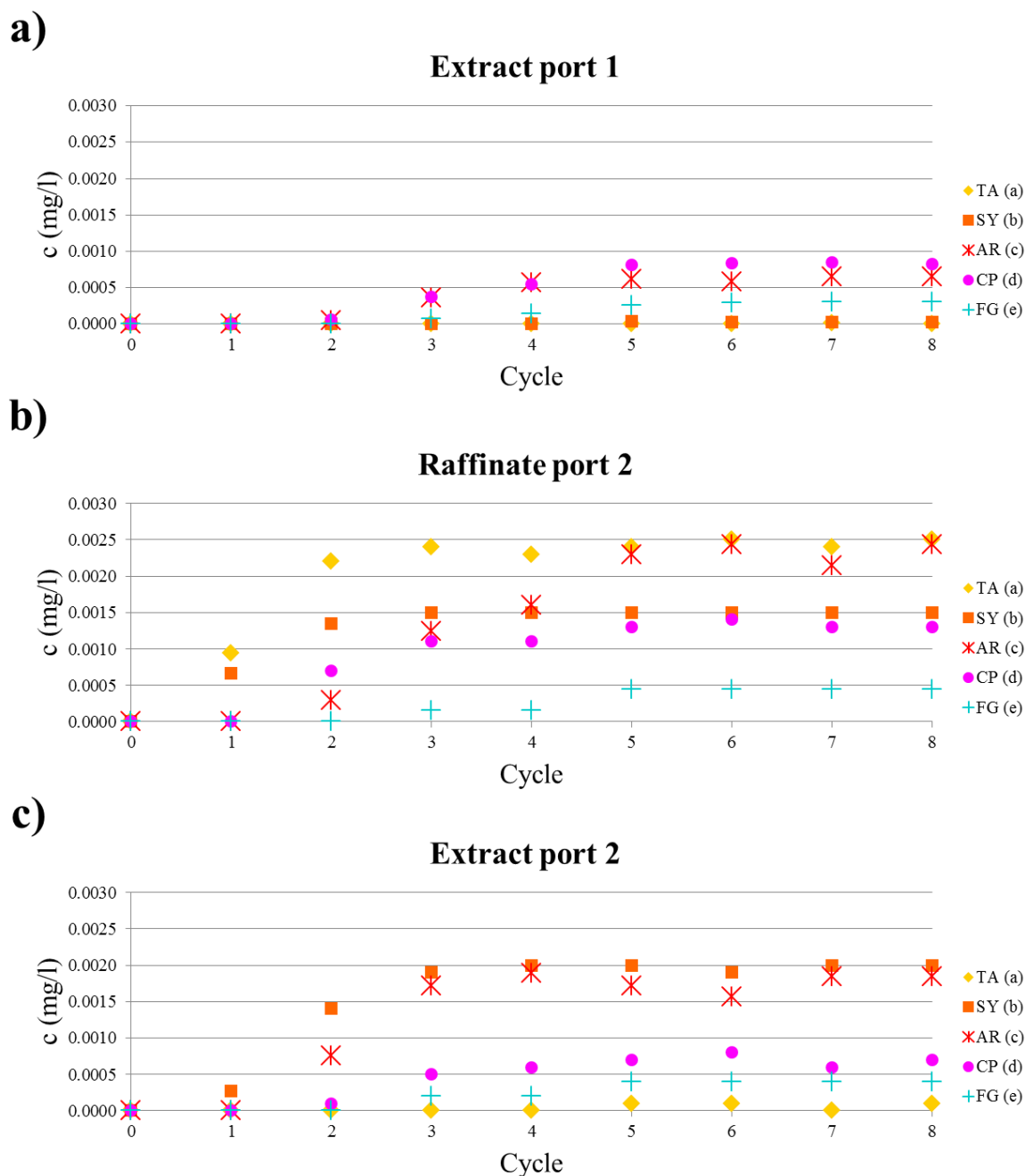


Figure 7-15 – Outlet concentrations averaged over each cycle of the second experimental run of 8-zone SMB with raffinate recycle. a) Extract Port 1 ($3.374 \text{ ml}\cdot\text{min}^{-1}$), b) Raffinate Port 2 ($2.058 \text{ ml}\cdot\text{min}^{-1}$), c) Extract Port 2 ($1.029 \text{ ml}\cdot\text{min}^{-1}$).

As shown in Table 7-6, the recovery yield of Allura Red (c) was only 25.58% (compared to the 27.12% of the first experimental run), with a purity of 36.44%. As shown in Figure 7-15 c), it was mostly contaminated with Sunset Yellow (b), although, as in the first experimental run (Figure 7-13 c), large amounts of Crystal Ponceau (d) and Fast Green (e) could also be found.

While Tartrazine (a) was, as expected, mostly obtained in the second raffinate port (at 79.64% of recovery, compared to the 65.89% recovery yield from the first experimental run), Figure 7-15 b) shows that it was still contaminated with Allura Red (c), Crystal Ponceau (d) and Fast Green (e), in the same way as the first experimental run. Sunset Yellow (b) was also expected to be present in fraction A, however, although a relatively large portion of the solutes in the second raffinate stream was composed of Sunset Yellow (b), it can be seen in Figure 7-15 c) that large amounts of Sunset Yellow (b) were also lost in the second extract stream, where it contaminated the product.

The performance of the first subunit also did not change very significantly compared to the first experimental run. Figure 7-15 a) shows that this fraction is still significantly contaminated with Allura Red (c). The recovery of Fast Green (e) in the first extract port, however, dropped to 34.09%, compared to the 45.77% of the first experimental run.

	TA (a)	SY (b)	AR (c)	CP (d)	FG (e)
Recovery (%)	79.64%	49.71%	25.58%	32.01%	34.09%
Purity (%)	34.32%	21.42%	36.44%	19.56%	14.79%

Table 7-6 – Performance of the second experimental run of 8-zone SMB with raffinate recycle.

7.7. Discussion and outlook

Food dyes were chosen as a model solute mixture to demonstrate a center-cut separation using 8-zone SMB with raffinate recycle, as these compounds are non-toxic and colorful compounds. As shown in sections 7.3.1 and 7.3.2, their differing visible light absorbance spectra can, not only, be used for the estimation of their concentration, but also for visually analyzing the composition of solutions. However, since the fractions obtained from the raffinate recycle 8-zone SMB experimental runs were too diluted to have absorbances over the sensitivity limit of the spectrophotometer Genesys 6 (Thermo Fisher Scientific, Germany) used in this work, the samples obtained had to be, instead, analyzed using a HPLC system.

Consequently, a HPLC method for the estimation of the concentrations of the food dyes was developed using a 25 cm long Luna C18 column (Phenomenex®, USA) and the Agilent Infinity 1260 (Agilent Technologies, USA), as described in section 7.2.1. With this method, it was possible to analyze the outlet fractions produced by the two raffinate recycle 8-zone SMB experimental runs. The chromatograms generated are shown in Figure 7-14 and

Figures A-1 to A-5 for each outlet port for every cycle of the two raffinate recycle 8-zone SMB experimental runs. The concentration of each food dye in each outlet port, estimated using the software Chromeleon™ (Thermo Fisher Scientific, Germany), are shown in Tables A-1 to A-6.

The eight LiChrorep® RP-18 columns used in the Modified Prochrom® ICLC-16-10 unit were characterized and the adsorption isotherms of Allura Red (c), Crystal Ponceau (d), Fast Green (e), Sunset Yellow (b) and Tartrazine (a) were estimated using 15% – 30% (v/v) ethanol complemented with 70mM acetic acid in water as solvent.

It was found that lower concentrations of ethanol in the solvent corresponded to larger adsorption Henry coefficients. As shown in Figure 7-9, this dependency could be explained using the Soczewinski equation [221], which describes an exponential dependency between the adsorption Henry coefficient of solutes and the organic modifier concentration, similar to the one suggested by Poole, C. F. [215], which is predicted by the partition equilibrium model explained in section 7.1 [213].

A mixture of 20/80 (v/v) ethanol / 70mM acetic acid in water generated the widest separation of the food dyes, without increasing the Fast Green (e) adsorption Henry coefficient, the strongest adsorbing dye used, over 10. Using the food dyes adsorption Henry coefficients, the raffinate and extract recycle 8-zone SMB operating parameter ranges were drawn using the methodology developed in the chapter 6. Flow rates and switching intervals inside and outside these operating regions were simulated using the mixing cell model in the ChromWorks™ 2016 platform in order to evaluate how the performance of the separation of Allura Red (c) using 8-zone SMB would respond to inadequate operating conditions and also to double-check the operating parameters chosen for the experimental runs.

The continuous purification of Allura Red (c) from a mixture containing Tartrazine (a), Sunset Yellow (b), Crystal Ponceau (d) and Fast Green (e) was tested with the Modified Prochrom® ICLC-16-10 Research Scale Continuous Chromatograph (Prochrom, Nancy, France) unit with raffinate recycle using the operating parameters validated in the ChromWorks™ 2016 simulations. However, during the first experimental run, the feed pump was automatically switched off two times and, therefore, a second run was performed.

The resulting outlet concentration profiles of the second experimental run did not differ much, despite of the feed interruptions of the first one. Nonetheless, in either case, the isolation of Allura Red (c) was not successful. Its recovery yield was, on average, 26.3% and

the average purity obtained was 36.3%. The product stream was mostly contaminated with Sunset Yellow (b) and, in smaller amounts, by Fast Green (e) and Crystal Ponceau (d).

Tartrazine (a) was the only dye mostly obtained in the fraction it was supposed to be (as shown in Figure 7-13 a) and in Figure 7-15 a)), therefore, its adsorption Henry coefficient must be higher than -0.54 (the dimensionless flow rate in zone IV(1) minus the correction factor of 0.14) and smaller than 0.81 (the dimensionless flow rate in zone II(1) minus the correction factor of 0.14). Therefore, the adsorption Henry coefficient of 0.17, estimated in the frontal analysis experiments, may be accurate.

Sunset Yellow (b) could not be found in the first extract stream (as shown in Figure 7-13 a) and in Figure 7-15 a)), therefore, it can be concluded that the dimensionless flow rate in zone II(1) was high enough to prevent it from contaminating fraction C. Hence, the adsorption Henry coefficient of Sunset Yellow (b) must be lower than 0.81 (the dimensionless flow rate in zone II(1) minus the correction factor of 0.14). The presence of Sunset Yellow (b) in the second extract port, however, indicates that its adsorption Henry coefficient must be higher than 0.46 (the dimensionless flow rate in zone II(2) minus the correction factor of 0.14) and, therefore, larger than the estimated 0.37 from the frontal analysis experiments described in section 7.3.3. Nonetheless, since that is a relatively small difference, it is also possible that the estimated adsorption Henry coefficient was accurate and the difference between its retention times in the raffinate recycle 8-zone SMB experimental runs and in the frontal analyses was instead caused by the dispersion of the concentration shocks in the dead volumes of the Modified Prochrom® ICLC-16-10 Research Scale Continuous Chromatograph SMB (Prochrom, Nancy, France) unit. Given that the dead volumes between the zones were approximately one quarter of the dead volumes inside the chromatographic columns, and the dead volume inside the recycle was even larger, this option cannot be discarded [84, 85, 222].

Both experimental runs show that Allura Red (c), Crystal Ponceau (d) and Fast Green (e) have much higher retention times in the raffinate recycle 8-zone SMB experiments than in the frontal analyses of section 7.3.3. This conclusion is supported by the fact that the adsorbent was not being completely regenerated at zone I(1), since these three food dyes were found in every outlet port. Conversely, it could also be deduced that Allura Red (c), Crystal Ponceau (d) and Fast Green (e) were, instead, much less retained in the SMB experimental runs than in the frontal analysis experiments, since this could also explain their presence in all of the outlet ports. However, their retention times must have been at least one

order of magnitude larger in the SMB experimental runs than the values estimated in the frontal analysis experiments of section 7.3.3, since they first leave the chromatographic columns only after two complete cycles. Fast Green (e), in particular, must have had even larger retention times than Allura Red (c) and Crystal Ponceau (d), since three complete cycles were over before it could be found in any significant amounts in the outlet ports of the second subunit. This conclusion is reinforced by the fact that in the first experimental run, when the feed pump was switched off two times, the recovery yield of Fast Green (e) was higher than in the second experimental run, when the SMB system was continuously fed, which can be explained by the reduction of the amount of Fast Green (e) fed into the system during the first experiment resulting in a relatively larger elution to loading time ratio that increased its recovery yield.

The significant difference between the adsorption behavior of Allura Red (c), Crystal Ponceau (d) and Fast Green (e) in the frontal analysis and in the raffinate recycle 8-zone SMB experiments cannot be explained by small experimental imprecisions in the estimation of the adsorption isotherms. Moreover, the outlet flow rates of the second experimental run of the 8-zone SMB with raffinate recycle unit were carefully measured, and the flow rate inaccuracies were always under 0.5%; too small to explain such large differences. The source of error in the prediction of their retention times must be, instead, in the assumptions made about their adsorption isotherms. One possibility is that the adsorption of Allura Red (c), Crystal Ponceau (d) and Fast Green (e) is much stronger than estimated in the frontal analysis experiments. However, both the front and rear concentration shocks of the food dyes were carefully recorded during the frontal analyses and their shapes closely analyzed and no sign of nonlinearity of the adsorption isotherms were noticed.

The main difference between the frontal analyses and the SMB experimental runs performed in the Modified Prochrom® unit with recycle of the raffinate stream were the relatively high concentrations used in the former compared to the internal concentrations of the latter. As shown in Figure 7-13 and in Figure 7-15, the concentrations of the raffinate recycle 8-zone SMB outlets were much lower than the 1 mg.l^{-1} used in the frontal analysis experiments, since it was assumed that if the adsorption isotherms appear to be linear at high concentrations they must remain so at low concentrations as well.

Although the adsorption isotherms of the concentrated food dyes appeared to be linear, they seem to have much stronger affinities for the C18-bound silica adsorbent at low concentrations. As explained in section 7.1, this could be explained by their ionization at

higher concentrations caused by a concentration increase at the surface of the adsorbent, since the food dyes used in this work have two sulfonyl groups each (three, in the case of Fast Green (e), as shown in Figure 7-1), therefore, their net charge can be anywhere from 0 to -2 (or -3, in the case of Fast Green (e)) in aqueous solutions [207].

As described in section 7.1, the adsorption behavior of charged molecules on octadecyl-coated silica particles is highly dependent on their charges, which are a function of the solution pH and, therefore, correlated to the concentration of the acetic acid buffer [207, 210, 223, 224]. Typically, molecules with high charge density do not have much affinity for the nonpolar octadecyl groups that coat the surface of the C18-silica particles [80, 210, 213, 219]. Consequently, if the food dyes have a neutral charge, they should adsorb with the highest affinity. Hence, it is possible that, at low concentrations, they become undissociated and bind more strongly to the column.

Another potential interfering factor in the adsorption behavior of the food dyes is the presence of contaminating byproducts of their synthesis processes as well as their degradations products, which could be interfering with the extent of their dissociation. However, these interactions, if present, are likely to be minor, since high grade standard food dyes were used in this work.

In order to increase the likelihood of a successful 8-zone SMB separation of Allura Red (c) from the dye mixture using the LiChroprep® RP-18 particles, larger chromatographic columns should be used in order to decrease the relative importance of the Prochrom® ICLC-16-10 unit dead volumes on the retention times of the solutes [84, 85, 222]. Moreover, the quality of the separation could be improved by adding process control to the system in order to prevent flow rate variations (as the ones seen in the first experimental run) and to adjust operating conditions to unexpected retention times [225-227]. Furthermore, more detailed experimental studies, taking into account the effects of pH, ionic strength and acetic acid concentration on the adsorption behavior of the food dyes, are necessary. Additionally, since the increased retention times of the food dyes in comparison to the frontal analyses was correlated to their lower concentrations in the 8-zone SMB experimental runs, it is possible that higher feed concentrations would result in improved separation performance.

Finally, it is worth emphasizing that most of the experimental challenges faced in this experimental study were caused by the ionic nature of the dyes used. Given the success of the protocol for estimating the concentrations of the individual dyes in mixed solutions using absorbance spectra deconvolution and that much of the experimental work was indeed

facilitated by the use of colorful solutions, the use of dyes for the study of different continuous liquid chromatography configurations has much potential. However, the use nonpolar dyes would be recommended instead, since their adsorption behavior should be easier to predict and to interpret [210].

7.8. Conclusions

The present chapter described the absorbance spectra and the adsorption isotherms of a pseudo-ternary mixture of five food dyes. A suitable solvent composition, yielding an adequate separation between the solutes, was chosen to demonstrate a raffinate recycle 8-zone SMB separation using eight LiChroprep® RP-18 columns in a Prochrom® ICLC-16-10 unit. The setup of the flow rates and switching time intervals was based on the methods developed in chapter 6 and independently confirmed using numerical simulations in the software ChromWorks™ 2016.

The experiments showed that, while theoretically feasible, an 8-zone SMB separation is not necessarily straightforward to realize, since it is influenced by several factors such as adsorption isotherm nonideality and dead volume effects. However, the potential of dyes for studying such advanced continuous liquid chromatography configurations as the 8-zone SMB was reaffirmed – as well as the need for greater care during adsorption isotherm estimation, solvent choice, dead volume estimation and process control.

8. Summary and general conclusions

The mixing cell and equilibrium models, taking into account economic factors, were used in chapter 5 to maximize the profitability of the 8-zone SMB with extract and raffinate recycle exploiting the TMB analogy. The economic performance at each respective best operating conditions were compared, which led to the derivation of simple criteria for the decision of which of the two separation sequences (easier separation or harder separation first) results in the highest profit (equations 5-56 and 5-57). Subsequently, a decision tree (Figure 5-11) was created to facilitate the choice between the two configurations as a function of the adsorption Henry coefficients and the specific process costs.

The differences between SMB with 8 zones and its geometric equivalent TMB analog were studied in depth in chapter 6, which resulted in more accurate predictions of its operating regions. These operating spaces were used for better estimating the performance of 8-zone SMB and for comparing it to the 4-zone SMB cascade, and it was shown that, in some cases, the former might be a better option.

The tools developed in chapter 6 were applied to an 8-zone SMB experimental center-cut separation of food dyes in chapter 7. Though, no pure intermediary eluting solute could be completely isolated, many of the hurdles of using food dyes as model experimental mixtures and of realizing an 8-zone SMB separation were unveiled. Additionally, the potential benefits of using 8-zone SMB for performing center-cut separations could be demonstrated.

The conclusions drawn in chapter 5 may motivate the development of similar decision trees for other continuous center-cut equilibrium-staged separations such as extraction, crystallization and distillation. Furthermore, in order to increase the scope of the methodologies developed in chapters 5 and 6, they should be extended for separation governed by nonlinear and competitive adsorption isotherms. The insight on how internal recycles may cause SMB and geometrically equivalent TMB models to perform significantly differently can be applied for other industrially relevant SMB systems, such as the Parex® process family (UOP Honeywell, USA). Although, dyes were established, in chapter 7, as attractive model solutes for demonstrating continuous liquid chromatography configurations, a selection of other (uncharged) dyes, the use of SMB systems with smaller dead volumes and the implementation of process control could, in the future, greatly support the success of this promising technology.

9. References

1. Broughton, D.B. and C.G. Gerhold, *Continuous Sorption Process Employing Fixed Bed of Sorbent and Moving Inlets and Outlets*. 1961: United States of America.
2. Guiochon, G., A. Felinger, and D.G.G. Shirazi, *Fundamentals of Preparative and Nonlinear Chromatography*. 2006: Elsevier Science.
3. Nicolaos, A., et al., *Application of equilibrium theory to ternary moving bed configurations (four plus four, five plus four, eight and nine zones) I. Linear case*. Journal of Chromatography A, 2001. **908**(1-2): p. 71-86.
4. Chiang, A.S.T., *Continuous chromatographic process based on SMB technology*. Aiche Journal, 1998. **44**(8): p. 1930-1932.
5. Agrawal, G. and Y. Kawajiri, *Comparison of various ternary simulated moving bed separation schemes by multi-objective optimization*. Journal of Chromatography A, 2012. **1238**: p. 105-113.
6. Agrawal, G., B. Sreedhar, and Y. Kawajiri, *Systematic optimization and experimental validation of ternary simulated moving bed chromatography systems*. Journal of Chromatography A, 2014. **1356**: p. 82-95.
7. Kessler, L.C. and A. Seidel-Morgenstern, *Theoretical study of multicomponent continuous countercurrent chromatography based on connected 4-zone units*. Journal of Chromatography A, 2006. **1126**(1-2): p. 323-337.
8. Nowak, J.J. and A. Seidel-Morgenstern, *Separation of Ternary Mixtures by Simulated Moving Bed Chromatography: Theoretical Study and Experimental Validation*. 2013: Docupoint-Verlag.
9. Nowak, J., D. Antos, and A. Seidel-Morgenstern, *Theoretical study of using simulated moving bed chromatography to separate intermediately eluting target compounds*. Journal of Chromatography A, 2012. **1253**: p. 58-70.
10. Kiwala, D., et al., *Center-cut separation of intermediately adsorbing target component by 8-zone simulated moving bed chromatography with internal recycle*. Journal of Chromatography A, 2016. **1453**: p. 19-33.
11. Seidel-Morgenstern, A., L.C. Kessler, and M. Kaspereit, *New developments in simulated moving bed chromatography*. Chemical Engineering & Technology, 2008. **31**(6): p. 826-837.
12. da Silva, F.V.S. and A. Seidel-Morgenstern, *Evaluation of center-cut separations applying simulated moving bed chromatography with 8 zones*. Journal of Chromatography A, 2016. **1456**: p. 123-136.
13. Storti, G., et al., *Robust design of binary countercurrent adsorption separation processes*. Aiche Journal, 1993. **39**(3): p. 471-492.
14. Nicoud, R.M., et al., *Enantiomeric enrichment of non-racemic mixtures of binaphthol with non-chiral packings*. Chirality, 1996. **8**(3): p. 234-243.
15. Schulte, M., et al., *Simulated moving-bed chromatograph - An efficient technique to producing optically active compounds on an industrial scale*. Chemie Ingenieur Technik, 1996. **68**(6): p. 670-&.
16. Blehaut, J. and R.M. Nicoud, *Recent aspects in simulated moving bed*. Analisis, 1998. **26**(7): p. M60-M70.
17. Kniep, H., et al., *Separation of enantiomers by simulated moving bed chromatography*. Chemie Ingenieur Technik, 1999. **71**(7): p. 708-713.
18. Kniep, H., et al., *Separation of enantiomers through simulated moving-bed chromatography*. Chemical Engineering & Technology, 2000. **23**(10): p. 853-857.
19. Lorenz, H., P. Sheehan, and A. Seidel-Morgenstern, *Coupling of simulated moving bed chromatography and fractional crystallisation for efficient enantioseparation*. Journal of Chromatography A, 2001. **908**(1-2): p. 201-214.

20. Denet, F., et al., *Enantioseparation through supercritical fluid simulated moving bed (SF-SMB) chromatography*. Industrial & Engineering Chemistry Research, 2001. **40**(21): p. 4603-4609.
21. Azevedo, D.C.S., L.S. Pais, and A.E. Rodrigues, *Enantiomers separation by simulated moving bed chromatography - Non-instantaneous equilibrium at the solid-fluid interface*. Journal of Chromatography A, 1999. **865**(1-2): p. 187-200.
22. Kaspereit, M., et al., *Impact of adsorption isotherm parameters on the performances of enantioseparation using simulated moving bed chromatography*. Journal of Chromatography A, 2002. **944**(1-2): p. 249-262.
23. Mihlbachler, K., et al., *Adsorption behavior of the (+/-)-Troger's base enantiomers in the phase system of a silica-based packing coated with amylose tri(3,5-dimethyl carbamate) and 2-propanol and molecular modeling interpretation*. Journal of Chromatography A, 2006. **1113**(1-2): p. 148-161.
24. Petrusavska, K., et al., *Chromatographic enantioseparation of amino acids using a new chiral stationary phase based on a macrocyclic glycopeptide antibiotic*. Journal of Separation Science, 2006. **29**(10): p. 1447-1457.
25. Elsner, M.P., G. Ziornek, and A. Seidel-Morgenstern, *Simultaneous preferential crystallization in a coupled, batch operation mode - Part 1: Theoretical analysis and optimization*. Chemical Engineering Science, 2007. **62**(17): p. 4760-4769.
26. Geddicke, K., et al., *Conceptual design and feasibility study of combining continuous chromatography and crystallization for stereoisomer separations*. Chemical Engineering Research & Design, 2007. **85**(A7): p. 928-936.
27. Perrin, S.R., et al., *Purification of difluoromethylornithine by global process optimization: Coupling of chemistry and chromatography with enantioselective crystallization*. Organic Process Research & Development, 2007. **11**(5): p. 817-824.
28. Zhanga, L., et al., *Application of an eremomycin-chiral stationary phase for the separation of DL-methionine using simulated moving bed technology*. Journal of Chromatography A, 2007. **1162**(1): p. 90-96.
29. Forssen, P., et al., *Effects of a strongly adsorbed additive on process performance in chiral preparative chromatography*. Journal of Chromatography A, 2008. **1212**(1-2): p. 89-97.
30. Rajendran, A., G. Paredes, and M. Mazzotti, *Simulated moving bed chromatography for the separation of enantiomers*. Journal of Chromatography A, 2009. **1216**(4): p. 709-738.
31. Katsuo, S. and M. Mazzotti, *Intermittent simulated moving bed chromatography: 2. Separation of Troger's base enantiomers*. Journal of Chromatography A, 2010. **1217**(18): p. 3067-3075.
32. Langel, C., et al., *Experimental Optimizing Control of the Simulated Moving Bed Separation of Troger's Base Enantiomers*. Industrial & Engineering Chemistry Research, 2010. **49**(23): p. 11996-12003.
33. Katsuo, S., et al., *Intermittent simulated moving bed chromatography: 3. Separation of Troger's base enantiomers under nonlinear conditions*. Journal of Chromatography A, 2011. **1218**(52): p. 9345-9352.
34. Palacios, J.G., et al., *Experimental validation of a new integrated simulated moving bed process for the production of single enantiomers*. Journal of Chromatography A, 2011. **1218**(16): p. 2232-2239.
35. Ribeiro, A.E., et al., *Chiral Separation of Flurbiprofen Enantiomers by Preparative and Simulated Moving Bed Chromatography*. Chirality, 2011. **23**(8): p. 602-611.
36. Ribeiro, A.E., et al., *Chiral Separation of Ketoprofen Enantiomers by Preparative and Simulated Moving Bed Chromatography*. Separation Science and Technology, 2011. **46**(11): p. 1726-1739.

37. Bentley, J., et al., *Optimizing the separation of gaseous enantiomers by simulated moving bed and pressure swing adsorption*. Adsorption-Journal of the International Adsorption Society, 2011. **17**(1): p. 159-170.
38. Garcia Palacios, J., M. Kaspereit, and A. Kienle, *Integrated Simulated Moving Bed Processes for Production of Single Enantiomers*. Chemical Engineering & Technology, 2011. **34**(5): p. 688-698.
39. Bentley, J., et al., *Optimizing the separation of gaseous enantiomers by simulated moving bed and pressure swing adsorption*. Adsorption-Journal of the International Adsorption Society, 2011. **17**(1): p. 159-170.
40. Gou, L.Z., et al., *A Hybrid Process for Chiral Separation of Compound-Forming Systems*. Chirality, 2011. **23**(2): p. 118-127.
41. Palacios, J.G., M. Kaspereit, and A. Kienle, *Integrated Simulated Moving Bed Processes for Production of Single Enantiomers*. Chemical Engineering & Technology, 2011. **34**(5): p. 688-698.
42. Munkelt, T., et al., *Recovery and Enantioseparation of Chiral Anesthetic Gases with Modified Porous Glasses*. Chemie Ingenieur Technik, 2013. **85**(11): p. 1686-1693.
43. Mutavdzin, I., A. Seidel-Morgenstern, and M. Petkovska, *Estimation of competitive adsorption isotherms based on nonlinear frequency response experiments using equimolar mixtures-numerical analysis for racemic mixtures*. Chemical Engineering Science, 2013. **89**: p. 21-30.
44. Swernath, S., M. Kaspereit, and A. Kienle, *Dynamics and Control of Coupled Continuous Chromatography and Crystallization Processes for the Production of Pure Enantiomers*. Chemical Engineering & Technology, 2013. **36**(8): p. 1417-1429.
45. Gong, R.J., et al., *Experiment and modeling for the separation of guaifenesin enantiomers using simulated moving bed and Varicol units*. Journal of Chromatography A, 2014. **1363**: p. 242-249.
46. Lorenz, H. and A. Seidel-Morgenstern, *Processes To Separate Enantiomers*. Angewandte Chemie-International Edition, 2014. **53**(5): p. 1218-1250.
47. Ngoc Lan, M., et al., *Recovery of ionic liquid and sugars from hydrolyzed biomass using ion exclusion simulated moving bed chromatography*. Journal of Chromatography A, 2012. **1227**: p. 67-72.
48. Caes, B.R., et al., *Simulated Moving Bed Chromatography: Separation and Recovery of Sugars and Ionic Liquid from Biomass Hydrolysates*. Chemsuschem, 2013. **6**(11): p. 2083-2089.
49. Rabelo, M.C., et al., *Chromatographic Separation of Isomaltooligosaccharides on Ion-Exchange Resins: Effect of the Cationic Form*. Adsorption Science & Technology, 2012. **30**(8-9): p. 773-784.
50. Ghazi, I., et al., *Beet sugar syrup and molasses as low-cost feedstock for the enzymatic production of fructo-oligosaccharides*. Journal of Agricultural and Food Chemistry, 2006. **54**(8): p. 2964-2968.
51. Nobre, C., et al., *Operating Conditions of a Simulated Moving Bed Chromatography Unit for the Purification of Fructo-Oligosaccharides*. 6th International Conference on Simulation and Modelling in the Food and Bio-Industry, ed. V. Cadavez and D. Thiel. 2010. 216-218.
52. Geisser, A., et al., *Separation of lactose from human milk oligosaccharides with simulated moving bed chromatography*. Journal of Chromatography A, 2005. **1092**(1): p. 17-23.
53. Subramani, H.J., K. Hidajat, and A.K. Ray, *Optimization of simulated moving bed and Varicol processes for glucose-fructose separation*. Chemical Engineering Research & Design, 2003. **81**(A5): p. 549-567.
54. Kurup, A.S., K. Hidajat, and A.K. Ray, *Comparative study of modified simulated moving bed systems at optimal conditions for the separation of ternary mixtures of xylene isomers*. Industrial & Engineering Chemistry Research, 2006. **45**(18): p. 6251-6265.

55. Jin, W.H. and P.C. Wankat, *Thermal operation of four-zone simulated moving beds*. Industrial & Engineering Chemistry Research, 2007. **46**(22): p. 7208-7220.
56. Lee, J., et al., *Modeling and simulation of a simulated moving bed for adsorptive para-xylene separation*. Korean Journal of Chemical Engineering, 2010. **27**(2): p. 609-618.
57. Bergeot, G., et al., *Intensification of Paraxylene Production using a Simulated Moving Bed Reactor*. Oil & Gas Science and Technology-Revue D Ifp Energies Nouvelles, 2010. **65**(5): p. 721-733.
58. Lim, Y.-I., et al., *Improvement of para-Xylene SMB Process Performance on an Industrial Scale*. Industrial & Engineering Chemistry Research, 2010. **49**(7): p. 3316-3327.
59. Sutanto, P.S., Y.-i. Lim, and J. Lee, *Flushing Flow Rates Analysis in Eight-Zone SMB Process for p-Xylene Separation*. Pres 2011: 14th International Conference on Process Integration, Modelling and Optimisation for Energy Saving and Pollution Reduction, Pts 1 and 2, 2011. **25**: p. 767-772.
60. Lim, Y.-I., *Optimal flushing flow rates in para-xylene simulated moving-bed considering geometric factor of dead volume*. Adsorption-Journal of the International Adsorption Society, 2012. **18**(5-6): p. 469-482.
61. Sutanto, P.S., Y.-I. Lim, and J. Lee, *Bed-line flushing and optimization in simulated moving-bed recovery of para-xylene*. Separation and Purification Technology, 2012. **96**: p. 168-181.
62. Cristancho, C.A.M. and A. Seidel-Morgenstern, *Purification of single-chain antibody fragments exploiting pH-gradients in simulated moving bed chromatography*. Journal of Chromatography A, 2016. **1434**: p. 29-38.
63. Wellhoefer, M., et al., *Continuous processing of recombinant proteins: Integration of inclusion body solubilization and refolding using simulated moving bed size exclusion chromatography with buffer recycling*. Journal of Chromatography A, 2013. **1319**: p. 107-117.
64. Bochenek, R., et al., *Evaluating the performance of different multicolumn setups for chromatographic separation of proteins on hydrophobic interaction chromatography media by a numerical study*. Journal of Chromatography A, 2013. **1301**: p. 60-72.
65. Palani, S., et al., *Recombinant protein purification using gradient-assisted simulated moving bed hydrophobic interaction chromatography. Part I: Selection of chromatographic system and estimation of adsorption isotherms*. Journal of Chromatography A, 2011. **1218**(37): p. 6396-6401.
66. Kessler, L.C., et al., *Step gradients in 3-zone simulated moving bed chromatography application to the purification of antibodies and bone morphogenetic protein-2*. Journal of Chromatography A, 2007. **1176**(1-2): p. 69-78.
67. Mihlbachler, K., F.B. Anspach, and A. Seidel-Morgenstern, *Experimental and theoretical studies on gradient chromatography of proteins*. Chemie Ingenieur Technik, 1998. **70**(4): p. 382-389.
68. Velayudhan, A. and C. Horvath, *Preparative chromatography of proteins analysis of the multivalent ion-exchange formalism*. Journal of chromatography, 1988. **443**: p. 13-29.
69. Kalbfuss, B., et al., *Size-exclusion chromatography as a linear transfer system: Purification of human influenza virus as an example*. Journal of Chromatography B-Analytical Technologies in the Biomedical and Life Sciences, 2008. **873**(1): p. 102-112.
70. Kroeber, T., et al., *Continuous purification of influenza virus using simulated moving bed chromatography*. Journal of Chromatography A, 2013. **1307**: p. 99-110.
71. Andreev, B.M., A.V. Kruglov, and Y.L. Selivanenko, *Continuous isotope separation by simulated countercurrent moving bed chromatography and ion exchange*. Fundamentals of Adsorption, 1996: p. 43-50.
72. Kruglov, A.V., B.M. Andreev, and Y.G. Pojidaev, *Continuous isotope separation in systems with solid phase .2. Separation of nitrogen isotopes with use of ion-exchange resin*. Separation Science and Technology, 1996. **31**(4): p. 471-490.

73. Zabokritsky, M.P., V.P. Chizhkov, and B.A. Rudenko, *Preparative-scale separation of close isomers and isotope-substituted compounds by high-resolution circulation gas-chromatography .1. state-of-the-art*. Journal of High Resolution Chromatography & Chromatography Communications, 1983. **6**(9): p. 460-470.
74. Zabokritsky, M.P., V.P. Chizhkov, and B.A. Rudenko, *Preparative-scale separation of close isomers and isotope-substituted compounds by high-resolution circulation gas-chromatography .2. applications*. Journal of High Resolution Chromatography & Chromatography Communications, 1985. **8**(4): p. 170-176.
75. Cheh, C.H., *Advances in preparative gas-chromatography for hydrogen isotope-separation*. Journal of Chromatography A, 1994. **658**(2): p. 283-291.
76. Schmidt-Traub, H., M. Schulte, and A. Seidel-Morgenstern, *Preparative Chromatography*. 2012: Wiley.
77. Lawler, K.V., et al., *Assessing zeolite frameworks for noble gas separations through a joint experimental and computational approach*. Microporous and Mesoporous Materials, 2016. **222**: p. 104-112.
78. Di Giovanni, O., et al., *Supercritical fluid simulated moving bed chromatography II. Langmuir isotherm*. Journal of Chromatography A, 2001. **919**(1): p. 1-12.
79. Cristancho, C.A.M., S. Peper, and M. Johannsen, *Supercritical fluid simulated moving bed chromatography for the separation of ethyl linoleate and ethyl oleate*. Journal of Supercritical Fluids, 2012. **66**: p. 129-136.
80. Snyder, L.R., J.J. Kirkland, and J.W. Dolan, *Introduction to Modern Liquid Chromatography*. 2011: Wiley.
81. Nicoud, R.M., *Chromatographic Processes*. 2015: Cambridge University Press.
82. Seidel-Morgenstern, A., *Optimization and comparison of different modes of preparative chromatography*. Analisis, 1998. **26**(7): p. M46-M55.
83. Ruthven, D.M. and C.B. Ching, *Countercurrent and simulated countercurrent adsorption separation processes*. Chemical Engineering Science, 1989. **44**(5): p. 1011-1038.
84. Faria, R.P.V. and A.E. Rodrigues, *Instrumental aspects of Simulated Moving Bed chromatography*. Journal of Chromatography A, 2015. **1421**: p. 82-102.
85. Lim, Y.I. and S.K. Bhatia, *Effect of dead volume on performance of simulated moving bed process*. Adsorption-Journal of the International Adsorption Society, 2011. **17**(1): p. 109-120.
86. Azevedo, D.C.S. and A.E. Rodrigues, *Design and optimization of new simulated moving bed plants*. Brazilian Journal of Chemical Engineering, 2006. **23**(2): p. 171-181.
87. Graca, N.S., et al., *Analysis of the synthesis of 1,1-dibutoxyethane in a simulated moving-bed adsorptive reactor*. Chemical Engineering and Processing, 2011. **50**(11-12): p. 1214-1225.
88. Cao, J., B. Shen, and J. Liu, *Optimal Operation of Simulated Moving Bed Technology on Utilization of Naphtha Resource*. Separation Science and Technology, 2012. **48**(2): p. 246-253.
89. Kusaba, T., Y. Kuranaga, and S. Miyamoto, *Separation of 2-Adamantanone from 1-Adamantanol and 2-Adamantanol by Simulated Moving Bed Chromatography*. Journal of Chemical Engineering of Japan, 2013. **46**(4): p. 262-270.
90. Acetti, D., et al., *Intermittent simulated moving bed chromatographic separation of (RS,RS)-2-(2,4-difluorophenyl)butane-1,2,3-triol*. Journal of Chromatography A, 2010. **1217**(17): p. 2840-2846.
91. Le, T.-H., et al., *Application of hmim BF₄ ionic liquid in reversed-phase simulated moving bed for the separation of 3-and 4-hydroxybenzoic acid*. Korean Journal of Chemical Engineering, 2009. **26**(5): p. 1334-1340.
92. Antos, D. and A. Seidel-Morgenstern, *Two-step solvent gradients in simulated moving bed chromatography - Numerical study for linear equilibria*. Journal of Chromatography A, 2002. **944**(1-2): p. 77-91.

93. Vanneste, J., et al., *Techno-economic evaluation of membrane cascades relative to simulated moving bed chromatography for the purification of mono- and oligosaccharides*. Separation and Purification Technology, 2011. **80**(3): p. 600-609.
94. Borges da Silva, E.A., I. Pedruzzi, and A.E. Rodrigues, *Simulated moving bed technology to improve the yield of the biotechnological production of lactobionic acid and sorbitol*. Adsorption-Journal of the International Adsorption Society, 2011. **17**(1): p. 145-158.
95. Long, N.V.D., et al., *Separation of D-psicose and D-fructose using simulated moving bed chromatography*. Journal of Separation Science, 2009. **32**(11): p. 1987-1995.
96. Nam, H.-G. and S. Mun, *Optimal design and experimental validation of a three-zone simulated moving bed process based on the Amberchrom-CG161C adsorbent for continuous removal of acetic acid from biomass hydrolyzate*. Process Biochemistry, 2012. **47**(5): p. 725-734.
97. Jeon, Y.-J., M.B. Park, and I.-H. Kim, *L-Ribose from L-arabinose by epimerization and its purification by 3-zone simulated moving bed chromatography*. Bioprocess and Biosystems Engineering, 2010. **33**(1): p. 87-95.
98. Mun, S., *Improving performance of a tandem simulated moving bed process for sugar separation by making a difference in the adsorbents and the column lengths of the two subordinate simulated moving bed units*. Journal of Chromatography A, 2013. **1277**: p. 48-57.
99. Vankova, K. and M. Polakovic, *Design of Fructooligosaccharide Separation Using Simulated Moving-Bed Chromatography*. Chemical Engineering & Technology, 2012. **35**(1): p. 161-168.
100. Lee, J.W., et al., *Design and sensitivity analysis of simulated moving bed chromatography to separate sugar alcohols*. Journal of Liquid Chromatography & Related Technologies, 2007. **30**(13-16): p. 1859-1877.
101. Nam, H.-G., S.-H. Jo, and S. Mun, *Comparison of Amberchrom-CG161C and Dowex99 as the adsorbent of a four-zone simulated moving bed process for removal of acetic acid from biomass hydrolyzate*. Process Biochemistry, 2011. **46**(10): p. 2044-2053.
102. Kim, J.-I., et al., *Analysis of "focusing" effect in four-zone SMB (Simulated Moving Bed) unit for separation of xylose and glucose from biomass hydrolysate*. Journal of Bioscience and Bioengineering, 2009. **108**: p. S65-S66.
103. Song, S.-M. and I.H. Kim, *A three-zone simulated moving-bed for separation of immunoglobulin Y*. Korean Journal of Chemical Engineering, 2013. **30**(8): p. 1527-1532.
104. Abel, S., et al., *Two-fraction and three-fraction continuous simulated moving bed separation of nucleosides*. Journal of Chromatography A, 2004. **1043**(2): p. 201-210.
105. Song, S.M., M.B. Park, and I.H. Kim, *Three-zone simulated moving-bed (SMB) for separation of cytosine and guanine*. Korean Journal of Chemical Engineering, 2012. **29**(7): p. 952-958.
106. Xie, Y., et al., *Standing wave design and experimental validation of a tandem simulated moving bed process for insulin purification*. Biotechnology Progress, 2002. **18**(6): p. 1332-1344.
107. Freydell, E.J., et al., *Size-exclusion simulated moving bed chromatographic protein refolding*. Chemical Engineering Science, 2010. **65**(16): p. 4701-4713.
108. Fuereder, M., S. Panke, and M. Bechtold, *Simulated moving bed enantioseparation of amino acids employing memory effect-constrained chromatography columns*. Journal of Chromatography A, 2012. **1236**: p. 123-131.
109. Cremasco, M.A., A. Starquit, and N.H.L. Wang, *Separation of L-tryptophan present in an aromatic amino acids mixture in a four-column simulated moving bed: experimental and simulation studies*. Brazilian Journal of Chemical Engineering, 2009. **26**(3): p. 611-618.
110. Gueorguieva, L., et al., *Recombinant protein purification using gradient assisted simulated moving bed hydrophobic interaction chromatography. Part II: Process design and experimental validation*. Journal of Chromatography A, 2011. **1218**(37): p. 6402-6411.

111. Nam, H.-G., et al., *Optimization of productivity in a four-zone simulated moving bed process for separation of succinic acid and lactic acid*. Chemical Engineering Journal, 2011. **171**(1): p. 92-103.
112. Wu, J., et al., *Model-based design of a pilot-scale simulated moving bed for purification of citric acid from fermentation broth*. Journal of Chromatography A, 2009. **1216**(50): p. 8793-8805.
113. Wu, X.D., et al., *Improving the Operating Conditions of Gradient Ion-Exchange Simulated Moving Bed for Protein Separation*. Industrial & Engineering Chemistry Research, 2013. **52**(15): p. 5407-5417.
114. Wang, Y., et al., *Identification and Separation of the Novel Antifungal Antibiotic of Streptomyces Hygroscopicus BOS-013 Strain by Simulated Moving Bed Chromatography*, in *Advanced Research on Material Engineering and Its Application*, H. Zhang and D. Jin, Editors. 2012. p. 245-248.
115. Grabski, A.C., A. Zilberman, and R.C. Mierendorf, *Highly efficient gram scale purification of monoclonal antibodies by simulated moving bed chromatography*. Abstracts of Papers of the American Chemical Society, 2010. **239**.
116. Nam, H.G., et al., *Experimental validation of the solvent-gradient simulated moving bed process for optimal separation of phenylalanine and tryptophan*. Process Biochemistry, 2012. **47**(3): p. 401-409.
117. Mao, N., et al., *Enhancement of MAb purification using simulated moving bed chromatography with HIC adsorbents*. Abstracts of Papers of the American Chemical Society, 2011. **241**.
118. Mun, S., *Effect of a partial-feeding application on product purities and throughput of a five-zone simulated moving bed process for the separation of a ternary nucleoside mixture*. Process Biochemistry, 2011. **46**(4): p. 977-986.
119. Nam, H.-G., et al., *Continuous separation of succinic acid and lactic acid by using a three-zone simulated moving bed process packed with Amberchrom-CG300C*. Process Biochemistry, 2012. **47**(12): p. 2418-2426.
120. Mun, S., *Optimal design of solvent gradient simulated moving bed chromatography for aminoacid separation*. Journal of Liquid Chromatography & Related Technologies, 2011. **34**(15): p. 1518-1535.
121. Cong, J. and B. Lin, *Separation of Liquiritin by simulated moving bed chromatography*. Journal of Chromatography A, 2007. **1145**(1-2): p. 190-194.
122. Wang, S.Y., Y. Liang, and S.W. Zheng, *Separation of epigallocatechin gallate from tea polyphenol by simulated moving bed chromatography*. Journal of Chromatography A, 2012. **1265**: p. 46-51.
123. Wei, F., et al., *Separation of alpha-Tocopherol with a Two-Feed Simulated Moving Bed*. Chinese Journal of Chemical Engineering, 2012. **20**(4): p. 673-678.
124. Xu, Q.Q., et al., *Separation and Purification of Desmosterol by Simulated Moving Bed Chromatography*. Chinese Journal of Analytical Chemistry, 2013. **41**(6): p. 851-855.
125. Kang, S.-H., J.-H. Kim, and S. Mun, *Optimal design of a tandem simulated moving bed process for separation of paclitaxel, 13-dehydroxybaccatin III, and 10-deacetylpaclitaxel*. Process Biochemistry, 2010. **45**(9): p. 1468-1476.
126. Kim, S.-G., et al., *Optimal design of a four-zone simulated moving bed process for separation of homoharringtonine and harringtonine*. Canadian Journal of Chemical Engineering, 2011. **89**(2): p. 304-313.
127. Zhang, W., Q. Li, and S.Y. Wang, *Macroporous Resin Column Simulated Moving Bed Chromatography Adsorption for Separation of Albiflorin and Paeoniflorin*. Asian Journal of Chemistry, 2013. **25**(8): p. 4271-4274.
128. Mun, S., *Enhanced performance of a tandem simulated moving bed process for separation of paclitaxel, 13-dehydroxybaccatin III, and 10-deacetylpaclitaxel by making a difference*

- between the adsorbent particle sizes of the two subordinate simulated moving bed units. *Process Biochemistry*, 2011. **46**(6): p. 1329-1334.
129. Grossmann, C., et al., *Experimental implementation of automatic 'cycle to cycle' control to a nonlinear chiral simulated moving bed separation*. *Journal of Chromatography A*, 2010. **1217**(13): p. 2013-2021.
130. Araujo, J.M.M., et al., *Chiral separation by two-column, semi-continuous, open-loop simulated moving-bed chromatography*. *Journal of Chromatography A*, 2010. **1217**(33): p. 5407-5419.
131. Wang, X. and C.B. Ching, *Chiral separation and modeling of the three-chiral-center beta-blocker drug nadolol by simulated moving bed chromatography*. *Journal of Chromatography A*, 2004. **1035**(2): p. 167-176.
132. Colin, H., *Foreword - Preparative chromatography today*. *Analisis*, 1998. **26**(7): p. M15-M17.
133. Hritzko, B.J., et al., *Standing-wave design of tandem SMB for linear multicomponent systems*. *Aiche Journal*, 2002. **48**(12): p. 2769-2787.
134. Wankat, P.C., *Simulated moving bed cascades for ternary separations*. *Industrial & Engineering Chemistry Research*, 2001. **40**(26): p. 6185-6193.
135. Kim, J.K., Y.F. Zang, and P.C. Wankat, *Single-cascade simulated moving bed systems for the separation of ternary mixtures*. *Industrial & Engineering Chemistry Research*, 2003. **42**(20): p. 4849-4860.
136. Kim, J.K. and P.C. Wankat, *Designs of simulated-moving-bed cascades for quaternary separations*. *Industrial & Engineering Chemistry Research*, 2004. **43**(4): p. 1071-1080.
137. Jo, S.-H., et al., *Comparative analysis of single-cascade five-zone and two-zone SMB systems for the separation of a ternary amino acid mixture*. *Canadian Journal of Chemical Engineering*, 2007. **85**(6): p. 874-882.
138. Khan, H. and M. Younas, *Theoretical analysis and simulation of five-zone simulating moving bed for ternary mixture separation*. *Canadian Journal of Chemical Engineering*, 2011. **89**(6): p. 1480-1491.
139. Mun, S., *Effect of subdividing the adsorbent bed in a five-zone simulated moving bed chromatography for ternary separation*. *Journal of Liquid Chromatography & Related Technologies*, 2008. **31**(9): p. 1231-1257.
140. Mun, S., *Enhanced Separation Performance of a Five-Zone Simulated Moving Bed Process by Using Partial Collection Strategy Based on Alternate Opening and Closing of a Product Port*. *Industrial & Engineering Chemistry Research*, 2010. **49**(19): p. 9258-9270.
141. Mun, S., *Improving performance of a five-zone simulated moving bed chromatography for ternary separation by simultaneous use of partial-feeding and partial-closing of the product port in charge of collecting the intermediate-affinity solute molecules*. *Journal of Chromatography A*, 2011. **1218**(44): p. 8060-8074.
142. Jermann, S., M. Meijssen, and M. Mazzotti, *Three column intermittent simulated moving bed chromatography: 3. Cascade operation for center-cut separations*. *Journal of Chromatography A*, 2015. **1378**: p. 37-49.
143. Jiang, C.W., F.M. Huang, and F. Wei, *A pseudo three-zone simulated moving bed with solvent gradient for quaternary separations*. *Journal of Chromatography A*, 2014. **1334**: p. 87-91.
144. Hur, J.S. and P.C. Wankat, *Hybrid simulated moving bed and chromatography systems for center-cut separation from quaternary mixtures: Linear isotherm systems*. *Industrial & Engineering Chemistry Research*, 2006. **45**(25): p. 8713-8722.
145. Palacios, J.G., et al., *Optimization and Analysis of Possible Column Arrangements for Multicomponent Separations by Preparative Chromatography*. *Industrial & Engineering Chemistry Research*, 2009. **48**(24): p. 11148-11157.
146. Hur, J.S. and P.C. Wankat, *Chromatographic and SMB center-cut separations of ternary mixtures*. *Separation Science and Technology*, 2008. **43**(6): p. 1273-1295.

147. Aumann, L. and M. Morbidelli, *A continuous multicolumn countercurrent solvent gradient purification (MCSGP) process*. Biotechnology and Bioengineering, 2007. **98**(5): p. 1043-1055.
148. Graca, N.S., L.S. Pais, and A.E. Rodrigues, *Separation of Ternary Mixtures by Pseudo-Simulated Moving-Bed Chromatography: Separation Region Analysis*. Chemical Engineering & Technology, 2015. **38**(12): p. 2316-2326.
149. Wei, F., et al., *Study on a pseudo-simulated moving bed with solvent gradient for ternary separations*. Journal of Chromatography A, 2012. **1225**: p. 99-106.
150. Jermann, S., S. Katsuo, and M. Mazzotti, *Intermittent Simulated Moving Bed Processes for Chromatographic Three-Fraction Separation*. Organic Process Research & Development, 2012. **16**(2): p. 311-322.
151. Wei, F., et al., *A novel pseudo simulated moving bed with solvent gradient for ternary separations*. Journal of Chromatography A, 2011. **1218**(20): p. 2906-2911.
152. Wei, F., et al., *Novel Simulated Moving-Bed Cascades with a Total of Five Zones for Ternary Separations*. Industrial & Engineering Chemistry Research, 2012. **51**(16): p. 5805-5812.
153. Lee, J.W. and P.C. Wankat, *Design of pseudo-simulated moving bed process with multi-objective optimization for the separation of a ternary mixture: Linear isotherms*. Journal of Chromatography A, 2010. **1217**(20): p. 3418-3426.
154. da Silva, E.A.B. and A.E. Rodrigues, *Design methodology and performance analysis of a pseudo-simulated moving bed for ternary separation*. Separation Science and Technology, 2008. **43**(3): p. 533-566.
155. Hur, J.S., et al., *Purification of L-phenylalanine from a ternary amino acid mixture using a two-zone SMB/chromatography hybrid system*. Separation Science and Technology, 2007. **42**(5): p. 911-930.
156. Abunasser, N. and P. Wankat, *Ternary separations with one-column analogs to SMB*. Separation Science and Technology, 2005. **40**(16): p. 3239-3259.
157. Rhee, H.K., R. Aris, and N.R. Amundson, *Theory and Application of Hyperbolic Systems of Quasilinear Equations*. 2001: Dover Publications.
158. Ching, C.B., D.M. Ruthven, and K. Hidajat, *Experimental-study of a simulated countercurrent adsorption system .3. SORBEX operation*. Chemical Engineering Science, 1985. **40**(8): p. 1411-1417.
159. Storti, G., et al., *Design of optimal operating-conditions of simulated moving-bed adsorptive separation units*. Industrial & Engineering Chemistry Research, 1995. **34**(1): p. 288-301.
160. Katsuo, S., et al., *Extra-column dead volume in simulated moving bed separations: Theory and experiments*. Journal of Chromatography A, 2009. **1216**(7): p. 1084-1093.
161. Nicolaos, A., et al., *Application of the equilibrium theory to ternary moving bed configurations (4+4, 5+4, 8 and 9 zones) II. Langmuir case*. Journal of Chromatography A, 2001. **908**(1-2): p. 87-109.
162. Kessler, L.C., *Enhancing the Potential of Simulated Moving Bed Chromatography*. 2009: Docupoint-Verlag.
163. Mazzotti, M., G. Storti, and M. Morbidelli, *Optimal operation of simulated moving bed units for nonlinear chromatographic separations*. Journal of Chromatography A, 1997. **769**(1): p. 3-24.
164. Migliorini, C., M. Mazzotti, and M. Morbidelli, *Simulated moving-bed units with extra-column dead volume*. Aiche Journal, 1999. **45**(7): p. 1411-1421.
165. Abel, S., M. Mazzotti, and M. Morbidelli, *Solvent gradient operation of simulated moving beds I. Linear isotherms*. Journal of Chromatography A, 2002. **944**(1-2): p. 23-39.
166. Kaspereit, M., A. Seidel-Morgenstem, and A. Kienle, *Design of simulated moving bed processes under reduced purity requirements*. Journal of Chromatography A, 2007. **1162**(1): p. 2-13.

167. Martin, A.J.P. and R.L.M. Synge, *A new form of chromatogram employing two liquid phases I. A theory of chromatography 2. Application to the micro-determination of the higher monoamino-acids in proteins*. Biochemical Journal, 1941. **35**: p. 1358-1368.
168. Storti, G., et al., *Adsorption separation processes - countercurrent and simulated countercurrent operations*. Computers & Chemical Engineering, 1988. **12**(5): p. 475-482.
169. Beltscheva, D., P. Hugo, and A. Seidel-Morgenstern, *Linear two-step gradient counter-current chromatography - Analysis based on a recursive solution of an equilibrium stage model*. Journal of Chromatography A, 2003. **989**(1): p. 31-45.
170. Kremser, A., *Theoretical analysis of absorption process*. Natural Petroleum News, 1930. **22**: p. 43-49.
171. Kawajiri, Y. and L.T. Biegler, *Nonlinear programming superstructure for optimal dynamic operations of simulated moving bed processes*. Industrial & Engineering Chemistry Research, 2006. **45**(25): p. 8503-8513.
172. Agrawal, G. and Y. Kawajiri, *Full Superstructure for Multiobjective Optimization of Multicolumn Chromatography for Ternary Separations*. Chemical Engineering & Technology, 2015. **38**(9): p. 1677-1682.
173. Nocedal, J. and S. Wright, *Numerical Optimization*. 2006: Springer New York.
174. Seidel-Morgenstern, A., *Experimental determination of single solute and competitive adsorption isotherms*. Journal of Chromatography A, 2004. **1037**(1-2): p. 255-272.
175. Moldoveanu, S.C. and V. David, *Essentials in Modern HPLC Separations*. 2012: Elsevier.
176. Rouessac, F. and A. Rouessac, *Chemical analysis: modern instrumentation methods and techniques*. 2007: John Wiley.
177. Witzel, C. and K.R. Gegenfurtner, *Categorical sensitivity to color differences*. Journal of Vision, 2013. **13**(7).
178. Rhee, H.K., R. Aris, and N.R. Amundson, *First-Order Partial Differential Equations*. 2014: Dover Publications.
179. Zhong, G.M. and G. Guiochon, *Analytical solution for the linear ideal model of simulated moving bed chromatography*. Chemical Engineering Science, 1996. **51**(18): p. 4307-4319.
180. Katti, A.M. and P. Jagland, *Development and optimization of industrial scale chromatography for use in manufacturing*. Analisis, 1998. **26**(7): p. M38-M46.
181. Mann, G., *Some considerations on the use of preparative liquid chromatography in the pharmaceutical industry*. Analisis, 1998. **26**(7): p. M76-M82.
182. Knox, J.H. and H.M. Pyper, *Framework for maximizing throughput in preparative liquid-chromatography*. Journal of Chromatography, 1986. **363**(1): p. 1-30.
183. Zhong, G.M. and G. Guiochon, *Steady-state analysis of simulated moving-bed chromatography using the linear, ideal model*. Chemical Engineering Science, 1998. **53**(6): p. 1121-1130.
184. Zhong, G.M., M.S. Smith, and G. Guiochon, *Effect of the flow rates in linear, ideal, simulated moving-bed chromatography*. Aiche Journal, 1997. **43**(11): p. 2960-2969.
185. Tedder, D.W. and D.F. Rudd, *Parametric studies in industrial distillation .1. design comparisons*. Aiche Journal, 1978. **24**(2): p. 303-315.
186. Wankat, P.C., *Equilibrium staged separations: separations in chemical engineering*. 1988: Elsevier.
187. Rajendran, A., *Equilibrium theory-based design of simulated moving bed processes under reduced purity requirements linear isotherms*. Journal of Chromatography A, 2008. **1185**(2): p. 216-222.
188. Bloch, H.S., et al., *Production of liquid olefins by PACOL-OLEX*. Abstracts of Papers of the American Chemical Society, 1972: p. 27-&.
189. Raverdino, V. and P. Sassetti, *Gas-chromatography in the identification of positional and geometrical-isomers of complex C8-C13 normal-alkene mixtures from the OLEX process*. Journal of Chromatography, 1979. **169**(FEB): p. 223-243.

190. Meyers, R.A., *Handbook of Petroleum Refining Processes*. 1997: McGraw-Hill.
191. Epp, D.N., *The Chemistry of Food Dyes*. 1995: Terrific Science Press.
192. Grumezescu, A.M. and A.M. Holban, *Natural and Artificial Flavoring Agents and Food Dyes*. 2017: Elsevier Science.
193. Fu, R., *Fast Separation of Synthetic/Artificial Food Colors on Agilent Poroshell 120 EC-C18*, in *Application Note*. 2012. p. 1-6.
194. Kirschbaum, J., et al., *Development and evaluation of an HPLC-DAD method for determination of synthetic food colorants*. *Chromatographia*, 2003. **57**: p. S115-S119.
195. Piccin, J.S., et al., *Adsorption of FD&C Red No. 40 by chitosan: Isotherms analysis*. *Journal of Food Engineering*, 2009. **95**(1): p. 16-20.
196. Dotto, G.L. and L.A.A. Pinto, *Adsorption of food dyes onto chitosan: Optimization process and kinetic*. *Carbohydrate Polymers*, 2011. **84**(1): p. 231-238.
197. Dotto, G.L., et al., *Removal of acid blue 9, food yellow 3 and FD&C yellow N degrees 5 dyes from aqueous solutions using activated carbon, activated earth, diatomaceous earth, chitin and chitosan: equilibrium studies and thermodynamic*. *Quimica Nova*, 2011. **34**(7): p. 1193-U110.
198. Piccin, J.S., G.L. Dotto, and L.A.A. Pinto, *Adsorption isotherms and thermochemical data of FD&C red N degrees 40 binding by chitosan*. *Brazilian Journal of Chemical Engineering*, 2011. **28**(2): p. 295-304.
199. Piccin, J.S., et al., *Kinetics and Mechanism of the Food Dye FD&C Red 40 Adsorption onto Chitosan*. *Journal of Chemical and Engineering Data*, 2011. **56**(10): p. 3759-3765.
200. Dotto, G.L., E.C. Lima, and L.A.A. Pinto, *Biosorption of food dyes onto Spirulina platensis nanoparticles: Equilibrium isotherm and thermodynamic analysis*. *Bioresource Technology*, 2012. **103**(1): p. 123-130.
201. Dotto, G.L., et al., *Application of chitosan films for the removal of food dyes from aqueous solutions by adsorption*. *Chemical Engineering Journal*, 2013. **214**: p. 8-16.
202. Cadaval, T.R.S., G.L. Dotto, and L.A.A. Pinto, *Equilibrium Isotherms, Thermodynamics, and Kinetic Studies for the Adsorption of Food Azo Dyes onto Chitosan Films*. *Chemical Engineering Communications*, 2015. **202**(10): p. 1316-1323.
203. Dotto, G.L., et al., *New physicochemical interpretations for the adsorption of food dyes on chitosan films using statistical physics treatment*. *Food Chemistry*, 2015. **171**: p. 1-7.
204. Sellaoui, L., et al., *Equilibrium modeling of single and binary adsorption of Food Yellow 4 and Food Blue 2 on modified chitosan using a statistical physics theory: new microscopic interpretations*. *Journal of Molecular Liquids*, 2016. **222**: p. 151-158.
205. Shabandokht, M., E. Binaeian, and H.A. Tayebi, *Adsorption of food dye Acid red 18 onto polyaniline-modified rice husk composite: isotherm and kinetic analysis*. *Desalination and Water Treatment*, 2016. **57**(57): p. 27638-27650.
206. Deniz, F. and R.A. Kepekci, *Biosorption of Food Green 3 by a novel green generation composite biosorbent from aqueous environment*. *International Journal of Phytoremediation*, 2017. **19**(6): p. 579-586.
207. Srivastava, V., et al., *Synthesis and application of polypyrrole coated tenorite nanoparticles (PPy@TN) for the removal of the anionic food dye 'tartrazine' and divalent metallic ions viz. Pb(II), Cd(II), Zn(II), Co(II), Mn(II) from synthetic wastewater*. *Rsc Advances*, 2015. **5**(98): p. 80829-80843.
208. Al-Ghouti, M.A., et al., *Multivariate analysis of competitive adsorption of food dyes by activated pine wood*. *Desalination and Water Treatment*, 2016. **57**(57): p. 27651-27662.
209. Xue, H.Y., F. Han, and B.Y. He, *Biosorption of Food Dye onto Gelatin Microspheres: Equilibrium Isotherm and Thermodynamic Analysis*, in *New Materials and Processes, Pts 1-3*, W.Z. Chen, et al., Editors. 2012. p. 2239-2242.
210. Foo, K.Y. and B.H. Hameed, *An overview of dye removal via activated carbon adsorption process*. *Desalination and Water Treatment*, 2010. **19**(1-3): p. 255-274.

211. Sanchez-Duarte, R.G., et al., *Chitosan-based adsorbents gels for the removal of tris-azo dye: isotherms and kinetics studies*. Environmental Engineering and Management Journal, 2016. **15**(11): p. 2469-2478.
212. Jandera, P., et al., *Characterization of the properties of stationary phases for liquid chromatography in aqueous mobile phases using aromatic sulphonic acids as the test compounds*. Journal of Chromatography A, 2009. **1216**(2): p. 237-248.
213. Gritti, F. and G. Guiochon, *Adsorption mechanism of acids and bases in reversed-phase liquid chromatography in weak buffered mobile phases designed for liquid chromatography/mass spectrometry*. Journal of Chromatography A, 2009. **1216**(10): p. 1776-1788.
214. Horváth, C., *High-performance liquid chromatography: advances and perspectives*. 1980: Academic Press.
215. Poole, C.F., *The Essence of Chromatography*. 2003: Elsevier.
216. Dill, K.A., *The mechanism of solute retention in reversed-phase liquid-chromatography*. Journal of Physical Chemistry, 1987. **91**(7): p. 1980-1988.
217. Wang, C.R., et al., *Overloading study of basic compounds with a positively charged C18 column in liquid chromatography*. Journal of Chromatography A, 2013. **1281**: p. 60-66.
218. Cavazzini, A., et al., *Understanding Mixed-Mode Retention Mechanisms in Liquid Chromatography with Hydrophobic Stationary Phases*. Analytical Chemistry, 2014. **86**(10): p. 4919-4926.
219. Gritti, F. and G. Guiochon, *Characteristics of the adsorption mechanism of acido-basic compounds with two pK(a) in reversed-phase liquid chromatography*. Journal of Chromatography A, 2009. **1216**(41): p. 6917-6930.
220. Ni, Y.N. and X.F. Gong, *Simultaneous spectrophotometric determination of mixtures of food colorants*. Analytica Chimica Acta, 1997. **354**(1-3): p. 163-171.
221. Soczewinski, E., *Solvent composition effects in thin-layer chromatography systems of the type silica gel-electron donor solvent*. Analytical Chemistry, 1969. **41**(1): p. 179-182.
222. Chin, C.Y. and N.H.L. Wang, *Simulated moving bed equipment designs*. Separation and Purification Reviews, 2004. **33**(2): p. 77-155.
223. Allen, S.J., G. McKay, and K.Y.H. Khader, *Multi-component sorption isotherms of basic-dyes onto peat*. Environmental Pollution, 1988. **52**(1): p. 39-53.
224. Gritti, F. and G. Guiochon, *Peak shapes of acids and bases under overloaded conditions in reversed-phase liquid chromatography, with weakly buffered mobile phases of various pH: A thermodynamic interpretation*. Journal of Chromatography A, 2009. **1216**(1): p. 63-78.
225. Bastin, G., et al., *Stability analysis of switching hyperbolic systems: the example of SMB chromatography*. 2014 European Control Conference (Ecc), 2014: p. 2153-2157.
226. Suvarov, P., et al., *Cycle to cycle adaptive control of simulated moving bed chromatographic separation processes*. Journal of Process Control, 2014. **24**(2): p. 357-367.
227. Suvarov, P., et al., *Control of incomplete separation in simulated moving bed chromatographic processes*. Ifac Papersonline, 2016. **49**(7): p. 153-158.

Appendix A – 8-zone SMB outlet concentrations

In this appendix, the concentrations of the food dyes in the outlet streams mentioned in sections 7.5 and 7.6, as well as the corresponding chromatograms of the pooled fractions from the first and second experimental runs are shown.

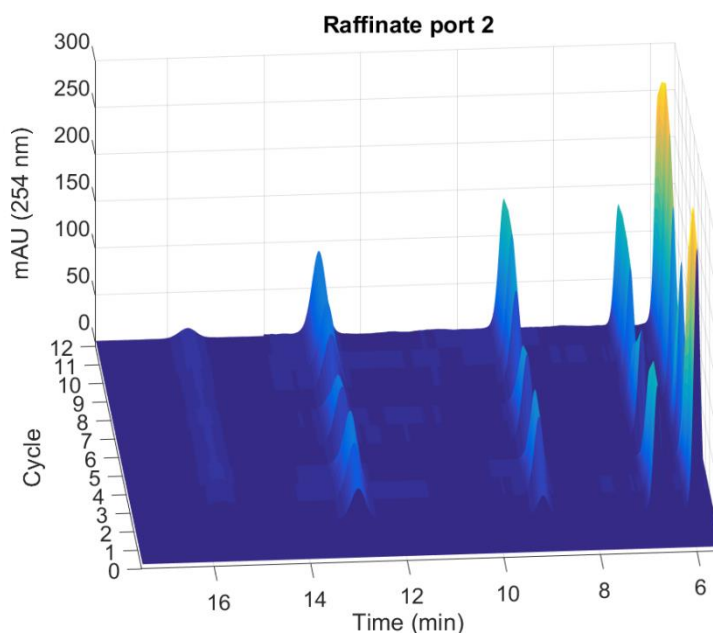


Figure A-1 – First experimental run of the 8-zone SMB with raffinate recycle - Chromatograms showing the composition of the pooled fractions from the second raffinate port of each of the 12 cycles. The time axis shows the chromatogram of each sample obtained using the HPLC method described in section 7.2.1. The “cycle” axis indicates from which cycle each sample was obtained from. The vertical axis shows the absorbance signal from the chromatograms at 254 nm. The first peak corresponds to Tartrazine, the second, to Sunset Yellow, the third, to Allura Red, the fourth, to Crystal Ponceau and the fifth, to Fast Green.

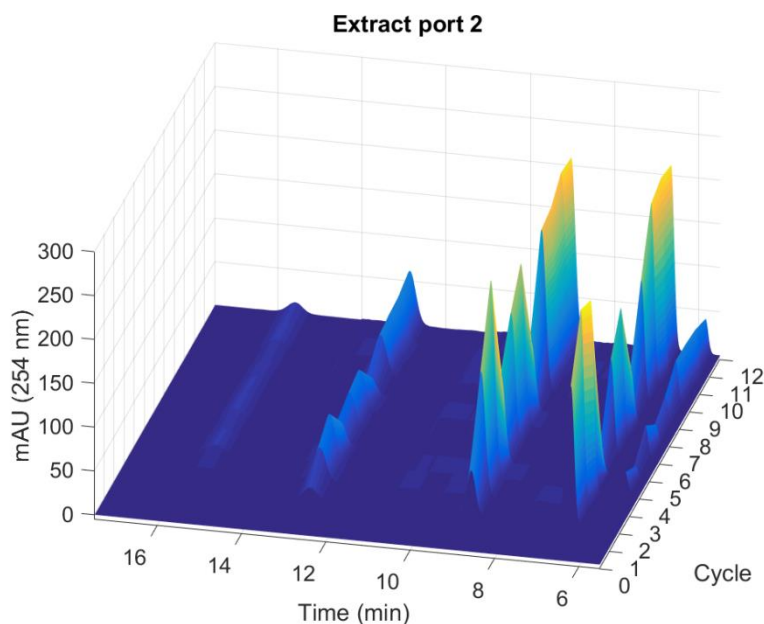


Figure A-2 – First experimental run of the 8-zone SMB with raffinate recycle - Chromatograms showing the composition of the pooled fractions from the second extract port of each of the 12 cycles. The time axis shows the chromatogram of each sample obtained using the HPLC method described in section 7.2.1. The “cycle” axis indicates from which cycle each sample was obtained from. The vertical axis shows the absorbance signal from the chromatograms at 254 nm. The first peak corresponds to Tartrazine, the second, to Sunset Yellow, the third, to Allura Red, the fourth, to Crystal Ponceau and the fifth, to Fast Green.

Cycle	Average concentration [$\text{mg.l}^{-1} \times 10^3$]				
	TA (a)	SY (b)	AR (c)	CP (d)	FG (e)
0	0.000	0.000	0.000	0.000	0.000
1	0.000	0.000	0.000	0.000	0.000
2	0.000	0.039	0.090	0.020	0.000
3	0.000	0.000	0.270	0.720	0.140
4	0.000	0.100	0.420	0.840	0.280
5	0.020	0.060	0.188	0.400	0.260
6	0.060	0.100	0.270	0.540	0.180
7	0.000	0.100	0.330	0.600	0.280
8	0.090	0.060	0.144	0.340	0.220
9	0.020	0.090	0.330	0.570	0.230
10	0.000	0.100	0.360	0.840	0.350
11	0.000	0.100	0.390	0.900	0.420
12	0.000	0.100	0.390	1.020	0.420

Table A-1 – Outlet concentrations averaged over cycle of the first experimental run of 8-zone SMB with raffinate recycle. Extract Port 1 ($3.374 \text{ ml.min}^{-1}$).

Cycle	Average concentration [$\text{mg.l}^{-1}\times 10^3$]				
	TA (a)	SY (b)	AR (c)	CP (d)	FG (e)
0	0.000	0.000	0.000	0.000	0.000
1	1.020	0.630	0.000	0.060	0.000
2	2.160	1.540	0.204	0.540	0.000
3	2.460	1.610	0.902	1.020	0.100
4	2.040	1.190	0.979	1.320	0.200
5	0.720	0.140	0.210	0.300	0.150
6	1.980	1.330	0.932	0.960	0.150
7	1.020	0.910	0.813	0.900	0.200
8	1.320	0.630	0.280	0.360	0.150
9	2.040	1.400	1.004	0.960	0.150
10	2.340	1.540	1.501	1.200	0.200
11	2.340	1.470	1.540	1.200	0.200
12	2.460	1.540	1.470	1.320	0.250

Table A-2 – Outlet concentrations averaged over cycle of the first experimental run of 8-zone SMB with raffinate recycle. Raffinate Port 2 ($2.058 \text{ ml.min}^{-1}$).

Cycle	Average concentration [$\text{mg.l}^{-1}\times 10^3$]				
	TA (a)	SY (b)	AR (c)	CP (d)	FG (e)
0	0.000	0.000	0.000	0.000	0.000
1	0.102	0.283	0.000	0.000	0.000
2	0.000	1.820	0.510	0.210	0.000
3	0.000	2.590	1.530	0.630	0.070
4	0.200	2.310	2.380	0.900	0.210
5	0.110	0.321	1.065	0.400	0.160
6	0.400	1.260	1.530	0.630	0.210
7	0.200	1.610	1.870	0.770	0.210
8	0.200	0.612	0.815	0.300	0.189
9	0.400	1.610	1.870	0.770	0.140
10	0.400	2.380	2.040	0.840	0.210
11	0.400	2.310	2.210	0.910	0.210
12	0.400	2.520	2.210	0.910	0.280

Table A-3 – Outlet concentrations averaged over cycle of the first experimental run of 8-zone SMB with raffinate recycle. Extract Port 2 ($1.029 \text{ ml.min}^{-1}$).

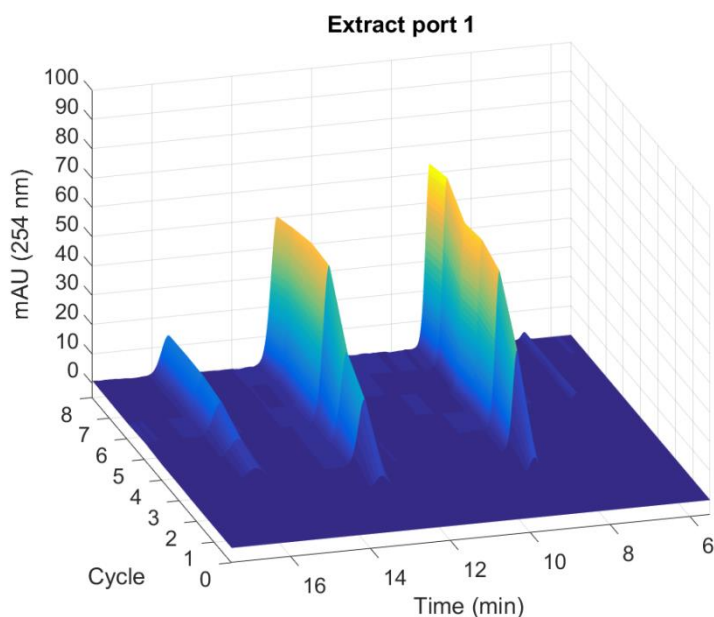


Figure A-3 – Second experimental run of the 8-zone SMB with raffinate recycle - Chromatograms showing the composition of the pooled fractions from the first extract port of each of the 8 cycles. The time axis shows the chromatogram of each sample obtained using the HPLC method described in section 7.2.1. The “cycle” axis indicates from which cycle each sample was obtained from. The vertical axis shows the absorbance signal from the chromatograms at 254 nm. The first peak corresponds to Tartrazine, the second, to Sunset Yellow, the third, to Allura Red, the fourth, to Crystal Ponceau and the fifth, to Fast Green.

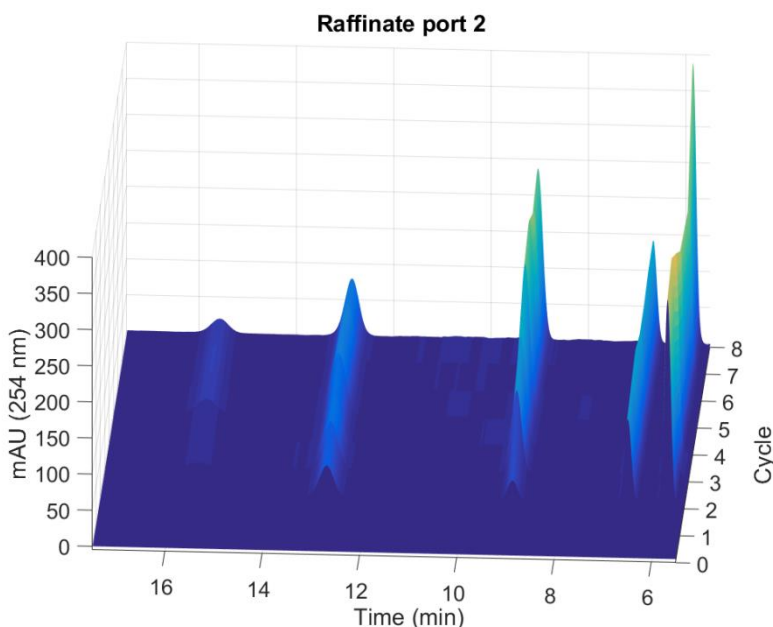


Figure A-4 – Second experimental run of the 8-zone SMB with raffinate recycle - Chromatograms showing the composition of the pooled fractions from the second extract port of each of the 8 cycles. The time axis shows the chromatogram of each sample obtained using the HPLC method described in section 7.2.1. The “cycle” axis indicates from which cycle each sample was obtained from. The vertical axis shows the absorbance signal from the chromatograms at 254 nm. The first peak corresponds to Tartrazine, the second, to Sunset Yellow, the third, to Allura Red, the fourth, to Crystal Ponceau and the fifth, to Fast Green.

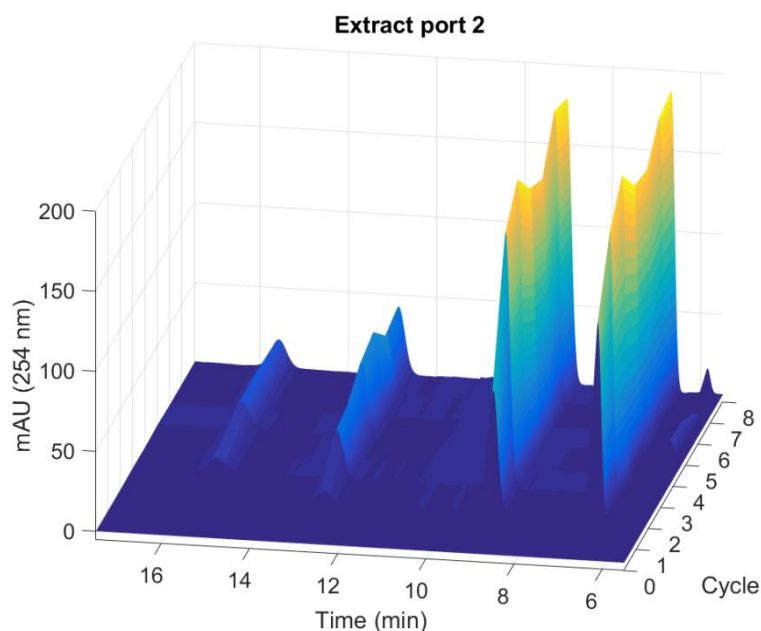


Figure A-5 – Second experimental run of the 8-zone SMB with raffinate recycle - Chromatograms showing the composition of the pooled fractions from the second extract port of each of the 8 cycles. The time axis shows the chromatogram of each sample obtained using the HPLC method described in section 7.2.1. The “cycle” axis indicates from which cycle each sample was obtained from. The vertical axis shows the absorbance signal from the chromatograms at 254 nm. The first peak corresponds to Tartrazine, the second, to Sunset Yellow, the third, to Allura Red, the fourth, to Crystal Ponceau and the fifth, to Fast Green.

Cycle	Average concentration [$\text{mg.l}^{-1} \times 10^4$]				
	TA (a)	SY (b)	AR (c)	CP (d)	FG (e)
0	0.000	0.000	0.000	0.000	0.000
1	0.000	0.000	0.000	0.000	0.000
2	0.000	0.000	0.530	0.700	0.000
3	0.000	0.000	3.700	3.700	0.700
4	0.000	0.000	5.700	5.500	1.400
5	0.000	0.340	6.200	8.116	2.600
6	0.019	0.300	5.800	8.400	2.900
7	0.160	0.300	6.500	8.500	3.080
8	0.000	0.300	6.500	8.300	3.090

Table A-4 – Outlet concentrations averaged over cycle of the second experimental run of 8-zone SMB with raffinate recycle. Extract Port 1 ($3.374 \text{ ml.min}^{-1}$).

Cycle	Average concentration [$\text{mg.l}^{-1}\times 10^3$]				
	TA (a)	SY (b)	AR (c)	CP (d)	FG (e)
0	0.000	0.000	0.000	0.000	0.000
1	0.900	0.700	0.000	0.000	0.000
2	2.200	1.350	0.300	0.700	0.000
3	2.400	1.500	1.200	1.100	0.150
4	2.300	1.500	1.600	1.100	0.150
5	2.400	1.500	2.300	1.300	0.450
6	2.500	1.500	2.400	1.400	0.450
7	2.400	1.500	2.100	1.300	0.450
8	2.500	1.500	2.400	1.300	0.450

Table A-5 – Outlet concentrations averaged over cycle of the second experimental run of 8-zone SMB with raffinate recycle. Raffinate Port 2 ($2.058 \text{ ml.min}^{-1}$).

Cycle	Average concentration [$\text{mg.l}^{-1}\times 10^3$]				
	TA (a)	SY (b)	AR (c)	CP (d)	FG (e)
0	0.000	0.000	0.000	0.000	0.000
1	0.000	0.300	0.000	0.000	0.000
2	0.000	1.400	0.800	0.100	0.000
3	0.000	1.900	1.700	0.500	0.200
4	0.000	2.000	1.900	0.600	0.200
5	0.100	2.000	1.700	0.700	0.400
6	0.100	1.900	1.600	0.800	0.400
7	0.000	2.000	1.800	0.600	0.400
8	0.100	2.000	1.800	0.700	0.400

Table A-6 – Outlet concentrations averaged over cycle of the second experimental run of 8-zone SMB with raffinate recycle. Extract Port 2 ($1.029 \text{ ml.min}^{-1}$).

Appendix B – List of Chemicals, equipment and suppliers

Designation	CAS	Abbreviation	Lot#	Supplier	Country
Acetic Acid 100% p.a. ROTIPURAN® 1.05 kg.l ⁻¹	64-19-7	-	-	Carl Roth GmbH + Co.	Germany
Allura Red AC (80% dye content)	25856-17-6	AR	MKBT6061V	Sigma- Aldrich	India
Blue Dextran	87915-38-6	BD	SCBP3949V	Sigma- Aldrich	Sweden
Crystal Ponceau 6R	2766-77-0	CP	MKBV8575V	Sigma Aldrich	India
Ethanol Absolute (>99.7%) HyperSolv CHROMANORM 0.79 kg.l ⁻¹	64-17-5	-	-	VWR Chemicals	France
Fast Green FCF	2353-45-9	FG	61580119	Thermo Fisher Scientific	Germany
Sunset Yellow FCF (90% dye content)	2783-94-0	SY	MKB56508V	Sigma- Aldrich	India
Tartrazine	1934-21-0	TA	10183745	Thermo Fisher Scientific	Germany

Table B-1 – Chemicals used in the experimental work described in this dissertation and their respective CAS number, abbreviation used, lot number and supplier.

Designation	Manufacturer	Country
LiChroprep® RP-18 (particle size: 25-40 µm) i.d. 1 cm, length: 10 cm. CAS 108688-10-4	Merck Millipore	USA
Luna C18 (particle size: 10 µm) i.d.0.5 cm, length: 25 cm.	Phenomenex®	USA
Modified Prochrom® ICLC-16-10 Research Scale Continuous Chromatograph SMB	Novasep SA.	France
Agilent Infinity 1260 HPLC	Agilent Technologies	USA
Special optical glass precision cell 10 mm light path. Type No. 100-O5	Hellma Gruppe GmbH.	Germany
Spectrophotometer Genesys 6 (190nm – 1100nm) ± 0.5% (5 mAU)	Thermo Fisher Scientific	Germany

Table B-2 – Equipment used in the experimental work described in this dissertation and their respective manufacturers.



Francisco Vitor Santos da Silva

Personal data and contact information

✉ **Email Address:** FranciscoVSSilva@Gmail.com
 ★ **Born:** 11/07/1990, Curitiba (Brazil)
 🇧🇷 **Nationality:** Brazilian

Study (2008-2012)

🎓 Federal University of Paraná (UFPR): **Bioprocess Engineering and Biotechnology**
 🏆 Prize for the **highest grade (93/100)**
 Thesis: Production of **anti-rabies vaccines** for veterinary use (grade: 92/100)

Professional experience

10/2013-09/2017 Max Planck Institute (Magdeburg): PhD candidate
 Project: Analysis and design of center-cut separations using **8-zone simulated moving bed chromatography**
Supervision 🎓: Master theses (3) Bachelor thesis (1)
Teaching: Tutoring exercises (1)

04/2013-10/2013 Federal University of Paraná (UFPR): Guest scientist
 Project: **Mathematical modeling** of **gas diffusion** in **bubble column bioreactors**

01/2012-04/2013 Max Planck Institute (Magdeburg): Guest scientist
 Project: Development of an **affinity chromatography** process for **erythropoietin** purification
Teaching: Tutoring exercises (1)

05/2010-07/2011 Carlos Chagas Institute (Fiocruz-PR): Internship
 Project: Use of mass spectrometry for the **quality control** of **recombinant proteins**

09/2009-09/2010 Solid State Fermentation Lab (UFPR): Internship
 Project: **Mathematical modeling** of **hyphae growth** in **solid state fermentation**

01/2009-08/2009 Biotechnological Processes Lab (UFPR): Internship
 Project: Screening of **fungi** for **phytase production**

Teaching experience

10/2014-04/2017 Otto von Guericke University (OvGU): Tutoring the exercises of the discipline: **Adsorption und Heterogeneous Catalysis**

04/2012-10/2012 Otto von Guericke University (OvGU): Tutoring the experiments for the discipline: **Downstream Processing of Biologicals**

07/2011-01/2012 Federal University of Paraná (UFPR): Tutoring the discipline: **Mathematics Applied to Biotechnology II**

Supervisions

Master thesis **Experimental** study of the application of **SMB** for the **separation** of pseudo-ternary mixtures (M.Sc. Bettina Kattein)

Master thesis **8-Zone SMB** for the separation of pseudo-ternary mixtures (M.Sc. Rita Ribeiro)

Master thesis **Experimental** estimation of the **adsorption isotherms** of **food colorants** for the designing of a **SMB process** (M.Sc. Rojia Piskari)